



Functional analysis of novel protein, PIERCE1, in motile ciliogenesis

By:

Priyanka Anujan

A thesis submitted in partial fulfilment of the requirements for the degree of

Doctor of Philosophy

September 2018

The University of Sheffield

Faculty of Medicine, Dentistry & Health

Department of Infection, Immunity & Cardiovascular Disease

Supervisors: Prof Colin D Bingle, Dr Lynne Bingle, Prof Sudipto Roy

Dedicated to my parents, Mr Anujan Krishnapillai and Mrs Indiradevi Anujan

For making it all possible for me!

I. Abstract

Motile cilia are localised to tissues and cells where fluid movement and cellular locomotion is required. Mutations in genes associated with ciliogenesis and cilia motility give rise to diseases called ciliopathies. Primary Ciliary Dyskinesia (PCD), a heterogeneous genetic disorder, is the most common form of ciliopathy that arises from defects in motile cilia. Several systematic approaches have led to the identification of numerous genes with putative function in ciliogenesis and ciliary motility. We interrogated existing data and identified several novel candidate genes temporally associated with ciliogenesis. Expression of these genes were analysed in mouse airway epithelial cells during mucociliary differentiation at the air liquid interface (ALI) and different mouse tissues. This thesis focuses on a poorly characterized gene encoding the protein 'PIERCE1'.

Transcriptional analysis of *Pierce1* revealed an expression pattern temporally associated with ciliogenesis during differentiation of ALI mouse airway epithelial cells. *Pierce1* also shows enriched expression in motile ciliated mouse tissues. Transient morpholino knock down of *pierce1* in zebrafish showed phenotypes consistent with abnormalities in motile cilia and live imaging showed severe cilia motility defects in Kupffer's vesicle. Finally, we generated maternal zygotic loss-of-function alleles at the zebrafish *pierce1* locus using the CRISPR/Cas9. These mutants showed mild laterality defects. A custom-made antibody against mouse full length PIERCE1 protein, was used to carry out immunofluorescence microscopy on ALI cultured mouse airway epithelial cells. It revealed that PIERCE1 is a cytoplasmic protein specifically

expressed in motile ciliated cells. A yeast 2-hybrid assay carried out on human lung and testis libraries identified PIAS2, as a possible interacting partner of PIERCE1. With these findings, we propose that PIERCE1 may be involved in the assembly and transport of components required for cilia motility.

II. Acknowledgement

First and foremost, I owe my deepest gratitude to my supervisor, Prof Colin D Bingle, for introducing me to the world of research and for giving fantastic opportunities that helped me grow in this field. It was due to his valuable guidance, cheerful enthusiasm and ever-friendly nature, I was able to complete my research in a respectable manner. I am also very grateful to Dr Lynne Bingle, for her kind supervision, guidance and encouragement whenever I got stuck in my path.

I consider myself very fortunate to also have the opportunity to be supervised by Prof Sudipto Roy (IMCB (A*STAR), Singapore). I owe a great debt of gratitude to him for his guidance, encouragement and patience. Thank you so much for uplifting me and for opening my mind to be a better researcher. Your support and guidance were essential for my success.

I would also like to express my sincere gratitude towards my lab colleagues in LU100 (Medical school, University of Sheffield), especially Dr Khondoker Akram and Dr Apoorva Mulay, for teaching me the cell culture techniques. I would like to thank Renata, Chloe, Saleni, Fawas, Azis and Zayed for their friendship, support and encouragement. I would also like to express my gratitude to the lab technicians for their incredible support especially Dr Benjamin Durham and Ms Yvonne L Stephenson. I wish to thank Mr Carl G Wright and Ms Jessica A Williams for helping us with culling the mice for dissection. Special thanks to Dr Helen Marriot for helping us with mice availability.

Equally, I would like to thank my lab colleagues in SR lab (IMCB, A*STAR, Singapore) especially, Dr Lu Hao, Dr Zhou Feng and Dr. Vijay Shankaranarayan Narasimhan, for teaching me all the zebrafish techniques and for helping me settle in the lab well. Special thanks to Stylianos Markrogkikas for his friendship, encouragement and nice little chats during our coffee breaks. I would also like to thank Yan Ling, Surin, Hui Li, Chalie and Lucy for their friendship, constant support with the experiments and help with miscellaneous things. Thank you very much Yan ling and Hui Li for taking over the experiments and looking after my *pierce1* mutant fishes. I would like to take this opportunity to thank the staff of the zebrafish facility at IMCB for the maintenance of the fishes and helping me with my mutant fishes.

I would also like to thank our collaborator, Dr Dominic Norris (MRC, Harwell), for giving us the polyclonal antibody against mouse full length PIERCE1 protein.

I also would like to thank University of Sheffield and A*STAR (Singapore) for giving me this opportunity and funding my scholarship.

Most importantly, I am indebted to my parents, Mr Anujan Krishnapillai and Mrs Indiradevi Anujan who made everything possible for me. They made me who I am today with their unconditional love, support and guidance. I would also like to thank my godparents – Mr Gopala Pillai and Mrs Gomathi Pillai for playing a pivotal role in my education during my childhood. I also wish to acknowledge my late maternal and paternal grandparents for their blessings and support.

Equally I wish to give my heartfelt thanks to my husband, Mr Bhagaval Prasad Bharath who came to my life during the latter part of my PhD. He was a constant source of emotional support, encouragement during challenging times. I would also like to thank my in-laws- Mr Bhagaval Prasad Nair, Mrs Asha Prasad and Miss Sreeparvathi Prasad for all the love and support

I also wish to express my gratitude to all teachers from my primary school, secondary school, A-levels and university. Many thanks to all my friends and family who were there for me through this journey.

Lastly but above all, I thank the almighty for everything.

III. Abstract publication

- Priyanka Anujan, Sudipto Roy, Colin D Bingle. **2017**. *Functional analysis of a novel protein, PIERCE1, in motile ciliogenesis in mammalian airway epithelial cells and zebrafish embryos*. **Mechanisms of Development, 145, S25.**

IV. Conference presentations

- **Poster presentation:** Functional analysis of a novel protein, PIERCE1, in motile ciliogenesis using in vitro cultured mammalian airway epithelial cells and zebrafish embryos. **Gordon Research Conference on Cilia, Mucus & Mucociliary Interactions** (12/02/2017-17/02/2017), Hotel Galvez in Galveston TX United States.
- **Poster presentation:** Functional analysis of a novel protein, PIERCE1, in motile ciliogenesis in mammalian airway epithelial cells and zebrafish embryos. **The 18th International Congress of Developmental Biology** (18/06/2017 – 22/06/2017), University Cultural Centre, National University of Singapore, Singapore.
- **Podium presentation:** Functional analysis of a novel protein, PIERCE1, in motile ciliogenesis in mammalian airway epithelial cells and zebrafish. **The 3rd BEAT-PCD Conference & 4th Training School** (06/02/2018 – 09/02/2018), NOVA Medical School|Faculdade de Ciências Médicas, Lisbon, Portugal.
- **Podium presentation:** Functional analysis of PIERCE1, in motile ciliogenesis. **2018 UK cilia networking meeting** (23/03/2018), Richard Doll Lecture Theatre, Oxford.

-
- **Podium presentation:** Functional analysis of a novel protein, PIERCE1, in motile ciliogenesis using in vitro cultured mammalian airway epithelial cells and zebrafish embryos. **The 14th Annual University of Sheffield Medical School Research Meeting** (14/06/2018 -15/06/2018), Students' Union Auditorium, University of Sheffield.
 - **Podium presentation:** Functional analysis of PIERCE1, in motile ciliogenesis. **European Respiratory Society International Congress 2018** (15/09/2018-19/09/2018), Paris, France.

V. Abbreviations

ALI	Air Liquid Interface
ANOVA	Analysis Of Variance
AP	Alkaline Phosphatase
ATP	Adenosine Triphosphate
BAL	Bronchoalveolar Lavage
BPIFA1	Bacterial Permeability Increasing Fold-Containing Protein A1
bp	Base Pairs
BSA	Bovine Serum Albumin
CBA	Curved Body Axis
CBF	Cilia Beat Frequency
CCPG1OS	Cell Cycle Progression 1, Opposite Strand
cDNA	Complementary DNA
CD	Centriolar Duplication
CF	Cystic Fibrosis
COPD	Chronic Obstructive Pulmonary Disease
CRISPR	Clustered Regularly Interspaced Short Palindromic Repeats
CT	Cycle Threshold
CP	Central Pair Of Microtubules
DAPI	4'6-Diamidino-2-Phenylindole
DD	Deutrosomal Duplication
DEPC	Diethylpyrocarbonate
dgRNA	Double Guide RNA
DNA	Deoxyribosenucleic Acid
dNTP	Deoxyribose Nucleotide Triphosphates
dpf	Days Post Fertilization
EDTA	Ethylenediamine Tetraacetic Acid
EM	Electron Microscope
ENaC	Epithelial Sodium Channel

FACs	Fluorescence Associated Cell Sorting
FBS	Foetal bovine serum
FGF	Fibroblast growth factor
FIG	Foxj-induced gene
FOXJ1	Forkhead box protein J1
Fwd	Forward
gDNA	Genomic DNA
GEMC1	Geminin Coiled-Coil Domain Containing
GFP	Green Fluorescent Protein
GMNN	Geminin
HBEC	Human bronchial epithelial cells
hrs	Hours
hpf	Hours post fertilisation
IDA	Inner dynein arm
IFC	Fluorescence Immunocytochemistry
IFT	Intraflagellar Transport
IHC	Immunohistochemistry
Kb	Kilobases
kDa	Kilo Dalton
KO	Knock-out
KV	Kupffer's vesicle
LB	Luria Bertani
LECA	Last evolutionary common ancestor
LRA	left-right asymmetry
MCC	Multiciliated Cells
MCIDAS	Multicillin
MeOH	Methanol
Min	Minutes
mNECs	Mouse nasal epithelial cells

mTECs	Mouse tracheal epithelial cells
MO	Morpholino oligonucleotides
MOE	Mainolfactory epithelium
MUC	Mucin
NHEJ	Non-Homologous End Joining
ODA	Outer Dynein Arm
PBS	Phosphate Buffered Saline
PCD	Primary Ciliary Dyskinesia
PCP	Planar Cellular Polarity
PCR	Polymerase Chain Reaction
PD	Pronephric Duct
PIERCE1	P53-Induced Expression In RB-Null Cells Protein 1
PTU	1-Phenyl-2-Thiourea
Rev	Reverse
rpm	Revolutions Per Minute
RS	Radial Spokes
s	Seconds
sgRNA	Single Guide RNA
Shh	Sonic Hedgehog signalling
TAE	Tris-Acetate EDTA
TALEN	Transcription Activator-Like Effectors Nuclease
TEM	Transmission Electron Microscopy
TZ	Transition Zone
PBS	Phosphate Buffered Saline
PCD	Primary Ciliary Dyskinesia
PCR	Polymerase Chain Reaction
PD	Pronephric Duct
PTU	1-Phenyl-2-Thiourea

WT	Wild type
X-gal	5-Bromo-4-Chloro-3-Indolyl-B-D-Galactopyranoside
3D SIM	3D Super Resolution Microscopy

VI. Table of contents

Contents

I. Abstract.....	I
II. Acknowledgement.....	III
III. Abstract publication.....	VI
IV. Conference presentations.....	VI
V. Abbreviations.....	VIII
VI. Table of contents.....	XII
VII. List of Figures.....	XVI
VIII. List of Tables.....	XX
Chapter 1 : Introduction.....	1
1.1 Cilia.....	1
1.1.1 Primary and motile cilia.....	1
1.1.2 Origins of Cilia.....	4
1.2 Motile cilia.....	4
1.2.1 Structure of motile cilia.....	5
1.2.2 Transcriptional control of ciliogenesis.....	7
1.2.3 Basal body formation.....	18
1.2.4 Basal body docking and cilia formation.....	22
1.2.5 Intraflagellar transport (IFT).....	25
1.2.6 Mechanisms of cilia motility.....	26
1.2.7 Role of cilia in airways.....	28
1.2.8 Role of cilia in establishing left-right symmetry.....	32
1.3 Disease manifestation by dysfunction of motile cilia.....	38
1.3.1 PCD.....	38
1.4 Previous attempts to define the cilium.....	39
1.6 <i>In vitro</i> culture of mouse tracheal and nasal epithelial cells at Air Liquid Interface as a model to study multiciliogenesis.....	40
1.5 Zebrafish as a model for characterising novel cilia markers and generating Primary Ciliary Dyskinesia phenotype.....	42
1.7 Aims and hypothesis of the thesis.....	45
Chapter 2 : Materials and methods.....	48
2.1 Studying ciliogenesis in primary mammalian airway epithelial cells cultured <i>in vitro</i>	48

2.1.1 Culture of mouse tracheal and nasal epithelial cells	48
2.1.2 RNA extraction	56
2.1.3 Reverse transcription	56
2.1.4 Amplification by Polymerase Chain Reaction (PCR)	57
2.1.9 siRNA transfection of primary mouse nasal and tracheal epithelial cells ..	57
2.1.10 Western Blotting	59
2.1.11 Immunofluorescence microscopy	60
2.1.12 Quantification of intracellular localization of epithelial cells	63
2.1.13 Quantitative PCR	63
2.2 Analysing ciliogenesis in zebrafish embryos	65
2.2.1 Zebrafish strains and husbandry	65
2.2.2 Zebrafish Morpholino experiments.....	65
2.2.3 Fixation of embryos for immunofluorescence.....	66
2.2.4 Whole mount immunohistochemistry on zebrafish embryos	67
2.2.5 Zebrafish molecular biology techniques.....	69
2.2.6 Making <i>pierce1</i> knockout with CRISPR/Cas9 gene editing technique	80
2.3 Statistical tests and analysis	84
Chapter 3 : Validation of mammalian airway epithelial cells cultured at air liquid interface as an <i>in vitro</i> model for analysing ciliogenesis.....	86
3.1 Preface	86
3.2 Results.....	87
3.2.1 Culturing and differentiation of mNECs and mTECs at the ALI.....	87
3.2.2 Transcriptional expression of airway epithelial markers during ALI culture of mNEC and mTEC.....	88
3.2.3 Secretion of BPIFA1 during ALI culture of mTEC and mNEC	91
3.2.4 Immunofluorescence microscopy of airway epithelial markers during ALI culture of mTEC and mNEC	92
3.2.5 mRNA analysis of cilia markers during ALI differentiation of mNEC and mTEC.....	97
3.2.6 ALI differentiation of mNEC from <i>Dnah11c^{iv/iv}</i> mice.....	98
3.2.7 Modulation of the number of ciliated cells with NOTCH inhibitor treatment.	100
3.2.8 Optimizing siRNA transfection into mNEC and mTEC	103
3.3 Discussion	106
Chapter 4 : Selecting potential novel candidate genes associated with ciliogenesis	115

4.1 Preface	115
4.2 Results	118
4.2.1 Expression levels of selected cilia candidate genes during mucociliary differentiation at ALI culture	120
4.3.2 Expression of the cilia candidate genes in mouse tissues	122
4.3.3 <i>Pierce1</i> (P53-Induced Expression in RB-Null Cells 1)	124
4.3.4 <i>RIKEN cDNA 1700013F07</i>	128
4.3.5 <i>RIKEN cDNA 1700001L19 gene</i>	132
4.3.6 <i>RIKEN cDNA 4833427G06 gene</i>	135
4.3.7 <i>Leucine Rich Repeat Containing 4B (LRRC4B)</i>	137
4.3.8 <i>RIKEN 1700028P14 gene</i>	140
4.3.9 <i>Maats1</i> (MYCBP associated and testis expressed 1)	144
4.3.10 <i>Erich2</i> (Glutamate rich protein-2)	147
4.3.11 <i>Spata24</i> (spermatogenesis associated 24)	149
4.3.12 <i>RIKEN cDNA 1110017D15 gene</i>	152
4.3.13 Expression analysis of the candidate genes during ALI differentiation of mTEC by RNA sequencing	156
4.4.14 Expression of candidate genes in developing lung by single cell gene expression	158
4.4 Discussion	160
Chapter 5 : Functional characterisation of <i>Pierce1</i> using zebrafish.....	166
5.1 Preface	166
5.1.1 Proposed method for investigating the functional role of <i>Pierce1</i> in zebrafish.....	166
5.2 Results	167
5.2.1 <i>pierce1</i> is upregulated by <i>Foxj1</i>	167
5.2.2 Transient knockdown of <i>pierce1</i> in zebrafish by morpholinos	168
5.2.3 Tagged expression vector systems shows cytoplasmic localisation of <i>Pierce1</i>	175
5.2.4 Creating a <i>pierce1</i> zebrafish mutant line using CRISPR/Cas9	177
5.3 Discussion	191
Chapter 6 : Localisation of <i>PIERCE1</i> to multiciliated cells may give clues to its function.....	200
6.1 Preface	200
6.2 Results	201
6.2.1 Validating <i>PIERCE1</i> antibody on testis cell lysate by Western blot.....	201

6.2.2 Localisation of PIERCE1 in differentiated mouse airway epithelial cells cultured at the ALI.....	203
6.2.3 PIERCE1 is upregulated in mNEC treated with DAPT	207
6.2.5 Determining the interactors of PIERCE1	209
6.3 Discussion	210
Chapter 7 : Discussion	217
7.1 Establishment of <i>in vitro</i> culture of mouse primary airway epithelial cells as a model for studying motile ciliogenesis.....	218
7.2 <i>Pierce1</i> was selected for further characterisation from a list of 10 randomly selected putative ciliary genes.....	220
7.3 <i>pierce1</i> zebrafish morphants showed severe situs abnormalities and curved axis associated with cilia defects.	225
7.4 Maternal zygotic zebrafish mutants of <i>pierce1</i> showed mild situs abnormalities	226
7.5 PIERCE1 has specific expression in multiciliated cells in mouse airway epithelial cells and has a cytoplasmic subcellular localization.....	229
7.6 C15ORF65, a paralog of PIERCE1.....	230
7.7 PIAS2 is a potential binding partner of PIERCE1	234
7.7 Proposed role of PIERCE1 in motile ciliogenesis	234
7.8 PIERCE1 and human diseases?	237
7.9 Future directions.....	237
Bibliography	239
Appendix 1.....	263
Appendix 2.....	264
Appendix 3.....	267
Appendix 4.....	270
Appendix 5.....	272

VII. List of Figures

Figure 1-1 Structure of cilium	3
Figure 1-2. Diversity in motile cilia is brought by different transcriptional modulators and signalling pathways working through FOXJ1.	11
Figure 1-3. Basal body synthesis in ciliogenesis.....	19
Figure 1-4. Functional role of cilia in airways.	30
Figure 1-5. Left–right (L–R) asymmetry of human body.....	34
Figure 1-6. Cilia in the left-right organiser.	36
Figure 1-7. Motile cilia in the zebrafish embryos.....	44
Figure 2-1. Harvest of mouse trachea.....	50
Figure 2-2. Harvest of mouse nasal septum.	52
Figure 2-3. Epithelial cells are extracted from mouse nasal septum and trachea and grown in submerged culture.	55
Figure 3-1 MRNA expression of airway epithelial markers during Air Liquid Interface (ALI) of MNEC and MTEC.....	89
Figure 3-2. Western blot shows secretion of BPIFA1 by ali cultures OF MNEC and MTEC	91
Figure 3-3. IF microscopy of differentiation of ciliated cells and secretory cells in the ALI cultured MNEC and MTEC.....	93
Figure 3-4. IF microscopy showing TP63 localised to basal cells during ALI culture.	95
Figure 3-5. IF staining of cells with PAN-CYTOKERATIN on differentiated airway epithelial cells.....	96
Figure 3-6. MRNA expression of genes involved in ciliogenesis during the ali differentiation of MNEC and MTEC	98
Figure 3-7. IF microscopy of differentiation of ali cultured MNEC from and DNAH11CI ^{V/IV} mice.....	99
Figure 3-8. The number of ciliated cells were increased in the DAPT treated MNEC.....	102
Figure 3-9. Optimizing SIRNA transfection with SIGLO (GREEN, Dharmacon) in primary mouse nasal and tracheal epithelial cells.	104
Figure 3-10. Optimizing SIRNA transfection with SIGLO (Green, Dharmacon) using 4 different transfection reagents.	105
Figure 4-1 A Flowchart for the selection process of candidate gene.	117

FIGURE 4-2 Expression of putative ciliary genes at different time-points in ALI culture of MNEC.....	121
Figure 4-3 Expression of novel candidate genes in whole mouse tissues. ...	123
Figure 4-4. <i>Pierce1</i> expression in mouse tissues based on the BioGPS database.	126
Figure 4-5. Localisation of PIERCE1 in motile ciliated tissues.....	127
Figure 4-6. C1ORF194 homolog expression in mouse tissues based on the BioGPS database.....	130
Figure 4-7. Localization of C1ORF194 in motile ciliated tissues.	131
Figure 4-8. C5ORF49 homolog expression in mouse tissues based on the BioGPS database.....	133
Figure 4-9. Localization of C5ORF49 in motile ciliated tissues.	134
Figure 4-10. C11ORF88 expression on mouse tissues based on the BioGPS database.	136
Figure 4-11. LRRC4B expression in mouse tissues based on the BioGPS database.	138
Figure 4-12. Localization of LRRC4B in motile ciliated tissues.	139
Figure 4-13. C9ORF135 homolog expression in mouse tissues based on the BioGPS database.....	142
Figure 4-14. Localization of C9ORF135 in motile ciliated tissues.	143
Figure 4-15. MAATS1 expression in mouse tissues based on the BioGPS database.	146
Figure 4-16. ERICH2 expression in mouse tissues based on the BioGPS database.	148
Figure 4-17. SPATA24 expression in mouse tissues based on the BioGPS database.	151
Figure 4-18. CBE1 expression in mouse tissues based on the BioGPS database.	154
Figure 4-19. Localisation of CBE1 in motile ciliated tissues.....	155
Figure 4-20. Expression of the candidate genes in ALI cultured WT MTEC vs TP73 KO MTEC.	157
Figure 4-21. Expression of the candidate genes in 9 distinct cell types of E18.5 fetal mouse lung.....	159
Figure 5-1. <i>perce1</i> is upregulated by Foxj1.....	168
Figure 5-2. <i>perce1</i> splice morpholino blocks splicing of <i>perce1</i> transcript..	170

Figure 5-3. <i>ierce1</i> morphants display phenotypes associated with ciliary structural defects.	171
Figure 5-4. <i>ierce1</i> morphants display laterality defects.	172
Figure 5-5. <i>ierce1</i> morphants have cilia motility defects in KV.	173
Figure 5-6. <i>ierce1</i> morphants have normal cilia length and number in KV.	174
Figure 5-7. Pierce1 has a cytoplasmic sub-cellular localisation in zebrafish embryos.	176
Figure 5-8. <i>ierce1</i> gRNA target sites identified by CHOPCHOP.	178
Figure 5-9. Validation of sGRNAs <i>in vitro</i>	179
Figure 5-10. Validation of sGRNAs <i>in vivo</i>	180
Figure 5-11. Validation of dGRNAs <i>in vitro</i> and <i>in vivo</i>	181
Figure 5-12. Transmission of 29 bp insertion in exon 2 from sGRNA1 injected F0.	183
Figure 5-13. Transmission of 5 bp deletion in exon 2 from a male founder injected with dGRNA.	184
Figure 5-14. Location of primers designed to identify homozygous mutants with c.176_180del allele.	185
Figure 5-15. Identification of F2 homozygous <i>ierce1</i> mutants for c.178_179ins(29 bp) and c.176_180del.	186
Figure 5-16. Maternal contribution of <i>ierce1</i> in zebrafish embryos.	187
Figure 5-17. Validation of mutation in <i>ierce1</i> transcripts of c.178_179ins(29 bp) maternal zygotic mutants.	188
Figure 5-18. Validation of mutation in <i>ierce1</i> transcripts of c.176_180del maternal zygotic mutants.	189
Figure 5-19. Conserved amino acid residues are missing in the mutants.	190
Figure 5-20. Maternal zygotic mutants showed mild situs abnormalities.	191
Figure 6-1. Western blot of PIERCE1 in mouse testis tissue lysate.	202
Figure 6-2. PIERCE1 is localised to ciliated cells in ALI MNECS at day 14.	204
Figure 6-3. Schematic diagram indicating the z-stacks created by the confocal laser scanning microscope from the ALI cultured MNEC samples.	205
Figure 6-4. PIERCE1 does not localize to cilia axoneme and is localized in the cytoplasm.	206
Figure 6-5. <i>Pierce1</i> is upregulated in DAPT treated MNEC.	208
Figure 7-1. Single-cell profiling of MTEC shows enriched expression of <i>ierce1</i> in ciliated cells.	223

Figure 7-2. Single-cell profiling of HBECs shows enriched expression of pierce1 in ciliated cells.	224
FIGURE 7-3. Expression of <i>Pierce1</i> and <i>Ccpg1os</i> in ALI cultured WT MTEC vs TP73 KO MTEC.....	231
FIGURE 7-4. <i>Ccpg1os</i> expression on mouse tissues based on the BioGPS database.	232
FIGURE 7-5. Expression of <i>Ccpg1os</i> in 9 distinct cell types of E18.5 fetal mouse lung.....	233
FIGURE 7-6. Schematic diagram showing the proposed role of PIERCE1.	236

VIII. List of Tables

Table 2-1. Primary antibodies in western blotting.	60
Table 2-2. Primary antibodies in immunostaining.	61
Table 2-3. Secondary antibodies in immunostaining.	62
Table 2-4. Components for quantitative pcr	64
Table 2-5. Zebrafish strains used in the study	65
Table 2-6. Morpholinos used in the study	66
Table 2-7. Primary antibodies in immunostaining	67
Table 2-8. Secondary antibodies in immunostaining	68
Table 2-9. Components for first-strand synthesis of cDNA	70
Table 2-10. Components for reverse transcription (RT).....	71
Table 2-11. Components for PCR with Roche expand high fidelity kit.....	72
Table 2-12. Components for PCR with MYFI mix	73
Table 2-13. Components for TOPO-TA cloning	74
Table 2-14. Components for restriction digest reaction.....	75
Table 2-15. Components for ligation reaction	76
Table 2-16. Components for Quantitative PCR.....	79
Table 2-17. components for gRNA template amplification	81
Table 2-18. Components for gRNA <i>in vitro</i> transcription.....	82
Table 2-19. Components for gRNA <i>in vitro</i> validation	83
Table 4-1. Novel cilia candidate genes	119



Chapter 1 : Introduction

1.1 Cilia

Cilia are one of the oldest known organelles, first described in protozoa by Antonie van Leeuwenhoek (father of microbiology and the first acknowledged microscopist) in 1675. He was fascinated by these 'incredibly thin feet, or little legs' used by cells to generate currents and swim in the fluid environment ((van Leewenhoek, 1932).

In 1785, a century later, the term 'cilium', from Latin word for eyelash, was coined by Otto Muller (Muller, 1786). Although the existence of cilia was known for centuries, only in the last few decades, an understanding of the formation, structure and function of cilia begun to emerge. They are membrane bounded hair-like cellular organelles, derived from centrioles and assembled by microtubules that have been conserved evolutionarily in eukaryotes (Satir, 1995, Satir and Christensen, 2008).

1.1.1 Primary and motile cilia

In vertebrates, cilia are broadly classified as immotile (primary cilium) and motile. These were traditionally distinguished on basis of the architecture of the axoneme, the central microtubular core, and their motile properties (WHEATLEY et al., 1996, Ibañez-Tallon et al., 2003, Satir and Christensen, 2007). As shown in Figure 1.1, the motile cilia have a central pair (CP) of singlet microtubules surrounded by 9 doublet microtubules and possess molecular motors, axonemal dyneins which are responsible for ciliary movement. In contrast, the CP is missing in primary cilia and they also lack the axonemal dyneins, radial spokes and nexin links, rendering them immotile (Choksi et al.,

2014d, Satir and Christensen, 2007, Takeda and Narita, 2012, Thomas et al., 2010, Satir et al., 2010). However, there are exceptions to this rule of distinction e.g. there are 9+0 cilia that lack radial spokes and CP in the node that are motile (Bellomo et al., 1996, Ishikawa, 2017).

Primary cilia are widely distributed in many cell types and are usually involved in sensory functions, for example, the monocilia lining the kidney tubules have a role in sensing urine flow (Praetorius and Spring, 2001, Pazour and Witman, 2003). Primary cilia were once thought to be vestigial organelles. This view has changed considerably since it is now known that they have important roles in physiology (Satir and Christensen, 2007, Abou Alaiwi et al., 2009, Veland et al., 2009, Satir et al., 2010). More and more research groups are studying these organelles, shedding further light into this area.

In contrast, motile cilia are highly restricted to tissues where fluid movement and cellular locomotion is required. They function by exerting mechanical force e.g. in the respiratory tract, ciliated cells are required for mucus clearance (Satir and Christensen, 2008, Roy, 2009, Satir and Christensen, 2007). Dysfunction in either motile or immotile cilia can give rise to devastating genetic disorders collectively known as ciliopathies (Fliegauf et al., 2007, Roy, 2009).

The understanding of a large portion of the genetic and biochemical pathways of ciliogenesis originated from studies on flagellation of *Chlamydomonas* and other model organisms (Pazour et al., 2005, Smith et al., 2005, Ostrowski et al., 2011). These studies lead to characterisation of many homologues in mammals and these are often associated in human ciliopathies.

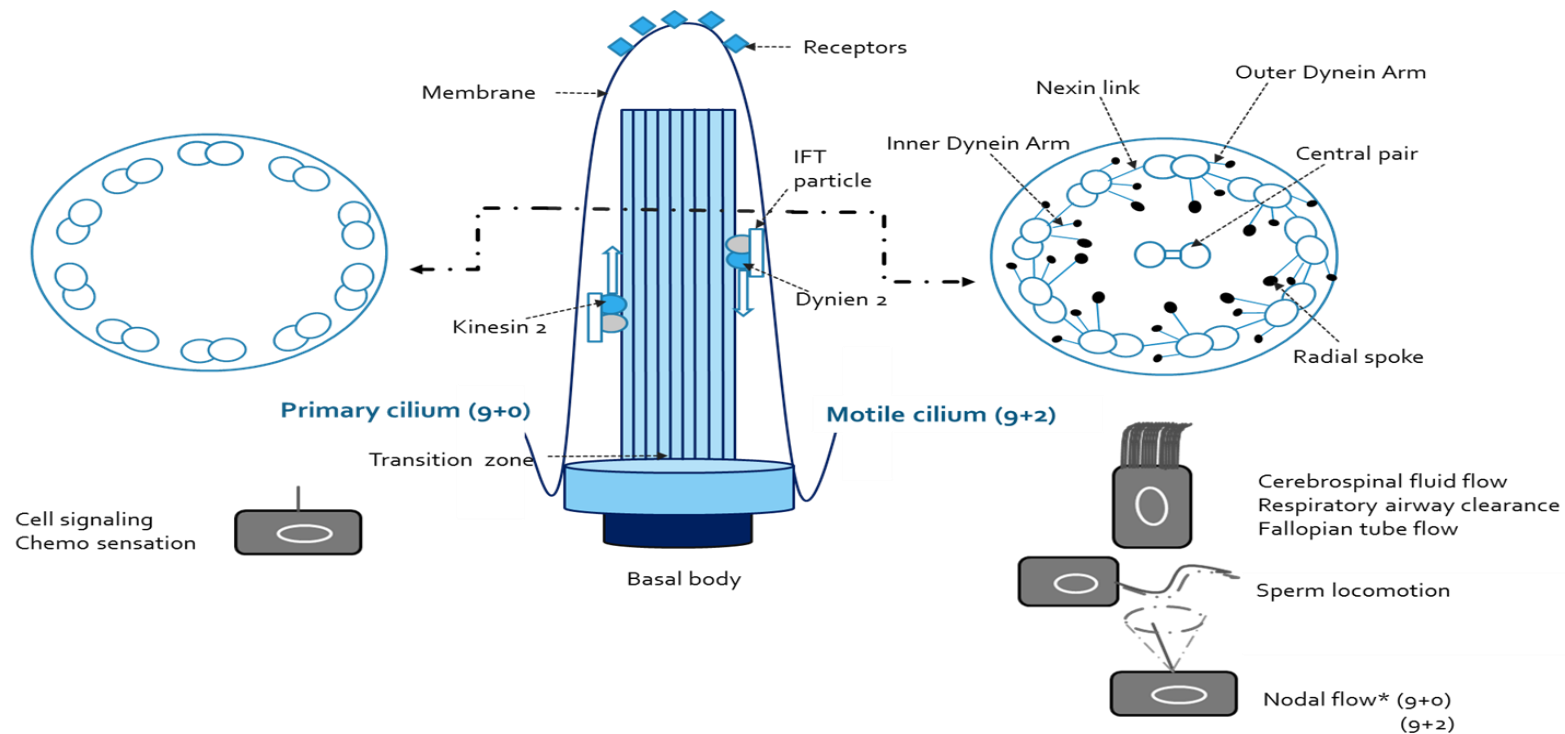


Figure 1-1 Structure of cilium

Cilia axoneme is nucleated by basal body that anchors itself on apical surface of plasma membrane through transition fibres. The elongation of axoneme requires bidirectional Intraflagellar transport (IFT) trafficking system in which kinesin-2 molecular motors carry protein and axonemal building blocks in to axoneme from cytoplasm and dynein-2 motors bring the turnover products from ciliary tips to basal body. The plus ends of microtubules at the ciliary tips allow the axoneme to grow and ciliary tip also harbours numerous receptors that allow cilia to sense the environment. Both primary cilium and motile cilium is basically formed of 9 sets of microtubule doublets enclosed by ciliary membrane. However, motile cilium possesses a pair of microtubule singlets that is connected to outer microtubule doublets through inner and outer dynein arms and radial spokes. Altogether, they function in a highly co-ordinated manner to enable motility.

1.1.2 Origins of Cilia

The origins of this multifunctional organelle are still a matter of debate. In 2011, Wickstead and Gull suggested that the ancestor cilium was a non-motile sensory organelle (Wickstead and Gull, 2011). On the other hand, most researchers believe that the prototype of cilia was a hybrid with both sensory and motility functions. These proposals arose through observations made in unicellular organisms that occupy the lower branch of evolutionary map (Silverman and Leroux, 2009, Mitchell, 2017). It is also thought that the motile 9+2 cilium was present in the last evolutionary common ancestor (LECA) (Mitchell, 2017). So how did cilia arise in the eukaryotes? One suggestion is that cilia came through the same cell lineage as the eukaryotic nucleus, by viral invasion. Hence, LECA might have had cilia for efficient motility and a nucleus for chromosome replication and information transfer (Satir et al., 2007, Satir, 2017). However, this area needs further clarity.

Nevertheless, my interests are more focused on motile cilia, captivated by the diverse functional roles they play in conception, development and physiology of vertebrate organisms. So, what makes these organelles so remarkable?

1.2 Motile cilia

Eukaryotic motile cilia/flagella are mainly involved in movement of extracellular fluids and cellular locomotion. Many unicellular organisms and some invertebrate larvae possess and utilize motile cilia for locomotion (Ibañez-Tallon et al., 2003, Pazour et al., 2005). On the other hand, in vertebrates, motile cilia are restricted to few tissues where fluid flow is required for physiology and the sperm cells that harbour flagella for movement (Figure 1.1). Interestingly, they

also show diversity in terms of their morphology and type of motility (Satir and Christensen, 2007). Early during development, the monomotile cilia present in the ventral node of the mouse, beat in a rotary fashion to drive nodal flow. This is the first step in breaking the bilateral symmetry of the organism (Wagner and Yost, 2000, McGrath and Brueckner, 2003). In adult physiology, multimotile ciliated cells (MCC) harbouring >200 cilia per cell, that move in a metachronal wave like pattern, line the respiratory tract and play a pivotal role in mucus clearance (Brooks and Wallingford, 2014a, Tilley et al., 2015). Multiciliated cells also line the brain ventricles and fallopian tubes for driving the cerebrospinal fluid flow and ovum transport, respectively (Brooks and Wallingford, 2014a). The core structure of the cilium and flagellum is very well conserved (Carvalho-Santos et al., 2011, Konno et al., 2015).

Although the traditional view regarding the function of motile cilia is fully focused on its motility, recent findings have shown that motile cilia also have sensory functions (Shah et al., 2009, Bloodgood, 2010, Jain et al., 2012). This suggests that there is more to be learnt about these well-conserved organelles, since their functions are more complex than previously thought. For decades, the structure and function of cilia have been studied extensively. However, recent advances in proteomics, molecular biology and gene editing have shed more light on the assembly and function of cilia.

1.2.1 Structure of motile cilia

Cilia are made up of three parts. 1) The basal body anchors cilia to the cell surface, 2) the axoneme forms the main extracellular part of cilia and 3) the transition zone (TZ) connects the basal body with the axoneme. These three

regions are connected continuously by microtubule cytoskeleton wherein the basal body is composed of 9 microtubule triplets, and has a cartwheel structure, (Li et al., 2012a, Geimer and Melkonian, 2004), and the 9 microtubule doublets make up the TZ and axoneme. The axoneme is encapsulated by the plasma membrane, which in turn is extended from the cell plasma membrane. The axoneme is composed of microtubule doublets and many other proteins (Satir and Christensen, 2008, Ishikawa, 2017).

In the typical motile cilia axoneme that has the 9+2 architecture, each microtubule doublet extends from the triplet microtubule (A-tubule, B-tubule and C-tubule) in the basal body and is enclosed in one complete cylindrical microtubule (A-tubule) and one incomplete tubule (B-tubule) bound to the A-tubule. A-tubules and B-tubules in the basal body are slightly different from the doublet in the axoneme (Paintrand et al., 1992, Nigg and Raff, 2009). Adjacent microtubule doublets are connected by dynein arms, nexin and the radial spokes that link the microtubule doublets and CP (Gibbons and Rowe, 1965, Smith and Yang, 2004, Ishikawa, 2017). Dyneins, radial spokes and nexin form a structure with a consistent 96-nm periodicity along the microtubule doublets (Lindemann, 2003, Ishikawa, 2017). The TZ is located on the microtubule doublet close to the edge of basal body and the dyneins, radial spokes and CP are positioned distal to the TZ (Omran, 2010, Williams et al., 2011, Fisch and Dupuis-Williams, 2012, Ishikawa, 2017). The current understanding of the structure between the TZ and cilia axoneme remains vague.

So, what are the mechanisms underlying the formation of this essential and sophisticated organelle? I will first start with the regulatory mechanisms that initiate the process of motile ciliogenesis.

1.2.2 Transcriptional control of ciliogenesis

1.2.2.1 FOXJ1 transcription factors are the master regulators of motile ciliogenesis

FOXJ1 (HFH4), a forkhead /winged-helix transcription factor, has been shown to be an essential factor required for motile ciliogenesis (Yu et al., 2008, Stubbs et al., 2008). In mice, *Foxj1* was found to be specifically expressed in motile ciliated tissues such including the embryonic node, airway epithelium, choroid plexus and testis and found to have a nuclear localisation (Clevidence et al., 1994, Hackett et al., 1995, Murphy et al., 1997, Blatt et al., 1999). High levels of expression was observed prior to motile ciliogenesis in the airway epithelium, oviducts, in ependymal cells lining the brain ventricles and the spinal column and also detected prior to the appearance of flagella in the spermatids (Blatt et al., 1999, Tichelaar et al., 1999). These findings strengthened the perception that FOXJ1 is a transcription regulator of motile ciliogenesis. Hereafter, two independent studies confirmed the importance of FOXJ1 in motile ciliogenesis. *Foxj1* knockout mice had complete absence of motile cilia axonemes in airways, brain ventricles and oviducts. They also exhibited *situs* abnormalities indicating defects in mono motile cilia present in the embryonic node (Brody et al., 2000). Independent studies also showed that *Foxj1* is also required for the formation of monomotile cilia present in the embryonic node and for flagella formation of spermatids (Chen et al., 1998). Loss of *Foxj1* resulted in loss of only motile cilia, not primary cilia. Using transmission electron microscopy, it

was also observed that in multiciliated cells, although generation of multiple basal bodies occurred normally, these failed to dock at the apical cell membrane to nucleate multiple cilia (Brody et al., 2000, Gomperts et al., 2004, You et al., 2004a, Alten et al., 2012, Choksi et al., 2014d). Thus, FOXJ1 is necessary for the docking of basal bodies at the apical membrane in multiciliated cells.

The functional role of FOXJ1 in motile ciliogenesis is not only shown in mammals but has also been studied in other vertebrates including *Xenopus* and zebrafish. The loss of Foxj1 in zebrafish embryos and *Xenopus* resulted in loss of motile cilia (Stubbs et al., 2008, Yu et al., 2008). FOXJ1 orthologues and associations with motile ciliogenesis are also found in invertebrate phyla such as Placozoa, Platyhelminthes and Echinodermata (Vij et al., 2012). This implies that FOXJ1 plays a conserved role in motile ciliogenesis.

So how does FOXJ1 regulate motile ciliogenesis? Remarkably, overexpression of *foxj1* induced ectopic motile cilia formation in different tissues in zebrafish and *Xenopus* embryos in (Stubbs et al., 2008, Yu et al., 2008). Furthermore, in chick neural tube and mouse embryonic fibroblast, formation of long cilia that resembled motile cilia, was induced by overexpression of *foxj1* (Cruz et al., 2010). These findings regarding the ciliogenic potential of FOXJ1 point towards a master regulatory role in the biogenesis of motile cilia.

Multiple high throughput screens carried out in mouse, zebrafish and *Xenopus* have identified genes that are regulated by FOXJ1. These lists mainly include genes required for structural and functional aspects of the motile cilia. Orthologs of *FOXJ1* was also used as a marker to conduct large scale genomic

screens that have produced lists of novel candidates that may play roles in cilia formation and function (Hoh et al., 2012, Choksi et al., 2014b, Stauber et al., 2017).

Members of the RFX family of transcription factors have also been implicated in ciliogenesis in many model organisms. This family of proteins is made up of seven members (RFX 1-7) in vertebrates and they all have a highly conserved 76-residue winged-helix DNA binding domain. These proteins are important for development and mutations in them are involved in many devastating disease conditions (Gajiwala et al., 2000, Choksi et al., 2014d). *Rfx1-4* have been found to be highly expressed in mouse testis indicating a possible role in spermatogenesis (Kistler et al., 2009).

The loss of *Rfx2* disrupted ciliary assembly in *Xenopus* embryos (Chung et al., 2012) and reduced cilia length in zebrafish Kupffer's vesicle (KV) and consequently laterality defects. In mouse, loss of RFX2 resulted in abnormal nodal cilia associated with laterality defects (Bisgrove et al., 2012, Wu et al., 2016). Recently, using data derived from studies on *Xenopus*, Quigley *et al* proposed that *Rfx2* acts as a scaffolding factor to recruit *Foxj1*, which is often bound to flanking enhancers, to the promoters of MCC genes (Quigley and Kintner, 2017).

On the other hand, *Rfx3* mouse mutants also displayed several phenotypes associated with ciliopathies including left-right asymmetry defects and hydrocephalus (Baas et al., 2006, Bonnafe et al., 2004). Didon *et al* proposed that RFX3 acts as a co-factor for FOXJ1 as it was shown to significantly increase *FOXJ1*-dependent transcription for ciliated cells in basal

cells in human airway epithelial cell culture. Furthermore, FOXJ1 and RFX3 were co-immunoprecipitated when these proteins were overexpressed (Didon et al., 2013). These results suggest a possibility that RFX factors and FOXJ1 form a transcriptional complex that confers specificity for motile cilia genes.

Furthermore, RFX4 has been identified to be a key regulator required for the formation of primary cilia that are crucial for the transduction of the Sonic Hedgehog (Shh) signalling pathway that specifies neuronal cell fates (Ashique et al., 2009, Bay and Caspary, 2012) .

1.2.2.2 Different transcriptional regulators and signalling pathways give rise to cilia diversity through FOXJ1

As was described in the previous section, FOXJ1 plays a master regulatory role in motile cilia biogenesis. But different transcriptional factors and signalling pathways give rise to the diversity in motile cilia as reviewed by Choksi *et al* (Choksi et al., 2014d). This is summarised in Figure 1-2.

To get an overview on how different signalling pathways and regulators come together to bring diversity in motile cilia through FOXJ1/RFX family, I will describe the transcription regulation of motile cilium biogenesis in the embryonic node and MCC biogenesis in airway epithelium in the next section.

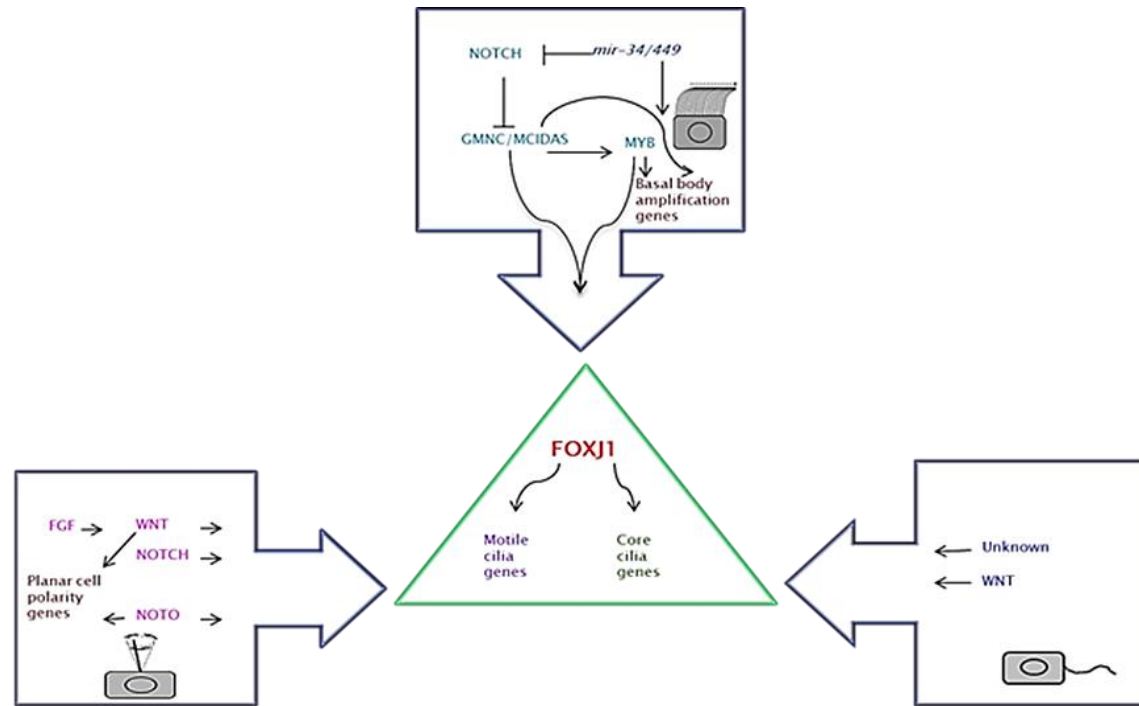


Figure 1-2. Diversity in motile cilia is brought by different transcriptional modulators and signalling pathways working through Foxj1.

There are different types of motile cilia. Different transcriptional regulators and signalling pathways give rise to this diversity. Multiciliated cells – the inhibition of Notch signalling is required for activation of mcc transcriptional pathway. The transcriptional cascade of GEMC1/MCIDAS activates the downstream targets such as MYB, FOXJ1 and RFX factors. MCIDAS/MYB also regulates genes required for basal body synthesis and docking. Monomotile cilia in the node- NOTCH and WNT (the latter acting downstream of FGF signalling) induce the formation of rotational monomotile cilia in organs of laterality. The NOTO transcriptional regulator activates FOXJ1 and an RFX factor in the ciliated cells of the mouse node. Pathways generating sperm flagella are largely unknown but acts through FOXJ1. (Adapted from (Choksi et al., 2014d).

1.2.2.2.1 Monomotile ciliated cells in embryonic node

In zebrafish, KV is the left-right organiser (Essner et al., 2005), in frog it is the gastrocoel roof plate (GRP) (Schweickert et al., 2007) and in chick and mouse, it is the node (Sulik et al., 1994, Nonaka et al., 1998b, Pownall and Isaacs, 2010). The dorsal forerunner cells (DRC) that express the *No tail* protein are the progenitors of KV. *No tail* expression is known to depend on Fibroblast growth factor (Fgf) signalling (Griffin et al., 1995). In zebrafish mutants of *fgf8*, the DRCs were deficient in number (Albertson and Yelick, 2005). In a different study, morpholino knockdown of *Fgf8* and other downstream effectors of Fgf signalling resulted in the loss of KV cilia and varied expression of laterality markers including *lefty* and *southpaw* (Hong and Dawid, 2009). Notch signalling has also been reported as being important in cilia length control in the KV. It has been shown that *Foxj1a* acts downstream of Notch signalling since *foxj1a* was downregulated in *DeltaD* (Notch ligand) mutants. *Foxj1* could also rescue the shortened KV cilia length in *DeltaD* mutants (Lopes et al., 2010). A role for Wnt/ β -catenin signalling in regulating *foxj1a* expression in KV ciliogenesis has also been reported, functioning through *Lef1* and *Tcf7* binding to *foxj1a* regulatory sequences (Caron et al., 2012). How all these different signalling pathways come together and interact with each other to regulate ciliogenesis in KV is an interesting area for further research.

Noto, a homeobox transcription factor, is expressed in the KV in bony fish, the GRP in amphibians and in the murine embryonic node (Von Dassow et al., 1993, Stein and Kessel, 1995, Knezevic et al., 1995, Ben Abdelkhalek et al., 2004, Alten et al., 2012). Loss of NOTO function in mice resulted in defects in length, number, ultra-structure and docking of cilia in embryonic node like in

the *Foxj1*-null mouse embryos (Alten et al., 2012, Stauber et al., 2017). *Noto* mutant mouse embryos displayed laterality defects. *Foxj1* is downregulated in the embryonic node of *Noto*^{-/-} mice as well as its molecular targets. The current notion is that *Noto* induces *Foxj1* which in turn activates other motile ciliary genes including *Rfx3*, *Dynlrb2* etc. Alten *et al* (2012) also attempted to rescue the phenotype of the *Noto* mutant by *Foxj1*. While *Foxj1* could restore the expression of ciliary genes and cilia axoneme formation and motility, the embryos continued to have laterality defects. This occurred due to the disrupted cilia polarity which is established by planar cellular polarity (PCP) pathway. This showed that *Noto* plays two independent roles in nodal ciliogenesis. First to activate *Foxj1* and consequently induce other motile ciliary genes for axoneme formation and secondly to establish correct cilia polarity by regulating the PCP pathway (Alten et al., 2012). Recently, Stauber *et al* carried out a systematic screen for downstream targets of *Foxj1* and *Noto* in mouse embryonic lung and node and identified 59 novel candidates as *Noto/Foxj1*-dependent factors in the embryonic node organiser that overlap in the airway epithelium (Stauber et al., 2017). Further experiments are required to establish the functional role of these candidates in motile ciliogenesis.

1.2.3.2.2 Multiciliated cells

Previous studies have shown that Notch signalling plays a key role in specifying the MCC fate during the differentiation (Morimoto et al., 2010). Notch/Delta signalling has a lateral inhibitory effect on ciliogenesis in airways and directs the cell differentiation towards the secretory cell. This was demonstrated from studies conditionally inactivating *Pofut1* and *Rbpjk* that inhibited Notch signalling in airway epithelium of mice (Morimoto et al., 2010). These mice

expressed a dramatic increase in number of MCCs and prevented formation of club (Clara) cells in airways. Likewise, when NOTCH1 intracellular domain was conditionally overexpressed in mouse airway epithelium, it resulted in an overwhelming specification of club cells and a reduced number of ciliated cells (Morimoto et al., 2010, Rock et al., 2011, Brooks and Wallingford, 2014a). However, the pathways behind the regulation of Notch signalling in ciliogenesis are not fully characterised.

A recent study on the evolutionarily conserved microRNA *miR-34/449*, that is found to be enriched in MCCs, has provided insights in to how this pathway may be regulated. This study showed that *miR-34/449* selectively accumulates in ciliated cells of human airways and *Xenopus* embryonic epidermis (Marcet et al., 2011). Further investigation in both models by inhibiting and overexpressing *miR-34/449* indicated it has a crucial conserved role in vertebrate multiciliogenesis by promoting centriole multiplication and by directly downregulating the Delta/Notch pathway (Song et al., 2014). This finding emphasises the significant role played by microRNAs in regulating essential aspects in developmental biology.

For MCC fate determination, two other major factors have been discovered recently; MCIDAS (Multicilin) and GEMC1 (Geminin Coiled-Coil Domain Containing). Both are related to Geminin (GMNN), a protein involved in cell-cycle progression and in the balance between cell proliferation and differentiation (Kroll, 2007). In fact, these three members of GMNN superfamily are involved in cell cycle progression and show high similarity in their coiled-coil domain. GMNN is an inhibitor of pre-replicative complex formation (Wu et al., 2014) and MCIDAS was found to bind with GEMININ to regulate DNA

replication and cell cycle progression (Pefani et al., 2011). Balestrini *et al* showed that GemC1 mediates initiation of chromosomal DNA replication by facilitating TopBP1- and Cdk2-dependent recruitment of Cdc45 onto replication origins in multicellular organisms (Balestrini et al., 2010).

MCIDAS was known as IDAS before it was identified by Stubbs *et al* as one of the main downstream targets induced by the inhibition of Delta/Notch pathway in MCC fate determination (Stubbs et al., 2012). Remarkably, *Mcidas* induced MCC fate when it was ectopically expressed in non-ciliated cells along with induction of mass centriole biogenesis and induction of cilia specific genes such as *Foxj1*, *Myb* etc. (Stubbs et al., 2012, Kyrousi et al., 2015). Moreover, a rare mucociliary clearance disorder called reduced generation of multiple motile cilia (RGMC) in humans was reported to cause by missense and recessive loss of function mutations in *MCIDAS*. RGMC results in formation of fewer cilia that are immotile; hence patients suffer from recurrent infections of the upper and lower airways (Boon et al., 2014). Mutations in *MCIDAS* were confirmed by family pedigree analysis and Sanger DNA sequencing of coding exons in 59 affected families (Boon et al., 2014). Ma *et al* (2014) characterised two of these mutations. They first showed that *MCIDAS* induces massive centriole assembly, a crucial step in multiciliogenesis, by binding to transcriptional factors such as E2F4, E2F5 and DP1 which then transcriptionally activate many genes essential for centriole biogenesis (Ma et al., 2014). One of those characterised mutations called G335D, cause failure to bind with E2F4 and DP1. The other mutant, R370H, can form complex with E2F4/5 and DP1, however, the complex is not functionally active to induce gene expression for centriole assembly (Ma et al., 2014, Balestra and Gönczy, 2014).

Besides MCIDAS, GEMC1 was recently found to be required for postmitotic commitment to MCC fate in *Xenopus* skin, zebrafish pronephros, and mouse brain (Kyrousi et al., 2015, Zhou et al., 2015). Like *Mcidas*, *Gemc1* was also found to be adequate to activate early commencement of differentiation of MCC progenitors in the mouse brain (Kyrousi et al., 2015). Both can induce ectopic differentiation of MCCs in mouse airway epithelia and *Xenopus* skin/kidney (Stubbs et al., 2012, Zhou et al., 2015, Kyrousi et al., 2015). In addition, GEMC1 can interact with E2F4/5, DP1 and MCIDAS to regulate specification of MCC precursors (Terré et al., 2016, Arbi et al., 2016). Despite these similarities between MCIDAS and GEMC1, GEMC1 appears to act upstream of MCIDAS since *Mcidas* is not induced in the absence of *Gemc1* and *Mcidas* was not able to activate *Gemc1* expression (Zhou et al., 2015, Arbi et al., 2016, Terré et al., 2016). Therefore, it makes GEMC1 the earliest transcriptional regulator in MCC formation downstream of Notch signalling. Recent unpublished findings from our group (Prof Sudipto Roy, IMCB) also provide insights into this pathway. A two-step model in the developmental pathway for MCC formation is proposed 1) GEMC1 regulates the specification of MCC precursors including MCIDAS and act downstream of Notch signalling 2) MCIDAS amplify the expression of cilia transcriptional regulators and drive basal body production for MCC formation. But, there are questions still unanswered. What are the molecular mechanisms that regulate Notch signalling in MCC biogenesis? How is the expression of *GEMC1* regulated?

In contrast, the third member of the family, GMNN, plays an inhibitory role in MCC formation while MCIDAS and GEMC1 are the activators. This trend is also conserved in their functional role in cell cycle progression since GEMC1

and MCIDAS play positive regulatory roles in DNA replication and GMNN is the negative regulator (Caillat et al., 2015, Ma et al., 2014, Vladar and Mitchell, 2016). How is this repression brought about? Data from biochemical experiments suggest that GMNN can form homo-heterodimers with MCIDAS and GEMC1, and thus repress their activity (Caillat et al., 2015, Vladar and Mitchell, 2016).

Other transcription factors that act downstream of GEMC1/MCIDAS include c-MYB, several members of RFX family and FOXJ1 (Stubbs et al., 2012, Kyrousi et al., 2015, Zhou et al., 2015). c-MYB is a transcription factor that upregulates S phase in many progenitor cells (Wang et al., 2015). A recent study identified the expression of *Myb* in airway epithelial cells destined to become multiciliated cells. They reported *Myb* is expressed transiently during multiciliogenesis. *Myb* is expressed in potential multiciliated cells as they exit cell cycle and during basal body biogenesis. Subsequently, *Myb* is switched off as the centrioles dock and multiciliated cells mature. When *Myb* was conditionally inactivated in airways, centriole amplification was impaired and *Foxj1* expression was not detected (Tan et al., 2013a). With primary cell culture studies, they also provided evidence that MYB act downstream of MCIDAS (Tan et al., 2013a, Brooks and Wallingford, 2014a). Consequently, MYB induces expression of *Foxj1* and centriole amplification. Recently, TAP73 was identified as another regulator of multiciliogenesis (Nemajerova et al., 2016a, Jackson and Attardi, 2016, Marshall et al., 2016). *Tp73* deficient mice show severe phenotypes associated with cilia defects e.g. hydrocephalus, female infertility and rhinitis/otitis media. They also showed that TP73 acts upstream to transcription factors involved in MCC biogenesis like *Foxj1*, *Rfx2/3*, *mir34bc*

and *Myb* by carrying out RNA sequencing on air liquid interface (ALI) cultured mouse tracheal epithelial cells extracted from wild type (WT) and *p73* deficient mice (Nemajerova et al., 2016a).

However, there is more to be learnt about the molecular interactions and regulation of these transcription factors and their downstream targets.

1.2.3 Basal body formation

The basal body or centriole where the cilia nucleate from, is cylindrically shaped and composed of 9 sets of triplet microtubules and a cartwheel enclosed in pericentriolar material (Li et al., 2012a, Geimer and Melkonian, 2004). In monociliated cells, formation of only one basal body from a centriole pair is required to generate a motile cilium (Carvalho-Santos et al., 2011, Yan et al., 2016). To exhibit multiciliogenesis, cells need to generate multiple basal bodies from which cilia axonemes are nucleated. Centriole replication and basal body formation prior to multiciliogenesis was first described by transmission electron microscopy (TEM) studies on MCCs in *Xenopus* epidermis, vertebrate airways and oviduct (Steinman, 1968, Sorokin, 1968, Kalnins and Porter, 1969, Dirksen, 1971). Two modes of basal body generation were reported in MCCs i.e. basal body generation from mass centriolar duplications (MCD) and acentriolar basal body formation through deuterosome pathway (DD) as shown in Figure 1.3. Conversely, the latter appeared to account for the formation of most basal bodies in multiciliated cells in the airways (Klos Dehring et al., 2013, Brooks and Wallingford, 2014a, Yan et al., 2016).

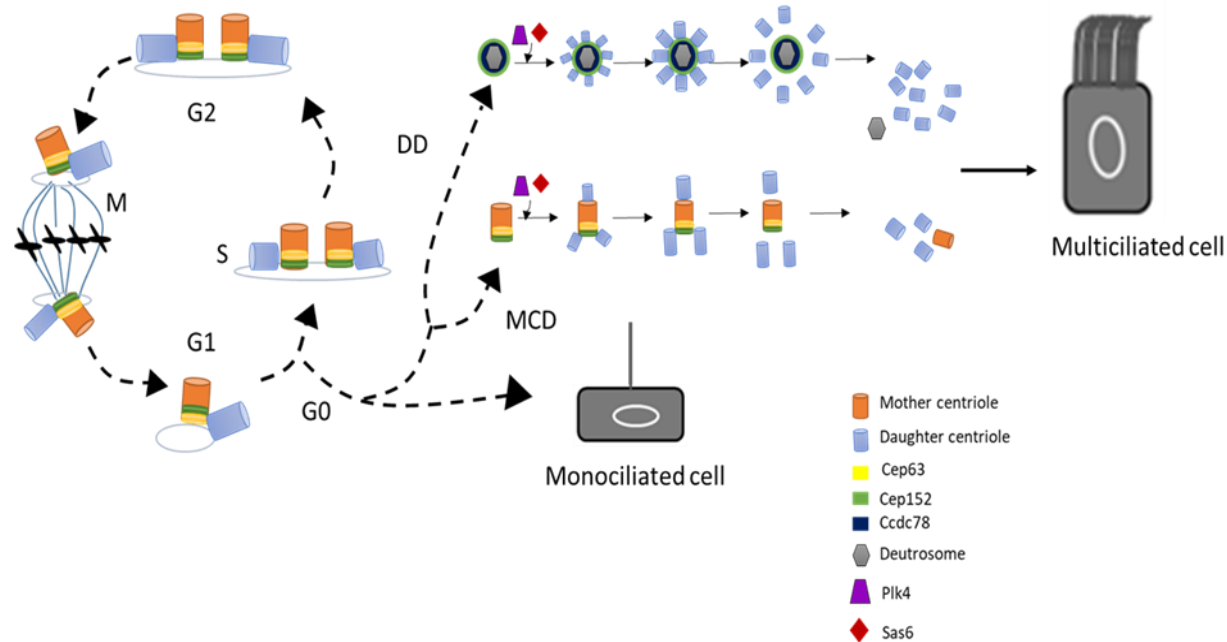


Figure 1-3. Basal body synthesis in ciliogenesis.

During the G1 phase of cell cycle, a cycling cell contains a pair of mother-daughter centrioles. Once it reaches the S-phase, each centriole will duplicate itself to give a daughter centriole so that the number of centrioles remain same after mitosis. During the G0 phase, the mother centriole can become basal body to support monocilium formation. In multiciliogenesis, 100s of basal bodies are synthesised by two distinct pathways. MCD (mother centriole pathway) pathway is mediated by CEP63–CEP152 complex and DD (deuterosome pathway) pathway is mediated by DEUP1–CEP152 in which CCDC78 recruit CEP152. The protein compositions and interactions of functional deuterosome are not fully characterised. Nascent centrioles or basal bodies detach from mother centriole (CD) and deuterosome (DD) and migrate to apical surface to form cilia (adapted from (Al Jord et al., 2014, Yan et al., 2016)).

In the centriolar mode of basal body generation in MCC, there is evidence from TEM studies for simultaneous development of multiple daughter centrioles from a single mother centriole whereas only one daughter centriole nucleates from mother centriole in other cycling cells (Carvalho-Santos et al., 2011). The latter would account for ciliogenesis in monociliated cells. Studies overexpressing and manipulating centriolar components required for centriolar replication, such as *Plk4* and *Sas6*, generated less than 10 centrioles in non-ciliated cells (Peel et al., 2007, Klos Dehring et al., 2013) indicating another mechanism other than mother centriole driven duplication, functions in these cells to produce >150 centrioles generated in MCCs (Klos Dehring et al., 2013) .

In acentriolar basal body generation, centrioles are derived from *de novo* biogenesis without mother centriole replication but involving a “nondescript electron-dense structure” called the deuterosome (Klos Dehring et al., 2013, Sorokin, 1968). This was described by TEM studies in various vertebrate models. This deuterosome is formed from fibrogranular material deposited in the apical cytoplasm and lies in close vicinity to Golgi bodies. The growth of procentrioles are organised around these spherical deuterosome bodies. When these newly centrioles/ basal bodies mature, they line up in rows underneath the apical plasma membrane and from each basal body a cilium arises from its apex (Hoyer-Fender, 2010, Klos Dehring et al., 2013).

The molecular biology of the deuterosome still remains somewhat obscure even 40 years after its discovery by TEM. Recent attempts to characterise their components identified a deuterosome protein, CCDC78, as an essential factor for centriole amplification. They also reported key centriolar

proteins such as Sas6, Plk4 and Cep152 localise to deuterosomes. In addition, localisation of Cep152 did not occur in *ccdc78 Xenopus* morphants and consequently centriole biogenesis was impaired (Klos Dehring et al., 2013). So, this indicates that in deuterostome-mediated centriole biogenesis, CCDC78-mediated recruitment of CEP152 is essential. CCDC78 is highly conserved in vertebrates as they conducted the studies in MCCs from various vertebrate models. In MCIDAS mutant cells, CCDC78 expression was not detected which further supports how MCIDAS regulates the deuterosomal pathway (DD) and hence centriole biogenesis in MCC (Klos Dehring et al., 2013, Brooks and Wallingford, 2014a, Boon et al., 2014, Nigg and Stearns, 2011).

Another study by Zhao *et al* (2013) pointed out another major component called *Deup1* as a mediator for acentriolar basal body biogenesis (Zhao et al., 2013a). They used 3D super resolution microscopy to demonstrate that MCCs use both mother centriole driven replication (MCD) and deuterosomal mode (DD) for basal body generation. Using 3D SIM visualisation, it was also reported these deuterosomes are dynamic structures that can change their morphology from granular to ring shaped according to the stage of the basal body amplification. They described DEUP1 as a vital structural component that facilitates deuterosome assembly mediated by CEP152 during *de novo* basal body amplification. Interestingly, when *Deup1* was overexpressed in non-multiciliated cells, it induced the augmentation of ring-like structures along with ectopic centriole amplification. Loss of *Deup1* in MCCs from mTEC resulted in a decrease in the number of deuterostomes and consequently *de novo* basal body amplification was impaired (Brooks and Wallingford, 2014a, Zhao et al., 2013a). Furthermore, DEUP1 was also found to accumulate on the daughter

centriole during deuterostome formation in MCCs of the mouse brain (Al Jord et al., 2014). This shows DEUP1 is a central player in deuterosomal amplification of basal bodies.

Another striking observation was that, CEP63, a paralogue of DEUP1, was identified as a key mediator in mother centriole dependent amplification of basal bodies. Both *Deup1* and *Cep63* interact with CEP152 to initiate centriole amplification in MCD and DD pathways respectively (Zhao et al., 2013a). So, it will be interesting to know how these interactions are regulated to ensure the balance between MCD and DD pathways to induce centriole biogenesis in MCCs.

CCNO, a cyclin-like protein, also plays a role in the acentriolar basal body generation mediated by deuterostome. The molecular pathway in which *CCNO* functions is not clear, however patients with mutations in *CCNO* have MCCs with reduced number of cilia (Wallmeier et al., 2014). Loss of *Ccno* in mouse airway epithelial cells showed larger deuterostomes with fewer basal bodies indicating a role for *CCNO* in the early onset of basal body amplification in MCCs (Funk et al., 2015, Meunier and Azimzadeh, 2016). Furthermore, it has been shown that a MCIDAS/E2F complex induces DD pathway by activating expression of *Deup1* but not *Cep63* in MCCs (Balestra and Gönczy, 2014, Ma et al., 2014). It will be an interesting area of research to study how all these factors mentioned earlier interconnect in centriole biogenesis.

1.2.4 Basal body docking and cilia formation

Once basal bodies are formed in the cytoplasm, they fuse with vesicles from one end of the cell and migrate apically (Ioannou et al., 2013, Al Jord et al.,

2014, Brooks and Wallingford, 2014a). Recent studies identified a basal body component called CHIBBY that plays an active role in vesicle formation. It is proposed that CHIBBY is recruited by basal body protein, CEP164, to the distal ends of basal bodies. Subsequently, recruitment and fusion of RAB8-positive vesicles is induced by CHIBBY, which in turn forms a ciliary vesicle at the distal appendages of basal bodies (Burke et al., 2014). Vesicles fuse with plasma membrane and thus dock the basal bodies to the apical surface of the plasma membrane. After docking, the ciliary axoneme, enclosed by the plasma membrane elongates from the basal body (Brooks and Wallingford, 2014a, Burke et al., 2014).

A few decades ago, Boisvieux-Ulrich *et al* studied basal body migration in ciliogenesis in quail oviduct using cytochalasin D (CD), an actin depolarising agent, and they reported that in the presence of CD, polarized basal body migration did not occur. So, this indicated that association of basal bodies with actin components is necessary for basal body migration (Boisvieux-Ulrich et al., 1990, Vladar and Axelrod, 2008). Only recently has light been shed on how this dynamic interaction between a meshwork of actin assemblies and basal bodies is regulated. Studies on *Xenopus* larvae by Park *et al* revealed the role of PCP proteins, including Fuzzy and Inturned, in regulating the assembly of actin filaments necessary for ciliogenesis (Park et al., 2006, Vladar and Axelrod, 2008). Studies conducted by Park *et al* concluded another PCP protein called Dishvelled is important for apical actin assembly by activating RhoA (Park et al., 2008, Vladar and Axelrod, 2008). Further studies indicated RHOA is essential for the formation of apical actin meshwork. RHOA inhibitors can block the actin web formation in ciliated cells. In addition to planar cell polarity

proteins FUZZY and INTURNED, other PCP proteins also appear to play an important part in ciliogenesis. RhoA functions downstream of PCP proteins and Foxj1 (Pan et al., 2007a) but the pathway by which RHOA mediates ACTIN assembly still remains unclear and further research is needed to understand this.

Earlier studies had reported that FOXJ1 plays a vital role in basal body docking and axoneme formation. In *Foxj1* null cells, actin web formation did not occur; it was also shown that FOXJ1 activates RHOA as the over expression of *Foxj1* leads to increased activity of *RhoA*. FOXJ1 also maintains cytoskeletal stability by maintaining Ezrin (EZR) and other cytoskeletal elements levels by regulating *Calpastatin* expression. EZR binds to basal bodies and mediates basal body docking to the apical surface (Gomperts et al., 2004, Pan et al., 2007a).

Subsequently, a bud emerges from each basal body after docking to the apical surface. From their tips, each bud undergoes elongation to form the axoneme, but structurally distinct basal part will become the transition zone (Williams et al., 2011). The inner two microtubules of the basal body microtubule triplets give rise to axonemal doublets and as the bud extends to form the axoneme, it also drives the extension of plasma membrane that latter becomes the ciliary membrane enclosing axoneme. Proteins that are important in axoneme formation can be found in the TZ. There are many ciliopathies associated with deficiency of these proteins (Garcia-Gonzalo and Reiter, 2012). Proteomic analysis of human airway cilia grown in ALI culture identified more than 200 axonemal proteins (Ostrowski et al., 2002b).

Furthermore, to elongate the axoneme, the ciliary membrane expands in parallel by vesicle fusion at the ciliary base and diffusion of proteins and lipids from the adjoining plasma membrane. Since, vesicle transport plays a vital role in ciliogenesis, proteins involved in vesicle trafficking and budding are also involved in ciliogenesis e.g. CLATHRIN and AP-1 for budding; TRAPP, RAB8 for targeting, Exocyst for tethering and SNAREs for fusion (Garcia-Gonzalo and Reiter, 2012)

1.2.5 Intraflagellar transport (IFT)

As the axoneme elongates, there is a constant turnover at the distal tip. A specialised transport process called intraflagellar transport (IFT), based on dynein and kinesin motors is used to build axonemes from basal bodies. It was Kozminski *et al.* who first initiated the series of experiments that lead to the discovery of this sophisticated process by observing bidirectional particulate movement in paralyzed flagella of *Chlamydomonas reinhardtii* (Kozminski et al., 1995). Subsequently, the biochemical nature of IFT was resolved by Piperno *et al* and Cole *et al* by purifying IFT components from the flagella of *Chlamydomonas* (Piperno and Mead, 1997). They identified two components termed complex A and complex B. Further analyses lead to the identification of the functional importance of these complexes. Complex B moves from base of the cilium to the tip, otherwise known as anterograde motion. In contrast, complex A moves in retrograde motion from the tip to the base of cilium. Furthermore, loss of complex B resulted in arrested cilia growth whereas mutation in complex A did not affect the cilium growth. Motor proteins such as kinesin-2 and dynein drive the transport in anterograde and retrograde directions, respectively, resulting in the bidirectional traffic system of IFT

(Piperno and Mead, 1997, Piperno et al., 1998, Cole et al., 1998, Cole, 2003). These processes are highly conserved in ciliogenesis in vertebrates. Ciliary precursors such as TUBULIN and other axonemal proteins are transported from the cytoplasm into the axoneme by the KINESIN-2 molecular motor. The turnover products are transported back from the axoneme tip by DYNEIN 2 (Satir and Christensen, 2008, Garcia-Gonzalo and Reiter, 2012). This complex IFT process presents numerous regulatory checkpoints for axoneme operation (Satir and Christensen, 2007, Satir and Christensen, 2008, Garcia-Gonzalo and Reiter, 2012).

1.2.6 Mechanisms of cilia motility

In MCCs, ciliary motility is achieved by interactions between the nine outer axonemal doublets, situated in opposite sides, in which one set of doublets (1-4) make the effective stroke and other set of doublets (5-9) make the recovery stroke. This is fuelled by ATP along with molecular motors, the dyneins. The dynein arms mediate the interactions between the axonemal doublets and the central pair of microtubules through radial spokes to generate the force required for ciliary beating. Axonemal dyneins are organised in two forms; the outer dynein arms (ODAs) composed of two heavy-chain dyneins made up of light and intermediate chains, and the more centrally located inner dynein arms (IDAs) composed of approximately seven monomeric and heterodimeric dynein isoforms. Ciliary beat frequency is modulated by ODAs through post translational modifications and the wave form of the beat is controlled in IDAs (Satir and Christensen, 2008, Wloga and Gaertig, 2010). Nonetheless, the pathway to switch from slow to fast modes in CBF and vice-versa is not clearly understood. Several studies have provided evidence that variation in CBF is

dependent on several post-translational modifications that can occur through multiple signalling cascades including Ca²⁺, cAMP, progesterone nitric oxide etc. (Salathe, 2007, Brooks and Wallingford, 2014a, Tilley et al., 2014, Satir and Christensen, 2008).

Unlike cilia in the MCCs which beat in a planar whip-like pattern, the nodal cilia have a rotational beating pattern in clockwise direction. In 1996, Bellamo *et al* reported that nodal cilia lack the CP and hence has a 9+0 arrangement in contrast to the typical 9+2 arrangement of motile cilia (Bellomo et al., 1996). This lead to the assumption that the absence of the CP could be the reason for the rotational manner or cilia beating pattern. Interestingly, in the zebrafish KV, both 9 + 2 and 9 + 0 cilia display rotational beating (Kramer-Zucker et al., 2005, Ferrante et al., 2008, Wilson et al., 2009, Kreiling et al., 2007). Recently, in contrast to the earlier belief, it was reported that cilia in mouse node also contain CP (Caspary et al., 2007). So, it seems that the lack of CP does not contribute to the rotational beating pattern. On the contrary, in humans and mice it was shown that gene mutations that disrupt CP assembly do not affect the cilia motility in the node and do not show laterality defects. But the motility of other cilia such as in the airways was severely affected (Lechtreck et al., 2008, Olbrich et al., 2012). Hence, it can be reasoned that CP is not required for motility of nodal cilia. However, the question remains: How do nodal cilia achieve the rotary beating pattern? In 2015, Shinohara *et al* proposed through computer simulations of structural data, that regular circular arrangements of microtubule doublets are necessary for a stable rotational motion of nodal cilia. They also reported that the lack of radial spokes plays a key role in creating the rotation beating pattern. To support this, they showed

that the mouse mutant of *Rsph4a* gene, that encodes the head of radial spoke, generated airway cilia with a clockwise rotational beating pattern (Shinohara et al., 2015). However, it is still not known how radial spokes regulate the switch between the beating patterns. Hamada also proposed that the clockwise rotation possibly arise from the orientation of the A and B tubules in the microtubule doublet and sliding direction of ODAs (Shinohara and Hamada, 2017). Further studies are required to validate this proposition.

1.2.7 Role of cilia in airways

The lung has evolved a series of defence mechanisms to protect the airways which are continually exposed to environmental pollutants and respiratory pathogens (Rawlins et al., 2007). The mucociliary epithelium in the respiratory tract is a major innate defence mechanism that acts as a chemical and physical barrier to all insults. The key components of this defence include physical barrier provided by cellular tight junctions, various receptors to sense the environment that send out signals to induce release of the innate defence molecules and antibodies against foreign particles and pathogens, and most importantly the mucociliary escalator that depend on mucins, periciliary fluid and concerted action of ciliated cells (Knowles and Boucher, 2002, Varelle et al., 2011). The mucociliary escalator cleans the airways by maintaining the flow of mucus gel that entrap pathogens and particulates from lower respiratory tract, into the pharynx, where is it swallowed. When the cilia are dysfunctional, it results in disorders like cystic fibrosis, asthma, PCD etc. (Braithwaite and Priel, 2008, Horani et al., 2014, Tilley et al., 2014).

Cilia in healthy human airways beat at 12 to 15 Hz with a metachronal motion (Braiman and Priel, 2008, Brooks and Wallingford, 2014a). As shown in Figure 1.4, cilia tips penetrate the mucus layer on the powerful and rapid forward stroke and on the slow reverse stroke, a bend in the axoneme allow the tip to go underneath the mucus layer, and this highly coordinated form of ciliary beat form allow the propulsion of mucus in forward direction and maintenance of a directional mucociliary escalator (Brooks and Wallingford, 2014a, Tilley et al., 2014).

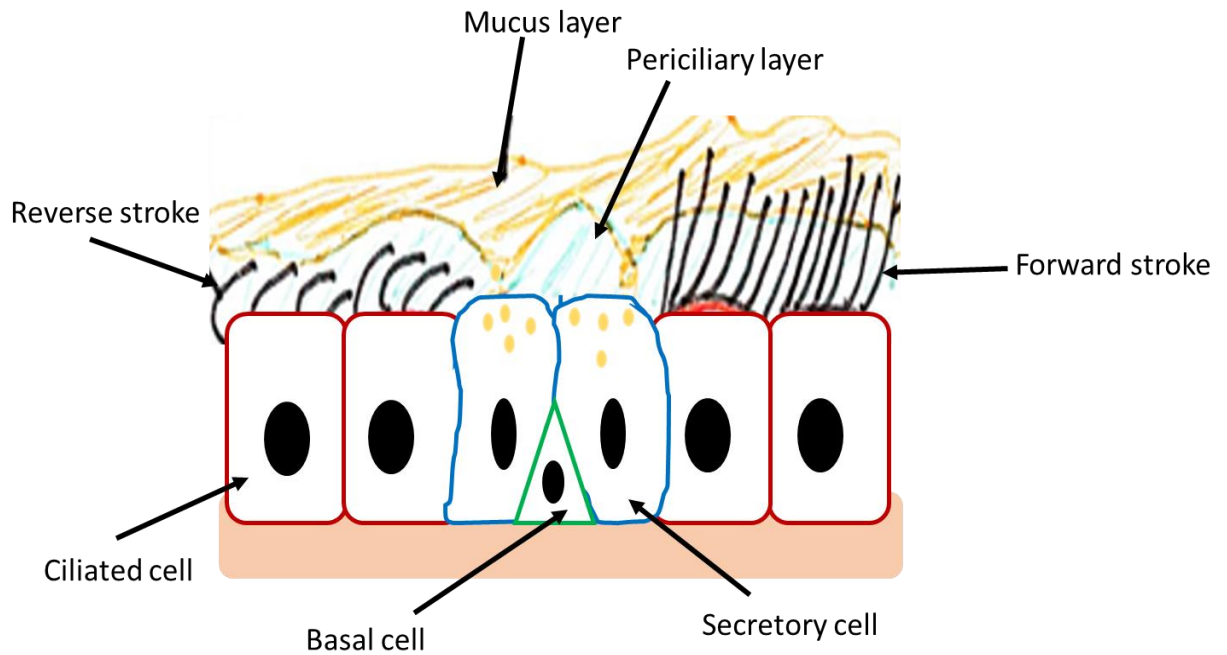


Figure 1-4. Functional role of cilia in airways.

The first line of innate defence in airways, mucociliary clearance, is achieved by concerted action of secretory cells that secrete mucins into mucus layer, periciliary layer that maintains the hydration between mucus layer and epithelial cells and ciliated cells that propel the mucus entrapping pathogens and other particulates out of airways through ciliary beating. Cilia beat constantly in a metachronal manner in which cilia contact mucus with a powerful and rapid forward stroke that enable ciliary tips to penetrate the mucus layer and then with a slow reverse stroke, mucus is propelled out of the airways in forward direction into the pharynx to be swallowed (adapted from (Tilley et al., 2015)).

Airway cilia have acquired several adaptations to aid their function in propelling mucus with its viscoelastic properties, including the ciliary length, which appears to be at 5-7 μm in the airways (Jing et al., 2017). This enables the cilia to engage more effectively with the mucus overlying the epithelium. Longer cilia would show considerable back bending, and hence would produce reduced kinetic energy that would not be sufficient to propel mucus in the normal direction of flow. Furthermore, the dense protein content at the distal tip of the axoneme makes it the strongest part of the cilium and therefore gives it adequate potential force to make contact and drive the mucus flow (Brooks and Wallingford, 2014a, Sedaghat et al., 2016). Lastly, ciliary motion exhibits metachronism phenomenon where cilia beat together with a uniform phase difference with adjoining neighbours displaying a moving wave pattern. This metachrony is particularly important when cilia are constantly in contact and propelling mucus that has elastic properties because it would not allow the mucus to discharge the imparted energy by back expansion that would impair the process (KNIGHT-JONES, 1954, Brooks and Wallingford, 2014a, Sedaghat et al., 2016). However, the mechanism of coordination that brings out this phenomenon is not clearly understood.

Furthermore, airway cilia are equipped with receptors that enable them to sense the environment, including recently identified sensory bitter taste receptors (T2R) found on human airway cilia (Shah et al., 2009). Other receptors include CFTR and ENaC that regulate the osmolality of periciliary fluid by controlling conductance of certain ions (Holtzman et al., 2014) . Disruption in any of these receptors results in increased fluid absorption that leads to thickening of mucus and consequently leads to respiratory disorders

like Cystic fibrosis (Brooks and Wallingford, 2014a, Satir and Christensen, 2008, Tilley et al., 2014).

1.2.8 Role of cilia in establishing left-right symmetry

One of the earliest events in a vertebrate's life, where motile cilia play an important function, is in establishing left-right asymmetry. Although from outside, the body appears symmetrical, the positioning of the internal organs and its vasculature exhibit left-right (L-R) asymmetry. For example, the stomach, spleen and the heart apex lie to the left and the liver to the right of the abdominal cavity of the human body. This asymmetry is strongly conserved throughout vertebrate lineage (Norris, 2012).

As shown in Figure 1.5, the normal arrangement of the sidedness is known as *situs solitus*. However, defects in the establishment of L-R asymmetry during development can result in deviant arrangements. There can be a complete mirror-reversal of organ L-R asymmetry and this arrangement is known as *situs inversus totalis*. However, this condition does not result in serious clinical complications. On the other hand, there can be *situs ambiguus* otherwise known as heterotaxy, where organ positioning can be randomised. This arrangement can result in a wide spectrum of congenital malformations that affects organ function. One such example is Congenital Heart Disease (CHD), a clinical condition with high morbidity and mortality. The heart is the most left-right asymmetrical organ in a vertebrate body. The asymmetry of the heart is important is for its function i.e. to establish systemic and pulmonary circulation for efficient oxygenation of blood. So, it is not surprising that CHD is

associated with heterotaxy (Ramsdell, 2005, Kathiriya and Srivastava, 2000, Blum and Ott, 2018).

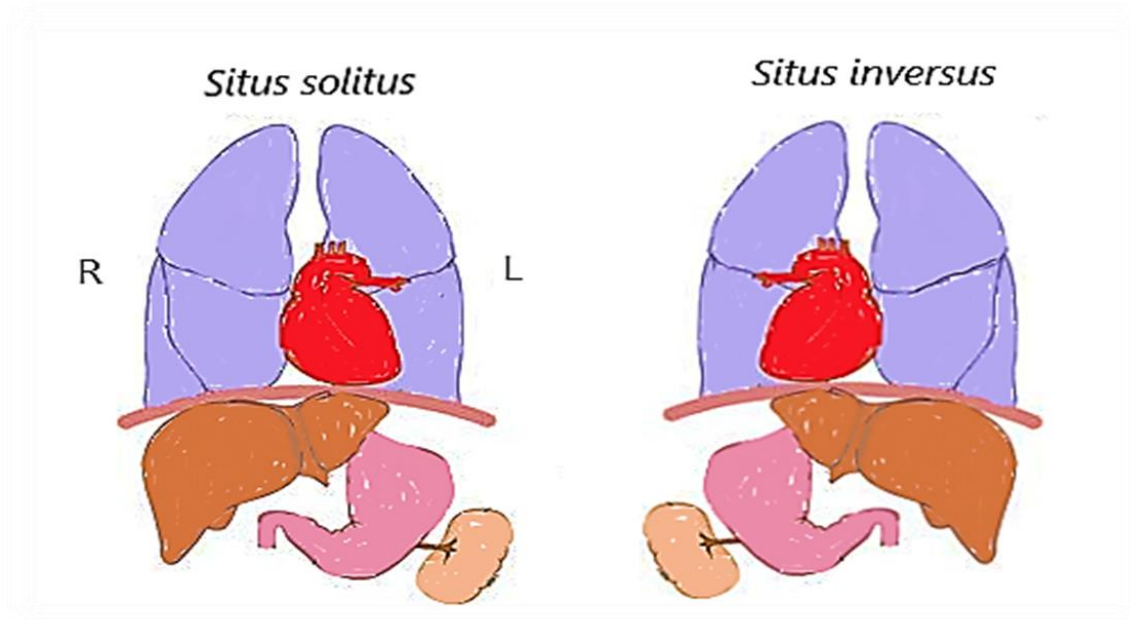


Figure 1-5. Left–right (L–R) asymmetry of human body.

The normal positioning of organs in a human body is known as '*situs solitus*', the heart, stomach and spleen are oriented to the left side, whereas the liver is present on the right side. In patients with '*situs inversus*', positioning of the visceral organs occurs in a mirror-image along the L–R axis. R indicates the right side, while L indicates the left side (adapted from (Babu and Roy, 2013, Patel and Honoré, 2010)).

The basis of how this L-R asymmetry is established remained a mystery until the discovery of the structure known as the node (Nonaka et al., 1998b, Sulik et al., 1994, Bellomo et al., 1996). This pit like structure is located at the anterior portion of the primitive streak. The process of establishing L-R asymmetry can be divided into 3 main steps: 1; Symmetry breaking from the node, 2; transfer of signals from node to lateral plate mesoderm; 3, asymmetric organogenesis (Hamada, 2016). There are around 200 monomotile cilia that protrude from the ventral side of the node that drive a leftward fluid flow to break the bilateral symmetry of gene expression to determine the left and right in the body (Nonaka et al., 1998b, Norris and Grimes, 2012, Sulik et al., 1994).

In contrast to the cilia in airway epithelium, the ciliary beat pattern is different in the node and displays a rotational motion (Nonaka et al., 1998a, Norris and Grimes, 2012, Hamada, 2016). The mechanisms underlying the rotational motion of nodal cilia is not as explained in section 1.2.6. So how does the rotary beating of cilia in the node generate nodal flow that results in breaking of symmetry?

Evidence from high speed video microscopy showed a posterior tilt in rotational axes in the nodal cilia. As shown in Figure 1.6, further studies showed that the nodal flow is generated by a combination of these two characteristics of node cilia: their clockwise beating and posterior tilt. The role of the PCP signalling pathway has been reported to be involved in establishing this posterior tilt (Nonaka et al., 2005, Klein and Mlodzik, 2005, Hamada, 2016). The molecular components of this pathway still need further clarification.

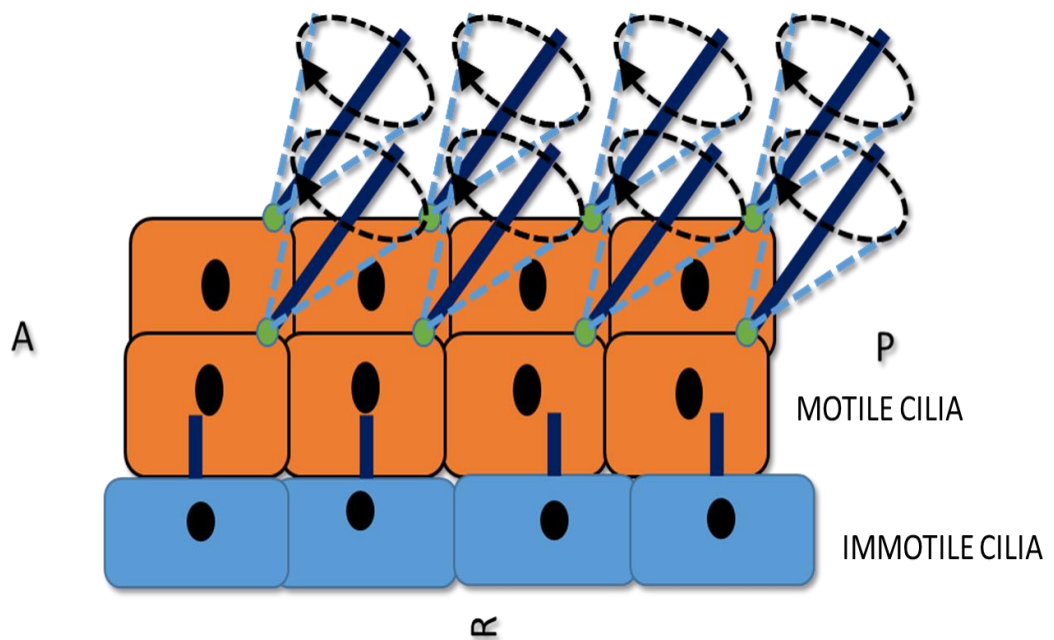


Figure 1-6. Cilia in the left-right organiser.

There are two types of cilia in the embryonic node- motile cilia and immotile cilia. Motile cilia is found in the central region of node and generate the nodal flow. They are posteriorly tilted and beat in rotation manner in the clockwise direction. The immotile cilia present in the periphery sense this flow and initiate the transcriptional cascade to establish left-right symmetry of the organism. A indicates anterior while P indicates posterior. R indicates the right side.

Furthermore the current consensus is that immotile cilia present on the crown cells at the periphery of the node then sense the nodal flow generated by motile cilia through Ca²⁺ channels composed of PKD1 and PKD2 (McGrath et al., 2003, Tabin and Vogan, 2003, Yoshiba et al., 2012, Pennekamp et al., 2002, Kamura et al., 2011). However, it is still not clear what exactly the immotile cilia sense during the symmetry-breaking event. On the other hand, in medaka, the node is devoid of primary cilia and only possess motile cilia which implies motile cilia should be able to generate, as well as sense, the flow in their system (Kamura et al., 2011).

The immediate effector of the nodal flow signal is *Cerl2*. Although initially, *Cerl2* expression is symmetric, it becomes restricted to the right side as the velocity of nodal flow increases and will be downregulated in the left. Since *Cerl2* is a *Nodal* antagonist, this asymmetric expression of *Cerl2* renders *nodal* expression to the left side of the crown cells (Marques et al., 2004, Schweickert et al., 2010, Shinohara et al., 2012). This asymmetry generated by *Cerl2* on the *Nodal* activity ($R < L$) at the node strongly correlates with the asymmetric pattern of *Nodal* expression in lateral plate mesoderm and further activates other factors required for asymmetric organogenesis (Kawasumi et al., 2011, Shinohara et al., 2012, Hamada, 2016).

In last few decades, considerable progress has been made in this area. However, there are many questions that need to be resolved. How is the anterior-posterior information deciphered into the posterior tilt of node cilia? How is the rotational motion and the direction of rotation in the nodal cilia

determined? What is the action of nodal flow and how is it sensed? What is the role of Ca²⁺ signalling and how does it induce degradation of Cer12 mRNA? Despite all the ambiguity, one thing that is clear is that motile cilia are required for establishing L-R asymmetry. Hence, it is not surprising that in patients with Primary Ciliary dyskinesia (PCD) (see session 1.3.1), 50% exhibit *situs inversus totalis* and heterotaxy occurs in at least 6% of individuals with PCD (Leigh, 2012).

1.3 Disease manifestation by dysfunction of motile cilia

1.3.1 PCD

Mutations in genes associated with ciliogenesis and cilia motility will result in cilia dysfunction and will give rise to ciliopathies. PCD is a heterogeneous autosomal recessive genetic disorder and occurs in 1 in 16000 individuals. PCD was first known as Kartagener syndrome, and patients display the triad of *situs inversus*, bronchiectasis, and chronic sinusitis (Cowan et al., 2001, Knowles et al., 2013a). Subsequently Kartagener syndrome was noted to be associated with male infertility. Later, the syndrome was renamed as immotile cilia syndrome and then PCD, after observing dynein arm defects in both airway epithelial cells and spermatozoa. The usual clinical symptoms of PCD patients are chronic sinusitis, chronic otitis media, recurrent infections in lower respiratory tract, bronchiectasis, male infertility and *situs* abnormalities (Knowles et al., 2013a, Rossman et al., 1980, Leigh, 2012, Tan et al., 2007).

In PCD patients, many structural defects in cilia are observed by electron microscopy, including short or absent ODA. Reduced or absent cilia beat frequency is also found in PCD, most commonly in patients with dynein arm

defects. Consequently, defects in mucociliary clearance are almost always occur in patients with PCD. Only a fraction of mutations leads to structural abnormalities in cilia and other mutations result in no ultrastructural defects in cilia, yet the cilia are immotile (Knowles et al., 2013a, Tilley et al., 2014).

A major confounding factor in the treatment of PCD is the difficulty of an early diagnosis. Many clinical manifestations of PCD overlap with other disorders such as cystic fibrosis, asthma etc. Therefore, in many cases that present with clinical symptoms, diagnosis can be made with examining the ultrastructure of cilia by electron microscopy. However, since many mutations do not present with ultrastructural defects in cilia, genetic testing is used as the gold standard diagnostic tool for testing known mutations of PCD. The currently known genes only account for 70% of PCD cases. Hence, to make genetic testing a comprehensive diagnostic tool, more genes must be uncovered that will account for the remaining PCD mutations. In order to do so, we need a better understanding of the molecular components and signalling pathways that is required for motile ciliogenesis and its function (Knowles et al., 2013a, Roy, 2009, Tilley et al., 2015).

1.4 Previous attempts to define the cilium

One of the biggest challenges in this field is identifying and characterising all molecular components of the motile cilium and filling the gaps left in the current knowledge on the formation and function of this organelle. To address this problem, multiple research groups have undertaken a series of high throughput analysis that identified numerous putative ciliary genes and proteins that may be important for motile ciliogenesis and ciliary function.

These large-scale screens can be classified into proteomic based and genomic based. In the proteomic approaches, ciliary proteins are identified through isolation of ciliary structures i.e. axoneme, centrosome or centrioles followed by protein separation by techniques like gel electrophoresis, and liquid chromatography-mass spectrometry (LC-MS) to identify the peptides (Pazour et al., 2005, Smith et al., 2005, Ostrowski et al., 2002a, Broadhead et al., 2006). These studies have yielded hundreds of putative proteins.

In addition, various genomic and transcriptomic based approaches were undertaken aimed at characterising the genetic makeup of the motile cilia, including their regulatory components. A common feature of the genomic approaches has been that they have produced thousands of putative ciliary genes and many of these require further functional characterisation to establish roles in motile ciliogenesis (Rosenbaum et al., 1969, Li et al., 2004, Stolc et al., 2005, Ross et al., 2007, Hoh et al., 2012, Choksi et al., 2014c, Nemajerova et al., 2016b, Stauber et al., 2017) .

This aspect is further explored on chapter 4. Functional characterisation of these putative genes in motile ciliogenesis is the basis of my thesis. For this purpose, mouse airway epithelial cells cultured at ALI were used as an *in vitro* model and the zebrafish was used as the *in vivo* model. So, what makes these models ideal for studying motile ciliogenesis?

1.6 *In vitro* culture of mouse tracheal and nasal epithelial cells at Air Liquid Interface as a model to study multiciliogenesis

The study of ciliogenesis *in vivo* is difficult and there are not many cell lines available that can form motile cilia. In 2002, You *et al* developed an ingenious protocol that can culture and differentiate primary airway epithelial cells *in*

vitro (You et al., 2002). Hence, this model offers a good system to study motile cilium biogenesis. Now, this model is very well established and is used extensively by many research groups to study various aspects of airway epithelium e.g. role of airway epithelial cells in chronic lung diseases and infection, molecular and genetic components involved in the differentiation of airway epithelial cells like ciliated cells etc. (Vladar and Brody, 2013, Tan et al., 2013b, Nichols et al., 2014, Nemajerova et al., 2016a, Eenjes et al., 2018a).

In brief, airway epithelial cells are freshly isolated from the trachea or nasal septum. These cells consist of multiple cell types. During *in vitro* culture, the cells are first grown in submerged conditions on inserts that allows the basal cell population (the epithelial progenitor population) to expand. Once the cells become confluent, cells are transferred into the air liquid interface (ALI) where the cells are exposed to air and media is supplied through the basal chamber. These conditions mimic the *in vivo* conditions in the airways and thus prompt the differentiation into mature airway epithelial cells that consist of multiciliated cells, secretory cells and basal cells (You et al., 2002, Vladar and Brody, 2013).

Studying transcriptomic and proteomic data derived from different time points during the differentiation of these cells, will allow the identification of genes and specific pathways involved in formation of MCCs. In addition, it facilitates the comparison and analysis of specific genetic and molecular pathways in the mutant or other genetically manipulated mouse strains by

extracting and culturing the airway epithelial cells from these animals (Vladar and Brody, 2013, Hoh et al., 2013, Nemajerova et al., 2016a).

Remarkably, motile ciliogenesis in these cultures can be modified by drug treatment to benefit our research needs (Pan et al., 2007b, Vladar et al., 2012, Vladar and Brody, 2013, Burke et al., 2014). Cell sorting can be used to extract individual cell populations that would allow further comparison among the MCCs and other cell types contained in airway epithelial cells cultured at ALI. Moreover, gene expression in airway epithelial cells grown at ALI can be modulated by gene transfer to study the protein of interest (Vladar and Stearns, 2007, Horani et al., 2013b, Vladar and Brody, 2013, Marshall et al., 2016).

1.5 Zebrafish as a model for characterising novel cilia markers and generating Primary Ciliary Dyskinesia phenotype

In the last few decades, the zebrafish, a tropical fish originally from river Ganges, has become a popular model for biomedical research due to its embryonic transparency, rapid development, high nucleotide and amino acid identity with humans, and its adaptability for genetic analyses (Song et al., 2016a). It has been reported that 70% of human genes have orthologues in zebrafish, and over 82% of genes implicated in human disease described in the Online Mendelian Inheritance in Man (OMIM) database have at least one zebrafish orthologue (Howe et al., 2013a, Song et al., 2016a). Hence, these characteristics make zebrafish a great tool for exploring and demonstrating the genetic and molecular basis of human development and disease.

For cilia research, zebrafish has many advantages and can be a tractable model for studying human ciliopathies. Zebrafish possess motile cilia

in diverse organs that can be easily observed in live transgenic embryos (Malicki et al., 2011). As outlined in the introduction above and is shown in Figure 2.7, during early stages of development, they have rotary beating monomotile cilia in KV, the equivalent of the embryonic node (Essner et al., 2005). As the embryos develop, more tissues that possess diverse motile cilia emerge. We can observe clustered motile cilia bundles from MCCs in the anterior and middle segment of pronephric ducts (embryonic kidney tubules) while monomotile cilia are seen in the posterior part of the pronephric ducts (Liu et al., 2007). There are motile cilia also present in the otic vesicle poles (Colantonio et al., 2009) (Stooke-Vaughan et al., 2012, Yu et al., 2011). The axoneme of the most motile cilia have the 9+2 architecture, however, the zebrafish spinal cord contains both 9+0 and 9+2 motile cilia (Kramer-Zucker et al., 2005, Sarmah et al., 2007).

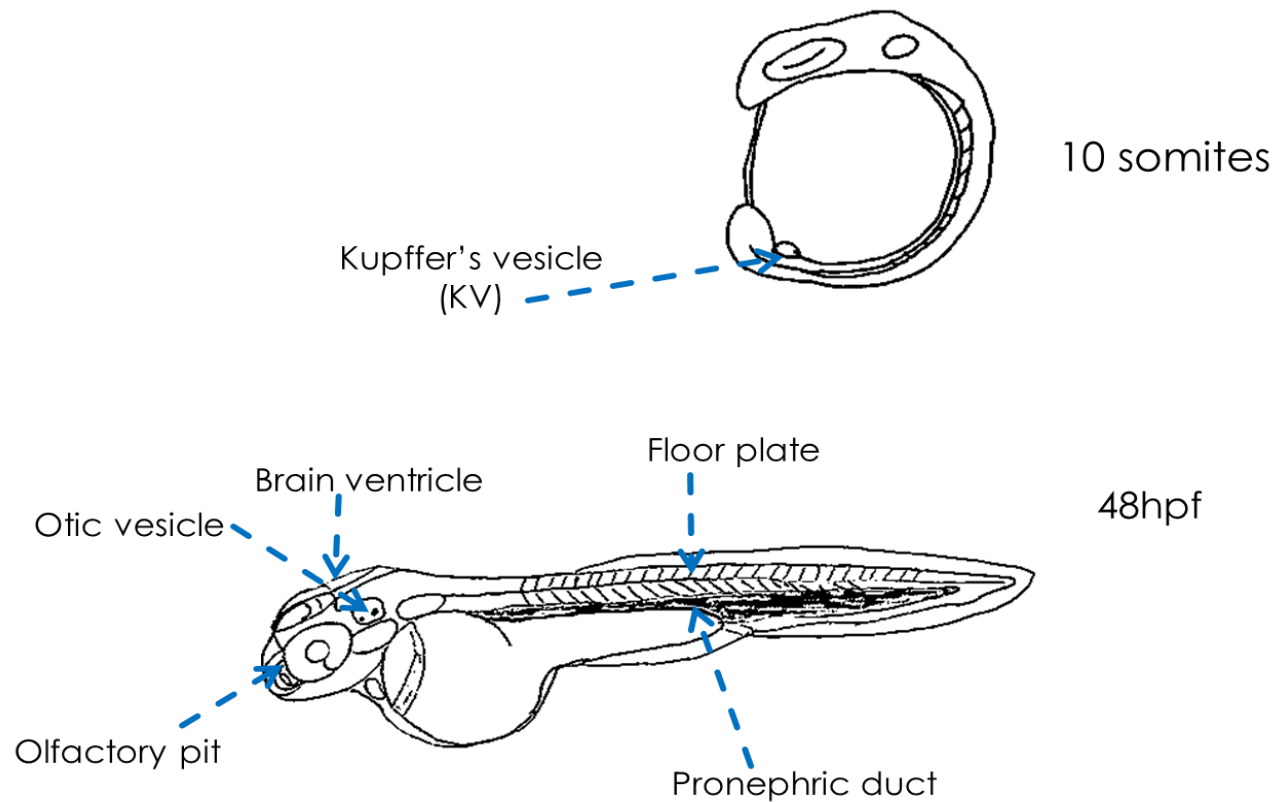


Figure 1-1-7. Motile cilia in the zebrafish embryos.

A) In the initial stages of development, monomotile ciliated cells are present in KV which is equivalent to the mammalian embryonic node.
 B) As the embryo develops, there are many different motile ciliated tissues such as pronephric duct, otic vesicle, brain ventricle, floor plate and olfactory pit. MCCs are found in pronephric duct, olfactory pit and brain ventricles.

Phenotypes associated with motile cilia defects can easily be characterized using bright field microscopy, antibody staining or transgenic analysis (Malicki et al., 2011). A large-scale mutagenesis screen done by Howe *et al* identified many zebrafish cilia mutants including genes that cause human ciliopathies (Howe et al., 2013a). Moreover, gene editing techniques like TALEN and CRISPR/Cas9 technologies are very well established and have been extensively used in the zebrafish, and therefore can be explored to model human ciliopathy gene mutations. Recently, Choksi *et al* carried out a systematic screen for novel ciliary genes by overexpressing *foxj1* in zebrafish embryos and identified hundreds of novel candidates with putative function in ciliogenesis and cilia motility (Choksi et al., 2014b). Overall, this information highlights the value of the zebrafish in ciliogenesis research.

1.7 Aims and hypothesis of the thesis

Despite the importance of cilia, the mechanisms regulating the transcriptional control and maintenance of motile ciliogenesis are incomplete, and we are only beginning to understand the mechanisms underlying the development and function of cilia. By identifying the transcriptional cascade that regulates these processes, it will give us a more thorough understanding of the biology of cilia and associated disorders. Therefore, better understanding of how signalling pathways modify this transcriptional cascade and identifying cell type-specific transcription factors that activate specific target genes will help in improving the diagnosis and treatment of ciliopathies like PCD.

To aid these goals, several systematic approaches have been taken including single cell transcriptome analysis in distal lung (Treutlein *et al.*, 2014)

and transcriptional profiling of FOXJ1 induced genes (Hoh et al., 2012, Choksi et al., 2014b). These, and other studies, have identified numerous novel ciliated cell markers involved in cilia formation and function. However, these data just form a map for treasure hunters since it requires further characterisation of individual candidates to understand and fill the gaps in the field of ciliogenesis. Identification and characterisation of novel ciliary genes would also help early diagnosis and treatment of ciliopathies like PCD.

Therefore, my project was focused on the following aims:

1. To undertake a systematic analysis of published data sets to identify potential novel ciliogenesis genes.
2. To establish primary mouse airway epithelial cell culture model and use it to characterise the expression of potential novel ciliogenesis genes to identify candidate gene for further analysis.

Having achieved these aims, *Pierce1* was selected as a potential ciliogenesis gene for further characterisation. Subsequently, my hypothesis was that *Pierce1* plays a role in motile ciliogenesis. This hypothesis was tested with following aims:

1. To characterise the functional role of PIERCE1 using an *in vitro* model and *in vivo* model with the following objectives.
 - A) To study the transcriptomic and proteomic expression of PIERCE1 in primary mouse airway epithelial cell culture.
 - B) To generate and phenotypically characterize the *pierce1* knockout zebrafish embryos.



Chapter 2 : Materials and methods

2.1 Studying ciliogenesis in primary mammalian airway epithelial cells cultured *in vitro*

2.1.1 Culture of mouse tracheal and nasal epithelial cells

Epithelial cells from mouse nasal septum and trachea were isolated from C57BL/6 mice and cultured in ALI culture conditions following published methodologies as outlined below.

2.1.1.1 Maintenance of mouse stock

C57BL/6 mice were obtained from Charles River and maintained in a specific pathogen free environment in open top cages. Animals were fed ad-lib rodent diet and provided with filtered tap water. All work involving animals was performed in accordance with the Animal (Scientific procedures) Act 1986 and was approved by the University of Sheffield animal welfare and ethical review body. Work was carried out under procedure project license 40/3726 (David Dockrell).

2.1.1.1 Harvest of mouse trachea

The mice were euthanized by administering 50mg/ml pentobarbital (100µl/mouse) by intraperitoneal injection that was followed by exsanguination by cutting the inferior *vena cava* by research technician with appropriate animal handling licence. Mouse carcasses were sprayed with 70% industrial methylated spirit (IMS) to sterilize the field. Using sterilized scissors and

scalpels, the skin around the tracheal area was removed until the trachea was exposed. After making an incision on the abdominal area a midline incision was made along the sternum and rib cage was removed to access the trachea within the thoracic cavity. With the aid of surgical forceps, the trachea was lifted, and blunt dissection was used to separate oesophagus from the posterior surface of trachea. Tracheae were then cut off at the proximal end and dissection was carried out down to the tracheal bifurcation. The resected tracheae were then placed in cold sterile filtered mTEC basic media (Ham's F12 Media (Life Technology, 31330-038) containing 2% Penicillin/ streptomycin (Life Technology, 15070-063). After transferring the resected tracheal tissues into a sterile 100 mm Petri dish containing 10 ml sterile antibiotics containing Ham's F12 media, the connective tissue and attached glands were dissected from the trachea and discarded under a dissection microscope using sterile forceps. The tracheae were subsequently transferred in to a new sterile 100 mm Petri dish with 10 ml Ham's F12 media containing antibiotics. Using a pair of sterile surgical scissors and forceps, the lumen of the tracheae was cut open before transferring into 5mL 0.15% Pronase (Sigma Aldrich, 10165921001) solution (1 trachea per ml) and was incubated overnight at 4°C. Dissection of mouse trachea is detailed in Figure 2.1.

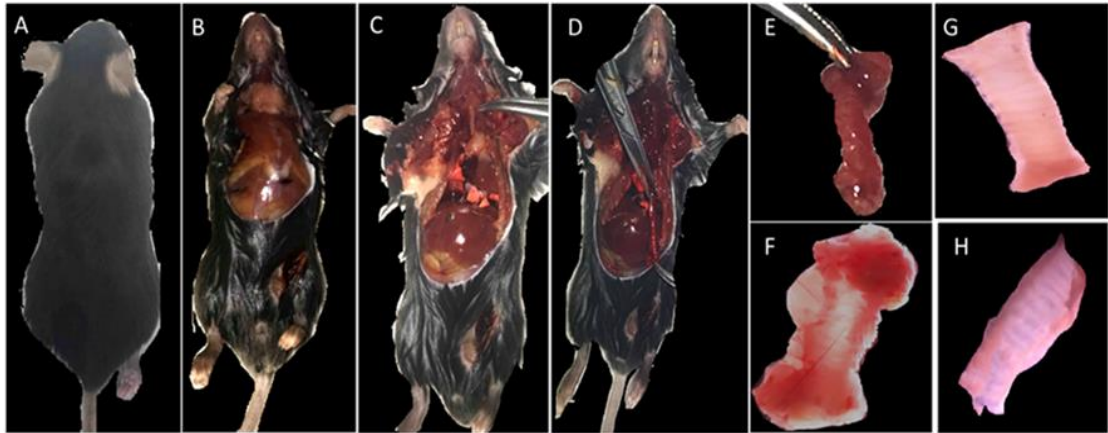


Figure 2-1. Harvest of mouse trachea.

A. WT C57BL/6J mice was used. **B.** Skin around tracheal area was removed. **C.** Midline incision was made along the sternum and rib cage was removed to access the trachea within the thoracic cavity. **D.** Trachea was lifted, and blunt dissection was used to separate trachea from surrounding tissues. **E.** Tracheas were then cut off from the proximal end and distal end. **F-H.** The connective tissue and attached glands were dissected from the trachea under a dissection microscope using sterile forceps the lumen was cut open.

2.1.1.2 Harvest of mouse nasal septum

Mice were euthanized by administering 50mg/ml pentobarbital (100uL/ mouse) by intraperitoneal injection that was followed by exsanguination by cutting as outlined above. Mouse carcasses were sprayed with 70% industrial methylated spirit (IMS) to sterilize the field. Using a sterile dissecting scissors, an incision was made at the nape of the neck that carried on around the entire neck through which the head was completely separated from the rest of the body. The loosely attached skin was then removed completely using the fine scissors that exposed the skull and nose. The posterior coronal plane in the skull was sectioned and bony outer layer was removed that exposed the brain followed by the complete removal of brain by forceps. The scissors were then inserted in to the oral cavity and the mandible (lower jaw) was separated which further exposed the upper palate. The scissors were then inserted into posterior nasal cavity and an incision was made along the suture line to extract the bony septum from the tissue. The resected nasal septae were then transferred into a 100 mm petri dish with 10 ml sterile Ham's F12 media with added antibiotics. Under the dissection microscope, further dissection was carried out to remove attached hairs, elastic tissues and anterior nasal tip. Subsequently, the tissues were transferred into a 15 ml falcon tube with 6 ml 0.15% Pronase solution (for 5 nasal septums) and were incubated overnight at 4°C. The dissection of the mouse nasal cavity is detailed in Figure 2.2.

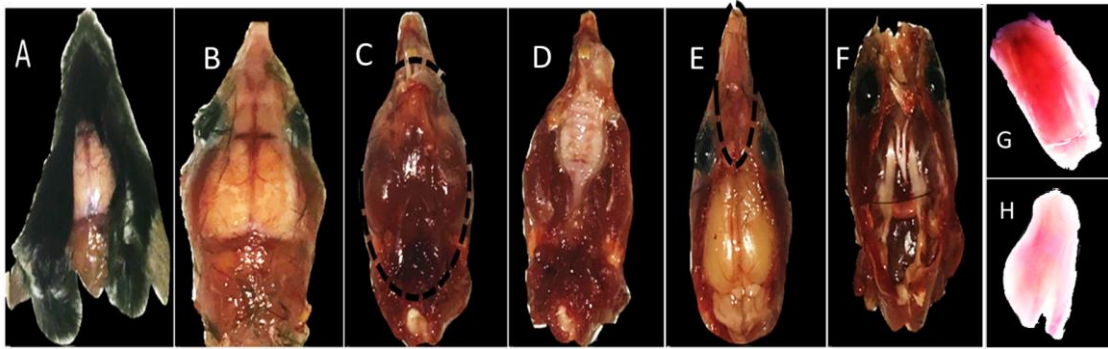


Figure 2-2. Harvest of mouse nasal septum.

A. WT C57BL/6J mice was decapitated. **B.** Head was skinned. **C-D.** The mandible (lower jaw) was separated which further exposed the upper palate. **E-F.** The posterior coronal plane in the skull was sectioned and bony outer layer was removed that exposed the brain followed by the complete removal of brain by forceps. The scissors were then inserted in to posterior nasal cavity and incision was made along the suture line to extract the bony septum from the tissue along the dotted lines. **G.** Extracted nasal cavity. **H.** Nasal cavity was cleaned under dissection microscope to expose nasal septum.

2.1.1.3 Epithelial cell isolation from mouse tracheal and nasal septum

Following pronase digestion, the tubes containing tracheae and nasal septae were left to stand in room temperature for 10 minutes and were given a gentle shake to dissociate more cells into the suspension. 500 µl of FBS (Sigma Aldrich, F2442) was added to the tubes to neutralise the pronase activity and the tubes were inverted 20 times. The tissues were then transferred to a second set of tubes (nasal and trachea separately) containing 2 ml Ham's F12 media with antibiotics and 10% FBS, inverted again 20 times. The tissues were again transferred into third set of tubes and step was repeated and subsequently tissues were discarded. The contents of three tubes were pooled together into fresh tubes for nasal septum and trachea. The cells were pelleted by centrifugation at 400g for 10 min at 8°C. The cell pellets were then suspended in 1 ml of Ham's F-12/pen strep containing crude pancreatic DNase I (Roche, 11284932001) and 10 mg/ml BSA (Sigma, A9418) and left to incubation in ice for 5 min. Meanwhile, 10µl of cell suspension was suspended in 10µl of Trypan blue and was loaded in to haemocytometer to take cell count using Nikon inverted light microscope at 10X magnification. Following the incubation, the cell suspension was again centrifuged at 400 g for 5 min at 8°C. The cell pellets were suspended in Ham's F12 media with 10% FBS and incubated in 15 mm tissue culture plates for 3-4 hours in 5% CO₂ at 37°C. Following the incubation, the non-adherent cells were collected from the plates and centrifuged at 400g for 5 min at 8°C. The pellet was resuspended in 1 ml of MTEC plus media (see appendix 1). An appropriate amount of this cell stock solution was then suspended in adequate volume of mTEC plus media to give the desired cell seeding density.

2.1.1.4 Culture of respiratory epithelial cells

The mTEC and mNEC were seeded on rat-tail collagen-1 coated 0.4 um porous transwells (BD Bioscience). The seeding density for both mTEC and mNEC were 30,000 cells per transwell. The culture conditions were already optimised and established in our laboratory (Akram et al., 2014, Mulay, 2017, Akram et al., 2015). The cells were cultured to confluence in submerged culture for 5-7 days using defined mTEC plus media (see appendix 1)(You and Brody, 2013). Cells were then induced to ALI culture using defined serum free media (MTEC-SF, see appendix 1) (You and Brody, 2013)and culture continued for 14 days in a standard culture environment to allow differentiation of cells that mimicked mouse tracheal and nasal airway epithelium. During ALI culture apical wash and cell lysates were collected on day-0, -2, -5, -7 and 14 of ALI culture for transcriptional and translational analysis of epithelial cell differentiation. At day 14, this epithelial cell layer mimics the original mouse tracheal/nasal epithelium. The cell culture model is illustrated in Figure 2.3. Original mTEC and mNEC cells which were isolated from mice but were not cultured, were utilised as positive control to validate the *in vitro* model.

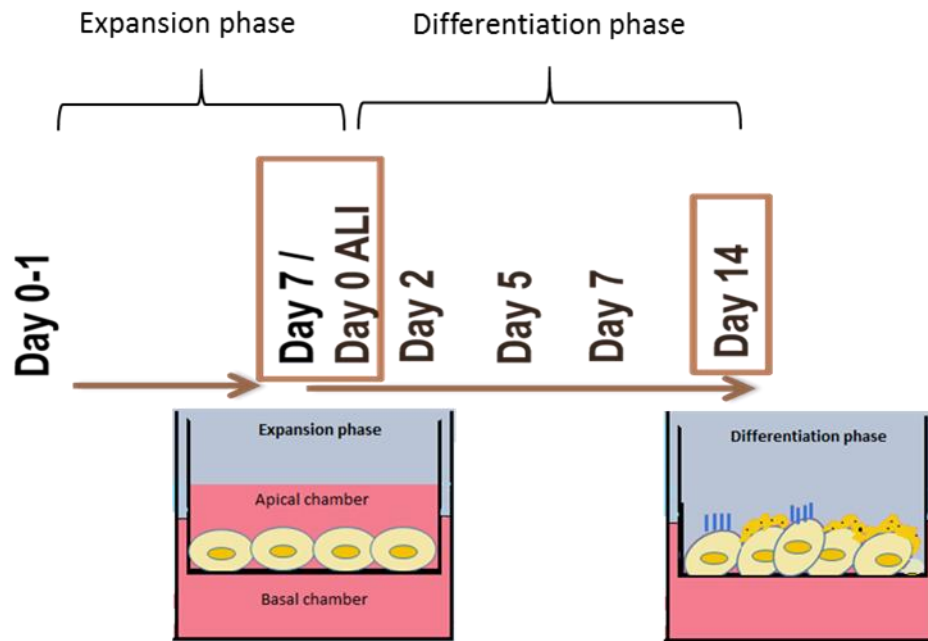


Figure 2-3. Epithelial cells are extracted from mouse nasal septum and trachea and grown in submerged culture.

Cells were seeded on collagen coated 0.4 μ m pore membrane transwells. Cells undergo proliferation while submerged in mTEC/ Plus medium for 6-7 days until fully confluent. Cells are then differentiated to day 14 by Air Liquid Interface (ALI) conditions using mTEC/ SF medium. ALI culture apical wash, cell lysates were collected and cells were fixed on day-0, -2,-5,-7 and 14 of ALI culture for transcriptional and translational analysis of epithelial cell differentiation.

2.1.2 RNA extraction

RNA was extracted from the cell lysates collected at different time points of ALI culture of mouse nasal and tracheal epithelial cells. 250µl of sample was initially thawed and equilibrated at room temperature for 10 minutes. 40µl of chloroform was added into the sample and mixed by vortex, followed by incubation in room temperature for 10 minutes. Following this step, the suspension was centrifuged at 13000 rpm at 8°C for 15 minutes. As a result, the suspension resolved in to 3 phases which was visible as 3 layers. The aqueous layer with the RNA was carefully extracted and transferred to a fresh Eppendorf tube and was suspended in 100µl isopropanol by vortex. The samples were then left to stand in room temperature for 10 minutes. Samples were centrifuged at 13000 rpm and 4°C for 10 minutes that allowed the formation of RNA pellet. After discarding the supernatant, 200µl of 75% ethanol was added to the pellet. Sample was again centrifuged at 13000 rpm at 8°C for 10 minutes and the supernatant was discarded. Subsequently the pellet was air-dried to remove any residual ethanol. The RNA pellet was then re-suspended in 20 µl of RNase-free water. RNA concentration was quantified using a nanodrop spectrophotometer. All extracted RNA underwent DNase free treatment to remove residual genomic DNA in the sample (see appendix 8.2).

2.1.3 Reverse transcription

Reverse transcription was carried out using Promega Reverse Transcription kit using AMV Reverse Transcriptase (Promega, A3500). 200 ng of RNA sample was suspended in 18.5µl water, 0.5 µl random primers and 0.5 µl oligo dt were

added followed by incubation at 70°C for 10 minutes. Then, 6µl master mix made up of 1.5µl dNTPs, 5µl Promega AMV buffer, 0.75µl RNAsin and 0.75µl AMV RT was added to the tube. Reaction mixture was then incubated at 42°C for 1 hour.

2.1.4 Amplification by Polymerase Chain Reaction (PCR)

End-point PCR was carried out using Maxima Hotstart (Thermo Scientific, K1051). For all PCR reactions, 1µl of appropriate forward and reverse primers and 1 µl of sample DNA was added to 10µl of Maxima Hot start master mix along with 6.5 µl nuclease free water. The PCR reaction was run on the following setting: 90°C for 1 minute, 60°C for 1 minute, 72°C for 1 minute for 25- 35 cycles. The primers used for amplifying mouse genes are shown in Appendix 3.

2.1.9 siRNA transfection of primary mouse nasal and tracheal epithelial cells

2.1.9.1 Transfection Reagents

Four different transfection reagents (Dharmafect 1, 2, 3, 4) from Dharmacon™ were tested. The efficiency and toxicity of transfections were compared by fixing the cells and assessing the number of cells emitting green fluorescence by transfection of siGLO and nuclear fragmentation by DAPI staining. All reagents were lipid based. All transfection reagents and volume ranges per transfection were used according to the manufacturer's instructions.

2.1.9.2 Transfection protocol

The siGLO green transfection indicator (Dharmacon™), a fluorescent oligonucleotide duplex that is restricted to the nucleus, thus concentrating its signal to permit explicit visual assessment of transfection efficiency, was first diluted with Opti-MEM® I (Gibco®, Invitrogen, Paisley, UK) with a concentration ranging from 25nM-200nM. Transfection reagents were also diluted in Opti-MEM® I. Reagent dilutions were mixed by pipetting and let to incubate in room temperature (RT) for 10 mins. 30 µl of the reagent dilution was suspended in 30µl of siRNA dilution. The siRNA Reagent complex was incubated at RT for 20 minutes. 240µl of antibiotic free mTEC plus media was added to the siRNA-Reagent complex and mixed well. Subsequently, this transection medium was added to the apical surface of the 60% confluent mNEC and mTEC cells growing on rat-tail collagen-1 coated 0.4 um porous transwells. After 48 hours incubation at 37°C, 5% CO₂ in cell incubator, the transfection medium was discarded. Cells were fixed with 10% formalin and stained with DAPI for visual assessment of toxicity and efficiency. Cells were also trypsinised for cell sorting.

2.1.9.3 Flow cytometry

Following transfection, the cells were trypsinised and suspended in 1 ml of mTEC plus media. The cell suspension was handed over to the Core Cell Sorting facility, Medical School, University of Sheffield to carry out cell sorting to separate transfected cells (green fluorescence attached) from non-transfected cells. Once the cells were sorted, the transfected cells and non-transfected cells were seeded separately on rat-tail collagen-1 coated 0.4 um

porous transwells. After proliferating them for 7 days, the cells were fixed with 10% formalin and stained with DAPI to visualise the transfected cells under epifluorescence microscope.

2.1.10 Western Blotting

Cell lysates and apical washed collected from ALI cultured cells at different time points were mixed with 2xSDS buffer (1:1) and heated at 95°C for 10 minutes. Samples were resolved on 12 % SDS-PAGE gels by loading 20 µl - 40µl of the sample. Gels were run at a voltage of 150V for 1 hr 30 minutes. Trans-Blot Turbo (Bio-rad) was used to transfer the gel to methanol activated PVDF membrane. Following the transfer, membranes were blocked in 5% non-fat milk (Anlene) dissolved in 1 xTris Buffered Saline-Tween (TBS-TWEEN) for 1hr at room temperature. Primary antibodies (see Table 2-1) diluted in the same blocking solution were added to the membrane and incubated overnight at 4°C. The primary antibodies were washed 3 times with TBS-TWEEN at 10mins interval. Secondary antibody (polyclonal goat-anti rabbit conjugated with HRP, DAKO P0448) diluted (1:2000) in same blocking solution were added to the membrane and incubated for 1 hour at room temperature, followed by vigorous 3 X TBS-TWEEN washes at 10mins interval. Enhanced chemiluminescent (ECL) substrate (Geneflow) was used to detect the signal from the HRP conjugated secondary antibody. Information regarding the preparation of the buffers used in Western blotting is given in Appendix 2.

Table 2-1. Primary antibodies in Western blotting.

Primary Antibody	Manufacturer	Dilution
BPIFA1 (Rabbit Ab, polyclonal)	Prepared in lab (Musa <i>et al.</i> , 2012)	1:200
PIERCE1 (Rabbit Ab, polyclonal)	Gift from Dr Dominic Norris (MRC, Harwell)	1:200

2.1.11 Immunofluorescence microscopy

2.1.11.1 ALI Culture Sample fixation

The apical surface of the transwell membrane was washed with warm (37°C) PBS and sample was incubated in the incubator for 30 minutes. After the incubation, the medium was aspirated from the basal compartment. 300µl of 10% buffered formalin (equilibrated at room temperature) was added to the apical chamber and 700 µl to the basolateral compartment of the transwell and left at room temperature for 1 hour. The apical and basolateral surfaces of transwells were washed 3 times by PBS (equilibrated at RT) by repeated pipetting. Finally, 300 µl of PBS was added to the apical chamber and 700 µl of PBS in to the basolateral chamber. The sample was stored at 4°C until the next step.

2.1.11.2 Fluorescence immunocytochemistry

PBS was aspirated from both compartments of the transwells. 300 µl of permeabilization/blocking buffer (Goat serum or Rabbit serum according to (the source of detection antibody) diluted 1:10 in PBS with 0.5% Triton X) was added to the apical surface. The plate was then placed on a shaker for 1 hour at room

temperature at 80 rpm. The permeabilization/blocking buffer was aspirated from the apical surface. Both apical and basal surfaces were washed with PBS once. The primary antibody (see Table 2-2) in permeabilization/blocking buffer was prepared as shown in the table below and 300 μ l primary antibody solution was added to the apical chamber of the transwell. The plate was then placed on a shaker in the cold room at 80 rpm overnight.

Table 2-2. Primary antibodies in immunostaining.

Primary antibody	Manufacturer	Dilution
BPIFA1 (Rabbit Ab, polyclonal)	Prepared in lab (Musa et al., 2012)	1:200
FOXJ1 (Mouse Ab, monoclonal)	Affymetrix eBioscience (2A5)	1:200
β -tubulin (Mouse Ab, monoclonal)	Sigma (T5201)	1:100
Mouse/human P63 (MOUSE Ab, monoclonal)	Santa Cruz Biotechnology (4A4)	1:500
MUC5B (Rabbit Ab, polyclonal)	Santa Cruz Biotechnology (H-300)	1:100
PIERCE1 (Rabbit Ab, polyclonal)	Gift from Dr Dominic Norris (MRC, Harwell)	1:80

Following the overnight incubation, the primary antibody was aspirated from the apical surface. The apical and basal surface of the transwell was washed three times with PBS by pipetting. The secondary antibody (see Table

2-3) solution in permeabilization/blocking buffer was prepared as shown in the table below and 300 µl antibody solution was added to the apical chamber of the transwell and the plate was wrapped in aluminium foil. The plate was placed on a shaker for 1 hour at 80 rpm at RT.

Table 2-3. Secondary antibodies in immunostaining.

Secondary antibody	Dilution	Primary antibodies used against
Alexa Fluor 568 Goat anti-rabbit Ab. Cat No- A11011. (Red)	1:200	PIERCE1, MUC5B, BPIFA1
Alexa Fluor 488 Goat anti-mouse Ab. Cat No- A11001. (Green)	1:200	P63, β -TUBULIN, FOXJ1

The secondary antibody was aspirated and the apical and basal surfaces of the transwell were washed three times with PBS under dim light. The membrane holding the cells were cut out using a scalpel and placed on a microscope slide (with the cell side up) using forceps. 1 drop of DAPI mounting medium (Vectashield, Vector Laboratories) was added on top of the cells and left to stand in RT for 2 minutes. The coverslip was transferred on to the prepared slide. Excess DAPI was diffused out to the edges. Nail polish was used to seal the coverslip to the slide and allowed the nail polish to set in RT for 30 minutes. The slides were then taken for analysis on the confocal microscope.

2.1.12 Quantification of intracellular localization of epithelial cells

ALI day 14 mNEC cells immunostained for FOXJ1 were analysed using Olympus Fluoview 1000 confocal microscope. Using 40x magnification, 8 adjacent fields spanning the whole membrane were imaged. Z-stacks were analysed and merged using ImageJ software to create the maximum intensity single image. The number of ciliated cells (FOXJ1^{+ve} cells) was studied using mean integrated fluorescence using ImageJ software. The percentage of cell expressing FOXJ1 was quantified using ImageJ as follows:

$$\frac{\text{Number of nuclei expressing FOXJ1}}{\text{Total number of nuclei stained by DAPT}} \times 100$$

2.1.13 Quantitative PCR

For qPCR to quantitate expression *Pierce1* and *Foxj1* in the differentiated mNEC grown at ALI treated with and without DAPT, 500 ng of total RNA was used for cDNA synthesis by Promega Reverse Transcription kit. Primer sequences (see Appendix 3) were taken from a recent study by Stauber *et al* (2017) that had identified downstream targets of FOXJ1 in murine embryonic airway epithelium and mouse embryonic node (Stauber et al., 2017). The internal control was *Hprt*. cDNA was diluted 1:50. The qPCR BIO SyGreen Blue Mix Lo-ROX (PCRBIOSYSTEMS, Cat. No- PB20.15-05) was used to carry out q-PCR (three repeats for each sample). qPCRs were carried out in a Rotor Gene Q qPCR cyler, using software Rotor Gene 2.1.0.9 (Qiagen). Reagents were assembled as shown below (Table 2-4).

Table 2-4 Components for Quantitative PCR

Reagent	Volume (each well)
cDNA	6 μ l
SYBR green master mix	3.5 μ l
Forward primer (5 μ M)	0.5 μ l
Reverse primer (5 μ M)	0.5 μ l

Fold differences in the gene expression levels were generated from the C_t values after normalizing against the internal controls using Microsoft excel. Three biological replicates were measured for *Pierce1* and *Foxj1*.

2.2 Analysing ciliogenesis in zebrafish embryos

2.2.1 Zebrafish strains and husbandry

Zebrafish strains used in the study were maintained at the Institute of Molecular and Cell Biology-zebrafish facility following standard protocols. The facility has a controlled temperature of 28.5°C and operates a 14-hr light and 10-hr dark light cycle. All the experiments with zebrafish were conducted with the approval of The Singapore National Advisory Committee on Laboratory Animal Research. The zebrafish strains used in the thesis are listed in the following Table 2-5.

Table 2-5 Zebrafish strains used in the study

Line	Purpose
AB	Wild-type
<i>hsp70::foxj1a</i>	Used to overexpress Foxj1
<i>pierce1</i> KO c.178_179ins(29 bp)	To assess the function of Pierce1
<i>pierce1</i> KO c.176_180del	To assess the function of Pierce1

hsp70: foxj1a line was generated in Prof Sudipto Roy's lab (Choksi et al., 2014c).

2.2.2 Zebrafish Morpholino experiments

2.2.2.1 Overview

All zebrafish morpholino experiments were conducted with the purpose of characterising the consequence of knockdown of a gene by either interfering with translation or splicing at mRNA level, on the subsequent development, focusing on structural and functional changes. We were particularly focused on

phenotypes that could arise from motile cilia defects such as abnormal otoliths, hydrocephalus, laterality defects, curved axis and pronephric cyst formation.

2.2.2.2 Morpholino design and preparation

Morpholino oligonucleotides (see Table 2-6) were designed and synthesized by GeneTools LLC. They were reconstituted to 1mM by suspending it in double distilled water and stored at room temperature. Using a N2 gas injector (PLI-100 from Harvard Apparatus), one cell stage zebrafish embryos were initially injected with a volume of 1nl, 0.75nl and 0.5nl of morpholino (100% concentration) into the animal pole. When there were embryos with more than 25% lethality, data were rejected. Reduced dose of morpholino was used to repeat the injection.

Table 2-6 Morpholinos used in the study

Type of Morpholino	Sequence
Pierce1 start (23 rd November 2015, Genetools)	TCGTTTGTGCTCATGTTTGTGTTGA
Pierce1 splice (4 th January 2016, Genetools)	GCTGGCTCTTCTTACCTGTATCTGA

2.2.3 Fixation of embryos for immunofluorescence

Approximately 30 embryos from each group were transferred into screw top eppendorfs. Embryos were fixed in 1 ml Fish fix (4% paraformaldehyde, 4% sucrose dissolved in PBS) for 2-3 hours in room temperature or overnight in 4°C. Subsequently, the fixed embryos were washed with 1x PBS for 4 times

with 30min intervals. PBS was then discarded, and embryos were kept in 100% methanol (MeOH) and stored in -20°C. In methanol, embryos can be kept up to 1 year.

2.2.4 Whole mount immunohistochemistry on zebrafish embryos

For immunohistochemistry, fixed embryos stored in 100% MeOH were rehydrated by washing with progression from 75%, 50% and 25% methanol to 1x PBS for 5 minutes at room temperature. Subsequently, embryos were washed in 1x PBS for 4 times with 2 minutes intervals. Then, PBS was discarded, and embryos were treated with 1ml ice-cold acetone and were stored in 20°C for 7 minutes. Acetone was then discarded, and embryos were further washed with 1x PBS for 4 times with 2 minutes intervals. Afterwards, embryos were incubated in blocking solution consisting of 2% sheep serum diluted in PBDT (PBDT consist of 1% BSA, 1 % DMSO and 0.5% Triton-X100 diluted in PBS and stored at 4°C) for 1 hour at room temperature in a glass cavity dish on a nutator at 65 rpm. The blocking solution were then removed and primary antibody (see Table 2-7) diluted in PBDT was added to the embryos.

Table 2-7.Primary antibodies in immunostaining

Primary antibody	Manufacturer	Dilution
Anti-GFP (polyclonal)	Torrey Pines, TP401	1:500
Anti-acetylated-alpha-tubulin (rabbit monoclonal)	Cell Signaling, 5335S	1:500

Anti-acetylated-tubulin (mouse monoclonal)	Sigma, T6793	1:500
A4.1025 (myosin heavy chain), mouse	Developmental Studies Hybridoma Bank (DSHB)	1:20
Anti-Myc (mouse monoclonal)	Santa Cruz Biotechnology (#sc-789)	1:500

Embryos were incubated overnight at 4°C. The following day, the primary antibody was removed, and the embryos were washed in PBDT for 4 times with 30 minutes intervals on a nutator (80 rpm). Appropriate secondary antibodies (Table 2.8) and DAPI (1:2000) diluted in PBDT was then added to the embryos and incubated for 3-4 hours at room temperature on a shaking platform at 60 rpm. After removing the secondary antibody, embryos were washed with PBDT for 4 times with 30 minutes intervals. Embryos were subsequently transferred to 70% glycerol (in sterile water). Stained embryos were mounted using 70% glycerol.

Table 2-8. Secondary antibodies in immunostaining

Secondary antibody	Dilution
Alexa Fluor 555 Goat anti-mouse Ab (Invitrogen)	1:500
Alexa Fluor 488 Goat anti-rabbit Ab. (Invitrogen)	1:500

2.2.5 Zebrafish molecular biology techniques

2.2.5.1 RNA isolation from zebrafish embryos

RNA was isolated from WT embryos, *hsp70: foxj1* embryos, morpholino injected embryos and *pierce1* mutant embryos to check for *pierce1* mRNA expression and to validate morpholino and mutations. RNA was first isolated and 1µg RNA was reverse transcribed to make cDNA. This cDNA was subsequently used for endpoint PCR and qPCR.

Approximately 30 embryos from each group were transferred into screw top eppendorfs. Embryos were first washed in 1 ml 0.1% DEPC treated sterile water. After discarding the water, 1 ml Trizol was added to embryos in a fume hood. Embryos were then lysed using 1 ml syringe and needle and incubated for 5 minutes at room temperature. 200 µl chloroform was added to the lysate and then vortexed for 15 seconds. The sample was then incubated for 3 minutes at room temperature. The chloroform-lysate solution was then centrifuged at 12,000 rpm for 15mins at 4°C, that resulted in separation of the mixture into three phases. The aqueous phase containing the RNA was moved into fresh 1.5 ml Eppendorf tube. RNA was precipitated by adding 500 µl isopropanol and incubated at room temperature for 10mins, then centrifuged at 12,000 rpm for 10mins at 4°C. Consequently, the RNA pellet was observed at the bottom of the Eppendorf tube. The RNA pellet was then washed and vortexed in 1ml of 75% ethanol and centrifuged at 7,500 rpm for 5mins at 4°C. Ethanol was then discarded, and the RNA pellet was air dried for 5-10mins at room temperature. The RNA pellet was then dissolved in 20 µl RNase free water. 1 µl DNase was added to the RNA solution and incubated for 20 minutes at 37°C to remove genomic DNA contamination. RNA concentration was

quantified using Nanodrop 1000 spectrophotometer (Thermo Scientific, US).

RNA stocks were stored at -80°C.

2.2.5.2 Reverse transcription

Equal concentrations of RNA were used in each experimental group by diluting with RNase free water where required. First-strand cDNA was synthesized using the Superscript First Strand Synthesis Kit (Invitrogen, USA). The reaction was assembled as indicated in Table 2-9 below.

Table 2-9. Components for First-strand synthesis of cDNA

Reagent	Volume
RNA	1 µg
Oligo dt	1 µl
10 mM dNTP	1 µl
DEPC water	Up to 10 µl

The mixture was incubated at 65°C for 5 min and was then left on ice for 5 min. The reverse transcription was carried out by the addition of the following reagents shown in the following Table 2-10.

Table 2-10. Components for Reverse Transcription (RT)

Reagent	Volume
10X buffer	2 μ l
25mM MgCl ₂	4 μ l
0.1M DTT	2 μ l
RNase Out	1 μ l
Superscript III reverse transcriptase	1 μ l

Afterwards, the mixture was incubated at 42°C for 1h. The reaction was terminated by a short incubation for 5 min at 85°C and subsequently chilled. Any excess RNA was removed by the addition of 1 μ l of RNase H and incubation at 37°C for 20 min. cDNA was stored at -20°C.

2.2.5.3 Polymerase Chain Reaction (PCR)

A web-tool, Primer3plus, (<https://primer3plus.com/>) was used to facilitate design of specific primers. Primers (see Appendix 4) for PCR were purchased from IDT (earlier1st-Base) Singapore. For PCR reactions to generate products for further sequencing and cloning, Roche Expand high fidelity kit (See Table 2-11) was used with PTC100 thermal cycler (MJ Research). A 50 μ l reaction volume was used. The cycling conditions consisted of denaturation at 95°C for 30s, followed by annealing for 30s at a range of temperatures from 55°C to 65°C, and finally, an extension at 68°C. Extension time was set at the rate of 1minute per Kb.

Table 2-11. Components for PCR with Roche Expand high fidelity kit

Reagent	Volume
10 mM dNTP	1 µl
10 µM Forward primer	1 µl
10 µM Reverse primer	1 µl
10 x buffer	5 µl
Enzyme	1 µl
cDNA	1 µl
dH ₂ O	40 µl

PCR products were then visualised by gel electrophoresis on 1-2% agarose gels in TAE buffer (See appendix section 2.2).

For PCR reaction for genotyping zebrafish embryos to identify *pierce1* mutants, a MyFi mix (Bioline) containing DNA Polymerase, dNTPs and MgCl₂ was used as shown in Table 2-12. A reaction volume of 20 µl was used. The cycling conditions consisted of initial denaturation at 95°C for 1 min, followed by denaturation for 30s at 95°C, annealing for 30s at a range of temperatures from 55°C, and finally, an extension at 72°C. This was followed by final extension at 72°C for 10 minutes.

Table 2-12. Components for PCR with MyFi mix

Reagent	Volume
MyFi Mix	10 μ l
dH ₂ O	7 μ l
10 μ M Forward primer	1 μ l
10 μ M Reverse primer	1 μ l
gDNA (~100 ng)	1 μ l

PCR products were then visualised by gel electrophoresis on 1-2% agarose gels in 1X TAE buffer (See Appendix 2.2).

2.2.5.4 Excision of RT-PCR bands and PCR clean-up

To extract a band of interest from agarose gel, the gel was positioned on top of a UV transilluminator. The band was cut away from the gel using a scalpel by cutting around the edges of band. Subsequently, the cut out gel containing the band was place in a 1.5 ml Eppendorf tube and subsequently weighed to determine the mass of the gel (e.g. 100 mg is equivalent to 100 μ l). Extraction of DNA from the gel was carried out using Qiagen gel extraction kit and the manufacture's protocol. An appropriate volume (3x volume of gel) of QG buffer was added to dissolve the gel by heating in 50°C up to 10 minutes. The gel mixture was then transferred to a spin column and centrifuged for 1 minute at 13000 rpm. The flow through was discarded. 500 μ l of buffer PB was added to the column and again centrifuged for 1 min at 13,000 rpm. The flow through was discarded and 700 μ l of buffer PE was added to the column followed by 2

times 1 min centrifugation at 13000 rpm. Subsequently, 15 µl RNase /DNase free water was added to the column and incubated in room temperature for 5 minutes. Afterwards, it was centrifuged for 1 min at 13,000 rpm and DNA was eluted as flow through. Eluted DNA was stored at -20°C.

2.2.5.5 TOPO-TA cloning

For sequencing PCR products and sub-cloning into zebrafish expression vectors, gel extracted PCR amplified product for a gene of interest i.e. *pierce1*, was used for TOPO cloning (Thermofisher, K4620-01). The cloning reaction consisted of mixing the following reagents:

Table 2-13. Components for TOPO-TA cloning

Reagents	Volume
DNA (25 ng/ µl)	4 µl
pCR II TOPO vector	1 µl
Salt	1 µl

The reaction mixture was incubated at room temperature for 20 minutes and subsequently transferred to ice. Afterwards, the reaction mixture was transferred in to One Shot DNH5α T1 competent E. coli cells and incubated on ice for 20 minutes before heat shocking in 42°C for 40 seconds. Subsequently, it was incubated on ice for another 5 minutes before plating antibiotic containing LB agar plate with 50 µl X-GAL and incubated overnight at 37°C. White colonies from the plate were picked for miniprep.

2.2.5.6 Extraction of plasmid DNA from bacterial cultures

Miniprep was carried out as per the manufacturer's protocol (QIAGEN, Valencia, CA, USA) from the 3 ml of bacterial culture using ion-exchange columns.

2.2.5.7 Restriction enzyme digestion

Restriction enzymes (New England Biolabs) were used for restriction digest to validate plasmids, cloning etc. To digest or linearize a particular vector or a construct, the following setup was used as shown in Table 2-14.

Table 2-14. Components for Restriction digest reaction

Reagents	Volume
DNA	3 µg
NEB Cutsmart buffer	5 µl
Restriction enzyme	2 µl (Double digest – 1.5 µl of each enzyme)
Water	Up to 50 µl

The reaction mixture was incubated for 3 hours at 37°C. Afterwards, digested fragments were resolved on a 1% agarose gel and the desired product was extracted from the gel.

2.2.5.8 DNA Sequencing

DNA sequencing was carried out at DNA sequencing facility at the Institute of Molecular and Cell biology, A*STAR, Singapore. Sequencing was performed using Big Dye Terminator v3.1 and appropriate primers. Results were viewed using the commercial software Finch TV.

2.2.5.9 Cloning and sub-cloning

In order to express tagged (MYC or GFP) Pierce1 in zebrafish embryos, primers were designed with appropriate restriction sites to amplify *pierce1* ORF with cloning restriction sites. PCR product was gel extracted and cloned into pCR II TOPO. *pierce1* TOPO plasmid with the engineered restriction sites were verified by miniprep followed by sequencing. Next, I proceeded to sub-clone *pierce1* (with the engineered restriction sites) in to either 6 x myc -PCS2 vector or PCS2-GFP xlt vector. Pierce1-TOPO plasmid with engineered restriction sites and the vector were digested with same restriction enzymes for 3 hours at 37°C. Digested *pierce1* (the insert) from the TOPO plasmid and digested vector was gel extracted. The insert and vector were mixed in a 3:1 molar ratio as shown in Table 2-15.

Table 2-15. Components for ligation reaction

Reagents	Volume
Insert (50 ng)	3 μ l
Vector (50 ng)	1 μ l
T4 DNA Ligation Buffer	10 μ l
T4 DNA ligase	1 μ l
Water	Up to 20 μ l

The ligation mixture was incubated at 16°C overnight. Following day, 6 μ l of the ligation mixture was mixed with 100 μ l One Shot DNH5 α T1 competent *E. coli* cells and incubated on ice for 20 minutes before heat shocking in 42°C for 40 seconds. Subsequently, it was incubated on ice for another 5 minutes

before plating antibiotic containing LB agar plate and incubated overnight at 37°C. Colonies were picked for miniprep to extract plasmid DNA. Restriction digest and sequencing was carried out on the extracted plasmid DNA to validate the construct.

2.2.5.10 *In vitro* transcription of linearized construct

1 µg linearized plasmid construct (6X myc-*ierce1*-PCS2, *ierce1*-PCS2-GFP xlt) were transcribed *in vitro* to synthesise mRNA using mMESSAGE mMACHINE SP6 or T7 kit (Ambion) according to manufacturer's protocol by adding transcription components and incubation for 2hrs at 37°C. Subsequently, excess DNA was removed by adding DNase1 followed by incubation for 15mins at 37°C. This was followed by lithium chloride precipitation at -20°C. Next day, RNA was pelleted by centrifugation at 12,000 rpm for 30mins followed by wash with 70% ethanol. After discarding the ethanol, pellet was dissolved in 20µl of 0.1% DEPC water. The synthesized mRNA was stored at -80°C. 1nl of synthesised RNA (200 ng µl) was injected into the animal pole of one-cell stage zebrafish embryos.

2.2.5.11 Quantitative PCR

For carrying out qPCR to look at the *ierce1* expression in *hsp70: foxj1* zebrafish embryos (heat shocked), WT (WT) embryos and *hsp70: foxj1* zebrafish embryos (non-heat shocked), embryos were collected at 24 hpf for RNA extraction. 1 µg of total RNA was used for cDNA synthesis by Superscript III (Invitrogen, #18080-051). Primers (see appendix 4) were designed at 3' end and flank exon-intron boundaries to test for genomic DNA contamination. Internal control was *rplpo*. cDNA was diluted 1:100. A Fast SYBR green master

mix (Invitrogen, 11780200) was used to carry out q-PCR on a 90 well plate (three repeats for each sample). Reagents were assembled as shown below in Table 2-16.

Table 2-16 : Components for Quantitative PCR

Reagent	Volume (each well)
cDNA (2 ng/ μ l)	6 μ l
SYBR green master mix	10 μ l
Forward primer (5 μ M)	2 μ l
Reverse primer (5 μ M)	2 μ l

Quantitative PCR was performed on a Fast 7900HT real time machine (Applied Biosystems) with the included SDS2.4 software. Fold differences in gene expression levels from experimental control were generated from the C_t values after normalizing against the internal controls using Microsoft excel.

Three biological replicates were measured for *pierce1*. Statistical significance was determined by using a Student's t-test, with p values < 0.05 considered significant. Primers for qPCR can be found in the appendix.

2.2.5.12 Extraction of genomic DNA from embryos

Individual embryos were picked and placed in 0.5 ml Eppendorf tubes. Embryos were washed with 200 μ l sterile water once. 10 μ l of lysis buffer (25 mM NaOH, 0.2 mM EDTA) was then added to each embryo and embryos were incubated for 20 min at 95°C. Subsequently, the reaction was chilled in ice for 5 minutes prior to addition of 10 μ l neutralisation buffer (40 mM Tris-HCl, pH 8.0). The mixture was vortexed for 1 minute. The DNA was subsequently used in PCR reactions.

2.2.5.13 Extraction of DNA from adult zebrafish

Adult zebrafish were anaesthetized in 0.02% 3-amino benzoic acid ethylester (tricaine). Roughly, 5 mm of the tail fin was cut and placed in 0.5 ml Eppendorf tube. 40µl of lysis buffer (25 mM NaOH, 0.2 mM EDTA) was then added to each tube and were incubated for 20 min at 95°C. Subsequently, the reaction was chilled in ice for 5 minutes prior to addition of 40µl neutralisation buffer (40 mM Tris-HCl, pH 8.0). The mixture was vortexed for 1 minute. The DNA was subsequently used in PCR reactions.

2.2.6 Making *pierce1* knockout with CRISPR/Cas9 gene editing technique

In order to generate stable genetic mutant lines for *pierce1* in zebrafish, the CRISPR/Cas9 system, a recently developed gene editing technique that induce double stranded breaks in the DNA, was utilised.

2.2.6.1 Designing and synthesising gRNAs

Target sites for CRISPR were identified by locating PAM sites (NGG) within the UTRs and exons of *pierce1* DNA. This was carried out using a web tool called “CHOPCHOP”. The 18bp sequence upstream of the identified PAM site was used as a template to generate gRNA along with the sequence that recruits Cas9 and the T7 promoter from which the guide RNA is transcribed. Subsequently, this ultramer was purchased from IDT. The ultramers were resuspended in sterile water to a final concentration of 100µM. Using a standard reverse primer, the ultramers (see appendix 4) were amplified with the reagents assembled as shown below in Table 2-17.

Table 2-17. Components for gRNA template amplification

Reagents	Volume
5 x Phusion buffer	20 μ l
Phusion polymerase	1 μ l
Designed ultramer (100 μ M)	2.5 μ l
Reverse primer	2.5 μ l
dNTP (10 mM)	2.5 μ l
DMSO	2.5 μ l
Water	64 μ l

The cycling conditions consisted of initial denaturation at 98°C for 30 seconds, followed by denaturation for 10s at 98°C, annealing for 30s at 60°C, and finally, an extension at 72°C for 15 seconds. This was followed by final extension at 72°C for 10 minutes. The PCR reaction was 35 cycles. PCR product was subsequently purified PCR purification kit by QIAGEN according to manufacturer's protocol. The PCR product was then eluted in 10 μ l of dH₂O.

The gRNA was transcribed from the purified PCR product using the MEGAshortscript T7 kit (Life Technologies) according to the manufacturer's instructions. The transcription reaction was assembled as shown below in Table 2-18.

Table 2-18. Components for gRNA *in vitro* transcription

Reagents	Volume
10 x buffer	2 μ l
ATP	2 μ l
GTP	2 μ l
CTP	2 μ l
UTP	2 μ l
PCR purified product	8 μ l
T7 enzyme	2 μ l

The reaction was incubated at 37°C for 3-4 hours. Subsequently, 2 μ l of DNase was added to the reaction to remove the remaining DNA incubating for further 20 minutes. In order to precipitate gRNA, 115 μ l nuclease free water along with 15 μ l ammonium acetate was added to reaction and mixed well by vortex. Afterwards 300 μ l EtOH (100%) was added and incubated at -20 °C overnight. Next day, the RNA is pelleted as shown in section 2.2.5.10. RNA concentration was measured by nanodrop.

2.2.6.2 *In vitro* validation of gRNAs

In order to test the efficiency of gRNAs, an *in vitro* reaction was assembled as follows in Table 2-19 in a 0.5 ml Eppendorf tube. The negative controls were assembled without Cas9 or gRNAs.

Table 2-19. Components for gRNA in vitro validation

Reagent	Volume
Plasmid DNA/ PCR product containing target site sequence (100 ng/ μ l)	1 μ l
NEB buffer 3	1 μ l
10 x BSA	1 μ l
gRNA (450 ng/ μ l)	1 μ l
Cas9 (400 ng/ μ l)	1 μ l
Water	5.5 μ l

The mixture was then incubated at 37 °C for 1 hour. Subsequently, the mixture was run on 1-2% agarose gels by gel electrophoresis and viewed under UV exposure to validate cleavage of plasmid DNA/ PCR product. If the DNA was cleaved, the gRNA was considered to be efficient.

2.2.6.3 Injection of gRNA + cas9 into zebrafish embryos

The injection mixture was made by adding 1 μ l of each gRNA (1.5 μ g/ μ l) and 1 μ l of cas9 RNA (1.6 μ g/ μ l). 1nl of this mixture was injected into the animal pole of one-cell stage embryos. The embryos were then incubated in petri dishes at 28°C until 7dpf and then transferred to the nursery.

2.2.6.4 Determination of CRISPR efficiency

gDNA was extracted from 8 CRISPR injected embryos and 8 uninjected embryos at 24 hpf. Primers were designed to amplify region spanning the target site. PCR was performed on injected and WT samples side by side with these primers using MyFi Hotstart kit. The PCR products were run on 1%-2.5% agarose gel to determine if any large deletions are detectable. The PCR products were then gel extracted and cloned to pCR II TOPO. 6 colonies were picked from each plate and plasmid was extracted by miniprep. The extracted plasmids were sent for sequencing to detect small insertions or deletions in the target site. If we were able to detect indels in target site, the CRISPR was considered efficient.

If the CRISPR cas9/gRNA injection was considered efficient, embryos were sent to nursery. Once the fishes became adults (2.5 months old), they were genotyped by fin-clip followed by gDNA extraction and PCR.

2.3 Statistical tests and analysis

All data analysis and statistical tests were performed using Graphpad prism V6.02 (Graphpad). The number of biological replicates of the experiments is indicated by the *n* number. Error bars represent the standard error of the mean (SEM). All data was analysed with a Student's t-test, one way ANOVA or two way ANOVA unless otherwise states. P values < 0.05 was considered significant. They are denoted as follows; * - $p < 0.05$, ** - $p < 0.01$, *** - $p < 0.001$.



Chapter 3 : Validation of mammalian airway epithelial cells cultured at air liquid interface as an *in vitro* model for analysing ciliogenesis

3.1 Preface

MCC beat in a coordinated and polarized manner to drive directional fluid flow across tissues and are essential for proper development and adult physiology. They are important for the function of airway, ependymal, and oviduct epithelia. Primary cells that can generate multiple motile cilia, such as mouse nasal epithelial cells (mNEC) and mouse tracheal epithelial cells (mTEC) described here, are of use since motile cilia formation is difficult to study *in vivo* and cell lines with multiciliated cells are not available. Protocols for culturing and differentiating primary airway epithelial cells from mouse nasal septum (mNEC) and trachea (mTEC) at an air-liquid interface (ALI) have been established (You et al., 2002, Antunes et al., 2007b).

mNEC and mTEC preparations generated using these protocols are valuable models to study different characteristics of airway epithelial cell differentiation and function, host response to infection, and disease pathology (Newby et al., 2007, Stubbs et al., 2012, Vladar and Brody, 2013). Vladar and Brody (2013) have shown mTECs cultured at ALI are a good *in vitro* model to study motile ciliogenesis. They are also suitable models to study specific genes and pathways from mutant or other genetically manipulated mouse strains. Several studies have shown that motile ciliogenesis in these *in vitro* culture systems can be manipulated by drug treatment (Vladar and Brody, 2013, Eenjes et al., 2018b).

The basic technique is as follows. mNEC and mTEC are isolated from mice, plated on transwells and cultured under submerged conditions for 5-7 days. Once confluent cells are transferred into ALI culture where the media is removed from the apical chamber of transwell Cells are cultured for up to 14 days when they become fully differentiated airway epithelium and can be used for functional studies as determined in previous studies using this *in vitro* model. Samples taken during this process can be used to study aspects of ciliogenesis.

In this chapter I describe how this *in vitro* model was validated as a good model to study MCC formation and function by analysing mRNA expression of epithelial cell markers by end-point RT-PCR, detection of airway epithelial secretory proteins by western blotting and visualization of the localization of airway epithelial markers by immunofluorescence microscopy. I also tested whether ciliogenesis could be modulated by drug treatment in ALI cultured model. The efficiency of siRNA transfection was also explored with the intention of modulating gene expression of putative ciliary genes.

3.2 Results

3.2.1 Culturing and differentiation of mNECs and mTECs at the ALI

The culture conditions for mTECs and mNECs were already optimised and established in our laboratory (Akram et al., 2014, Mulay, 2017). The average number of mNECs isolated was 231,250 cells per nasal septum (n=17 WT batches). The average number of mTECs isolated was 156,250 cells per trachea (n=12 WT batches). The cells were grown in the presence of ROCKi as it enhances airway epithelial basal cell proliferation (Horani et al., 2013b). A

seeding density of 30,000 cells per transwell was used for both mNEC and mTEC. The formation of a confluent monolayer was achieved within 5-7 days of seeding.

3.2.2 Transcriptional expression of airway epithelial markers during ALI culture of mNEC and mTEC

In order to validate the differentiation of mNEC and mTEC cultured at the ALI, end-point RT-PCR was carried out. This was carried out on cells at ALI day 0, (cell population of progenitor cells), ALI day 14 (expected to be a population of differentiated airway epithelial cells), the original cells taken prior to establishment of culture (representative of differentiated airway epithelial cells present in the original tissue) and fibroblasts isolated from the same mice (as an additional control).

The *Oaz1* gene is a housekeeping gene (de Jonge et al., 2007) and this was used as the control for all of the PCRs carried out. As shown in the Figure 3.1, *Oaz1* was expressed consistently in all samples including mouse fibroblasts.

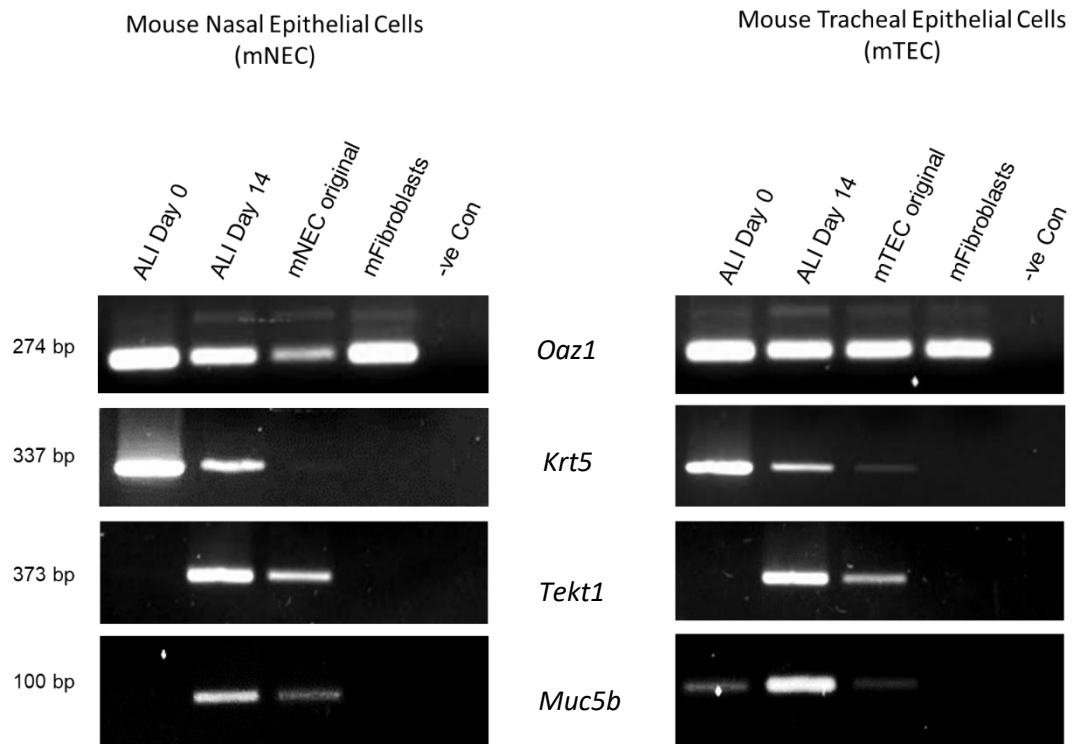


Figure 3-1 mRNA expression of airway epithelial markers during air liquid interface (ALI) of mNEC and mTEC.

End-point RT-PCR was carried out on samples collected on day 0 and day 14 of ALI cultured mNEC and mTEC to compare mRNA expression of epithelial markers and to validate that the cells have differentiated at Day 14. The original samples (org), airway epithelial cells isolated from nasal septum and trachea before plating, were used as the positive control. Fibroblasts extracted from mouse nasal septum and trachea were used as a negative control. (n=3)

Tekt1 encodes TEKT1 protein that is expressed in the axoneme of motile cilium and is required for cilia motility (Ryan et al., 2018). Therefore, *Tekt1* is a marker for ciliated cells. The expression of *Tekt1* is absent on day 0 in both mNECs and mTECs, indicating absence of ciliated cells. On day 14, expression is comparable with that in the original cells denoting presence of differentiated ciliated cells. Mouse fibroblasts cDNA was used as the negative control and absence of band as expected indicates absence of ciliated cells.

The *Muc5b* gene, encodes the secretory gel forming mucin protein MUC5B that is secreted by secretory cells of airway epithelium (Fahy and Dickey, 2010). Expression of *Muc5b* was very low on day 0 in both in both mNECs and mTECs whereas the presence of a dense band on day 14 for both mNEC and mTEC indicates the presence of more differentiated secretory cells. These results indicate our day 14 ALI cultured cells from both mNEC and mTEC show gene expression signatures consistent with mature airway epithelial cells.

The *Krt5* gene encodes KRT5 protein, a known marker of basal cells, which are considered as the progenitors of the airway epithelium (Rock et al., 2009, Zuo et al., 2015). On day 0, band intensity was highest and as expected, during cell differentiation at the ALI, the band intensity decreased by ALI day 14 in both mNECs and mTECs. This suggested that the population of basal cells at ALI day 0 has differentiated into distinct airway epithelial cell types including secretory and ciliated cells. Again, fibroblasts served as a negative control and absence of band confirms the absence of fibroblast cells in the ALI cultures.

3.2.3 Secretion of BPIFA1 during ALI culture of mTEC and mNEC

In order to further validate whether our cells differentiated in ALI culture, I compared the production of BPIFA1, a protein that is secreted by differentiated airway epithelial secretory cells (Musa et al., 2012, Akram et al., 2015, Akram et al., 2017). I carried out western blot on the apical washes of the mTEC and mNEC collected at ALI day 0 and day 14 time points by western blot. As shown in the Figure 3.2, BPIFA1 was not detected in the washes collected at ALI day 0 but a band of size between 25 kDA and 30 kDA representing BPIFA1 was detected from washes collected at ALI day 14 indicating the presence of differentiated secretory cells that secrete BPIFA1 at this time.

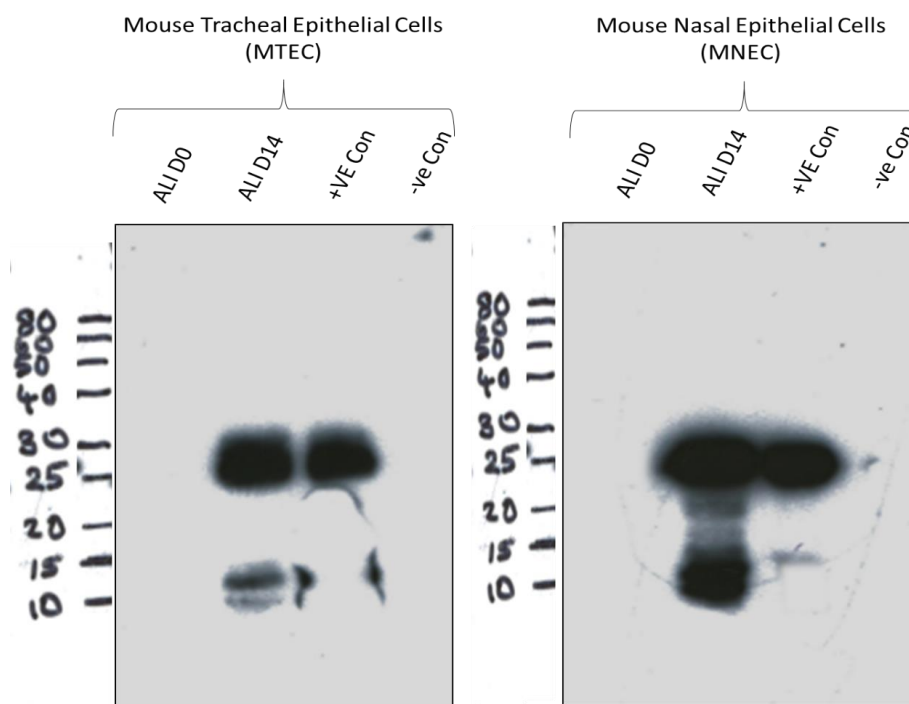


Figure 3-2. Western blot shows secretion of BPIFA1 by ALI cultures of mNEC and mTEC

BPIFA1 is a secretory protein secreted by differentiated airway secretory epithelial cells. There is no secretion of BPIFA1 in day 0 but expression is found on day 14 of ALI of both nasal and tracheal cells as denoted by bands at 25 kDA. The same volume of apical wash fluid was loaded in each lane. Positive control is WT mouse bronchoalveolar lavage fluid (Akram et al., 2017). The negative control is SDS buffer. A smaller band was also observed at 10 kD due to protein degradation (n=3).

3.2.4 Immunofluorescence microscopy of airway epithelial markers during ALI culture of mTEC and mNEC

To visualize the differentiated airway epithelial cells in the ALI culture, cells were fixed with 10% formalin and stained with various airway epithelial markers such as TP63 (basal cells), BPIFA1 (secretory cells), β -TUBULIN (Cilia) and PAN- CYTOKERATIN (epithelial cells) and DAPI (cell nuclei). The stained cells were visualized under confocal microscopy, which allows for optical sectioning in the Z-axis.

As shown in Figure 3.3 Cells were co-stained with β -tubulin that allowed us to visualise the cilia and BPIFA1 to detect secretory cells. On day 0, expression of BPIFA1 and ciliated cells were absent. On day 14, cilia projection was found on cells in both mNEC and mTEC and BPIFA1 staining was present in a different cell type.

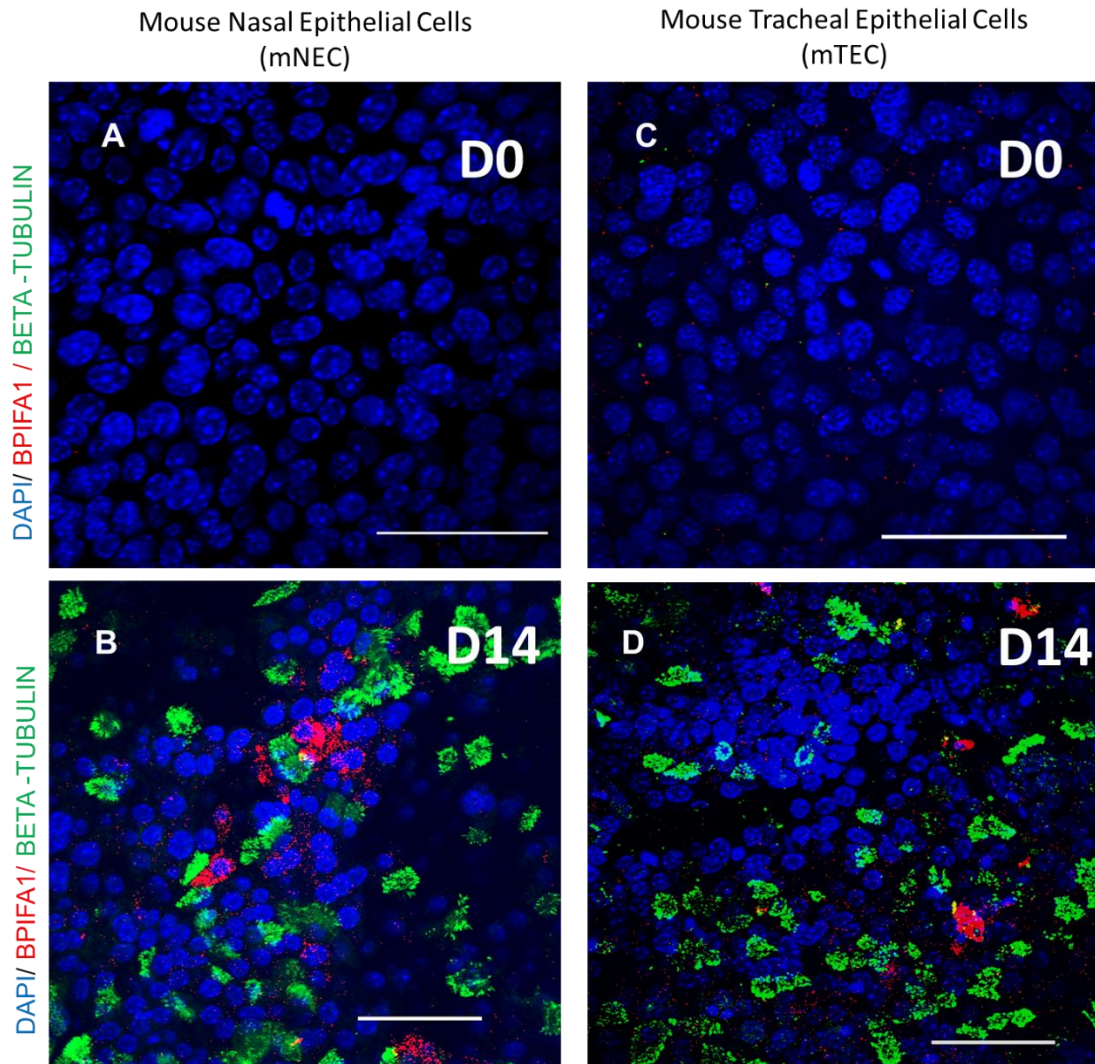


Figure 3-3. IF microscopy of differentiation of ciliated cells and secretory cells in the ALI cultured mNEC and mTEC

At ALI day 0, secretory cells that express secretory protein **BPIFA1**, and ciliated cells (**BETA-TUBULIN** staining the cilia axoneme) cannot be detected in either culture. At day 14, secretory cells that express BPIFA1 and ciliated cells that express Beta-Tubulin are seen (n=5). Scale = 50 μ m.

As shown in the Figure 3.4, when the cells were co-stained with TP63 and BPIFA1 on day 0, almost all nuclei were shown to be positive for TP63 indicating these are basal cells but BPIFA1 staining was not seen in either mNEC or mTEC cultures. In day 14 cultures, cytoplasmic BPIFA1 staining was present denoting differentiated airway secretory cells and the number of Tp63 stained nuclei were much fewer than in the day 0 cultures. This suggests that the cells had differentiated from a population of basal cells (airway progenitor cells) on day 0 to a differentiated airway epithelial cell population on day 14.

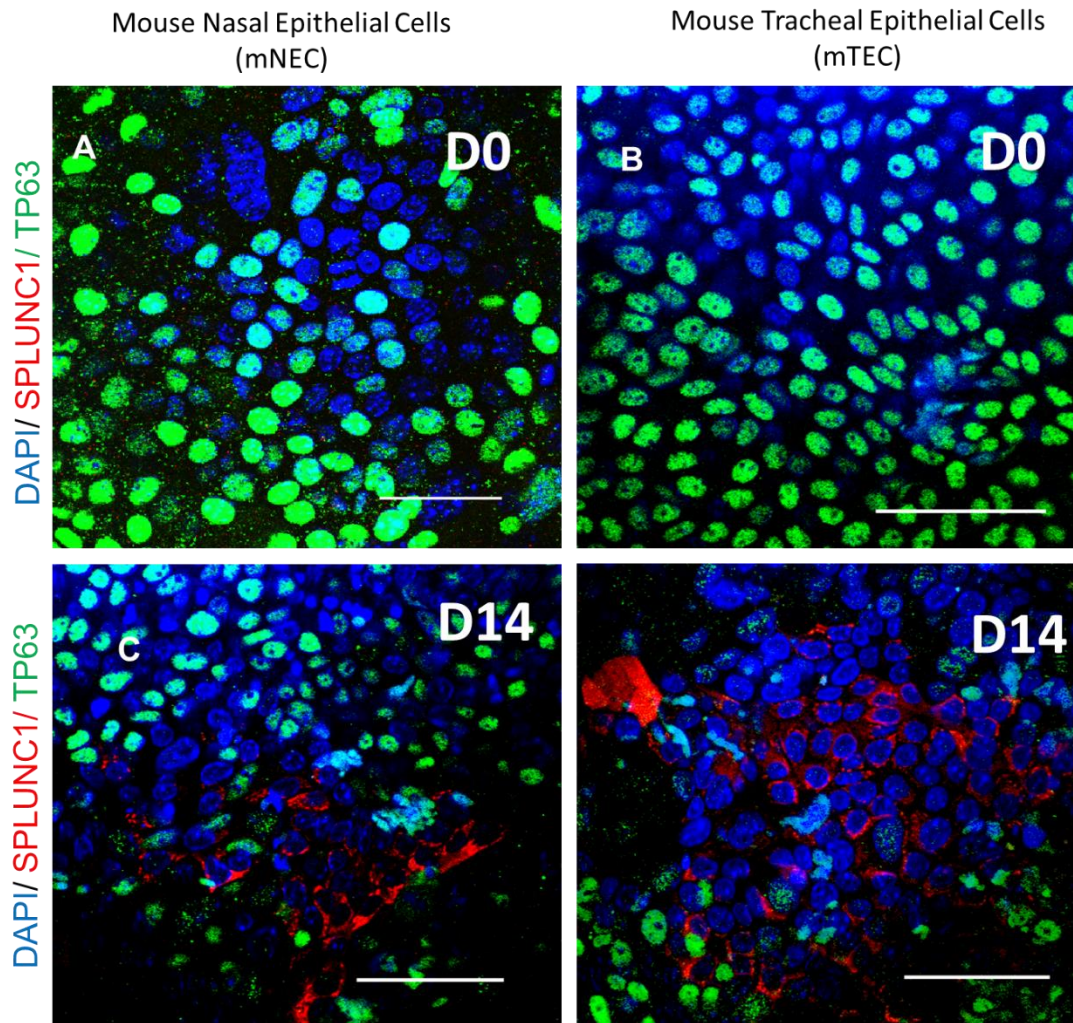


Figure 3-4. IF microscopy showing TP63 localised to basal cells during ALI culture.

At ALI day 0, most cells are found to be positive for Tp63 denoting they are airway progenitor cells. At day 14, there are fewer Tp63 positive progenitor cells and secretory cells that contain SPLUNC1 (BPIFA1) can also be seen (n=5). Scale = 50µm.

Both mNEC and mTEC cells from ALI day 14 cultures were stained for Pan-cytokeratin, marker of all epithelial cells. As shown in Figure 3.5, all the cells at ALI day 14 for both mNEC and mTEC were stained which indicates successful and efficient airway epithelial cell extraction and culture.

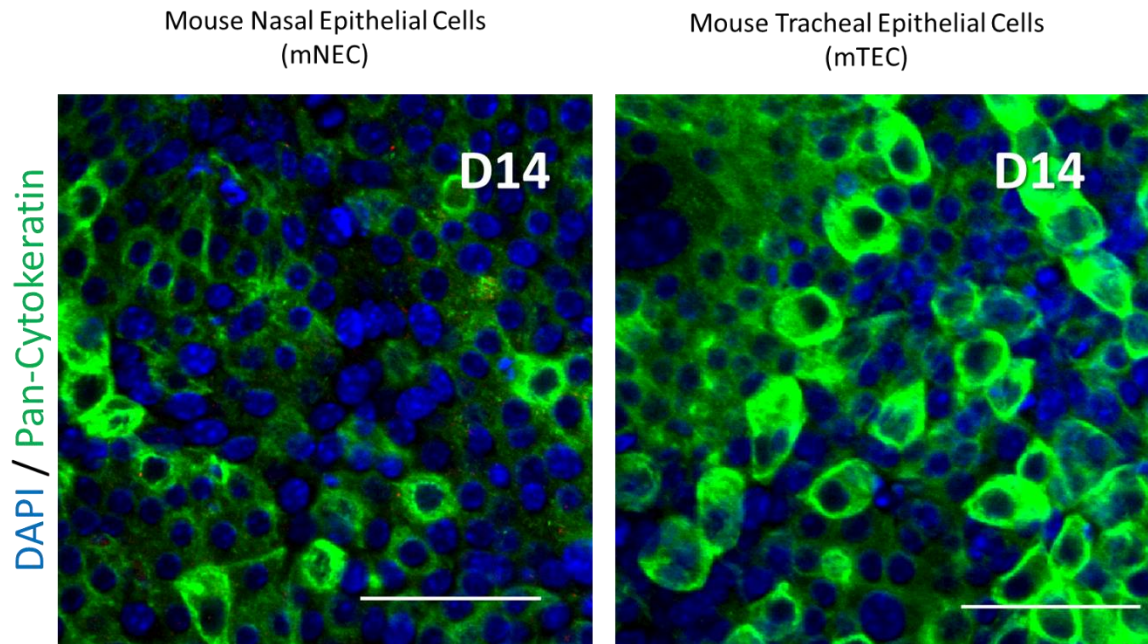


Figure 3-5. IF staining of cells with Pan-cytokeratin on differentiated airway epithelial cells.

In both mNEC and mTEC cultures all cells appear to stain for Pan-Cytokeratin, a marker for epithelial cells for (n =1). Scale = 50 μ m.

3.2.5 mRNA analysis of cilia markers during ALI differentiation of mNEC and mTEC

In order to study the expression pattern of genes known to be required for or associated with ciliogenesis during ALI differentiation, endpoint RT-PCR was carried out on cDNA collected on days 0, 2, 5, 7, and 14 of ALI culture from both mNEC and mTEC. Original cells were used as a positive control whilst fibroblast served as a negative control.

As shown in Figure 3.6, genes encoding major regulators of ciliogenesis such as *Mcidas* and *Foxj1* were expressed from day 0 and were upregulated during the differentiation of both cell types at the ALI. *Mcidas* had peak expression at day 2-5 and appeared to decrease from day 7. The peak expression for *Foxj1* was found from day 5/7. Expression of *Tekt1* was detected from day 2 and a gradual increase occurred until peak expression was observed on day 14.

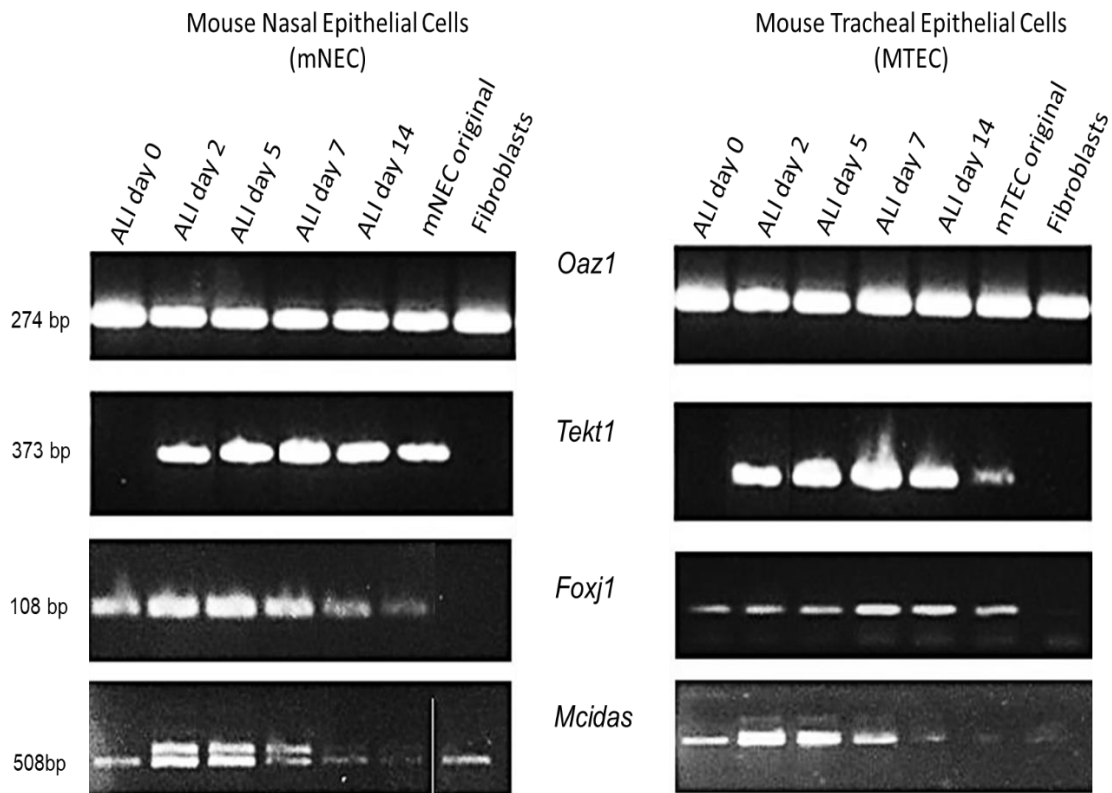


Figure 3-6. mRNA expression of genes involved in ciliogenesis during the ALI differentiation of mNEC and mTEC

End point RT-PCR was performed as described. *oaz1* is a housekeeping gene used as a positive control. *Foxj1* and *Mcidas* encode main transcription factors involved in multiciliogenesis and expression can be seen from day 0. *Tekt1* encodes structural component of cilia and transcriptional expression can be seen from day 2 of ALI culture of mNEC and mTEC. All genes involved in ciliogenesis are upregulated during the differentiation of mNEC and mTEC at ALI (n=3).

3.2.6 ALI differentiation of mNEC from *Dnah11c^{iv/iv}* mice

Next, I wanted to know whether the mNEC and mTEC cultured at ALI were able to recapitulate the functional phenotype of original cells *in situ*. To do this, we used *Dnah11c^{iv/iv}* mice. These mice harbour a missense mutation at the outer arm dynein heavy chain 11 locus (*Dnah11c*). Hence, they have immotile tracheal cilia with normal ultrastructure and reduced sperm motility. These mice exhibit gross rhinitis, sinusitis, and otitis media and therefore an excellent model of many aspects of human PCD (Lucas et al., 2012).

3.2.5.2 Identification of cilia in ALI culture of mNEC from *Dnah11c^{iv/iv}* mice

To visualize the differentiation of airway epithelial cells in WT and *Dnah11c^{iv/iv}* mNEC cells at day 14 of ALI, the cells were fixed and stained for FOXJ1 (ciliated cells) and MUC5B (secretory cells). As shown in Figure 3.7, ciliated cells (FOXJ1+) and secretory cells (MUC5B+) were detected on mNEC at ALI day 14 derived from both WT and *Dnah11c^{iv/iv}* mice. This experiment was only carried out once.

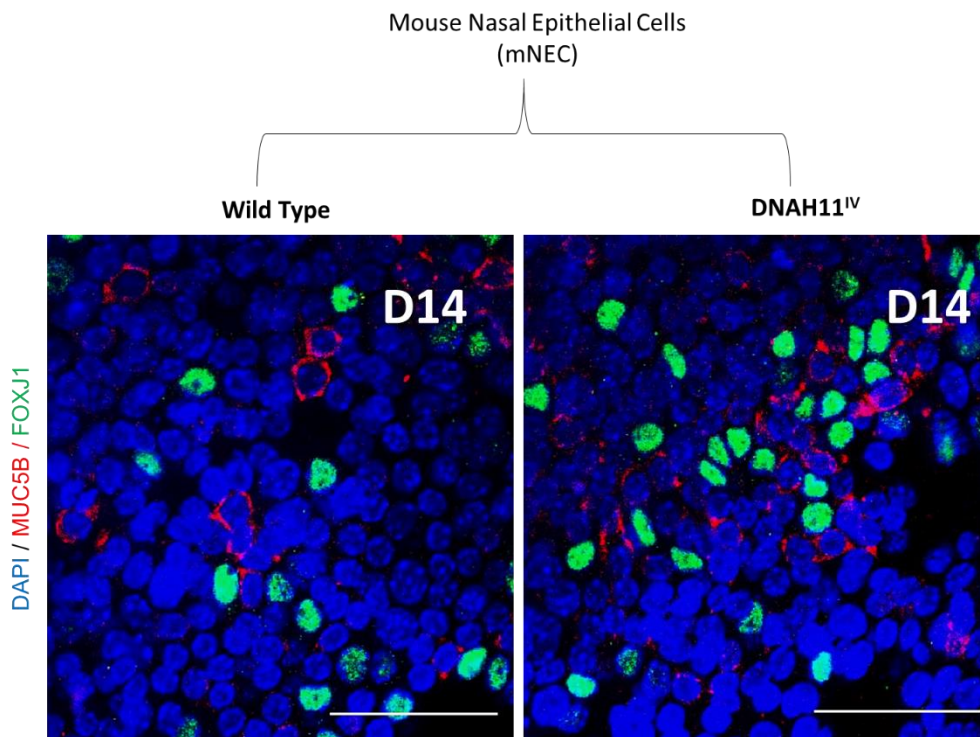


Figure 3-7. IF microscopy of differentiation of ALI cultured mNEC from and *Dnah11c^{iv/iv}* mice.

At ALI day 14, differentiation of *Dnah11c^{iv/iv}* mNEC cultures was similar to wt. Secretory cells were stained with MUC5B and ciliated cells by FOXJ1 (n=1). Scale = 50 μ m

I next wanted to test whether mNEC cells isolated from *Dnah11c^{iv/iv}* retained their cilia abnormality. These mice have immotile cilia due to a missense mutation in the dynein heavy chain gene *Dnah11c*. The IF microscopy showed that the cultures have normal ultrastructure however cilia motility was shown to be absent. This was confirmed by high-speed video microscopy of day 14 mNEC from WT and *Dnah11c^{iv/iv}* mice. Ciliary beating was visible in WT cells but absent in *Dnah11c^{iv/iv}* cells (See attached video files). This indicates that the ALI cultured cells recapitulated the morphological phenotypical characteristics of the original tissue.

3.2.7 Modulation of the number of ciliated cells with NOTCH inhibitor treatment.

Many studies have shown that the differentiation of multiciliated cells in ALI culture can be modulated by drug treatment (Pan et al., 2007b, Vladar et al., 2012, Vladar and Brody, 2013, Burke et al., 2014). Notch signalling plays an important role in the differentiation of MCCs such that cells with lower Notch signalling levels differentiate into MCCs (Deblandre et al., 1999, Tsao et al., 2009). DAPT, an inhibitor of Notch signalling, was shown to increase the number of ciliated cells in mTEC cultures (Stubbs et al., 2012, Vladar and Brody, 2013). In order to understand whether the DAPT treatment gives same results in mNEC, I treated the mNEC cells with 1mM DAPT from ALI day 0 to day 4.

IF microscopy was performed with FOXJ1 antibody and the number of FOXJ1^{+ve} cells out of DAPI stained nuclei were counted with and without DAPT treatment in 3 independent batches. FOXJ1 is a precursor for MCC and the

FOXJ1^{+ve} cell are expected to become MCCs. As shown in Figure 3.8, the results showed that the number of FOXJ1^{+ve} nuclei when normalised to DAPI stained nuclei were significantly (p-value <0.05) increased by ~2-fold in the ALI cultures treated with DAPT.

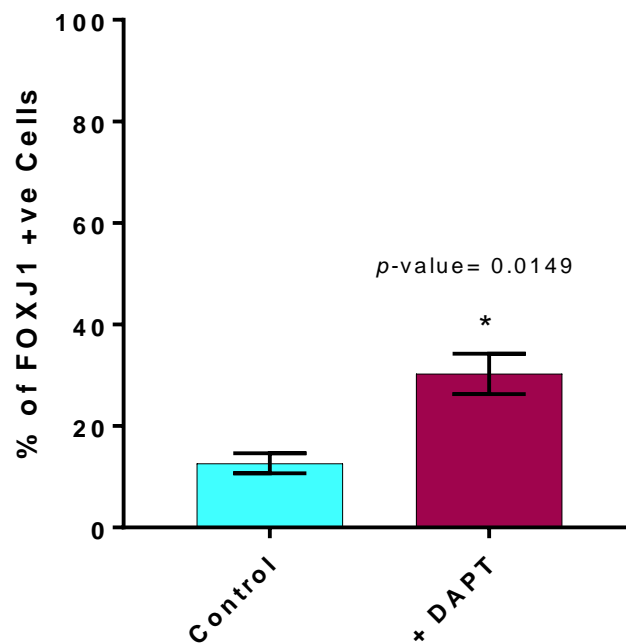
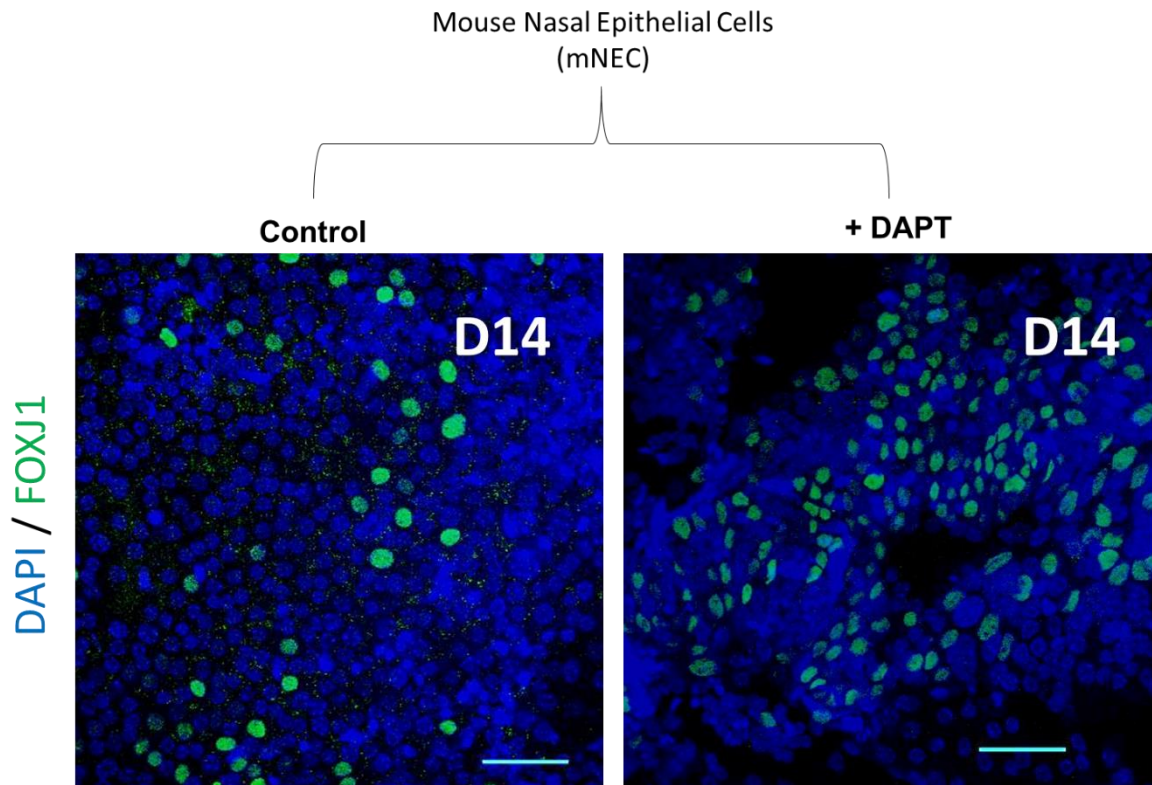


Figure 3-8. The number of ciliated cells were increased in the DAPT treated mNEC.

(A) IF microscopy was carried out on ALI day 14 of control (untreated) and DAPT^{+ve} mNEC. At day 14, there are more (~x2) FOXJ1^{+ve} cells in DAPT treated mNEC compared to the control. Error bars indicate standard error of mean (SEM) (n=3 independent batches of culture). *p<0.05 using paired t-test (two tailed). scale =50 μ m.

3.2.8 Optimizing siRNA transfection into mNEC and mTEC

Next, I wanted to test whether siRNA transfection was efficient in these primary cells. To determine optimal conditions of siRNA transfection into mNEC and mTEC cells *in vitro*, the efficiency of different Dharmacon transfection reagents and siGLO was evaluated. Different concentrations of siRNA from 25-200nM were combined with Dharmafect 1 to carry out siRNA transfection into both cells when they were 50% confluent. As shown in Figure 3.9, maximum transfection efficiency of approximately 10 to 12% was achieved using 50 nM siGLO. The transfection efficiency was assessed by eye counting under fluorescence microscope. The transfection efficiency seemed to be higher in mNEC compared to mTEC.

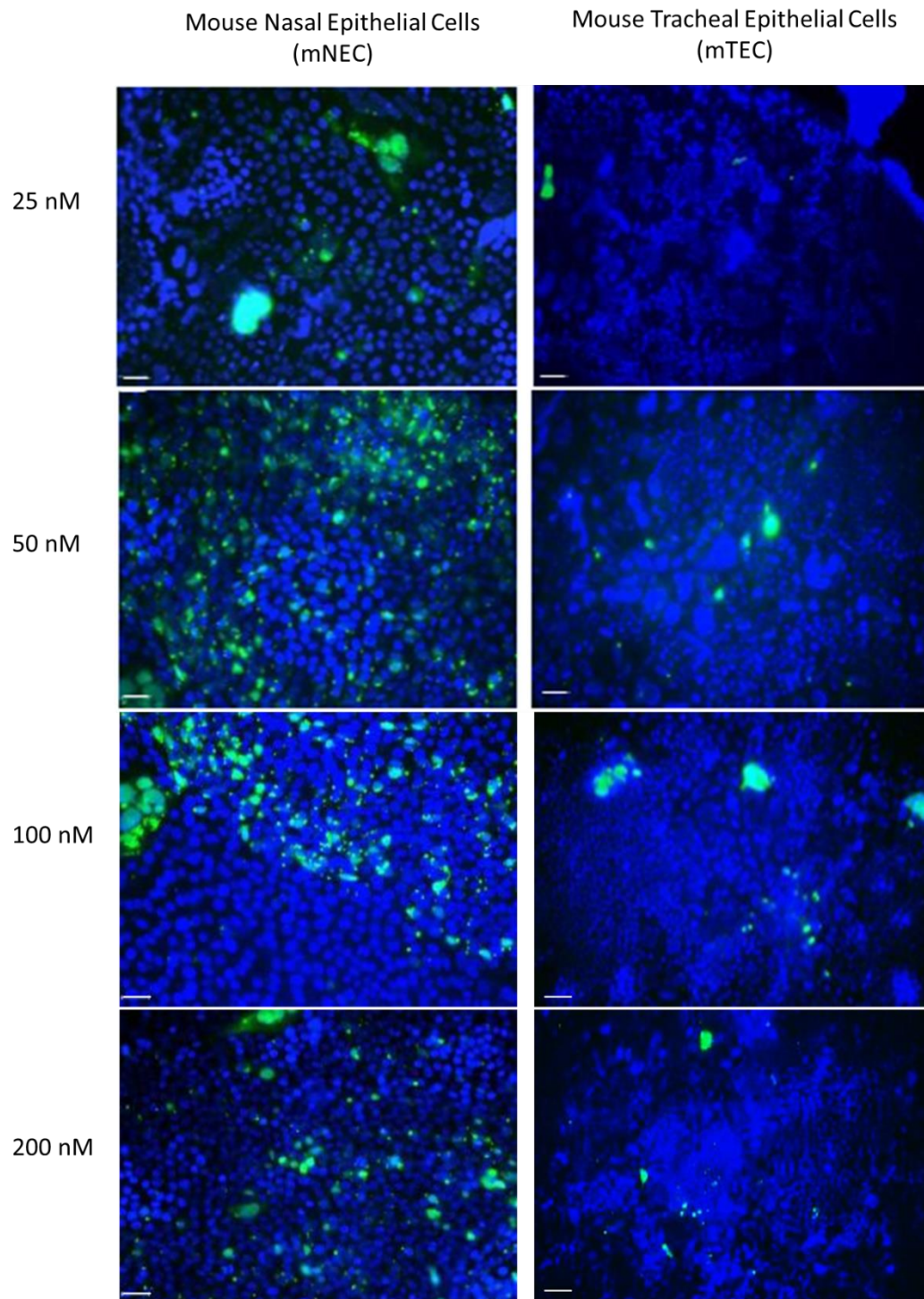


Figure 3-9. Optimizing siRNA transfection with siGLO (green, Dharmacon) in primary mouse nasal and tracheal epithelial cells.

Transfection was carried out at different concentrations; i) 25nM, ii) 50nM, iii) 100nM. iv) 200nM. Maximum transfection efficiency achieved was around 15% in mNEC cells with 50nM siGLO. Transfection efficiency was higher in mNEC compared to mTEC (n=2 independent batches of culture). (Image magnification = 20X, scale = 50µm)

I also tested Dharmacon transfection reagents Transfect 2, 3 and 4 to evaluate whether they produced a difference in transfection efficiency. As shown in Figure 3.10, higher transfection efficiency was achieved with transfection reagent 1. Lower transfection efficiency was achieved using transfect 2, 3.and 4. The transfection efficiency was assessed by eye counting under fluorescence microscope. Transfection efficiency was also shown to be variable in different batches of cells. The experiment was repeated twice.

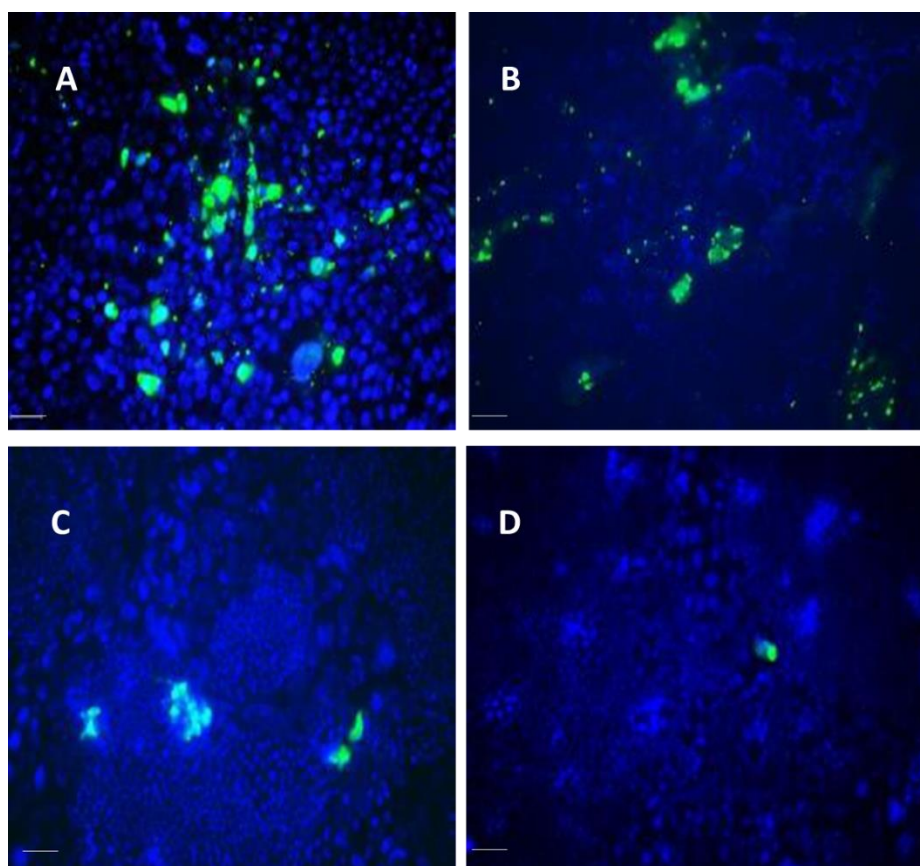


Figure 3-10. Optimizing siRNA transfection with siGLO (green, Dharmacon) using 4 different transfection reagents.

Transfection was carried out using 4 different Dharmacon reagents. Maximum transfection efficiency was achieved with transfect 1 (A). Transfect 2 (B), Transfect 3 (C) and Transfect 4 (D) had lower transfection efficiency (n=2). (Image magnification = 20X, scale = 50µm)

To attempt to improve the success of this technique, transfected wells were trypsinised and pooled together. The pooled sample was sent for cell sorting to sort transfected cells from non-transfected cells. The recovered transfected cells were then reseeded onto new collagen coated transwells and then grown in submerged culture for 7 days to allow proliferation. However, these cells did not proliferate well and did not reach confluency. I concluded that this technique may have had potential to be useful for introducing siRNA into the cells for functional work but decided that significant improvements in the technique would be required to allow this to be valuable for my work.

3.3 Discussion

In vertebrates, the functional role and morphology of multiciliated airway epithelial cells are conserved. In airways, the first line of host defence is accomplished by concerted action of multiciliated cells that drive mucus clearance (Brooks and Wallingford, 2014b, Tilley et al., 2015). Ciliary impairment and resulting mucostasis are central players in many airway disorders (Tilley et al., 2015, Brooks and Wallingford, 2014b).

PCD also known as immotile cilia syndrome is one of the most common forms of ciliopathy. It is a heterogeneous genetic disorder that arises due to mutations in many genes involved in ciliogenesis and cilia motility (Kennedy et al., 2007, Knowles et al., 2013b). Identifying novel genes involved in ciliogenesis and ciliary motility can greatly improve early PCD diagnosis (Kennedy et al., 2007, Daniels and Noone, 2015, Knowles et al., 2013b).

Recently, several high throughput studies have identified numerous genes specifically expressed in cilia and ciliogenesis (Ross et al.,

2007, Hoh et al., 2012, Choksi et al., 2014c). Characterising these genes and their function is an important step in identifying signalling pathways and mechanisms in ciliogenesis and its function that will be valuable in understanding aetiology of and finding a cure for ciliopathies.

The ALI differentiation of primary mNEC and mTEC shown here is a particularly useful model for the study of motile cilia biogenesis because it is difficult to study *in vivo* and due to the nonavailability of cell lines with multiple cilia. To appropriately model the *in vitro* airway epithelium, we replicated the ALI culture of primary mNEC and mTEC, as these cells simulate the morphological and functional characteristics of the airway epithelium (Antunes et al., 2007, Vladar and Brody, 2013). For instance, basal cells from the proximal human airway differentiate into a mucociliary pseudostratified epithelium containing ciliated, goblet and basal cells. In this *in vitro* cell culture environment, cells display beating cilia, mucus secretion, barrier properties similar to the native airway epithelium.

For my studies it was important that I could establish these cultures with both nasal and tracheal cells. I was able to show expression of the well-established airway epithelial markers *Muc5b*, *Tekt1*, and *Krt5* indicating that cultures contained the secretory cells, ciliated cells and basal cells present in airway epithelium. The absence of *Muc5b* and *Tekt1* in day 0 and expression on day 14 indicated that the cells differentiated successfully during the 14-day ALI culture period. The downregulation of *Krt5* from day 0 to day 14 suggested that the number of progenitor cells decreased but the presence of *Krt5* on day 14 indicated that a population of progenitor basal cells were maintained throughout the culture period.

It was important to test that the differentiated epithelium was capable of secreting proteins onto the apical surface. I was able to show this by western blotting apical washes from the abundant secretory protein BPIFA1. *BPIFA1* has been reported to be one of the most highly expressed genes in differentiated ALI cultures (Ross et al., 2007). It has also previously been shown to be a major secretory product from both mouse (Akram et al., 2017) and human cells (Campos et al 2004). My cultures showed the presence of BPIFA1 in apical washes collected from day 14 ALI cultures of both mNEC and mTEC which confirming the presence of functional secretory cells in the cultures. As expected BPIFA1 was absent from washes of undifferentiated cells.

Using IF microscopy with a range of airway epithelial markers such including TP63, BPIFA1, β -TUBULIN and Pan-Cytokeratin it was clear to see that the cultures showed a distribution of different cell types including basal cells, secretory cells and ciliated cells. Consistent with the *Krt5* expression data and as we expected, the number of basal cells was lower in the differentiated ALI day 14 cells compared to the undifferentiated ALI day 0 cells.

Several studies have investigated the process of ciliogenesis during mTEC differentiation. For example, Vladar and Brody described distinct stages of multiciliogenesis in ALI culture of primary mouse tracheal epithelial cells (Vladar and Brody, 2013). Here, we similarly used RT-PCR to analyse the mRNA levels of genes encoding some of the main regulators and protein components of cilia structure. Our results revealed that the mRNA transcripts for ciliogenesis regulators such as *Mcidas* and *Foxj1* were detectable from day 0 of the ALI culture. Previous studies revealed MCIDAS functions upstream of

FOXJ1 (Tan et al., 2013, Takahashi et al., 2015) and in our culture model the peak expression appears on day 2, while peak expression of FOXJ1 was on day 5-14. Since the endpoint RT PCR is only semi-quantitative, it showed variability. Therefore, our culture model appears to agree with the findings from previous studies. Since, FOXJ1 is a specific marker for ciliated cells (Yu et al., 2008) we can presume the cell fate decision is made prior to the induction of differentiation through the ALI culture process. However, the translation only appears to start after inducing ALI as the protein was absent from our day 0 IF analysis. You *et al* showed expression of *foxj1* from day 2 in ALI culture of mTEC (You et al., 2004b). This suggests that the transcription of the main regulators involved in ciliogenesis start before the induction of ALI differentiation of the culture in mouse cells. This could potentially be induced through paracrine signalling as the cells reach confluency. The transcript of a gene encoding a protein component of cilia, *Tekt1*, appeared from day 2 of ALI culture followed by the induction of the regulators.

In this study I used endpoint RT-PCR which may have limited the sensitivity of transcript detection. This method is semi-quantitative and hence not efficient for absolute quantification and more quantitative data could have been generated using qPCR. I carried out these experiments in 2014-2015 and very similar results were shown by the RNA sequencing studies undertaken on differentiating mTEC cultures (Nemajerova et al., 2016c). Comparison with all other data does confirm that our model was suitable to test and analyse the expression of potential candidate genes involved in ciliogenesis.

I also had the opportunity to grow mNEC cells from *Dnah11c^{iv/iv}* mice that harbour a missense mutation in dynein heavy chain gene DNAH11 and hence show immotile cilia with normal ultrastructure. These animals display a variety of disorders such as gross rhinitis, sinusitis, and otitis media and are considered to be a model of many aspects of human PCD (Lucas et al., 2012). I used these mice to confirm that the defect in cilia function was maintained *ex vivo* when the cells were established in ALI cultures. Time-lapse imaging confirmed that ciliary beating was absent in mNEC from *Dnah11c^{iv/iv}* mice but present in the WT cultures. This therefore confirmed that the cells cultured at ALI recapitulated the characteristics of original cells derived from the tissue. Recently, cells derived from potential PCD patients cultured at ALI have been utilised as useful aid in diagnosing PCD (Hirst et al., 2014, Shapiro et al., 2018).

Many studies have successfully modulated the process of ciliogenesis in mTEC by treatment of different drugs. Nocadazole and Taxol have been used by several groups to arrest ciliogenesis by inhibiting centriole assembly (Vladar et al., 2012, Vladar and Brody, 2013, Burke et al., 2014). Likewise, DAPT, a known NOTCH inhibitor has been used to increase the number of ciliated cells in mTEC (Stubbs et al., 2012, Vladar and Brody, 2013). For my further work I needed to ensure that I could modulate ciliated cell numbers in my cultures. So, I treated mNEC with DAPT. Consistent with results from previous studies performed on mTEC, the number of the ciliated cells was significantly increased in the mNECs. The ability to modulate ciliogenesis in this cell culture model is a very useful tool since it allows assessment of whether expression of putative ciliary genes correlates with the presence and absence of ciliated cells. Such

modulation would also be a useful model to study the functional role of cilia when it comes to studies of host pathogen interactions.

Another way of potentially modulating ciliogenesis would be by genetically modulating the level of specific genes. As yet we have not undertaken this type of work in our group. In this study, I attempted to test whether siRNA transfection was an efficient tool in our primary mTEC and mNEC ALI culture. My plan was to use this to modulate expression of my novel candidate genes. To do this, siGLO (Dharmacon) was transfected to mNEC and mTEC cells when they were 50% confluent on submerged culture using Dharmafect transfection reagents (transfect 1, 2, 3, 4). siGLO (Dharmacon) is a fluorescent oligonucleotide duplex that restricts to the nucleus, thus concentrating its signal to permit explicit visual assessment of transfection efficiency. However, maximum transfection efficiency that I achieved was only around 10-12%. Transfection efficiency did appear to be higher in mNEC compared to mTEC, which may point out difference in the biophysical properties of cells obtained from two different niches. Consistent with the manufacturer's notes, cell toxicity was not observed during these studies confirming that these transfection reagents had limited toxicity in the primary cells. Previous studies have reported difficulties in delivering siRNA into well differentiated epithelial cells (Griesenbach et al., 2006). This is thought to be due to the high molecular weight and polyanionic nature of siRNA that makes it difficult to cross the epithelial cell membrane freely. Pseudostratified epithelium presents significant barriers such as airway secretions, physical barriers and host defence mechanisms to the delivery of nucleic acid (Griesenbach et al., 2006, Ramachandran et al., 2013) Thus,

we decided to attempt to transfect cells when they were in submerged culture and proliferating since we thought actively proliferating cells might be more susceptible to nucleic acid uptake. Also we needed to establish a method that might allow use to repress gene expression in the early phases of ciliogenesis in the differentiating cultures. My results were not as useful as I had anticipated. Previous studies have reported tight junctions that prevent paracellular passage of molecules, are present within one day of seeding (Ramachandran et al., 2013). Furthermore, I could not be certain whether I had a homogenous population of a basal cells before inducing ALI and so cell make up could have differed which could partially explain the variability seen in transfections. Ramachandran et al described “reverse transfection “as an efficient method for the delivery of RNA interference oligonucleotides to polarised pig airway epithelial cell in *in vitro*”. In this method, siRNA-reagent complexes are added at the time of seeding as opposed to standard transfection in which transfection is done on the pre-plated cells. However, they recommended using a high seeding density of 150,000 cells (Ramachandran et al., 2013). Since, I used mouse models, my seeding density was about 30000 cells. The cell yields I obtained per mouse nasal septum and trachea ranged from 100,000-230,000 cells. Therefore, the reverse transfection seemed inefficient and impractical for my studies. I also attempted to sort transfected cells and grow them to confluency. However, my results showed that cell proliferation after FACS was not achieved. This suggests that the primary cells did not tolerate the FACS procedure following transfection.

Multiple studies have successfully utilised lentivirus infection to modulate gene expression in mTEC (Vladar and Stearns, 2007, Horani et al., 2013b,

Marshall et al., 2016). This technique has not been established in our laboratory and therefore in the interest of time, I decided not to proceed with modulating gene expression in ALI cultured cells.

In conclusion, I was able to establish mNEC and mTEC cultured at the ALI and show that they are a good *in vitro* model to study the formation and function of multiciliated cells in the airway epithelium. The experiments presented here and by other groups, show that this cell culture model facilitates the characterisation of novel ciliogenesis regulators and the assessment of cilia formation and function. To continue to utilise this model more efficiently in the future, further enhancement of current techniques and development of additional methodologies may be necessary. The main improvements can be focused on attaining larger cultures volumes, formulating methods to passage cells without loss of differentiation potential and adapting culture vessels for high-throughput screening.

Chapter 4 : Selecting potential novel candidate genes associated with ciliogenesis

4.1 Preface

This chapter describes analysis of data from high throughput studies to select potential novel candidate genes associated with the process of ciliogenesis.

Many of the genes and signaling pathways involved in the formation and function of motile cilia are still not completely resolved. This poses many challenges when it comes to diagnosing heterogeneous genetic disorders such as PCD, (Knowles et al., 2013a). One of the key goals in ciliary research is to identify novel molecular constituents of the cilium. A series of high throughput genomic and proteomic screens have identified multiple genes, thought to be involved in the formation and function of the cilium (Ostrowski et al., 2002a, Ross et al., 2007, Geremek et al., 2011, Hoh et al., 2012, Choksi et al., 2014b).

A common feature of these studies is that they identify hundreds of genes. These studies have identified a few genes with direct relevance to human ciliopathies. However, nothing much can be inferred about many of the genes revealed by these studies.

The main aim of this research project was to functionally characterize novel ciliary genes using an *in vitro* model, murine airway epithelial cells cultured at an ALI and an *in vivo* vertebrate model, using zebrafish embryos. In order to select candidate genes for the study, I reviewed the data generated by Hoh *et al* on the transcriptional profile of multiciliated cells in culture (Hoh et al., 2012). They used the same *in vitro* model (mouse airway epithelial cells cultured at ALI) I was using for my studies, to generate this data.

Hoh *et al* determined the transcriptional profile of multiciliated cells during the mucociliary differentiation of mouse tracheal epithelial cells at ALI culture (Hoh et al., 2012). In the study, the mouse tracheal epithelial cells for the differentiation in the *in vitro* culture, were derived from mice expressing GFP from the ciliated-cell specific *Foxj1* promoter (*Foxj1*: GFP). The differentially expressed genes in ciliating (GFP+) cells from these cultures were characterized at an early and a late time point during differentiation. They were filtered by removal of the profile of the non-ciliated GFP- cells. This study identified ~650 genes that were upregulated during the early phase of ciliogenesis, during the formation and replication of basal bodies, and ~80 genes that were upregulated during a later timepoint, after cilia were fully formed (Hoh et al., 2012).

The data generated by Hoh *et al*, had identified many known ciliary genes as well as many uncharacterized genes that were not previously identified as ciliary genes culture (Hoh et al., 2012). Therefore, I chose the top 10 most differentially expressed (between FOXJ1^{+ve} and FOXJ1^{-ve} cells) uncharacterized genes for further assessment on their potential association with motile ciliogenesis.

To select a candidate gene for further characterization, I proposed that we would select one out of the selected 10 genes that would show enriched expression in motile ciliated tissues, specifically localisation to ciliated cells, show differential expression during differentiation of mNECs and have also been identified in other high throughput screens for ciliary genes done in more than 2 organisms.

Several online databases like Cildb, Human Protein Atlas, bioGPS and LungGens were used to gather information needed for selecting a good candidate. In addition, expression of these genes were analyzed using endpoint RT-PCR using RNA from mNEC differentiated at the ALI, where most of them showed differential expression like other genes known to be involved in ciliogenesis. Expression of these genes was also analyzed in different mouse tissues and some of them were found to be enriched in tissues containing abundant motile cilia. The proposal for selecting a candidate gene for further characterization of its role in motile ciliogenesis is summarized in following flow chart.

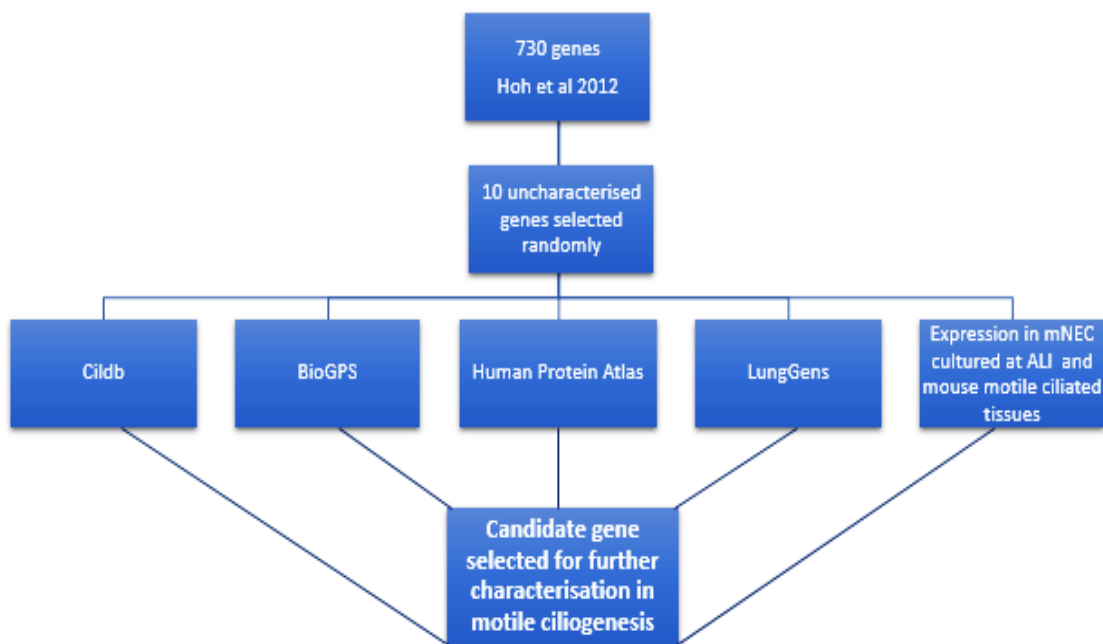


Figure 4-1 A flowchart for the selection process of candidate gene.

There is little information on these genes in the literature. It seems likely that functionally characterizing the role of these genes in cilia formation or function may unravel novel pathways and mechanisms that are linked to the process of ciliogenesis.

4.2 Results

Cildb (<http://cildb.cgm.cnrs-gif.fr>), a knowledge database that incorporates ciliary data from various sources, was used to see if these genes or any of their orthologues had been identified in ciliary screens undertaken other organisms. Cildb links orthology relationships among 44 species (44 eukaryotes and 3 bacteria) to high throughput ciliary studies (Arnaiz et al., 2009, Arnaiz, 2014). The selected candidate genes and the ciliary screens that have identified them as shown in Cildb are shown in Table 4.1.

Table 4-1. Novel cilia candidate genes

Gene / Accession	Accession	Studies	Gene Ontology (Biological function)
<i>RIKEN cDNA 1700007K13 (Pierce1)</i>	NM_027040	4,5,7,8,10,13	N/A
<i>RIKEN cDNA 1700013F07 (C1orf194 homolog)</i>	XM_131080	2, 4, 5, 6, 7, 12, 13,14	N/A
<i>RIKEN cDNA 1700001L19 (C5orf49 homolog)</i>	XM_127414	1,2,3,4,7,9,10,13	N/A
<i>RIKEN cDNA 4833427G06 (C11orf88 homolog)</i>	NM_177702	4, 5,13	Skeletal muscle fibre development
<i>Lrrc4b</i>	NM_177656	1,4,5,8,9,13	Negative regulation of protein kinase activity, Cytokine-mediated signalling pathway, Negative regulation of JAK-STAT cascade, Positive regulation of synapse assembly
<i>RIKEN cDNA 1700028P14 (C9orf35 homolog)</i>	NM_026188	1,4,5, 7,10,11	N/A
<i>Maats1</i>	XM_489540	1,4,5, 6,7,10,13	N/A
<i>Erich2</i>	NM_025744	4,5	N/A
<i>Spata24</i>	NM_027733	4,5	Transcription, DNA-templated, Spermatogenesis, Cell differentiation
<i>RIKEN cDNA 1110017D15 (Cbe1)</i>	NM_001048005	4,5,7,8	Spermatogenesis, Cell differentiation

1- McClintock et al. 2008, 2- Baker et al. 2008 ,3- Guo et al. 2010, 4- Hoh et al.,2012 ,5- Treutlein B. 2014,6- Ostrowski et al. 2002 ,7- Ross et al. 2007,8- Geremek et al. 2010 ,9- Datta et al. 2011, 10- Ivliev et al. 2012,11- Geremek et al. 2014, 12- Baker et al. 2008 13- Choksi et al.2014 14. Nakachi et al. 2011

■ Mouse ■ Human ■ Rat ■ Zebrafish

4.2.1 Expression levels of selected cilia candidate genes during mucociliary differentiation at ALI culture

To study the expression of these genes during ciliogenesis, I used end-point RT-PCR to study the transcriptional expression of the selected candidate genes during the mucociliary differentiation of mNEC cultured at the Air Liquid Interface (ALI). Original cells (from the primary isolation) were used as a positive control. *Oaz1* was used as positive control in this experiment. The negative control was dH₂O.

All the selected genes were shown to be differentially expressed during establishment of the ALI culture, implying that these genes are temporarily associated with the process of mucociliary differentiation as shown in Figure 4.1. Although, all the genes were upregulated during the ALI differentiation the pattern of expression was slightly different for each. *Pierce1*, *C11orf88 Homolog*, *Lrrc4b*, *C9orf135 Homolog*, *Maats1*, *Spata24* and *Cbe1* were all observed from day 0 to day 14 at ALI. The peak expression was observed from day 5 to day 14, as denoted by the band density. For *Spata24*, the peak expression was observed from day 2 to day 14. This pattern corresponds to expression of ciliary transcriptional regulators such as *Foxj1* and *Mcidas* (Chapter 3).

Expression of *C1orf194 homolog* and *Erich2* was observed from day 2 to day 14 of ALI. The peak expression was observed on day 14. This pattern corresponds to expression of genes encoding cilia structural components such as *Tekt1* (Chapter 3). Expression of *C5orf49 homolog* was only observed from day 5 to day 14 at ALI.

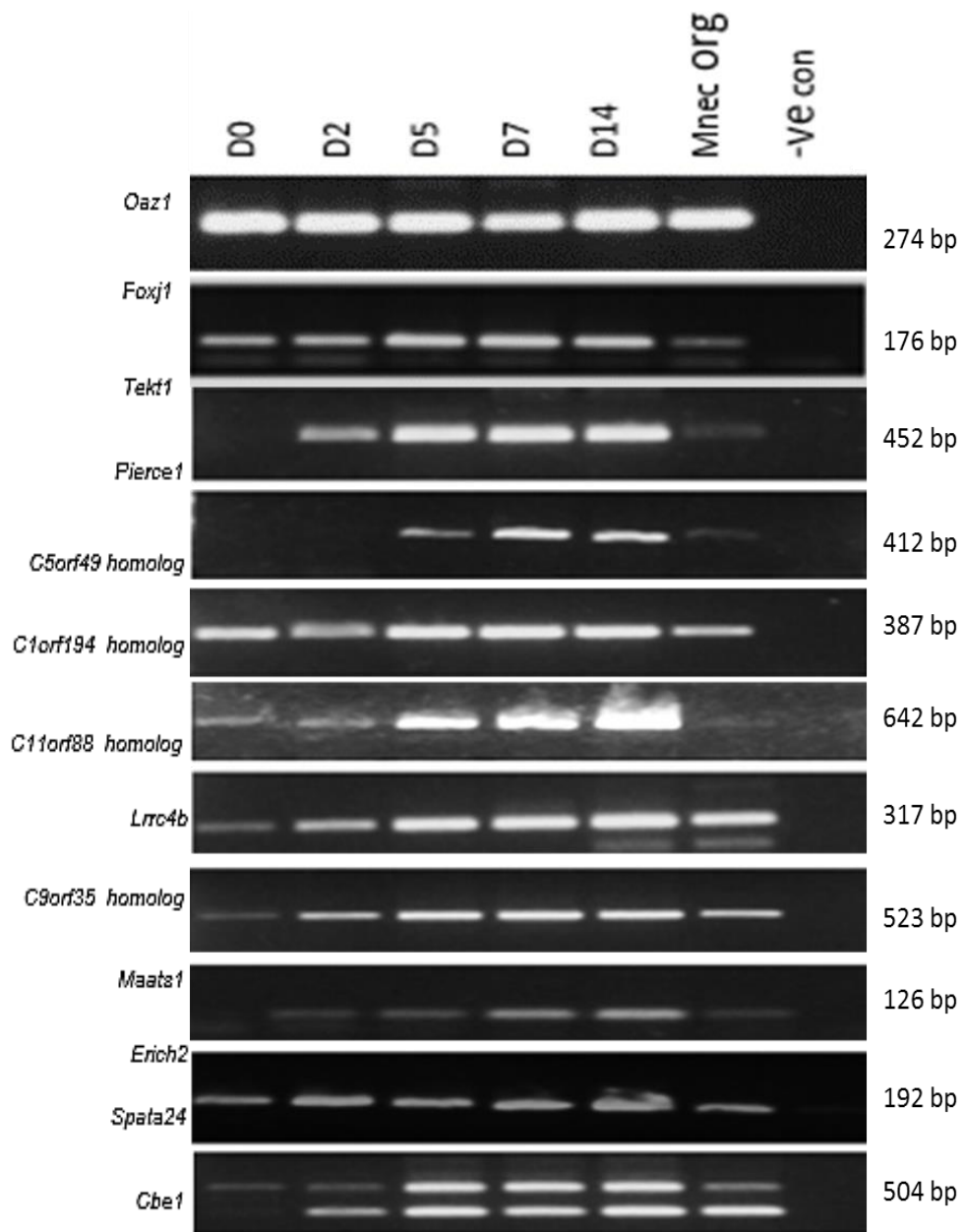


Figure 4-2 Expression of putative ciliary genes at different time-points in ALI culture of mNEC.

RT-PCR was performed as described in the materials and methods section using primers to the ten putative cilia genes. *Oaz1* was used as a positive control (n=1).

4.3.2 Expression of the cilia candidate genes in mouse tissues

Next, expression of the candidate genes in a range of whole mouse tissues was investigated alongside several known cilia genes. Within these tissues abundant motile cilia are found in lung, embryo, testes, brain and ovary. As shown in Figure 4.2, *Foxj1* and *Tekt1* were expressed only in tissues associated with motile cilia.

Like *Foxj1* and *Tekt1*, *Pierce1*, *C1orf194 homolog*, *C5orf49 homolog*, *C9orf135 homolog* and *Cbe1* also exhibited expression in the tissues associated with motile cilia. Some of the genes were expressed in a few of the tissues associated with motile cilia tissues, *Lrrc4b*, *Maats1*, *Erich2* and *Spata24*. In contrast *C11orf88 homolog* was observed to be expressed in all tissues essentially equally.

Having provided some evidence that these genes may be associated with the process of ciliogenesis, the next section outlines more details of each individual gene.

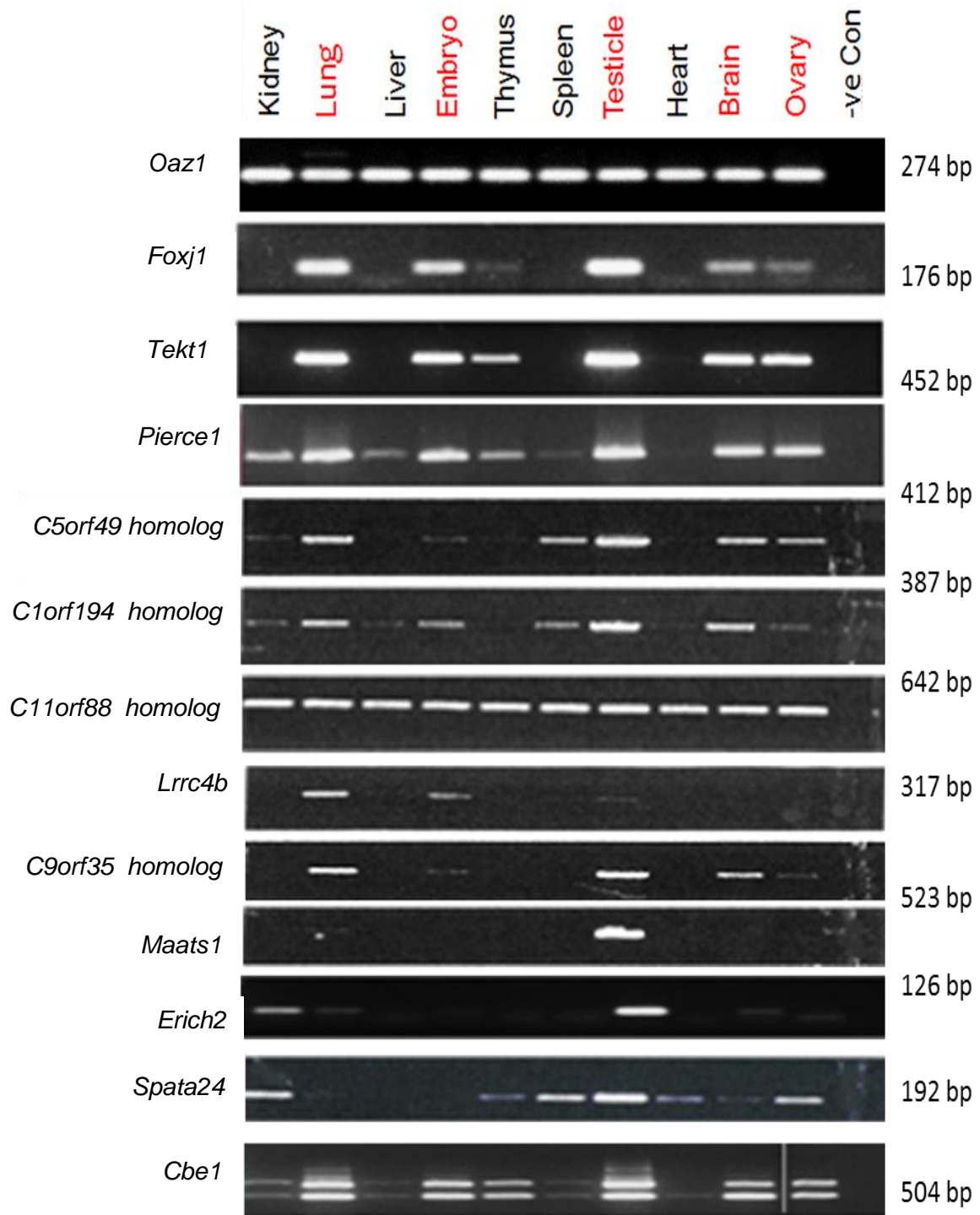


Figure 4-3 Expression of novel candidate genes in whole mouse tissues.

RT-PCR was performed as described in the materials and methods section. (n=1). Tissues with abundant motile cilia are highlighted in red.

4.3.3 *Pierce1* (P53-Induced Expression in RB-Null Cells 1)

PIERCE1 was first identified as a target of TP53 and was also found to be upregulated in retinoblastoma (RB) protein deficient mouse embryonic fibroblasts (Sung et al., 2007, Sung et al., 2010). *Pierce1* has been mapped on to Chromosome 2, 19.38 cM, cytoband A3 in mouse and the gene encodes a protein of 169 amino acids. The human orthologue is known as *C9ORF116*.

As shown in Table 4.1, *Pierce1* was identified in ciliary gene screens performed on mouse airway epithelial cells (Hoh et al., 2012, Treutlein et al., 2014a) and was identified as being expressed in ciliated cells. In addition, the study of human airway epithelial cells cultured at the ALI (Ross et al., 2007) and studies on PCD patient samples (Geremek et al., 2011, Geremek et al., 2014) also identified *PIERCE1* as a putative ciliary gene. PIERCE1 was also identified in a proteomic study of human ciliated tissues, with expression in epithelia of the oviduct and lung (Ivliev et al., 2012). *pierce1* was also found to be a downstream target of FOXJ1 in zebrafish (Choksi et al., 2014c).

In humans, *PIERCE1* encodes for a protein of 136 amino acids with a predicted molecular mass of 15.26 kDa. Multi-alignment analysis with Blastp and Clustal X indicates that PIERCE1 shares a high identity with orthologues in other species, with the highest identity of 100 % to chimpanzee, 78% identity to mouse, 54% identity to frogs and 44% identity to zebrafish (See Appendix 5.1). They share a common predicted domain of unknown function, DUF4490, which spans 39 to 137 amino acids in the human protein. In addition, the chimpanzee PIERCE1 orthologue is predicted to contain a domain of Atrophin-

1 superfamily, from 25 to 108 amino acids, that is not found in other orthologues.

Analysis of the Biology Gene Portal System (BioGPS) microarray data set (expression in different mouse tissues, *Dataset: GeneAtlas GNF1M, gcrma*), suggests that *Pierce1* is abundantly expressed in tissues with motile cilia, such as nasal septum, the main olfactory epithelium (MOE), trachea, lung and testis (Figure 4.3). The graphs from bioGPS presented in this chapter are from public data therefore it is not reliable to use as a standalone evidence.

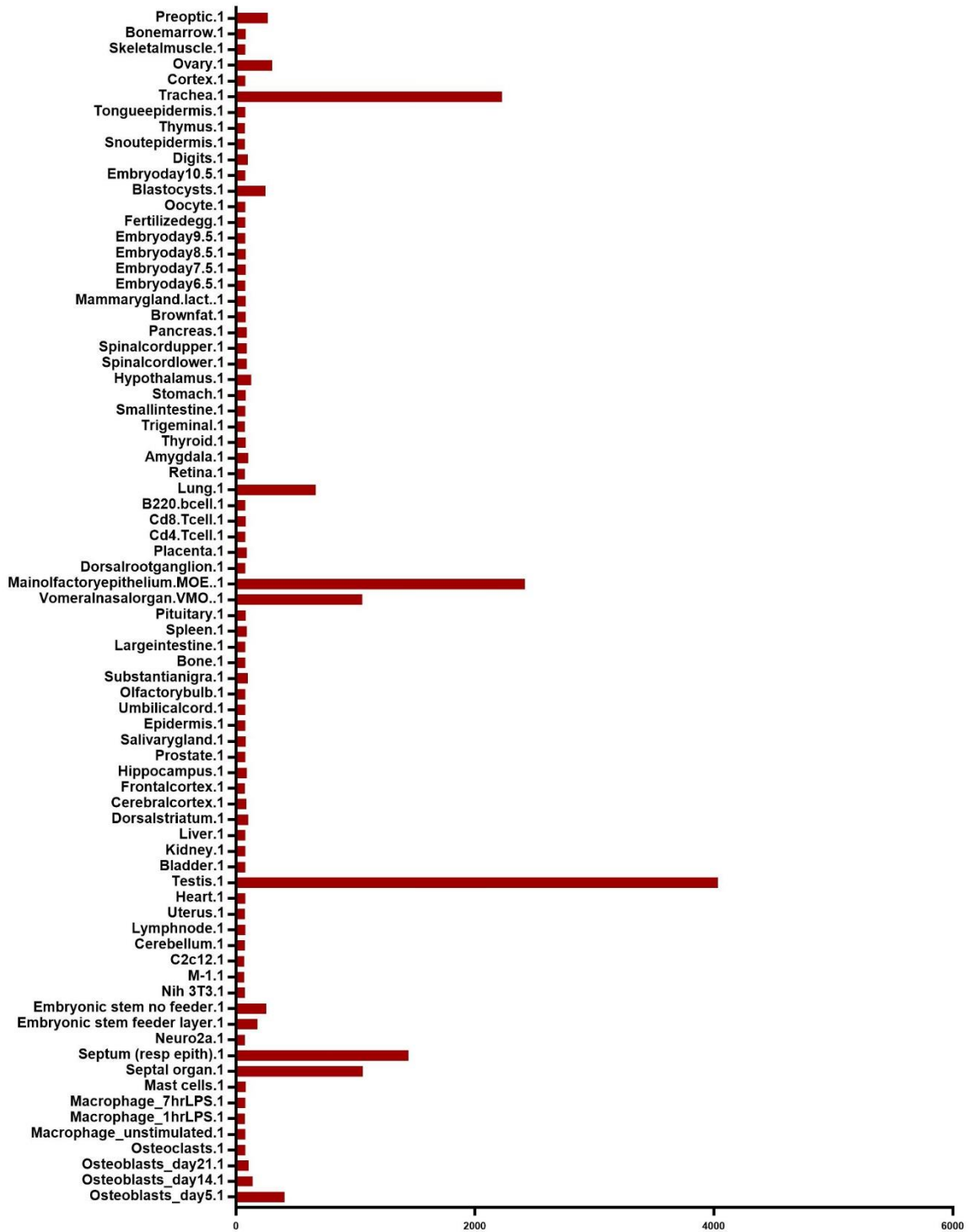


Figure 4-4. *Pierce1* expression in mouse tissues based on the BioGPS database.
 (Dataset: GeneAtlas GNF1M, gcrma; Probeset: gnf1m29796_a_at)
<http://biogps.org/#goto=genereport&id=69327>

The localisation of PIERCE1 was investigated by analysis of protein-level immunostaining data from the Human Protein Atlas – a large-scale antibody-based resource examining protein expression in human tissues. The immunostaining images from airways and fallopian tubes were analysed and data for FOXJ1 was used as the positive control. PIERCE1 is seen to be enriched in ciliated cells in the airway epithelium and in the fallopian tube. It appears that the protein is in both the cytoplasm and axoneme of ciliated cells (Figure 4.4).

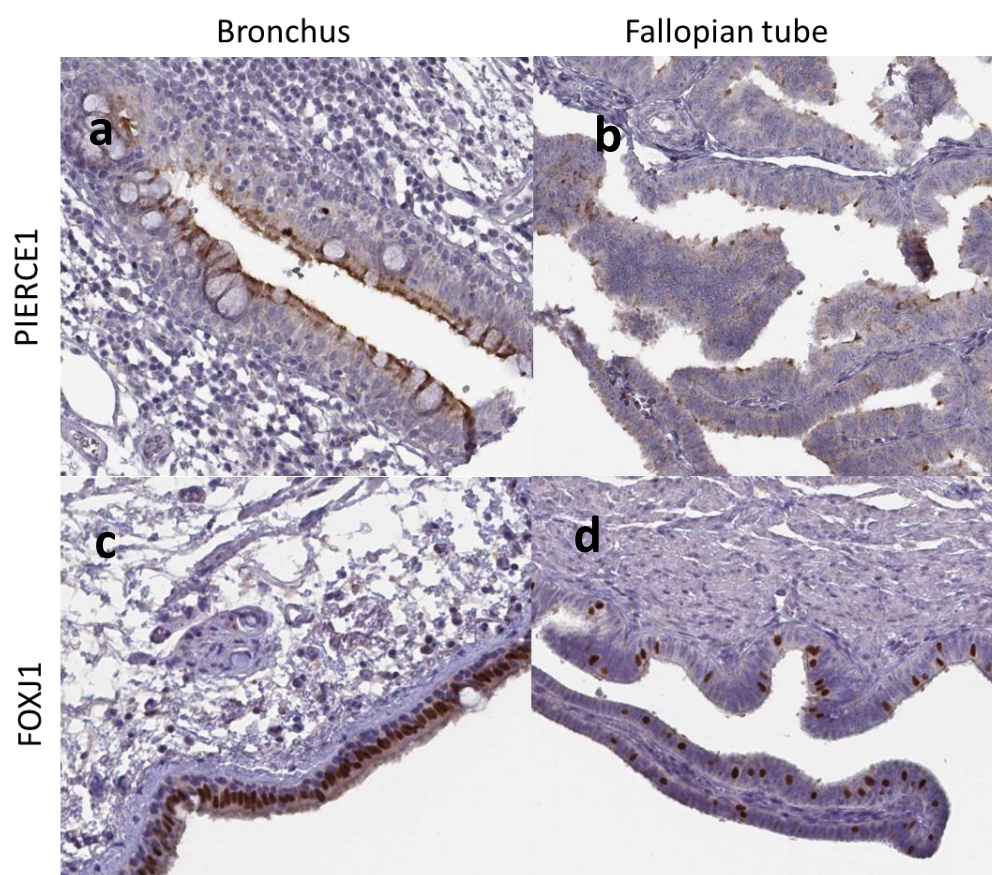


Figure 4-5. Localisation of PIERCE1 in motile ciliated tissues.

The images were attained by immunohistochemical staining of bronchus and fallopian tubes with protein-specific antibodies in the Protein Atlas project (Uhlen et al., 2010). The antibodies were against the following proteins: PIERCE1 (a,b), FOXJ1 (c,d). The antibody-based staining is shown in brown and staining of nuclei with DAPI in blue. The airways ciliated cells form a continuous layer, while in fallopian tubes they are separated from each other by non-ciliated epithelial cells.

Together these data, and the identification of this gene in several other cilia genomic and proteomic screens, suggest that *PIERCE1* may have a conserved functional role in motile ciliogenesis.

4.3.4 RIKEN cDNA 1700013F07

RIKEN cDNA 1700013F07 is mapped to chromosome 3 in the mouse and encodes a protein of 168 amino acids. The human orthologue is called C1ORF194, an uncharacterised protein. It was identified in the ciliary genes screens undertaken by Ross et al (2007), Hoh et al (2012) and Choksi et al (2014). Analysis of Cildb identified that other ciliary genomic and proteomic screens also identified this gene. It was identified in the proteomic profiling of mouse spermatozoa ((Baker et al., 2008b), the proteomic analysis of spermatozoa in rat (Baker et al., 2008a) and a proteomic study on sperm tails from *Ciona intestinalis* (Nakachi et al., 2011). Ostrowski et al (2002) also identified the protein in proteomic analysis of cilia axonemes was isolated from these ALI cells (Ostrowski et al., 2002b). All these findings indicate *RIKEN cDNA 1700013F07* as a conserved component of motile ciliary axoneme.

In humans C1ORF194 encodes a protein of 157 amino acids without a signal peptide. The C1ORF194 protein has a predicted molecular mass of 19.35 kD. Multi-alignment analysis with Blastp and Clustal X indicates that C1ORF194 shares a high identity with orthologues in other species, with the highest identity of 99% to chimpanzee, 74% identity to mouse, 43% identity to frog and 45% identity to zebrafish (See Appendix 5.2). The human protein contains a domain of unknown function (DUF3695) between amino acids 23 to 115.

Analysis of a BioGPS microarray data set (expression in different mouse tissues, *Dataset: GeneAtlas GNF1M, gcrma*), show it is abundantly expressed in testes (Figure 4.5).



Figure 4-6. C1orf194 homolog expression in mouse tissues based on the BioGPS database.

Dataset: GeneAtlas GNF1M, gcrma; Probeset: gnf1m29836_a_at
<http://biogps.org/#goto=genereport&id=75504>

As shown in Figure 4.6, immunostaining data from the Human Protein Atlas, shows the protein to be localised into axoneme of ciliated cells in the airway and fallopian tube.

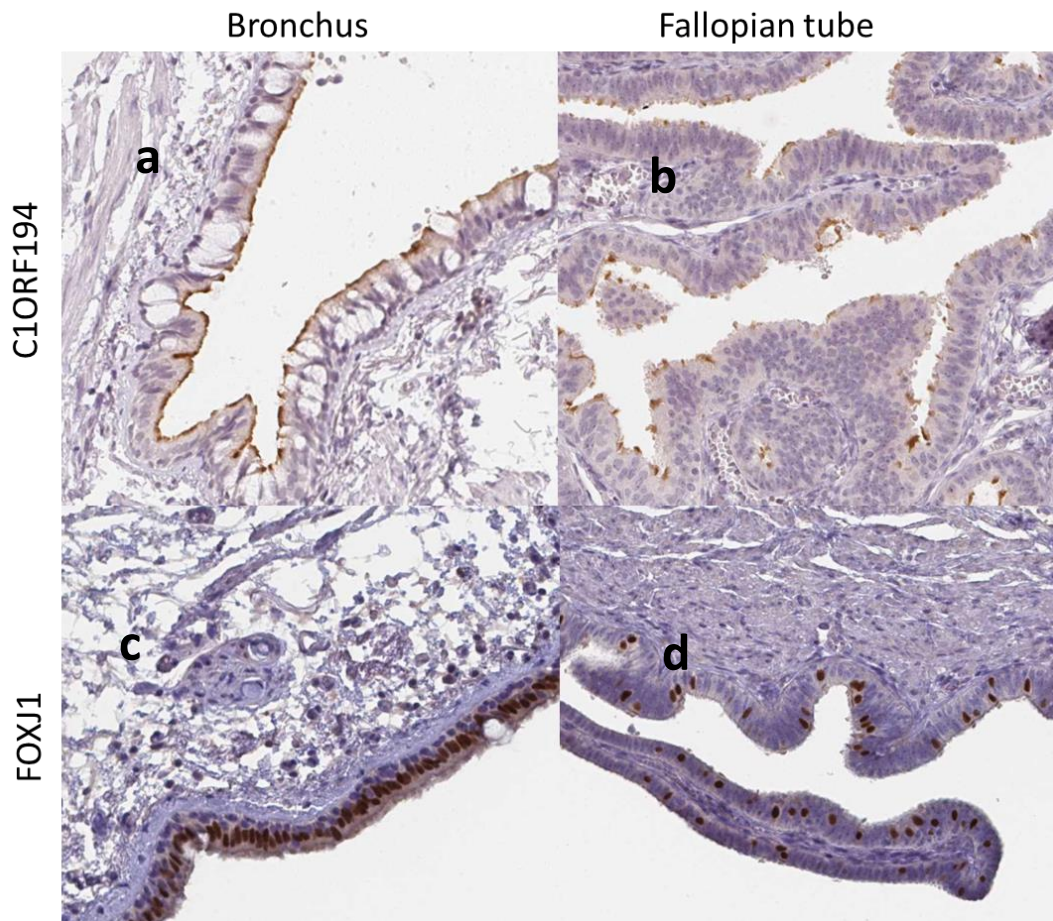


Figure 4-7. Localization of C1ORF194 in motile ciliated tissues.

The images were attained by immunohistochemical staining of bronchus and fallopian tubes with protein-specific antibodies in the Protein Atlas project (Uhlen et al., 2010). The antibodies were against the following proteins: C1ORF194 (a,b), FOXJ1 (c,d). The antibody-based staining is shown in brown and staining of nuclei with DAPI in blue. The airways ciliated cells form a continuous layer, while in fallopian tubes they are separated from each other by non-ciliated epithelial cells.

4.3.5 RIKEN cDNA 1700001L19 gene

RIKEN cDNA 1700001L19 gene is mapped on to Chromosome 13, in mice and encodes a protein made up of 182 amino acids. The human orthologue is called C5ORF49. It is conserved in all vertebrates. This gene was identified in many ciliary gene screens undertaken on mouse airway epithelial cells and ciliated tissues (Hoh et al., 2012, Baker et al., 2008b, McClintock et al., 2008) and in the proteomic analysis of spermatogenesis (Guo et al., 2010). It was also identified in screens done in human airway epithelial cells and proteomic analysis on human ciliated tissues (Ross et al., 2007, Ivliev et al., 2012). The gene was also identified as a FOXJ1 induced genes in the functional screen performed in zebrafish (Choksi et al., 2014c).

In humans *C5ORF49* encodes a protein of 147 amino acids without a signal peptide. The C5ORF49 protein has a predicted molecular mass of 16.99 kDa. Multi-alignment analysis with Blastp and Clustal X indicated that C5ORF49 shared a high identity with orthologues in other species, with the highest identity of 99% to chimpanzee , 75% identity to mouse, 60% identity to chicken and 45% identity to zebrafish. No orthologue was identified in frogs (see Appendix 5.3). All these proteins share a common predicted domain of unknown function (DUF4541) spans amino acids 42 to 131 in the human protein.

Analysis of a bioGPS data set (mRNA analysis in different mouse tissues), shows it to be enriched in testis and MOE (Figure 4.7).

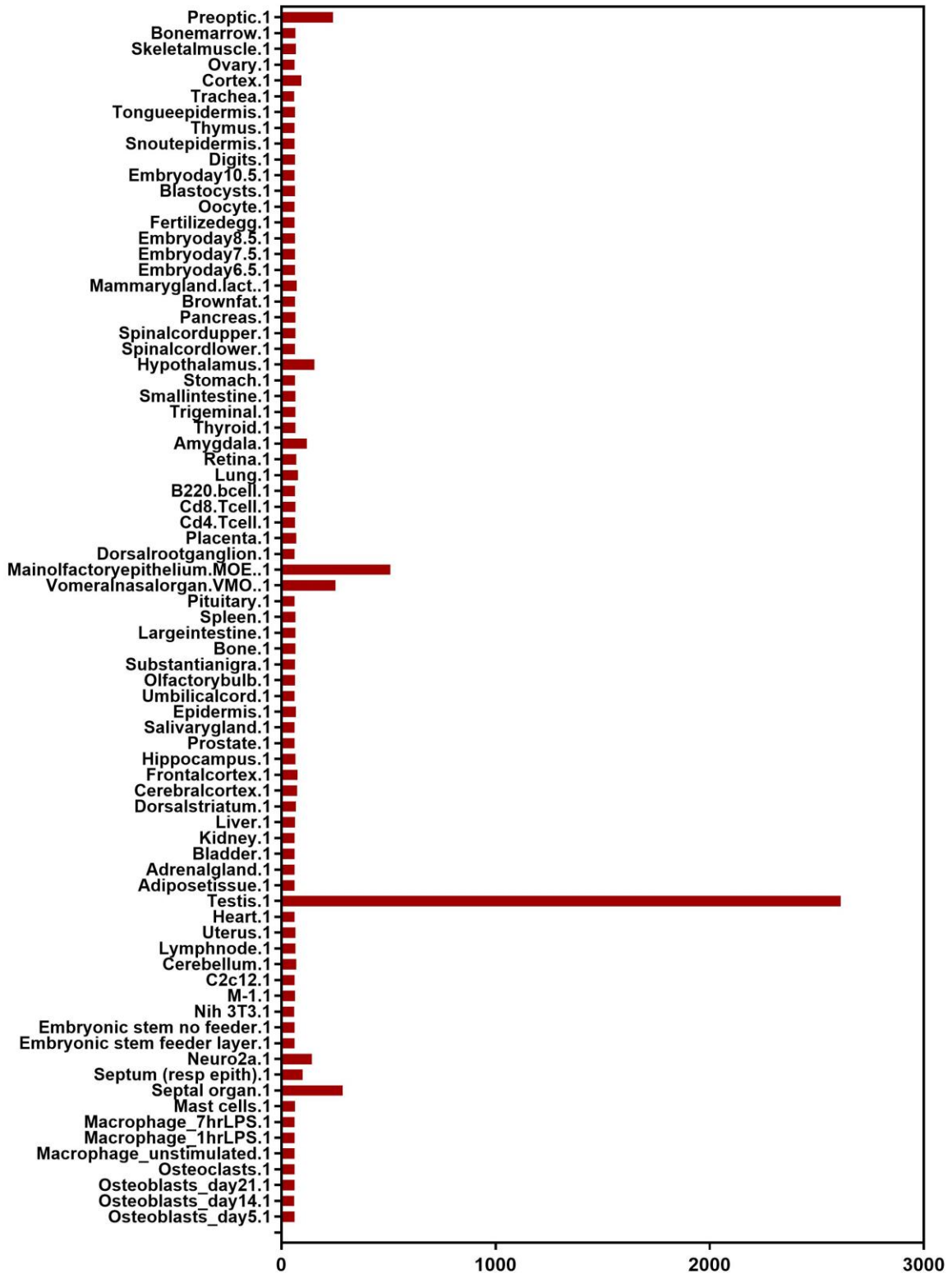


Figure 4-8. C5orf49 homolog expression in mouse tissues based on the BioGPS database.

Dataset: GeneAtlas GNF1M, gcrma; Probeset: gnf1m16743_a_at

<http://biogps.org/#goto=genereport&id=75504>

As shown in Figure 4.8, immunostaining from the Human Protein Atlas, shows C5ORF49 to be localised to the mucociliary epithelium of bronchus and the fallopian tube. This data shows strong staining in the cytoplasm and axoneme of ciliated cells.

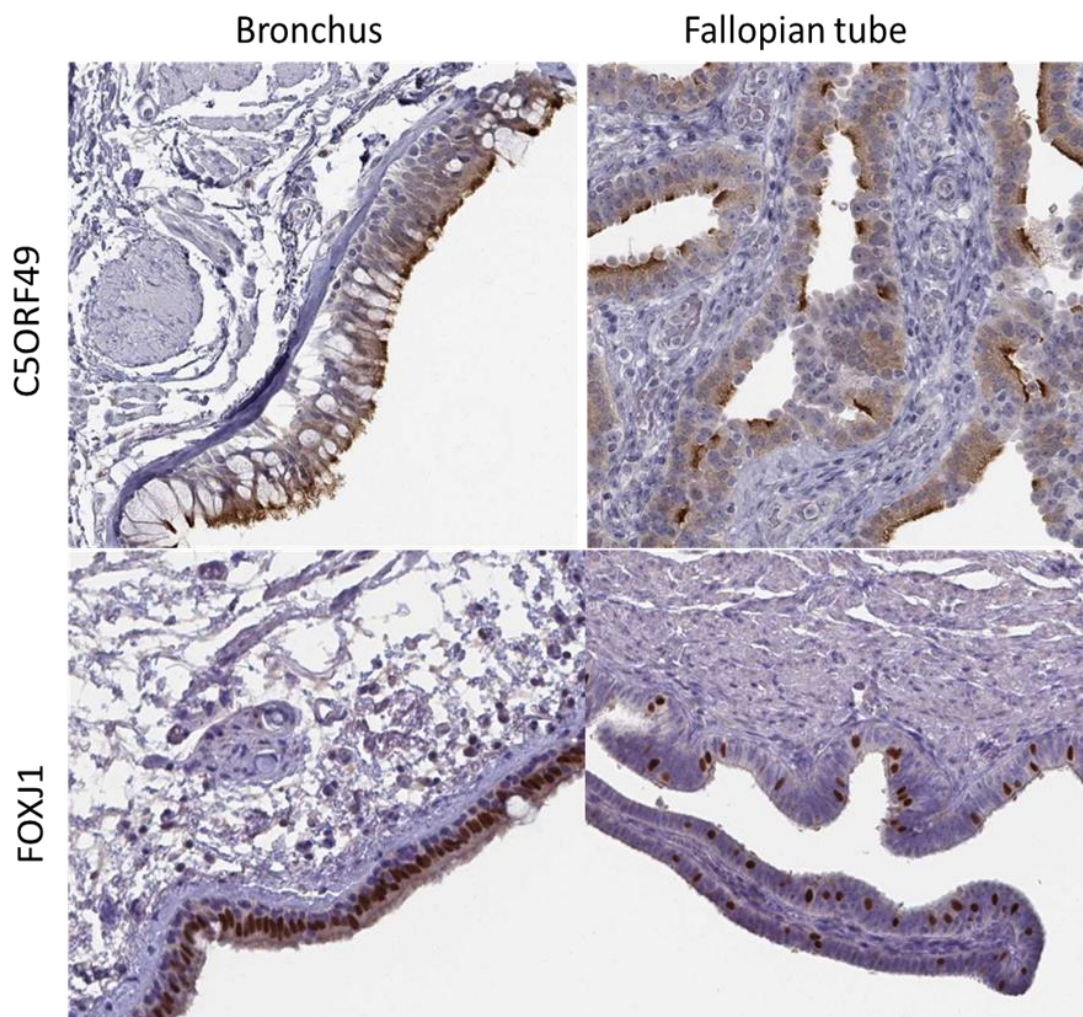


Figure 4-9. Localization of C5ORF49 in motile ciliated tissues.

The images were attained by immunohistochemical staining of bronchus and fallopian tubes with protein-specific antibodies in the Protein Atlas project (Uhlen et al., 2010). The antibodies were against the following proteins: C5ORF49 (a,b), FOXJ1 (c,d). The antibody-based staining is shown in brown and staining of nuclei with DAPI in blue. The airways ciliated cells form a continuous layer, while in fallopian tubes they are separated from each other by non-ciliated epithelial cells

4.3.6 RIKEN cDNA 4833427G06 gene

RIKEN cDNA 4833427G06 gene is mapped to chromosome 9 in mice and it encodes a protein of 168 amino acids. The human orthologue is called C11ORF88. This protein is conserved in all vertebrates. This gene was identified in ciliary gene screens undertaken in the mouse (Hoh et al., 2012, Treutlein et al., 2014a), in human airway epithelial cells (Ross et al., 2007) and in zebrafish (Choksi et al., 2014c). Using Cildb, other studies that identified this gene were also found, including the study on the tissue expression pattern in mouse tissues to identify cilia genes (McClintock et al., 2008) and a proteomic study of human ciliated tissues identifying the protein in the epithelia of the oviduct and lung (Ivliev et al., 2012).

In humans, *C11ORF88* encodes a protein of 196 amino acids without a signal peptide. It has a predicted molecular mass of 19.34 kDa. Multi-alignment analysis with Blastp and Clustal X indicates that it shares a high identity with orthologues in other species, with the highest identity of 98% to chimpanzee, 61% identity to mouse, 35% identity to frog and 35% identity to zebrafish (See Appendix 5.4). No putative conserved domains have been identified in the protein.

Analysis of expression in a BioGPS microarray data set (expression in different mouse tissues, *Dataset: GeneAtlas GNF1M, gcrma*), shows it to be abundantly expressed in motile ciliated tissues such as nasal septum, MOE, trachea, lung with the highest expression in testis (Figure 4.9). It was also shown to be expressed in osteoblast.

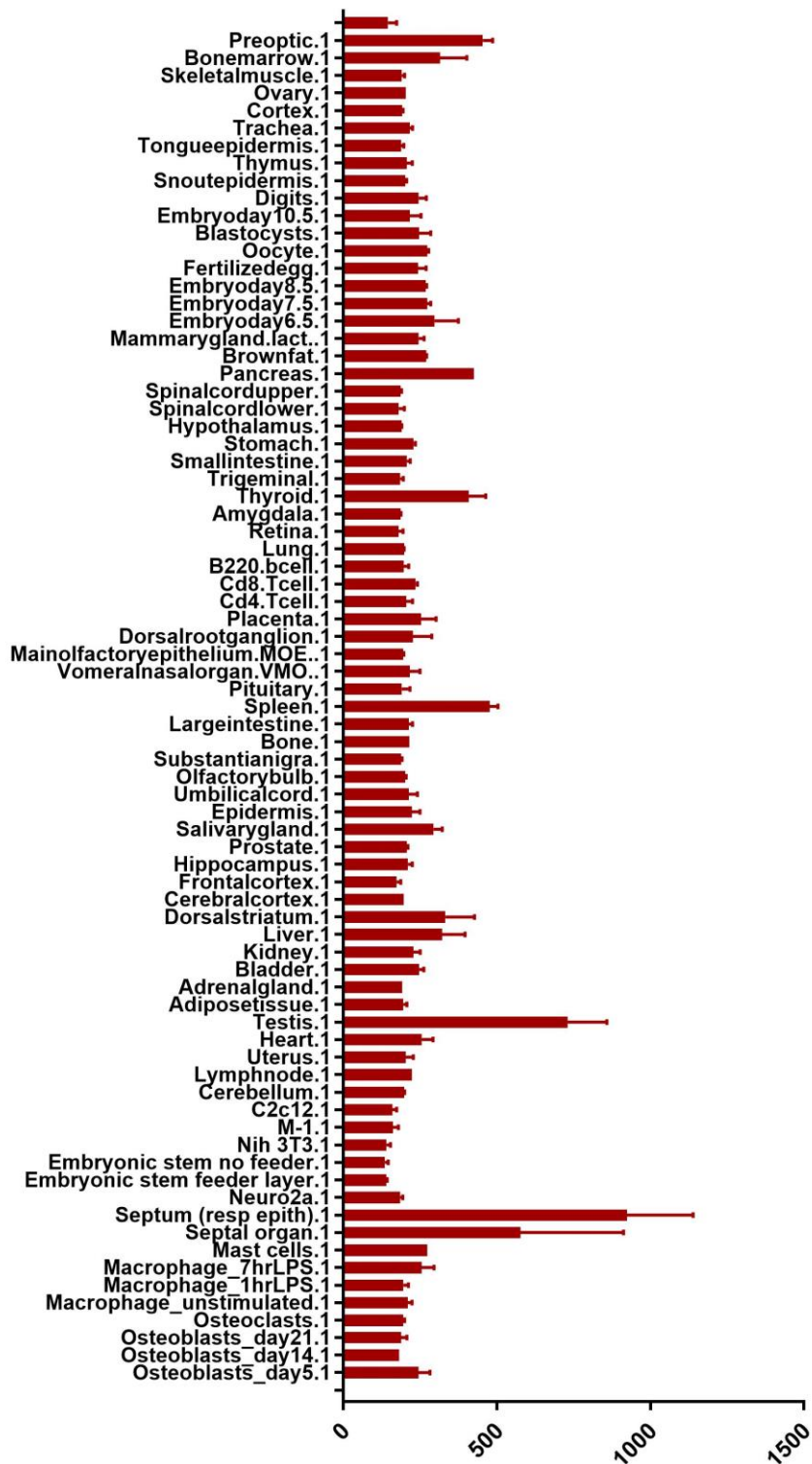


Figure 4-10. C11orf88 expression on mouse tissues based on the BioGPS database.

(Dataset: GeneAtlas GNF1M, gcrma; Probeset: gnf1m17154_a_at
<http://biogps.org/#goto=genereport&id=235345>)

No data are found in the Human Protein Atlas for protein localisation of C11ORF88.

4.3.7 Leucine Rich Repeat Containing 4B (LRRC4B)

Lrrc4b gene is mapped on to Chromosome 7, in mice and encodes a protein of 709 amino acids. It is conserved in all vertebrates. Proteins like LRRC4B, that contain the Leucine-rich repeats (Lrrc), are an evolutionarily conserved class of proteins found across all organisms.

In humans, *LRRC4B* encodes a protein of 715 amino acids without a signal peptide. It has a predicted molecular mass of 76.71 kDa. Multi-alignment analysis with Blastp and Clustal X indicated that LRRC4B shared a high identity with orthologues in other species, with the highest identity of 100% to chimpanzee, 96% identity to mouse, 76% identity to chicken and 65% identity to zebrafish (See Appendix 5.5). The importance of leucine-rich repeats containing proteins in the formation of cilia have been studied since late 90s. Other than the leucine-rich repeat superfamily domain in the N-terminus of the protein, it also contains an immunoglobulin-like domain that spans amino acids 360 to 460.

Analysis of mRNA expression in a BioGPS microarray data set (expression in different mouse tissues, *Dataset: GeneAtlas GNF1M, gcrma*), shows it to be expressed in brain and spinal cord. (Figure 4.10). There is no specific enrichment of expression in tissue associated with multiciliated cells.

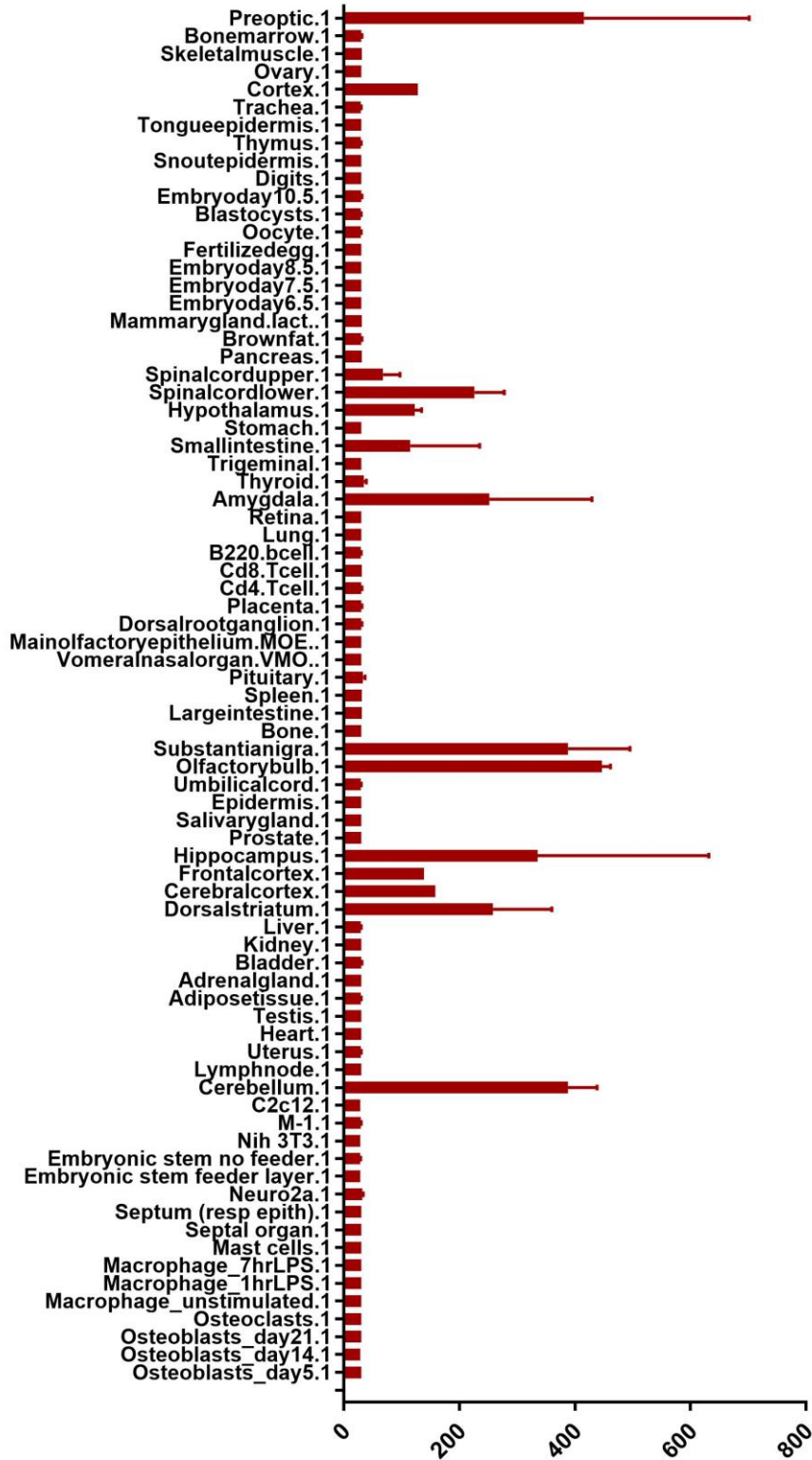


Figure 4-11. *Lrrc4b* expression in mouse tissues based on the BioGPS database.
 (Dataset: GeneAtlas GNF1M, gcrma; Probeset: gnf1m28823_a_at)
<http://biogps.org/#goto=genereport&id=272381>

Immunostaining data from the Human Protein Atlas (Figure 4.11) identifies weak LRRC4B staining in the mucociliary epithelium of the bronchus and fallopian tube. The staining appears to be localised to the cytoplasm of the cells.

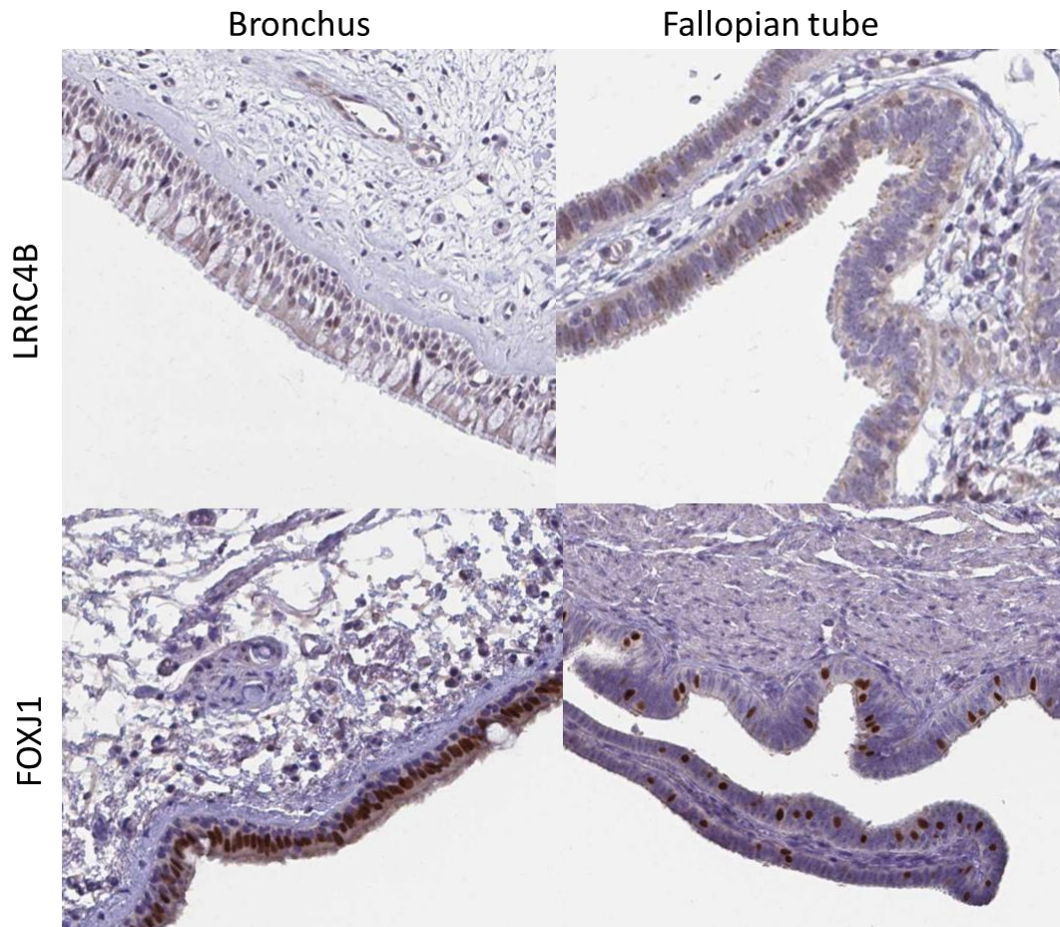


Figure 4-12. Localization of LRRC4B in motile ciliated tissues.

The images were attained by immunohistochemical staining of bronchus and fallopian tubes with protein-specific antibodies in the Protein Atlas project (Uhlen et al., 2010). The antibodies were against the following proteins: LRRC4B (a,b), FOXJ1 (c,d). The antibody-based staining is shown in brown and staining of nuclei with DAPI in blue. The airways ciliated cells form a continuous layer, while in fallopian tubes they are separated from each other by non-ciliated epithelial cells.

4.3.8 RIKEN 1700028P14 gene

The *RIKEN 1700028P14* gene is mapped on to Chromosome 19, in the mouse and it encodes a protein of 228 amino acids. The human orthologue is called C9ORF135. An orthologue has not been identified in zebrafish however orthologues are found in other fishes e.g. spotted gar. As shown in Table 4.1, this gene was identified in gene screens undertaken in mouse airway epithelial cells, tissues and spermatozoa (Hoh et al., 2012, Baker et al., 2008b, McClintock et al., 2008, Treutlein et al., 2014a). It was also identified in the screen undertaken in human airway epithelial cells and in PCD patient samples (Ross et al., 2007, Geremek et al., 2011, Geremek et al., 2014).

In humans, the 825 bp ORF of *C9ORF135* encodes a protein of 229 amino acids without a signal peptide. The C9ORF135 protein has a predicted molecular mass of 26.45 kDa. Multi-alignment analysis with Blastp and Clustal X indicated that C9ORF135 shares identity with orthologues in other species, with the highest identity of 97% to chimpanzee , 64% identity to mouse, 43% identity to frog and 42% identity to spotted gar (See Appendix 5.6). The protein contains a predicted domain of unknown function (DUF4572) which spans amino acids 28 to 220 in the human protein.

By analysis of BioGPS a microarray data set (expression in different mouse tissues, *Dataset: GeneAtlas GNF1M, gcrma*), it was found to have high enriched expression in testis (Figure 4.12).



Figure 4-13. C9orf135 homolog expression in mouse tissues based on the BioGPS database.

(Dataset: GeneAtlas GNF1M, gcrma; Probeset: gnf1m04869_a_at)
<http://biogps.org/#goto=genereport&id=67483>

Immunostaining data from the Human Protein Atlas shows, C9ORF135 is weakly expressed in the mucociliary epithelium of bronchus and fallopian tube (Figure 4.13). The staining is very weak and appears to have cytoplasmic/membranous localisation. It is not clear if there is specific staining in ciliated cells.

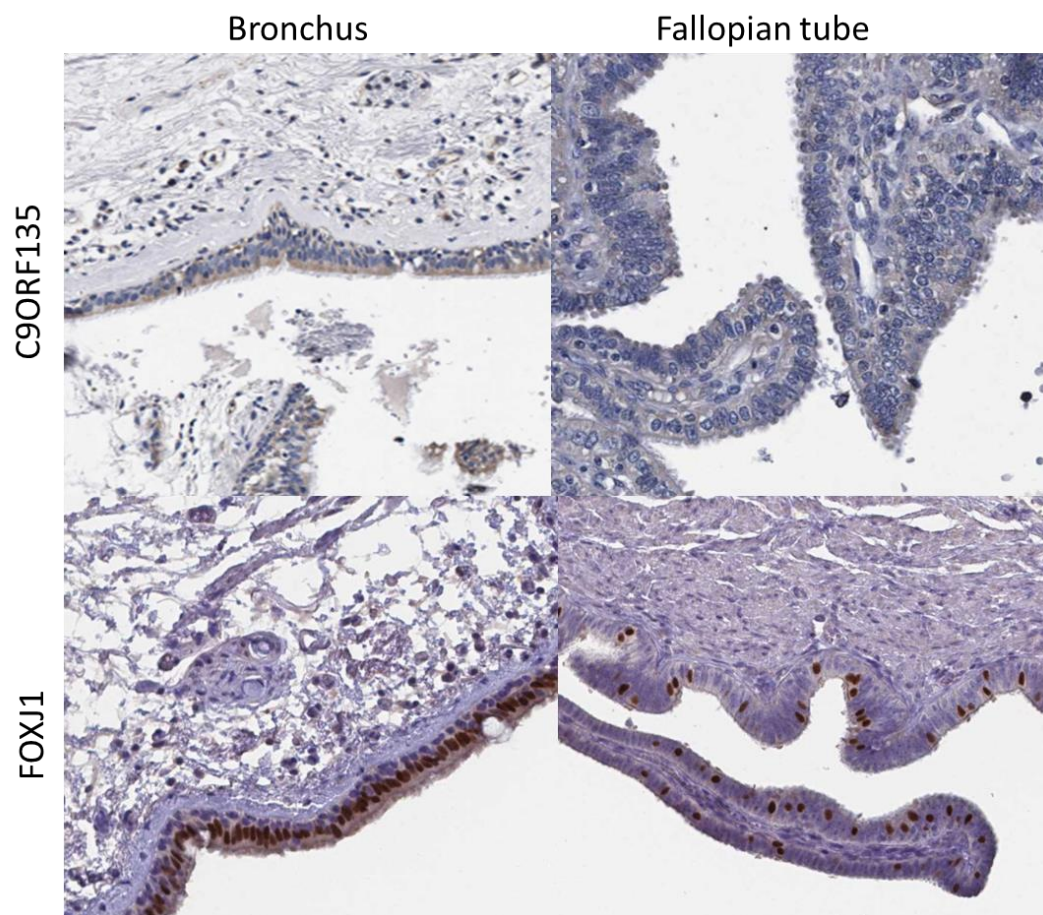


Figure 4-14. Localization of C9ORF135 in motile ciliated tissues.

The images were attained by immunohistochemical staining of bronchus and fallopian tubes with protein-specific antibodies in the Protein Atlas project (Uhlen et al., 2010). The antibodies were against the following proteins: C9ORF135 (a,b), FOXJ1 (c,d). The antibody-based staining is shown in brown and staining of nuclei with DAPI in blue. The airways ciliated cells form a continuous layer, while in fallopian tubes they are separated from each other by non-ciliated epithelial cells

4.3.9 *Maats1* (MYCBP associated and testis expressed 1)

Maats1 is mapped on to Chromosome 16, in the mouse and the gene encodes a protein made up of 783 amino acids. It is also known as AAT1 (AMY-1-associating protein expressed in testis 1) and CFAP91 (Cilia- and flagella-associated protein 91). The human orthologue is also known as MAATS1 (formerly known as C3ORF15). The *Chlamydomonas* orthologue was shown to be a component of a spoke-associated complex that mediates regulatory signals between the radial spokes and dynein arms to regulate flagellar dynein activity (Dymek and Smith, 2007). It was also shown to form a complex with AMY-1, A-kinase Anchor Protein 84, in the mitochondria of somatic cells and sperm (Yukitake et al., 2002). Both MAATS1 and AMY-1 were also found to be expressed specifically in the testis during the process of spermatogenesis and to be localized in the spermatid and mature sperm (Yukitake et al., 2002). As shown in table 4.1, this gene was identified in multiple ciliary genomic screens undertaken in mouse tissues and airway epithelial cells (McClintock et al., 2008, Hoh et al., 2012, Treutlein et al., 2014a), as well as in several screens performed on human airway epithelial cells and ciliated tissues (Ostrowski et al., 2002b, Ross et al., 2007, Ivliev et al., 2012). Since, it was identified in the axonemal proteome screen done human airway multiciliated cells by Gostkowski et al (2002), this protein could be a component of axoneme. The gene is also a target of FOXJ1 in zebrafish (Choksi et al., 2014a).

In humans, *MAATS1* encodes a protein of 767 amino acids without a signal peptide. The MAATS1 protein has a predicted molecular mass of 89.97 kDa . Multi-alignment analysis with Blastp and Clustal X indicated that MAATS1

shares a high identity with orthologues in other species, with the highest identity of 99% to chimpanzee, 79% identity to mouse, 61% identity to frog and 56% identity to zebrafish (See Appendix 5.7). The protein contains two domains, a solute carrier (proton/amino acid symporter) spanning amino acids 171 to 323 and a SMC_N super family domain spanning amino acids 394 to 608 in human protein.

Analysis of a BioGPS microarray data set (expression in different mouse tissues, *Dataset: GeneAtlas GNF1M, gcrma*), shows it to be abundantly expressed in testis and relative high expression in other tissues associated with motile cilia, such as nasal septum, the MOE and trachea (Figure 4.14).

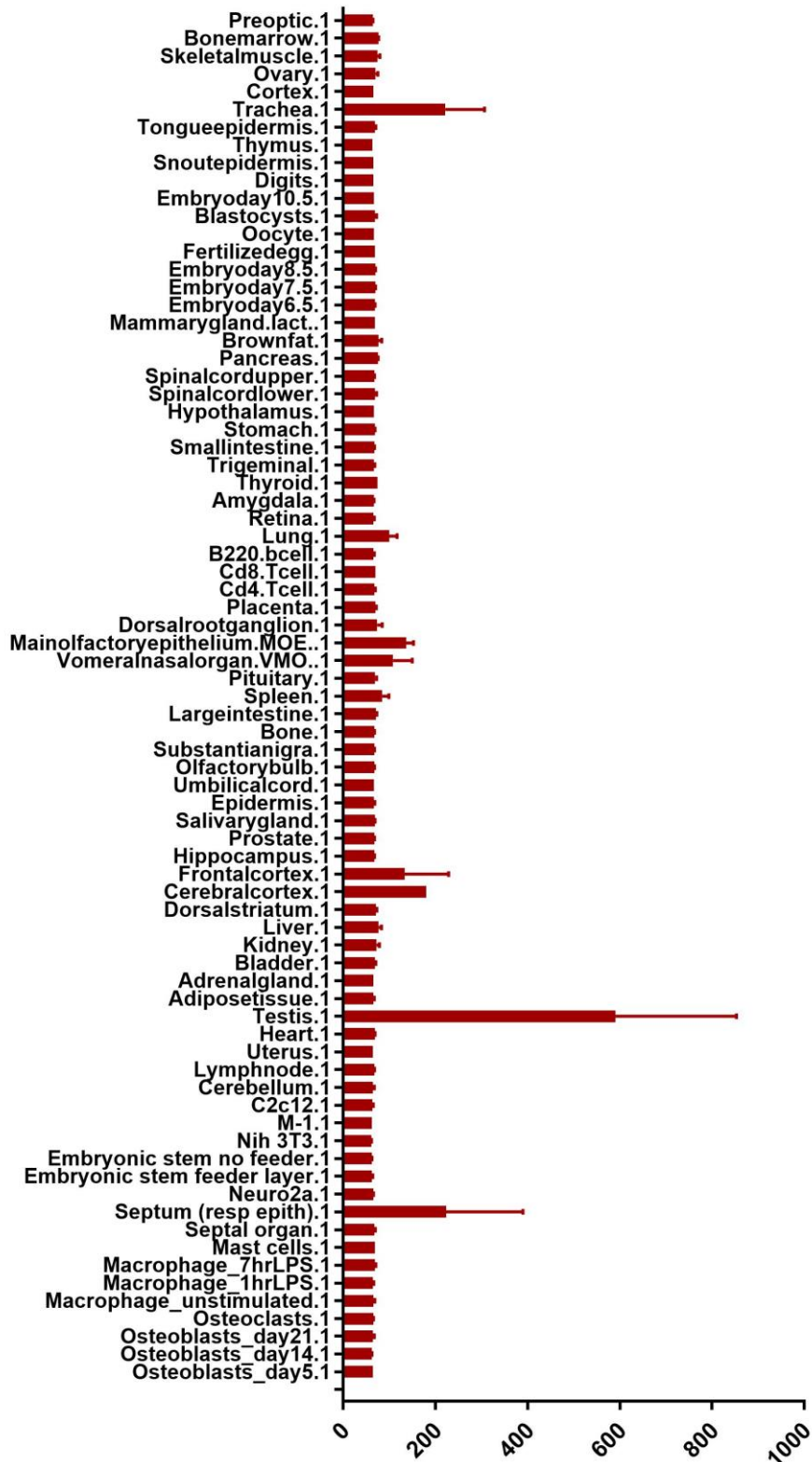


Figure 4-15. *Maats1* expression in mouse tissues based on the BioGPS database.

(Dataset: GeneAtlas *GNF1M*, *gcrma*; Probeset: *gnf1m19069_a_at*)

<http://biogps.org/#goto=genereport&id=320214>

No data for protein localization was found in Human Protein Atlas.

4.3.10 *Erich2* (Glutamate rich protein-2)

Erich2 is mapped on to Chromosome 2, in the mouse and the gene encodes a protein of 456 amino acids. *Erich2* was one of the differentially expressed genes found in ciliating GFP+ cells by Hoh et al at (2012) during the ciliary differentiation of mTECs at the ALI (Hoh et al., 2012).

In humans, *ERICH2* encodes a protein of 156 amino acids without a signal peptide and with a predicted molecular mass of 17.67 kDa. Multi-alignment analysis with Blastp and Clustal X indicates that ERICH2 shares a high identity with orthologues in other species, with the highest identity of 99% to chimpanzee, 68% identity to mouse, 49% identity to frog and 75% identity to zebrafish (See Appendix 5.8). No conserved domains were identified in the sequence.

Analysis of a BioGPS microarray data set (expression in different mouse tissues, *Dataset: GeneAtlas GNF1M, gcrma*), shows it to be abundantly expressed in testis (Figure 4.15).



Figure 4-16. Erich2 expression in mouse tissues based on the BioGPS database.

(Dataset: GeneAtlas GNF1M, gcrma; Probeset: gnf1m09582_a_at)
<http://biogps.org/#goto=genereport&id=66748>

No data for protein localization was found in Human Protein Atlas.

4.3.11 *Spata24* (spermatogenesis associated 24)

Spata24 is mapped on to Chromosome 18 in the mouse and the gene encodes a protein of 205 amino acids. It is also known as TIPT and TIPT2. *Spata24* has been shown to be important for spermatogenesis. SPATA24 associate with TATA-binding protein (TBP)-related protein 2 (TRF2) and HP1, thus establishing an interesting link between transcription and chromatin modelling (Brancorsini et al., 2008). Pitulescu et al (2009) showed SPATA24, as a strong binding partner of GEMININ and suggested that interactions with basal transcription factors allow it to regulate transcription (Pitulescu et al., 2009). As shown in the Table 1, this gene came up in ciliary gene screens undertaken in mouse airway epithelial cells (Hoh et al., 2012, Treutlein et al., 2014a).

In humans, *SPATA24* encode a protein of 205 amino acids without a signal peptide and has a predicted molecular mass of 23.59 kDa. Multi-alignment analysis with Blastp and Clustal X indicates that SPATA24 shares a very high identity with orthologues in other species, with the highest identity of 100% to chimpanzee, 100% to pig and 91% identity to mouse. No orthologues are found in frog and zebrafish (See Appendix 5.8). The protein contains an unknown conserved functional domain spanning between amino acids 25 to 191.

Analysis of a BioGPS microarray data set (expression in different mouse tissues, *Dataset: GeneAtlas GNF1M, gcrma*), shows the gene to be abundantly expressed in testis (Figure 4.16).

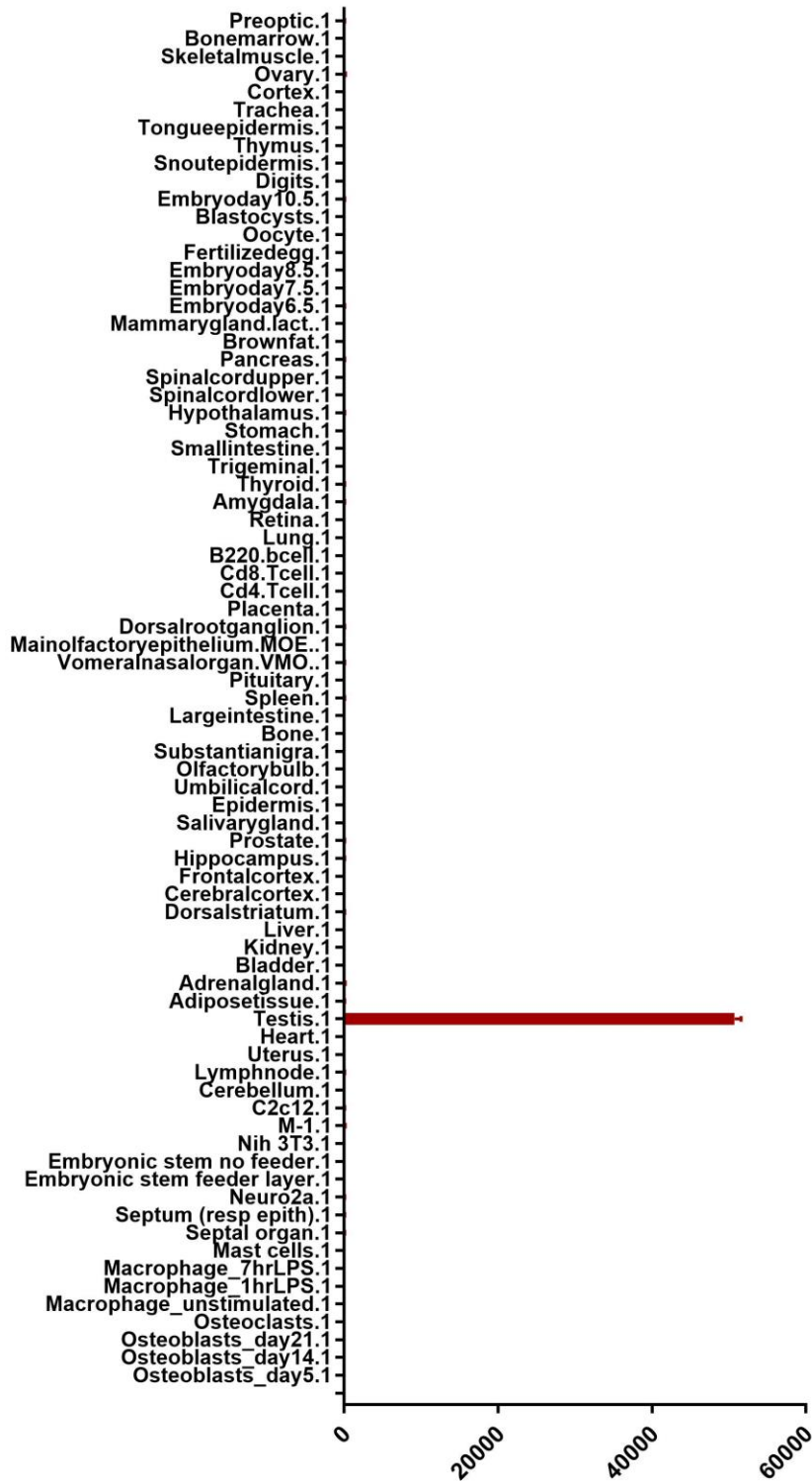


Figure 4-17. Spata24 expression in mouse tissues based on the BioGPS database.

(Dataset: GeneAtlas GNF1M, gcrma; Probeset: gnf1m13353_a_at)
<http://biogps.org/#goto=genereport&id=71242>

No data for protein localization was found in Human Protein Atlas.

4.3.12 *RIKEN cDNA 1110017D15* gene

RIKEN cDNA 1110017D15 gene is mapped on to Chromosome 4, in mouse and generates two transcripts, resulting in open reading frames with different carboxyl termini, but which show no homology to known proteins. The human orthologue is C9ORF24 and it is also known as CBE1. There are no known orthologues in zebrafish. It was first identified from the random sequencing of a cDNA library from human lung biopsies and expression was shown to be induced during the *in vitro* differentiation of bronchial epithelial cells. Immunohistochemistry showed expression of CBE1 in ciliated cells (Yoshisue et al., 2004). In addition, Haitichi et al also showed expression in airway epithelial cells in relation to FOXJ1 (Haitichi et al., 2009). As shown in Table 4.1, this gene was identified in ciliary gene screens undertaken in mouse cells (Hoh et al., 2012, Treutlein et al., 2014a) and was also identified in studies on human mTEC cells (Ross et al., 2007) and in PCD patient samples (Geremek et al., 2011).

In humans, *CBE1* encodes a protein of 262 amino acids, without a signal peptide that has a predicted molecular mass of 30.17 kDa. Multi-alignment analysis with Blastp and Clustal X indicates that CBE1 shares a high identity with orthologues in other species, with the highest identity of 99% to chimpanzee, 81% to pig and 76% identity to mouse. No orthologues are found in frog and zebrafish (See Appendix 5.9). The protein contains a conserved functional domain (SMRP1- Spermatid-specific manchette-related protein 1) that spans from almost the entire protein, amino acids 1-249 amino in human.

Analysis of a BioGPS microarray data set (expression in different mouse tissues, *Dataset: GeneAtlas GNF1M, gcrma*), shows that *Cbe1* was found to be abundantly expressed in tissues associated with motile such as nasal septum, the MOE, trachea, lung and testis (Figure 4.17).

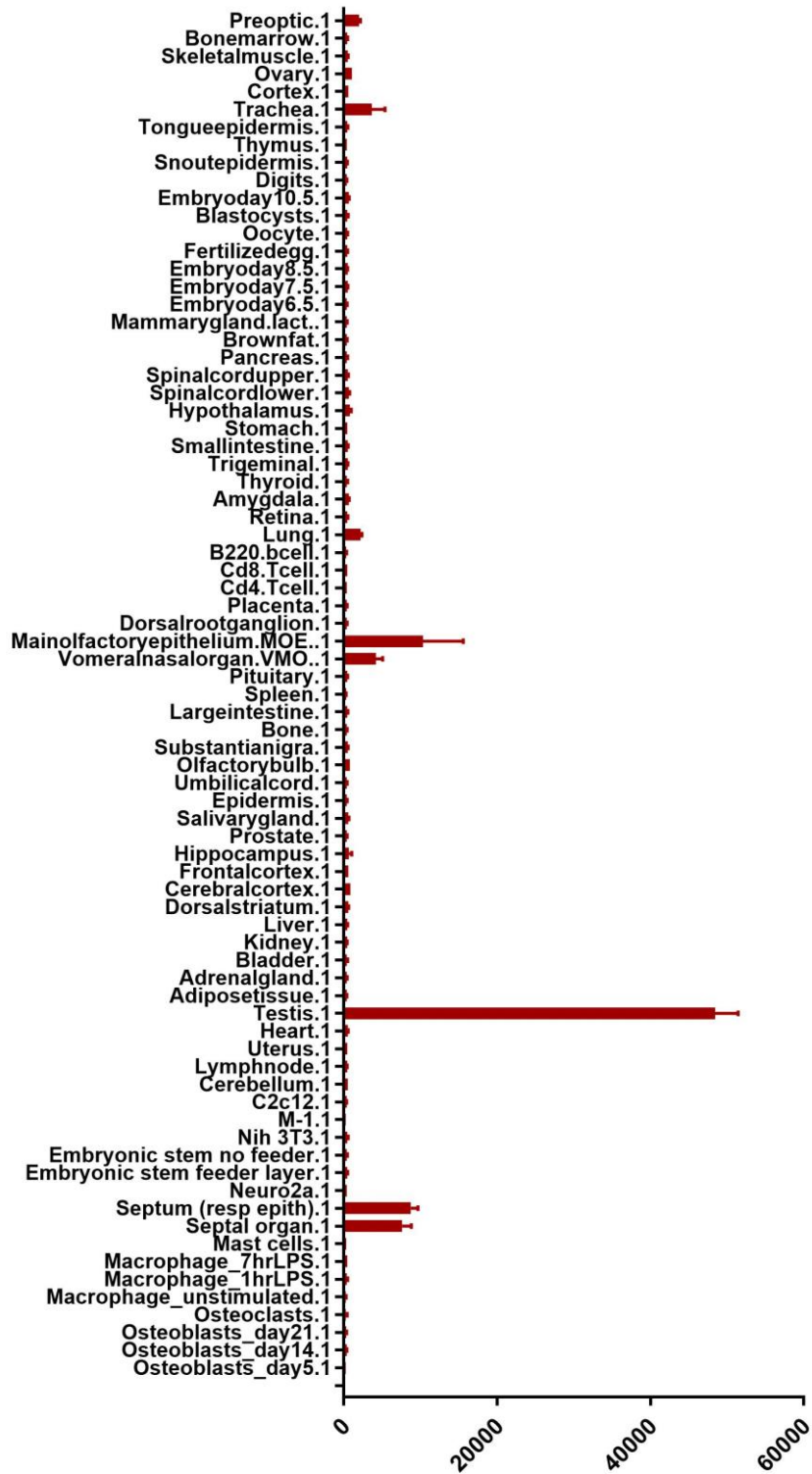


Figure 4-18. *Cbe1* expression in mouse tissues based on the BioGPS database.
 (Dataset: GeneAtlas GNF1M, gcrma; Probeset: gnf1m16773_a_at)
<http://biogps.org/#goto=genereport&id=73721>

Human Protein Atlas images, suggest that CBE1 was not detected in airway epithelial cells but low intensity staining was detected in the fallopian tube (Figure 4.18) with a cytoplasmic/membranous location. It does not appear to be specific for ciliated cells.

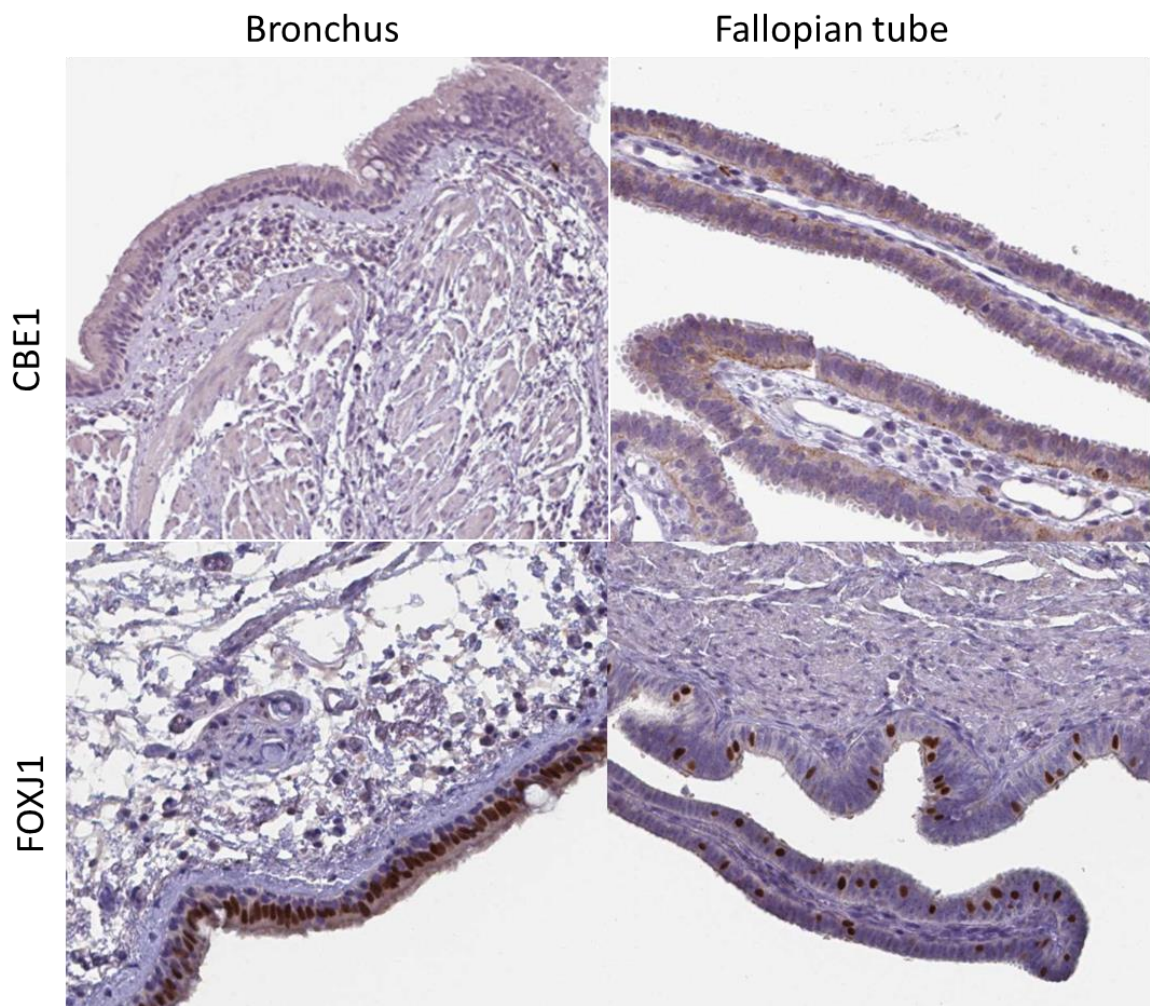


Figure 4-19. Localisation of CBE1 in motile ciliated tissues.

The images were attained by immunohistochemical staining of bronchus and fallopian tubes with protein-specific antibodies in the Protein Atlas project (Uhlen et al., 2010). The antibodies were against the following proteins: CBE1 (a,b), FOXJ1 (c,d). The antibody-based staining is shown in brown and staining of nuclei with DAPI in blue. The airways ciliated cells form a continuous layer, while in fallopian tubes they are separated from each other by non-ciliated epithelial cells.

4.3.13 Expression analysis of the candidate genes during ALI differentiation of mTEC by RNA sequencing

To characterise the functional role of TP73 in multiciliogenesis, Nemajerova et al compared the transcriptomes of WT and *Tp73*^{-/-} mTECs at day 0, 4, 7 and 14 of ALI differentiation (Nemajerova et al., 2016a). They used RNA sequencing to generate lists of all genes expressed during distinct stages of cell differentiation at ALI. I used the raw data showing the RNA sequencing (seq) read counts to plot the graphs in Figure 4.19 that show how the transcriptional expression of these genes change during the differentiation of cells at ALI. This helps to further validate my endpoint PCR results (Figure 4.1) that were generated in 2015. All the candidate genes, with the exception of *Lrrc4b* were upregulated during the ALI differentiation of mTEC (Figure 4.30). In the *Tp73*^{-/-} mTEC, many of these genes were shown to be downregulated. *Pierce1*, *C1orf194 Homolog*, *C9orf135 Homolog*, *Maats1*, *Erich2* and *Cbe1* were shown to have lower expression during the ALI differentiation of *Tp73*^{-/-} mTEC. It is also important to note that the scales of the graphs are not same since the levels of expression were very different from gene to gene. It was better to use different scales for the graphs to show the change in expression during differentiation.

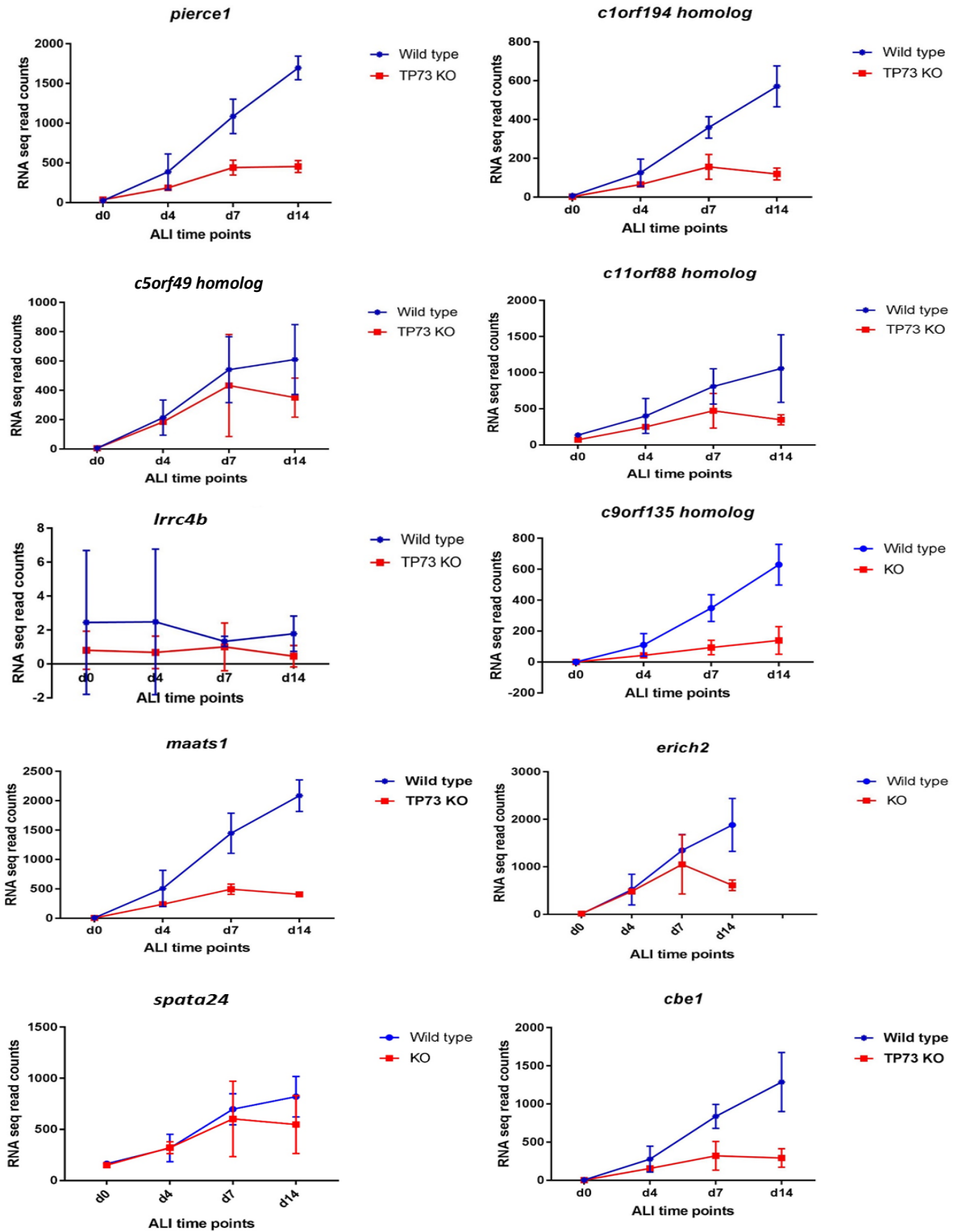


Figure 4-20. Expression of the candidate genes in ALI cultured WT mTEC vs TP73 KO mTEC.

Nemajerova *et al* (2016) acquired RNA seq reads from 3 independent cultures for WT and 2 independent cultured of *tp73*^{-/-} mTEC. Error bars represent standard error of the mean.

4.4.14 Expression of candidate genes in developing lung by single cell gene expression.

Using data from 'LungGENS', an online tool for mapping single-cell gene expression in the developing lung the expression of the candidate genes in diverse types of airway epithelial cells was also investigated. The LungGENS website is based on single-cell RNA sequencing data from normal fetal mouse lung (Du et al., 2015, Du et al., 2017).

The data for average RNA expression for each gene in 9 distinct cell types of developing lungs of embryonic day 18.5 mice, was used to plot the graphs in Figure 4.20. The cell types that were included in the study were Type I alveolar cells, Type II alveolar cells, Ciliated cells, Club cells, Endothelial cells, Myeloid/immune cells, Lipofibroblast, Matrix fibroblast and Myofibroblast. As shown in the graphs, 9 out of 10 of the candidate genes were significantly expressed in expressed in ciliated cells. *Lrcc4b* was the outlier and showed expression in Ciliated cells, Myeloid/immune cells, Lipofibroblast, Matrix fibroblast and Myofibroblast.

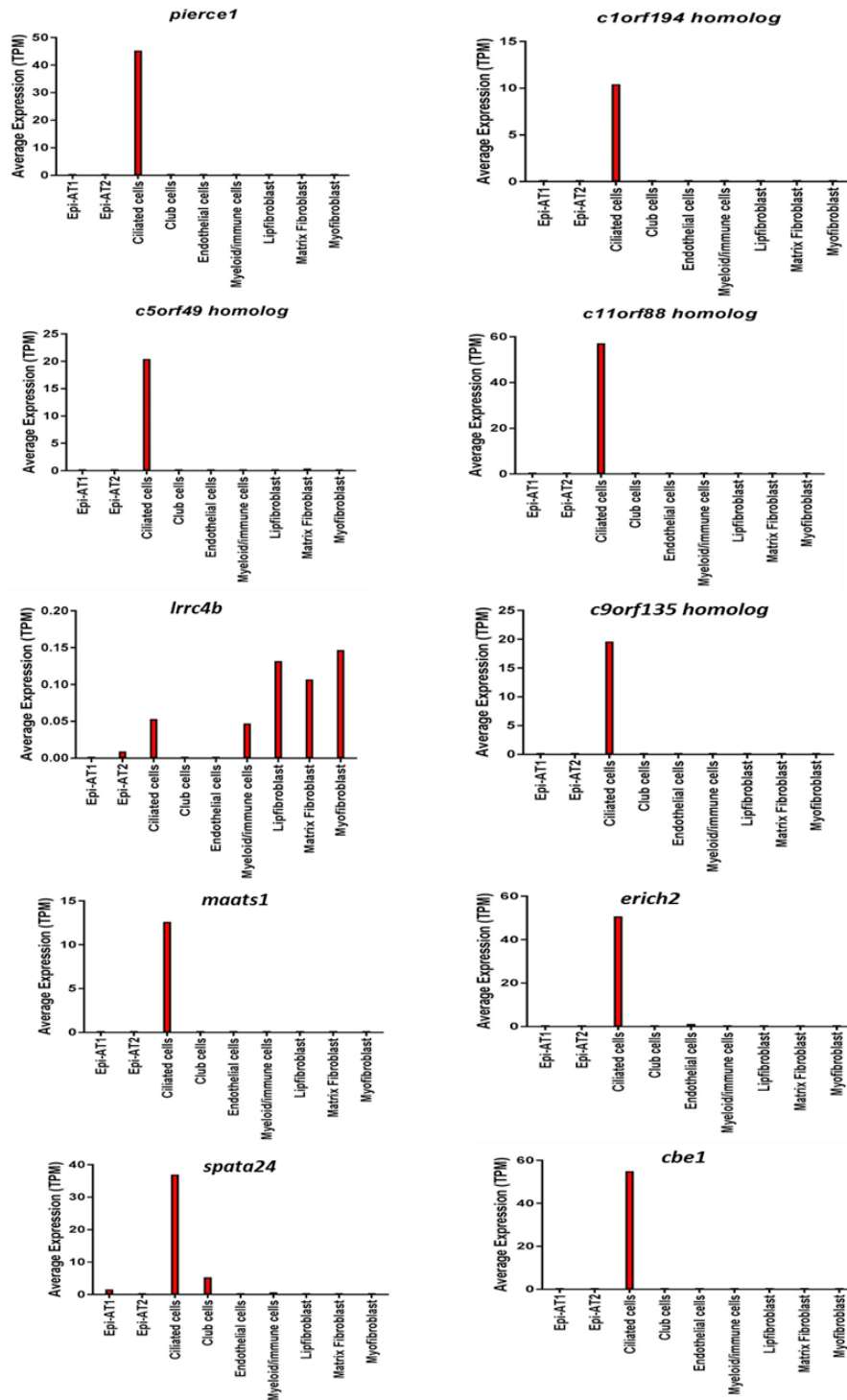


Figure 4-21. Expression of the candidate genes in 9 distinct cell types of E18.5 fetal mouse lung.

The graphs were plotted from the average mean expression data acquired from the LungGENS. The data were collected from mouse fetal airway cells sequenced from E18.5 mouse lung, processed using Fluidigm C1 microfluidics technology. The count of samples for each cell types are as follows: Epi-AT1-7, Epi-AT1-9, Ciliated cells-2, Club cells- 2, Endothelial cells- 18, Myeloid/ Immune cells-8, Lipofibroblast-8, Matrix fibroblast- 9 and myofibroblast-9.

4.4 Discussion

The complexity of the pathways involved in ciliogenesis has prompted many research groups to perform high throughput genomic and proteomic screens to identify putative ciliary genes and components. The results of these studies have identified lists of thousands of genes. A few of these have been functionally characterised and their relevance to human ciliopathies have been resolved. However, little can be said about the rest of the genes revealed by these studies. The causative genes for 30% of the PCD cases are still not known and analysis of novel ciliary genes is still required to fully elucidate the pathways governing ciliogenesis

To identify novel genes involved in this process, I selected 10 uncharacterised genes that came up on the high throughput screen carried out by Hoh et al to define the transcriptome of multiciliated cells in mouse airways. The difficulties with using confident interpretation of data mined from high throughput studies are that the sensitivity of the high-throughput screens can be variable and it can include false positives or omit true positives.

Once I had selected the 10 candidate genes, I used Cildb to find more genomic and proteomic screens that had identified them. This analysis allows estimation of the conservation level of the signature genes. Most of my candidate genes had come up on 5 or more studies undertaken in distinct species; human, mouse and zebrafish. It seems likely that the more ciliary screens that identified a specific gene, the more relevant the gene could be in the process of ciliogenesis.

Vladar and Brody described distinct stages of multiciliogenesis at ALI culture of primary mouse tracheal epithelial cells (Vladar and Brody, 2013). In chapter 3, I described how I used endpoint RT-PCR to analyse the mRNA levels of genes encoding some of the main transcription factors and protein components of cilia structure. The transcriptional expression of main transcription regulators such as *Mcidas* and *Foxj1* are expressed early (from day 0) during mucociliary differentiation of mTEC at ALI and undergo upregulation. The genes encoding ciliary components such as *Tekt1* are expressed later (from day 2). Therefore, we studied the pattern of transcriptional expression of the candidate genes during mucociliary differentiation at ALI. All the genes appeared to upregulate during the differentiation of mTECs at the ALI. Some genes were observed to be expressed from day 0 and while others were only seen from day 2 or later. These PCRs were carried out in January 2015.

Consistent with our end-point PCR data, many of these candidate genes were shown to be upregulated in the data sets of RNA seq during cell differentiation at ALI found by RNA sequencing by Nemajerova et al (2016). This data set was generated to find the downstream effects of TP73 in multiciliogenesis in mTEC cells, by comparing the transcriptome of WT and *Tp73* knockout (KO) mTECs at day 0, 4, 7 and 14 of ALI differentiation. In these data, all the genes, except *Lrrc4b*, were shown to be upregulated from day 0 to day 14. This increase in expression during the mucociliary differentiation at ALI mirrors what has already observed for established ciliary genes such as *Foxj1*, *Mcidas* and *Tekt1*. Again, this shows that these genes could be playing a role in the mucociliary differentiation of airway epithelial cells.

All the genes except *Lrrc4b*, were also shown to be downregulated in *tp73* KO mTECs. TP73 is shown as a central transcriptional regulator of multiciliogenesis that works upstream of many cilia genes (Nemajerova et al., 2016a, Marshall et al., 2016) including FOXJ1, the master regulator of motile ciliogenesis (Yu et al., 2008, Stubbs et al., 2008). So, it can be expected that cilia genes will be downregulated when TP73 is not expressed. Unfortunately, they only undertook 2 replicates of the experiment, so I was not able to perform statistical analysis to validate the significance of the result.

By end-point RT-PCR, the expression of the potential candidate genes was examined on a panel of whole mouse tissues; kidney, lungs, liver, embryo, thymus, spleen, testicle, heart, brain, ovary. Motile cilia can be found in lung, embryo, testicle, brain and ovary. *Foxj1* and *Tekt1* was shown to have specific enriched expression in motile ciliated tissues. Similar pattern of expression was observed for *Pierce1*, *RIKEN cDNA 1700013F07* and *RIKEN cDNA 1700001L19*, *RIKEN cDNA 1700028P14* and *Cbe1*. The dataset in bioGPS that looked at expression of these genes in mouse tissues shows enriched expression in testis for most of these genes. In the testis, the sperm harbours flagellum and many of the mechanisms in ciliogenesis are conserved in sperm flagella formation (Fisch and Dupuis-Williams, 2012).

Human Protein Atlas described localization patterns for some of my ciliary candidates. For the analysis, I used images of staining done in multiciliated tissues such as bronchus and fallopian tube. The positive control was FOXJ1 as that has a strong nuclear staining in cells with motile cilia and lack staining in non-ciliated cells. Staining restricted to ciliated cells was observed for proteins encoded by three of my candidate genes; *Pierce1*, *RIKEN*

cDNA 1700013F07 and RIKEN cDNA 1700001L19. It should be remembered that not all proteins are well represented in Protein atlas. Although the presence of a particular protein associated with ciliated cells is a useful source to boost the confidence in the gene's role in ciliogenesis, the lack of staining may mean only that the antibody is not very reactive.

Finally, I studied the expression of the candidate genes in distinct cell types of E18.8 mouse lung using the data from 'LungGens'. As expected for a ciliary gene, 9 out of 10 candidate genes were specifically expressed in ciliated cells. *Lrrc4b* had comparatively low expression in the cell types studied in mouse fetal lung. Interestingly, *Spata24* showed low expression in club cells and high expression in ciliated cells. Previous studies performed on tissue cultures of human respiratory epithelium and lung segments have established unequivocally that club cells are one of the primary sources of stem cells in the airways. Researchers have shown that club cells can differentiate into ciliated cells (Rawlins et al., 2009, Reynolds and Malkinson, 2010, Rokicki et al., 2016). The gene ontology (GO) term for biological function for SPATA24 is shown as transcriptional regulation. It was also shown as a strong binding partner of GEMININ, a coiled coil domain protein belonging to same family of MCIDAS. The expression pattern for *Mcidas* in LungGens is very similar to that of *Spata24*. (https://research.cchmc.org/pbge/lunggens/genequery_E18_p3.html?geneid=mcidas). So, it can be assumed that *Spata24* may also have transcriptional regulatory role in ciliogenesis. This is further supported by the pattern of expression during the mucociliary differentiation of mNEC at ALI. The peak expression of *Spata24* was observed at earlier stages of differentiation (day 2) like *Mcidas*.

After comparing all these results, I selected one gene for further functional characterisation. This gene had to be novel and should have fulfilled most of the criteria, I thought would give it more significance to be a ciliary gene.

The criteria were as follows

- The gene should be listed in 5 or more ciliary genomic and proteomic studies and at least in 3 species, including zebrafish.
- The gene should have differential expression like known cilia genes e.g. *Foxj1*, *Tekt1*, during the mucociliary differentiation of airway epithelial cells at ALI.
- The gene should have enriched expression in motile ciliated tissues as evidenced by the RT-PCR and bioGPS.
- The gene should have enriched expression in ciliated tissues as evident by human protein atlas.
- The gene should be specifically expressed in ciliated cells as evident by LungGens data.

I selected *PIERCE1* as my candidate gene since it fulfilled all criteria. I decided to study the role of *PIERCE1* using an *in vitro* model; mouse primary airway epithelial cell cultured at ALI and an *in vivo* vertebrate model; zebrafish. I have described these in the following chapters.

Chapter 5 : Functional characterisation of Pierce1 using zebrafish

5.1 Preface

In the previous chapter, I presented results that lead me to select *PIERCE1* for further characterisation. This choice was based on data from several ciliary genomic and proteomic screens, transcriptional expression during differentiation of airway epithelial cells at the ALI, expression in tissues containing motile cilia and enriched expression in ciliated cells.

Since *pierce1* was shown to be induced by Foxj1 in zebrafish by Choksi *et al* (2014) (Choksi *et al.*, 2014c), I hypothesised that Pierce1 has a conserved functional role in zebrafish in motile ciliogenesis downstream of Foxj1.

Many human ciliopathy causative mutations were identified in a large-scale mutagenesis screen undertaken in zebrafish (Howe *et al.*, 2013b). Many groups have also utilised zebrafish vertebrate organism model to functionally characterise roles of novel genes in motile ciliogenesis (Knowles *et al.*, 2013c, Narasimhan *et al.*, 2015, Song *et al.*, 2016b). I decided to follow the same strategy to functionally characterise the role of Pierce1 in motile ciliogenesis.

5.1.1 Proposed method for investigating the functional role of Pierce1 in zebrafish

In zebrafish, the most economic and rapid method for performing reverse genetic analysis is by utilising modified anti-sense oligonucleotides known as morpholinos (MOs), which provide transient gene knockdown by binding to RNA and inhibiting protein synthesis (Nasevicius and Ekker, 2000, Timme-

Laragy et al., 2012). Most commonly, researchers use two types of MOs. The first is a translation blocking MO that targets sequence in the post-spliced mRNA in the region from the 5' cap to about 25 bases 3' to the AUG translational start site and thus blocks translation of the transcript. Secondly, there is splice blocking MO that targets an exon-intron boundary (splice donor) or intron-exon boundary (splice acceptor) that results in disruption of the ORF and translation of protein (GeneTools, 2018). I decided to undertake initial characterisation of *Pierce1* by designing two independent MO; one a translation blocking MO and one a splice blocking MO.

In the past few years, CRISPR/Cas9 has become a favourite gene-editing tool to make stable zebrafish genetic mutants (Hwang et al., 2013a). I also decided to make a genetic mutant for *pierce1* in zebrafish as I considered it would be a good model to study functional role of *Pierce1* in adult fish. It would also function as a model to study molecular pathways and protein interactions of *Pierce1*. Furthermore, I also decided to utilise zebrafish expression plasmids to study the subcellular localisation of *Pierce1* *in vivo*.

5.2 Results

5.2.1 *pierce1* is upregulated by *Foxj1*

Microarray indicated that *pierce1* was upregulated by *Foxj1* (5.22 fold up) in zebrafish (Choksi et al., 2014c). I initially further validated this result by qRT-PCR and found that *pierce1* was greater than 7-fold upregulated by *Foxj1* as shown in Figure 5.1. For this experiment, I made the cDNA from embryos from the zebrafish transgenic line (*hsp70: foxj1*) that temporally overexpresses *Foxj1* upon heat shock. This was the same transgenic line used for identifying the

Foxj1 targets by Choksi *et al* (2014). cDNA from *hsp70: foxj1* embryos, that was not subjected to heat-shock and hence does not overexpress *Foxj1*, was used as the control.

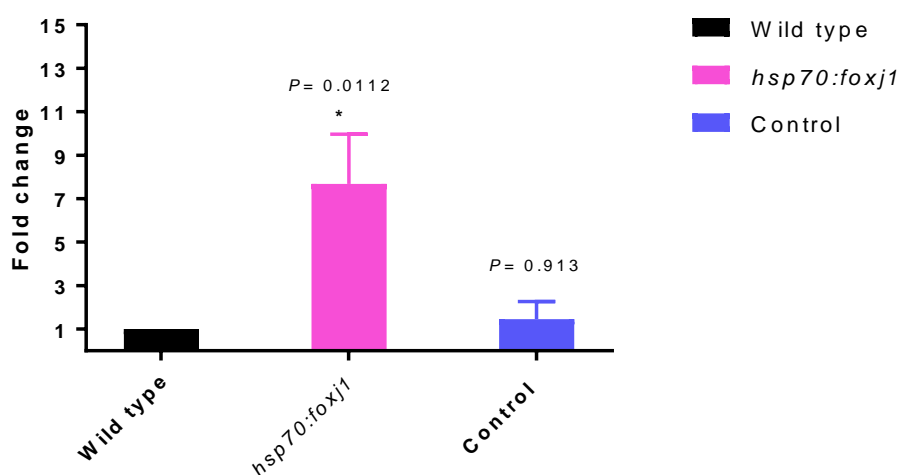


Figure 5-1. *pierce1* is upregulated by *Foxj1*.

qPCR results indicate that *Foxj1* upregulates *pierce1* by >7 folds compared to wild-type. The embryos that were not subjected to heat shock were the negative control. (n=3 independent batches of experiments). The error bars represent standard error of the mean (SEM). *-p<0.05 using 1way ANOVA.

5.2.2 Transient knockdown of *pierce1* in zebrafish by morpholinos

I injected the 2 independent MOs designed against *pierce1*, into the animal pole of WT zebrafish embryos at the one cell stage. One was a start MO that should block translation of the protein by binding to the translation start site of the *pierce1* transcript. Secondly, a splice blocking MO was designed that targeted the splice junction of exon 1-intron 1 of the *pierce1* transcript. Dose titration was carried out to determine the optimal dose and I found that the start MO works best (i.e. less than 20% mortality at maximum dose) at a concentration of 0.25 mM and an injection volume of 1 nl. The splice MO works best at a concentration of 0.6 mM and an injection volume of 1 nl.

To validate the splice MO, primers were designed to amplify a region from exon 1 to intron 1 of *pierce1* as shown in Figure 5.2.2 (a). If the splice MO was able to block the splicing, a product would be amplified. I carried out a RT-PCR on the cDNA made from DNase1 treated RNA from morphant embryos at 24 hours post fertilisation (hpf), while uninjected WT embryos served as the control. The products of the PCR were resolved on a 1.5% agarose gel as shown in Figure 5.2 (b). As expected, a 766 bp band was detected for *pierce1* splice morphants and not detected in WT control. This band was gel extracted and cloned into pCR II TOPO. After miniprep, the plasmids were sent for sequencing. The sequencing results revealed that in splice morphants, splicing event was blocked in splice junction between exon 1 and exon 2.

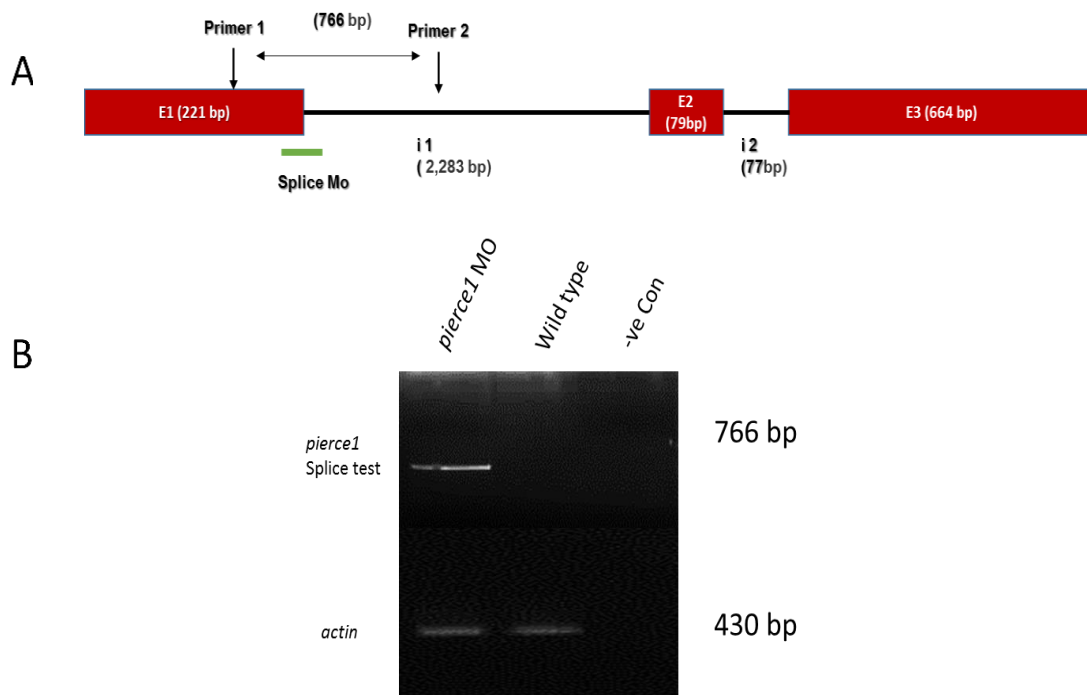


Figure 5-2. *pierce1* splice morpholino blocks splicing of *pierce1* transcript.
 (A) Primers were designed to amplify a product that span from exon 1 to intron 1 of *pierce1* transcript. (B) As expected, a band was only detected for *pierce1* splice morphant. β -actin was used as the loading control.

5.2.2.1 *pierce1* morphants display ciliopathy phenotypes

The embryos were assayed for various phenotypes arising due to loss of Pierce1 function. Data for the phenotypes was obtained from analysis of morphants as well as controls from three independent trials. In each trial, 50-70 embryos for each variable were used.

5.2.2.2 *pierce1* morphant embryos display phenotypes associated with motile ciliary defects

The embryos were examined at 22 hpf, 48 hpf and 72 hpf to look for phenotypes associated with ciliary defects such as otolith defects, curved body axis, hydrocephalus and pronephric cysts. As shown in Figure 5.3, both morphants displayed curved body axis and heart oedema. Splice morphants also displayed hydrocephalus. These defects were not found in WT embryos.

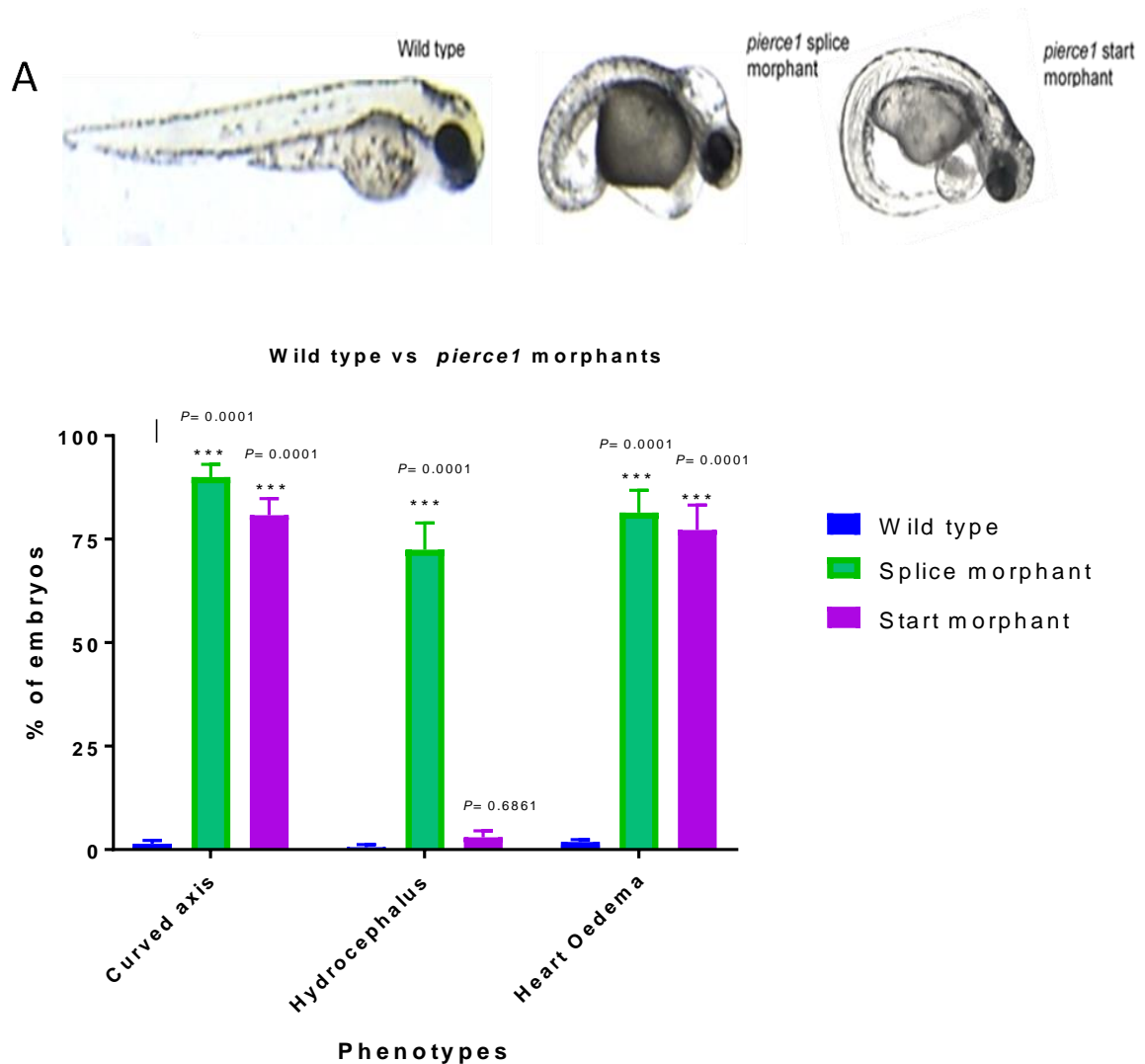


Figure 5-3. *pierce1* morphants display phenotypes associated with ciliary structural defects.

A) The figure shows embryos at 48 hpf. Both *pierce1* morphants showed significant curved body axis and heart oedema. Splice morphants also displayed hydrocephalus. The WT embryos did not show these phenotypes. B) The phenotypical assay was done in 3 independent batches. In each trial, 50- 70 embryos for each variable was used. Error bars indicate standard error of mean (SEM) (n=3 independent batches of experiments). *** $p < 0.001$ using 2way ANOVA.

5.2.2.3 *pierce1* morphants have laterality defects

Since the *pierce1* morphants showed phenotypes corresponding to ciliary phenotypes, I hypothesised the morphants would also have laterality defects associated with ciliary defects in KV. To test this hypothesis, WT and *pierce1*

morphant embryos fixed at 48 hpf were stained with an antibody against myosin heavy chain (A4.1025 antibody) to visualize the looping of the heart. In the WT zebrafish embryos, the heart is looped to the left. The immunostaining revealed that in both splice and start morphants, over 60% had bilateral looping, 15- 20% had right side looping and 20-25% with left sided looping as seen in WT. Therefore, both splice morphants and start morphants of *pierce1* had significant alteration in L-R symmetry.

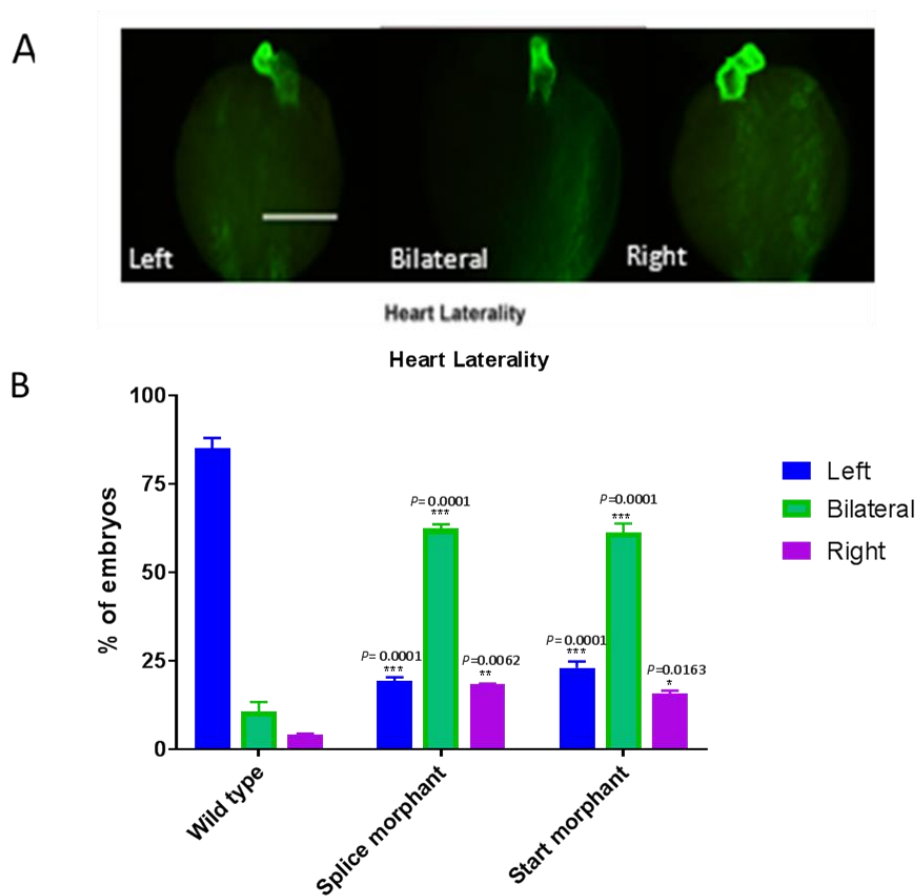


Figure 5-4. *pierce1* morphants display laterality defects.

A) Both *pierce1* morphants showed laterality defects as shown by the altered left-right sidedness in the heart looping. In both morphants (36 hpf), majority showed bilateral heart looping while in WT it was left sided heart looping. B) In each trial, 50- 70 embryos for each variable was used. Error bars indicate standard error of mean (SEM) (n=2 independent batches of experiments). ***p<0.001 using 2way ANOVA.

5.2.2.4 *pierce1* morphants have cilia motility defects in KV

Since the *pierce1* morphants showed laterality defects as shown by altered left-right sidedness of heart looping in Figure 5.4, I hypothesised that cilia motility would be abnormal in KV. Live imaging for studying cilia beating in KV was carried out on the morphants and WT embryos at the 10-somite stage (see attached video files). It revealed that in both morphants, the ciliary motility in KV were severely affected as shown in Figure 5.5.

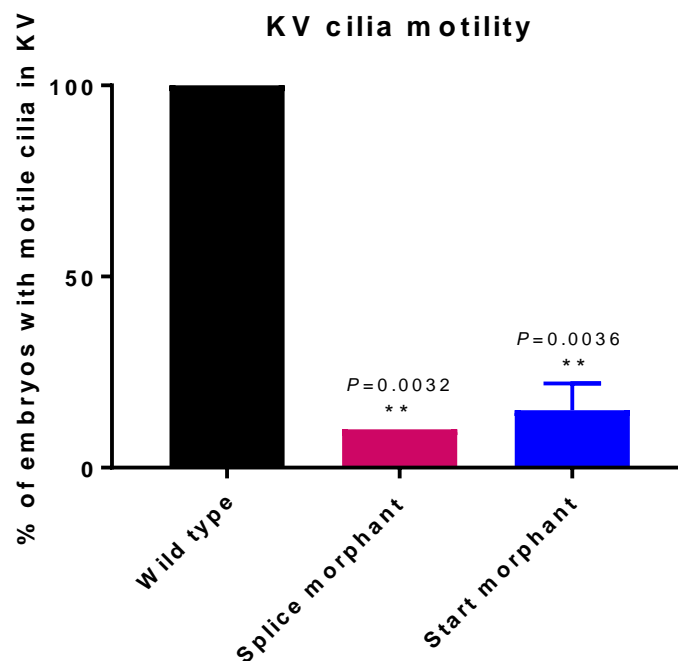


Figure 5-5. *pierce1* morphants have cilia motility defects inKV.

Live imaging was carried out on both start and splice morphants to examine the cilia motility. This showed severe KV cilia motility defects in 80%-90% of morphants embryos. In WT embryos, we could observe normal KV cilia beating in counter clockwise manner in 100% embryos. This data is representative of 2 biological replicates. 5-6 embryos were screened in each replicate for different variables. Error bars indicate standard error of mean (SEM) (n=2 independent batches of experiments). ** $p<0.01$ using 2way ANOVA.

5.2.2.5 Analysis of cilia number and length in KV in *pierce1* morphants

After studying the morphology of *pierce1* morphants, I considered that cilia length and number of cilia might be altered in the morphants. To address this question, I visualized cilia in the KV of both *pierce1* morphants at 10 somites by immunolabelling cilia with an antibody against Acetylated Tubulin. As shown in Figure 5.6, no gross difference was observed between WT embryos and morphant embryos. The staining was performed in 2 batches of MO injected and WT controls. In each batch, 3-4 embryos were imaged and examined.

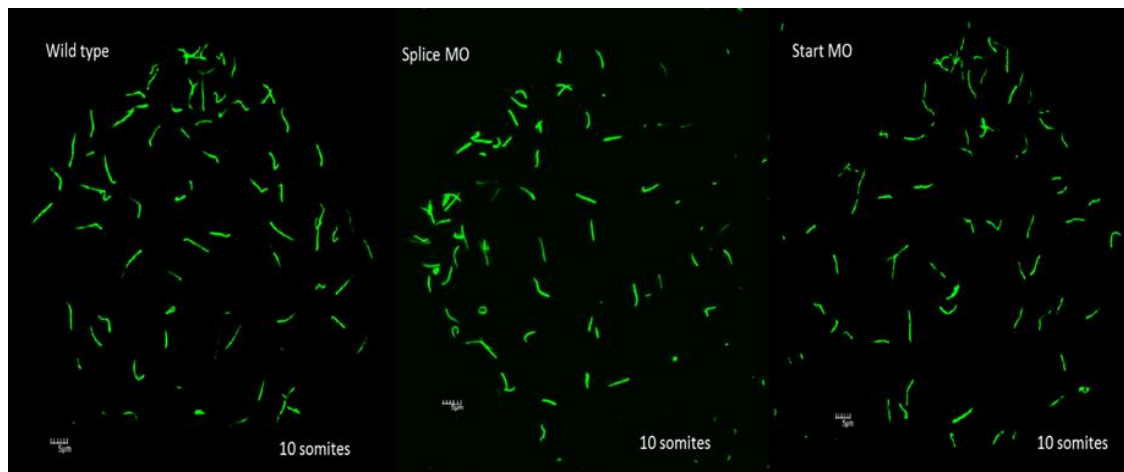


Figure 5-6. *pierce1* morphants have normal cilia length and number in KV.

At 10 somites, Cilia were immunolabelled using an antibody against acetylated α -tubulin in wild-type and morphant embryos. Cilia length and number were observed by confocal microscopy. No clear differences were observed between WT and morphant embryos.

5.2.3 Tagged expression vector systems shows cytoplasmic localisation of Pierce1

To understand the function of Pierce1, I first wanted to determine where the protein is localised in ciliated cells. The best approach to solve this would be by using an antibody directed against Pierce1 that could be used to determine the subcellular localization by immunohistochemistry. During my study, no commercial antibody was available against Pierce1 that would work in zebrafish. However, there was an antibody generated by SIGMA against human PIERCE1, in which, the epitope shared some conserved amino acid residues with the zebrafish protein. However, no signal was detected on immunofluorescence (data not shown). Therefore, I decided to clone *pierce1* into two tagged zebrafish expression vectors that would allow me to express Pierce1 with a C-terminus GFP tag and an N-terminus Myc (6x) tag. After *in vitro* transcription, I injected mRNA encoding *pierce1-gfp* and *6xmyc-pierce1* into 1-cell stage embryos. After double labelling the embryos with anti-Acetylated Tubulin and either anti-GFP or anti-Myc, both tagged versions of Pierce1 were shown to be localized to the cytoplasm as shown in Figure 5.7. The negative control was uninjected embryos that were stained with the same antibodies at the same time as the injected embryos.

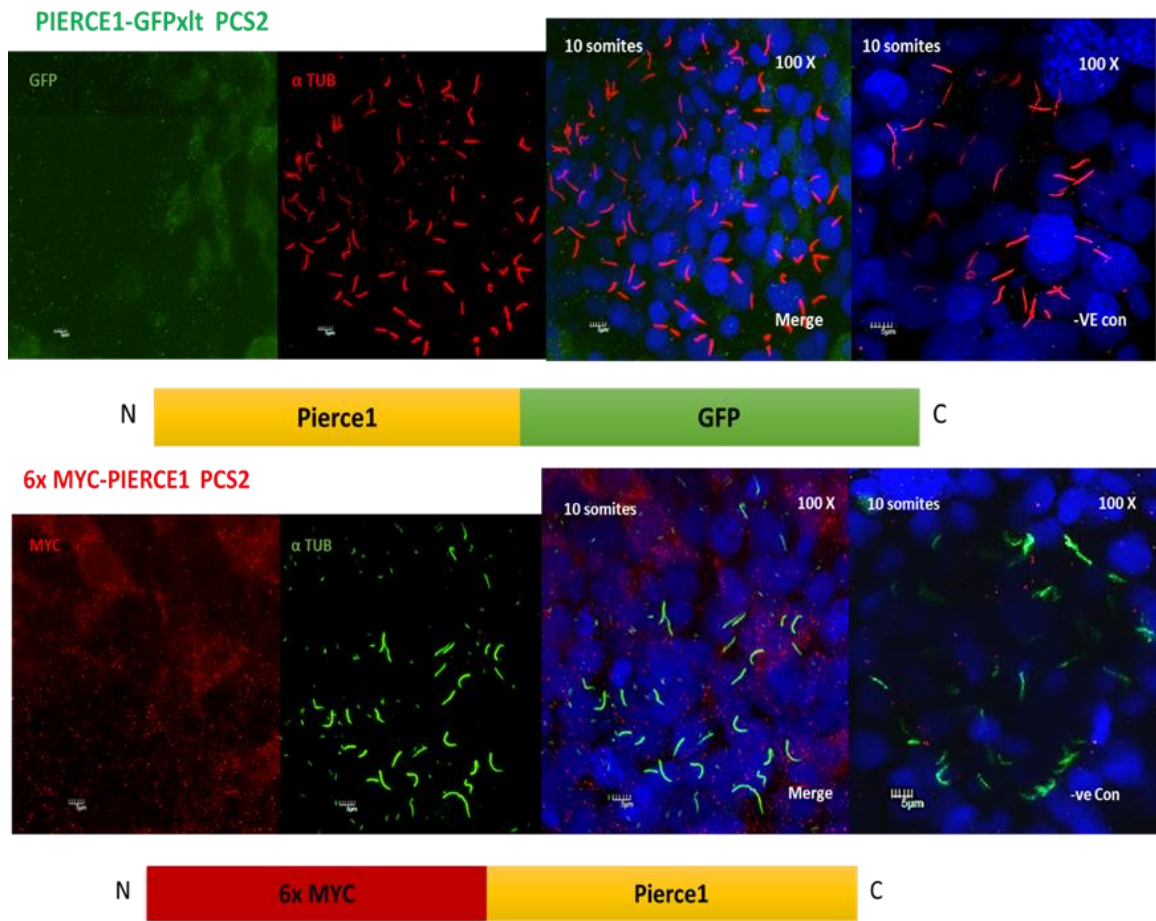


Figure 5-7. *Pierce1* has a cytoplasmic sub-cellular localisation in zebrafish embryos.

pierce1 with a C-terminus GFP tag and an N-terminus Myc (6x) tag was injected into 1-cell stage embryos. After double labelling the 10 somites embryos with anti-Acetylated tubulin and either anti-GFP or anti-Myc, both tagged versions of *Pierce1* was shown to be localized to the cytoplasm in KV by confocal imaging. The negative control was uninjected embryos that were stained with the same antibodies at the same time as the injected embryos as shown in the right hand panels.

I attempted to rescue the *pierce1* morphants by injecting the 6 x Myc-*Pierce1* mRNA. However, there was no significant difference between rescue and morphants.

5.2.4 Creating a *pierce1* zebrafish mutant line using CRISPR/Cas9

Many research groups have utilised antisense MOs to perform targeted transient knockdowns in zebrafish embryos to assess the developmental functions of genes of interest. However, many groups have now argued that this technique is flawed by potential off target effects (Kok et al., 2015, Place and Smith, 2017, Eve et al., 2017). On the other hand, some groups still support the value of the use of morpholinos with proper controls (Stainier et al., 2015, Blum et al., 2015). Despite the controversy, the zebrafish community are moving towards making stable genetic mutants as a more reliable approach to assess the functional roles of genes of interest.

The CRISPR/Cas9 system was utilised to generate a stable mutant line deficient for *Pierce1*. This technique was recently introduced as a new type of gene editing tool, even for organisms with a genome difficult to edit like the one of zebrafish (Hwang et al., 2013b, Seruggia and Montoliu, 2014). The CRISPR/Cas9 system is present in prokaryotes and archaea as part of their adaptive immune defence mechanism. Bacteria store fragments of DNA from invading viruses, which are then spliced into the bacterial genome region containing CRISPRs (Clustered Regularly Interspaced Short Palindromic Repeats). This region is then transcribed to make a guide-RNA that is used to guide Cas9 nucleases to viral DNA and cleave it thus prevent virus replication (D'Agostino et al., 2016).

The type II CRISPR/Cas9 system from *Streptococcus pyogenes* can be utilised *in vitro* by synthesising a guide RNA (gRNA) from the target site of the gene of interest and Cas9 RNA, which are co-injected in one-cell stage

zebrafish embryos. The 20 bp long target site must be immediately upstream a Protospacer Adjacent Motif (PAM) 5'-NGG/NCC (Ran et al., 2013, D'Agostino et al., 2016).

5.2.4.1 Validating the guide RNAs (gRNAs) that target *pierce1*

In order to find potential target sites from *pierce1* for synthesising gRNA, I utilised a webtool called 'CHOPCHOP' that identifies potential target sites without off targets and list them according to their quality (Labun et al., 2016).

As shown in Figure 5.7, CHOPCHOP results showed potential target sites in *pierce1* for gRNAs. The green coloured target sites were predicted to be the best quality to achieve expected mutations. Since, *pierce1* has a small coding region composed of 3 exons, only a few sites were identified. I decided to use two approaches; 1) to use a single gRNA that would result in indels (insertion/deletion) in the target site, 2) to use double gRNAs to make a deletion of the region spanning between the two target sites.

ENSDART00000081909.4

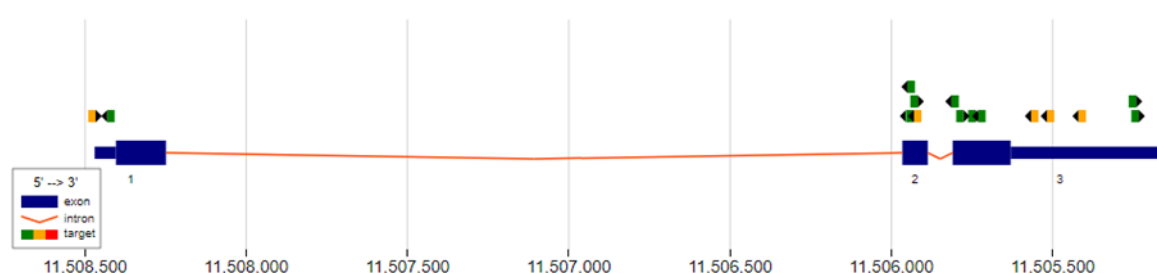


Figure 5-8. *pierce1* gRNA target sites identified by CHOPCHOP.

The results are displayed across the genomic region of *pierce1*. The target colour shows the quality of each sgRNA (green [best] to red [worst]). <http://chopchop.cbu.uib.no/search.php>

For the sgRNA approach, I chose three target sites found on exon 2 and made gRNAs targeting those sites. The efficiency of the gRNAs was first tested

in vitro with PCR amplified coding region of *pierce1* from WT zebrafish cDNA. As shown in Figure 5.9, only 1 of the 3 gRNAs was able to cleave the PCR product.

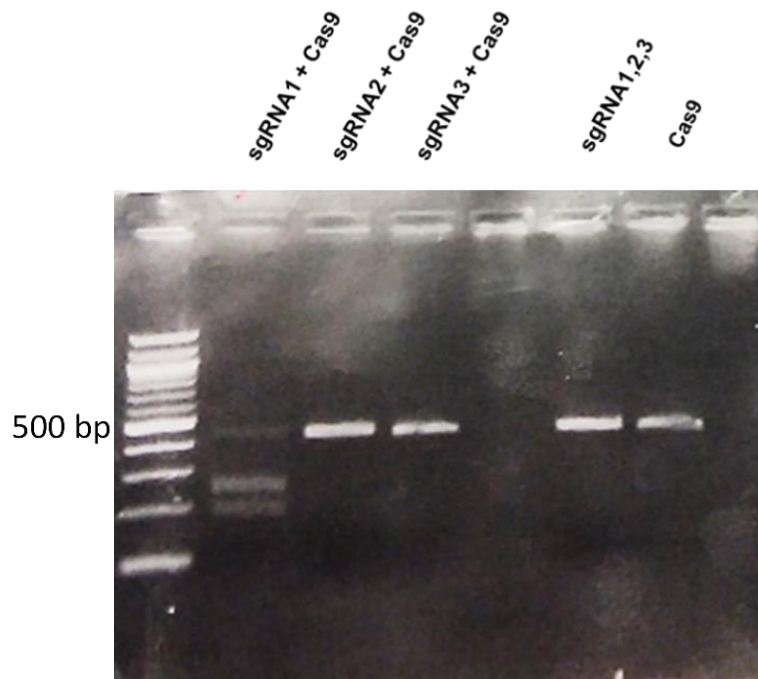


Figure 5-9. Validation of sgRNAs *in vitro*.

sgRNAs that target 3 different target sites of exon 2 on *pierce1* gene were added along with Cas9 in to PCR amplified *pierce1* transcript. As controls, *pierce1* transcript was incubated with sgRNAs without Cas9 and Cas9 without sgRNAs. Only with sgRNA1, Cas9 was shown to cleave the PCR product.

Once validated *in vitro*, I injected sgRNA1 with Cas9 protein into one cell stage zebrafish embryos. At 24 hpf, 8 injected embryos were pooled together for gDNA extraction. The region spanning the target site was amplified as shown in Figure 5.10.

There was no difference in band size observed between WT and sgRNA1 injected embryos. This was expected because small indels would not be visible in the gel. So I gel extracted these bands and cloned into pCR II TOPO vector. These were sent for sequencing. For the sgRNA injected

embryos, 1 out of the 5 colonies picked for sequencing had a 12 bp deletion in the target site as shown in Figure 5.10. This experiment validated the efficiency of this sgRNA1 *in vivo*. Once validated, I continued injecting embryos with sgRNA1 + Cas9 RNA and sent them to the nursery to grow into adults.

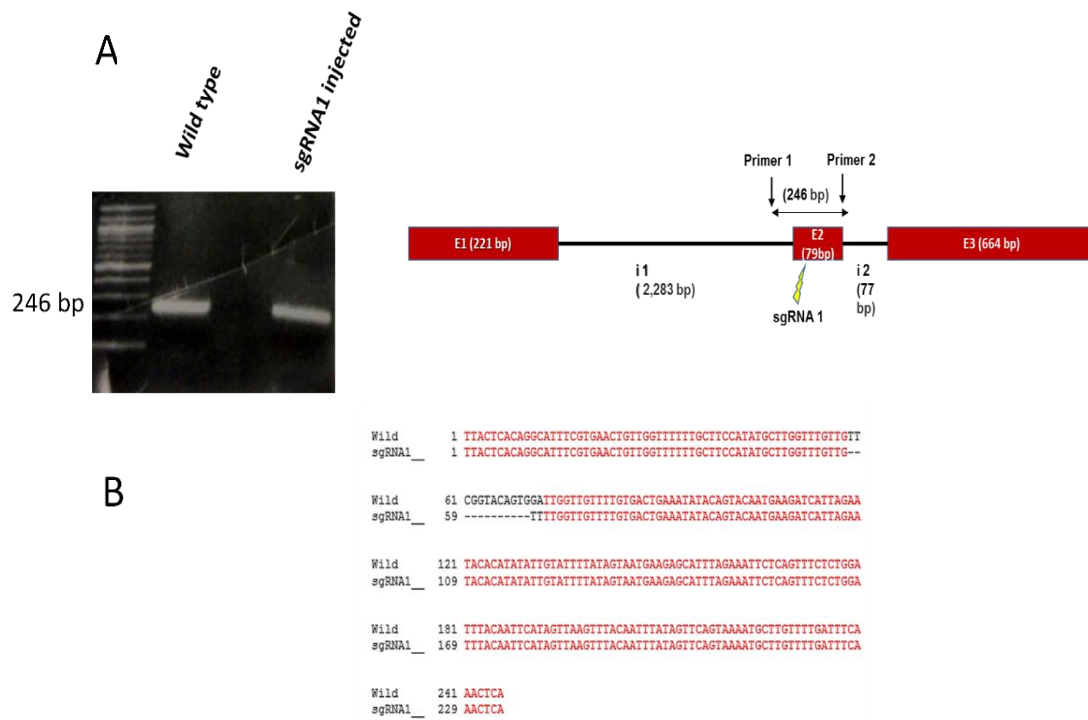


Figure 5-10. Validation of sgRNAs *in vivo*.

sgRNA1 was injected into one cell stage WT zebrafish along with Cas9. 8 injected embryos were pooled to extract gDNA. The gDNA was used to amplify the region spanning the target site using the primers indicated in the Figure. The products were gel extracted and cloned in to pCR II TOPO. Out of the 6 clones sequenced, one had a 12 bp deletion at the target site validating the efficiency of the sgRNA *in vivo*.

For my second approach with dgRNAs for deleting a large region, I chose the green coloured target site in the 5'UTR of *pierce1* as shown in Figure 5.8. I made a gRNA against this target site. I proposed that the combination of the newly made gRNA with the previously used gRNA would result in a deletion that span from 5'UTR to exon 2 of *pierce1*.

The efficiency of the newly made gRNA was also tested *in vitro* with *pierce1* cDNA with 5' and 3' UTRs cloned into pCR II TOPO. The gRNA was tested alone and in combination with previously used gRNA. It was compared with the plasmid with just Cas9 (negative control). As shown in Figure 5.11a, the gRNAs were shown to cleave the plasmid.

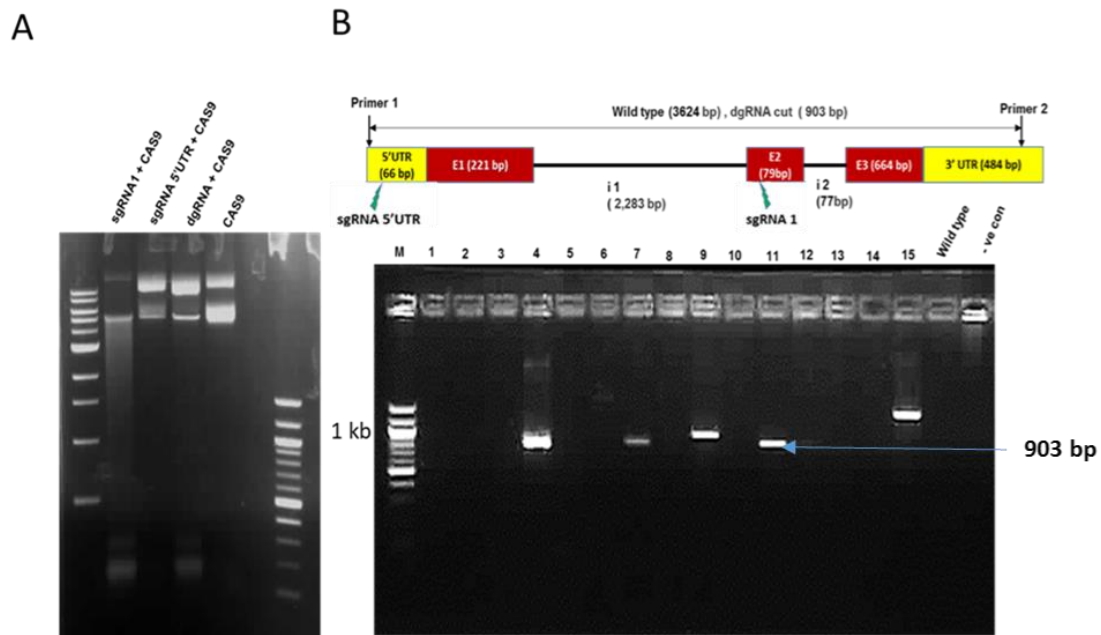


Figure 5-11. Validation of dgRNAs *in vitro* and *in vivo*.

A new gRNA was designed against a target site on 5'UTR. This was validated *in vitro* alone and in combination with sgRNA1 on a plasmid containing 5'UTR-*pierce1*-3'UTR. A) sgRNA5'UTR was shown to cleave the plasmid by itself and in combination with sgRNA1. B) sgRNA5'UTR + sgRNA1 (dgRNAs) were injected into one cell stage zebrafish embryos along with Cas9. gDNA was extracted from injected embryos and PCR was carried out using the primers indicated in the Figure. As shown, deletions generated by dgRNAs were found in several embryos validating the dgRNA approach.

After validation *in vitro*, the two gRNAs were injected into one cell stage zebrafish embryos along with Cas9. As shown in Figure 5.11b, primers were designed to amplify from 5'UTR to 3'UTR of *pierce1*. In the WT embryos, the PCR would not be expected to generate a product as it is too large to amplify (3824 bp) with the PCR conditions used. With the deletion generated by dgRNAs, the PCR would amplify a 903 bp product.

gDNA was extracted from 15 injected embryos and PCR was carried out using these primers. As shown in Figure 5.11b, the expected 903 bp product was amplified from some injected embryos along with larger products from few embryos. Subsequently, these were gel extracted and cloned into pCR II TOPO for sequencing.

As expected, the 903 bp product resulted from dgRNA deletion of the region spanning between the target sites. Sequencing of the larger products revealed that the allele had a partial deletion due to the NHEJ repair mechanism existing in the fish embryos (Certo et al., 2011, Cong et al., 2013). So, I continued injecting embryos with dgRNAs with Cas9 and these were sent to the nursery to grow into adults.

5.2.4.2 Generating *pierce1* mutant zebrafish line from sgRNA/dgRNA+Cas9 injected F0 fish.

Since, injected zebrafish embryos (F0) are mosaics, a screening step was required to identify founders with mutations induced in the germline for transmission into the next generation. F0 fish were crossed with WT and gDNA was extracted from the progeny to check for transmission of mutant alleles. With the sgRNA approach, PCR for progeny from a female F0 fish was found to amplify a larger product than the expected product from WT. This band was gel extracted and sequenced. Sequencing revealed that an allele with a 29-base pair insertion (c.178_179ins (29 bp)) in the target site of exon 2 of *pierce1* was being transmitted as shown in Figure 5.12. Hence, this F0 female fish was outcrossed to raise an F1 generation with carriers, from where I could generate F2 zygotic mutants.

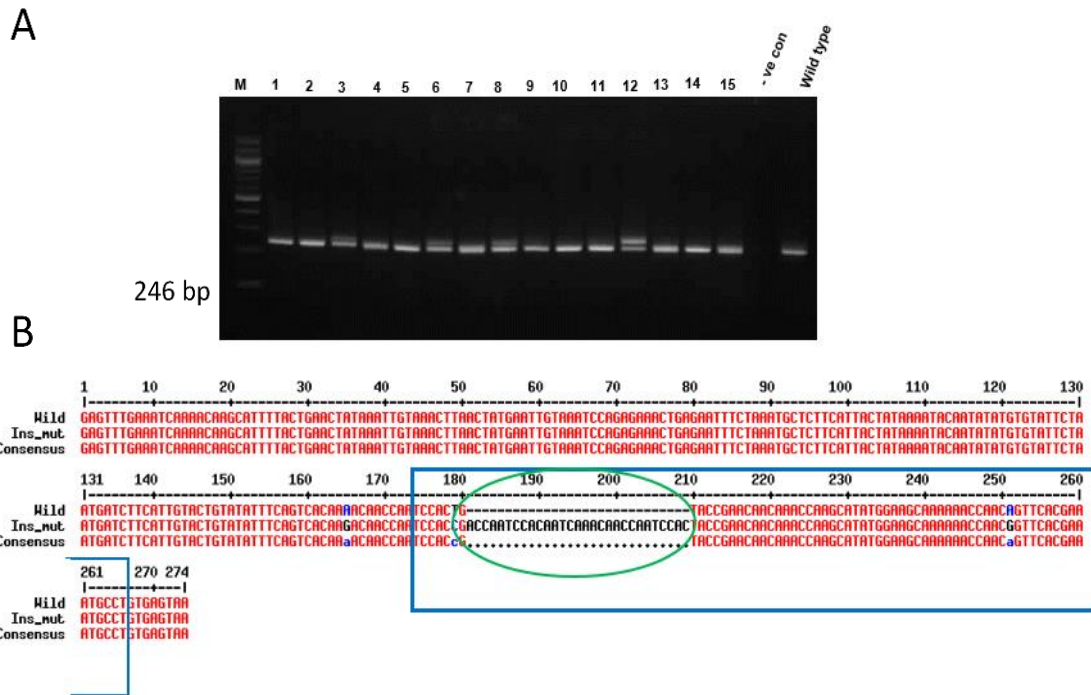


Figure 5-12. Transmission of 29 bp insertion in exon 2 from sgRNA1 injected F0. A) gDNA from progeny from outcross of sgRNA1 injected F0 female was used to carry out PCR to amplify region spanning target region. A larger product in addition to the expected product was observed in some embryos. B) These products were gel extracted and cloned into pCR II TOPO for sequencing. The results revealed that larger product was caused by 29 bp insertion (circles in green) in the target site on exon 2 (boxed in blue) resulting in a frameshift.

Similarly, with the dgRNA approach, a male founder was found that transmitted an allele with partial deletion of the intron1 and a 5 base pair deletion in the target site in exon 2 (c.176_180del) resulting in a frameshift as shown in Figure 5.13. Again, this founder was outcrossed to raise F1 generation with heterozygous fishes. These heterozygous fish could be used to generate F2 homozygous zygotic mutants.

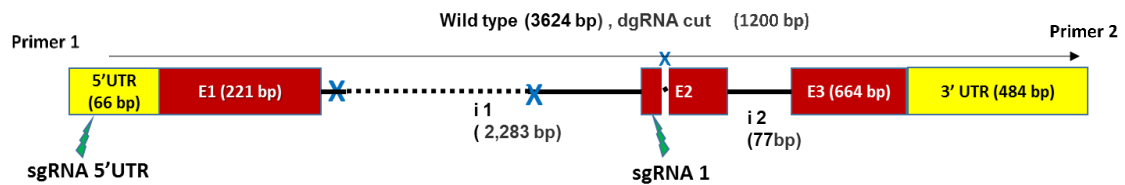
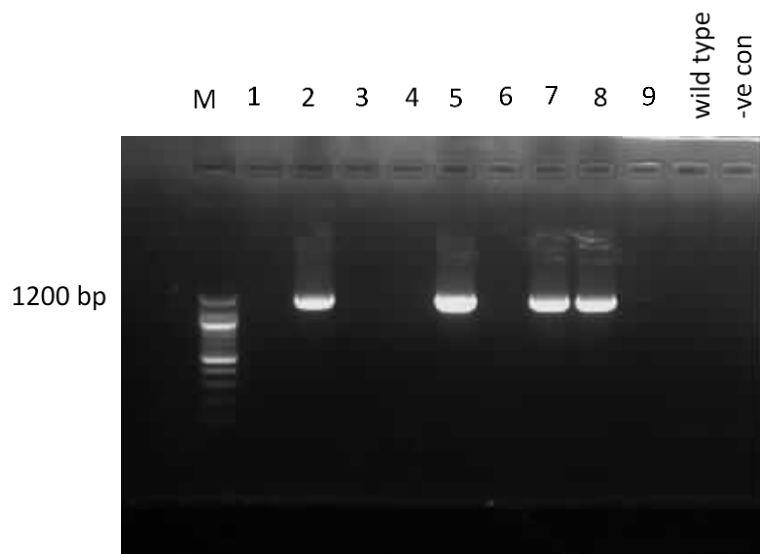


Figure 5-13. Transmission of 5 bp deletion in exon 2 from a male founder injected with dgRNA.

gDNA from progeny from outcross of dgRNA1 injected F0 male was used to carry out PCR to amplify region spanning target region. A product of size 1200 bp was observed in some embryos. These products were gel extracted and cloned into pCR II TOPO for sequencing. The results showed that larger product was resulted by a partial deletion of the targeted region. This allele had a partial deletion of intron 1 and a 5 base pair deletion in exon 2.

Subsequently, F1 fish for both alleles were fin-clipped to extract gDNA and screened by PCR to identify heterozygous fish. To raise homozygous mutants, the F1 heterozygous fish were in-crossed to generate F2 generation. According to the Mendelian ratio, we expect 25% of F2 fish to be homozygous.

gDNA was extracted from progeny of the F1 heterozygous fish in-cross and PCR was carried out to confirm the existence of homozygous progeny

using primers spanning the deleted intron region as shown in Figure 5.14 for the c.176_180del allele.

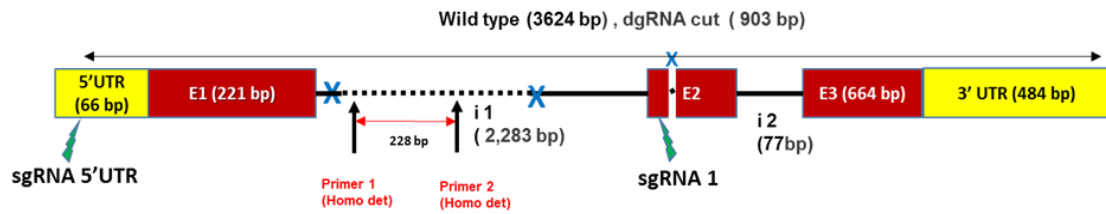


Figure 5-14. Location of primers designed to identify homozygous mutants with c.176_180del allele.

In the c.176_180del mutants, the expected product size of 228bp was not amplified in the homozygous but it was amplified in the WT and heterozygous embryos as shown in Figure 5.15 b.

For c.178_179ins (29 bp) allele, the same primers from Figure 5.10 were used. Product of 2 different sizes was observed in heterozygous whereas only the larger product was observed in homozygous embryos (Figure 5.15 a). The smaller product was observed in WT.

However, for both mutant alleles, we did not see any phenotypical difference between F2 zygotic mutants (homozygous) embryos from WT and heterozygous embryos. The number of homozygous embryos identified corresponded to the expected 25% as per Mendelian ratio indicating embryonic lethality did not occur.

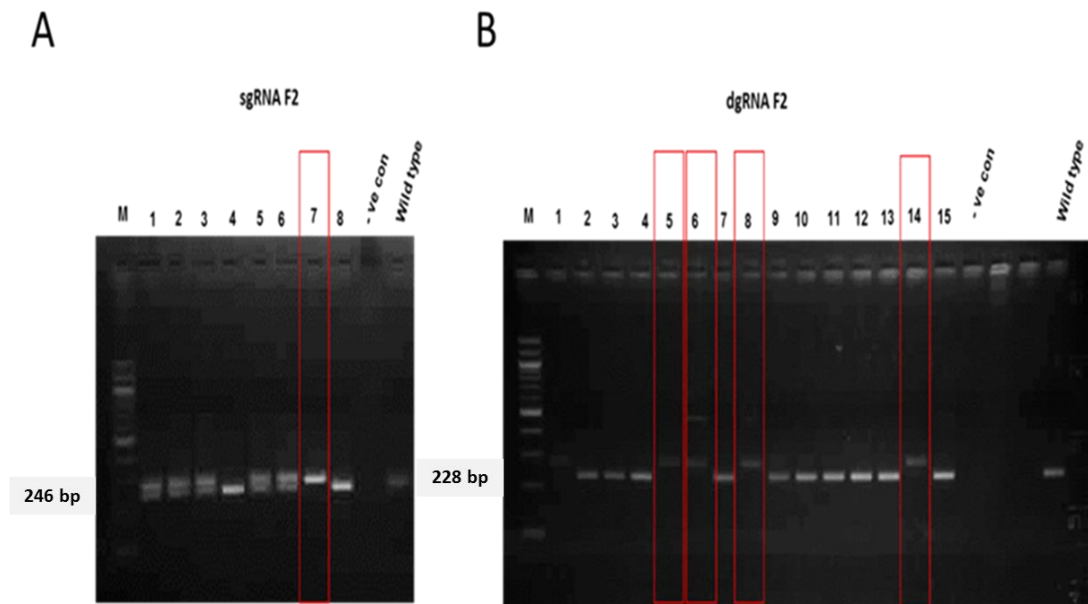


Figure 5-15. Identification of F2 homozygous *pierce1* mutants for *c.178_179ins(29 bp)* and *c.176_180del*.

A) For the *c.178_179ins(29 bp)* allele, a homozygous embryo was identified by PCR that is highlighted by red column by using primers shown in Figure 5-10B. B) For *c.176_180del* allele, homozygous embryos were identified by PCR using the primers shown in Figure 5.14. Homozygous embryos are highlighted by red column.

5.2.4.3 Maternal contribution of *pierce1* mRNA in zebrafish embryos

Since the zygotic mutants for *pierce1* did not show any significant difference from WT, I decided to check if *pierce1* mRNA is contributed from the maternal side into the embryos. I thought that the maternal contribution of WT *pierce1* mRNA from the heterozygous mother into the zygotic mutants would be acting as a rescue factor and thus be masking the phenotypes.

To check for maternal contribution, I extracted RNA and made cDNA from embryos at earlier developmental stages, 1.5 hpf, 3 hpf, 5 hpf, 6 somites, 10 somites, 18 somites and 24 hpf. As shown in Figure 5.16, *pierce1* mRNA

was found from earliest developmental stages indicating there is maternal contribution of *pierce1* mRNA.

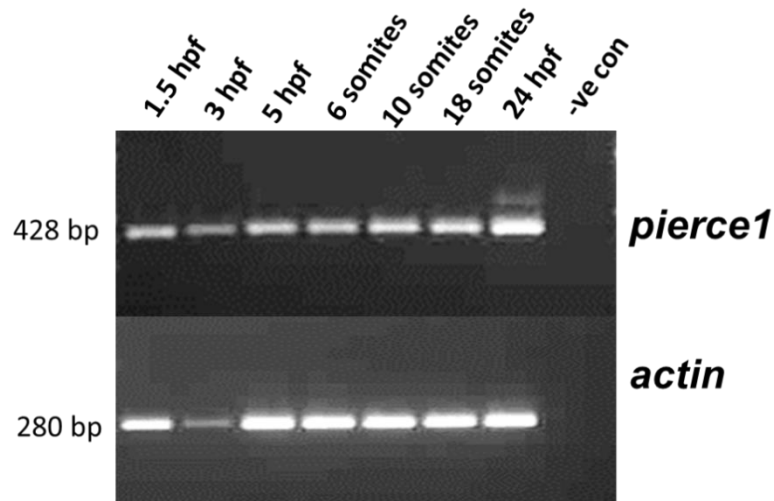


Figure 5-16. Maternal contribution of *pierce1* in zebrafish embryos.

cDNA was made from zebrafish embryos at early developmental stages, 1.5 hpf, 3 hpf, 5 hpf, 6 somites, 10 somites, 18 somites and 24 hpf. PCR for *pierce1* and *actin* (loading control) was carried out on these cDNAs. *pierce1* transcripts were identified from earliest developmental timepoint when the embryonic transcription is not carried out. Hence, it was concluded that there is maternal contribution of *pierce1*.

5.2.4.4 Maternal zygotic mutants for *pierce1*

Since there is maternal contribution of *pierce1* mRNA in zebrafish embryos, I in-crossed F2 *pierce1* homozygous mutants (zygotic mutants) for both mutant alleles to generate maternal zygotic mutants. Zygotic mutants from both alleles were able to generate progeny. Therefore, it can be concluded that both mutants did not have fertility issues and sperm motility was normal.

There was no commercial antibody to confirm that Pierce1 protein was not generated in mutants. Therefore, I used cDNA from pooled F3 maternal zygotic mutants to carry out PCR to amplify *pierce1* transcripts.

As shown in Figure 5.17A, a larger PCR product was observed for c.178_179ins(29 bp) maternal zygotic mutants compared to WT. These products were cloned into pCR II TOPO and sent for sequencing. As shown in Figure 5.17B, the sequencing showed that the 29 bp insertion is integrated in the *piece1* transcript.

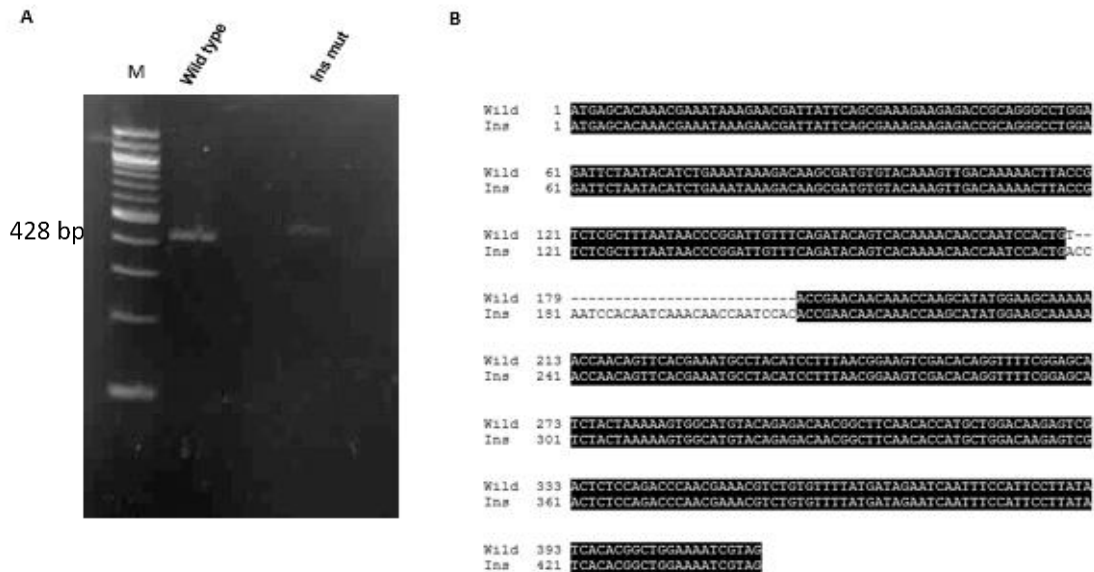


Figure 5-17. Validation of mutation in *piece1* transcripts of c.178_179ins(29 bp) maternal zygotic mutants.

A) *piece1* transcripts amplified by PCR from mutants and WT. Product is larger in mutants. B) Sequencing of PCR products showed 29 bp insertion in the *piece1* transcripts from mutants.

As shown in Figure 5.18A, no significant size difference was observed for PCR products generated by c.176_180del maternal zygotic mutants compared to WT. The PCR products were cloned into pCR II TOPO and sent for sequencing. As shown in Figure 5.18B, the sequencing showed that the 5 bps are deleted from the *piece1* transcripts.

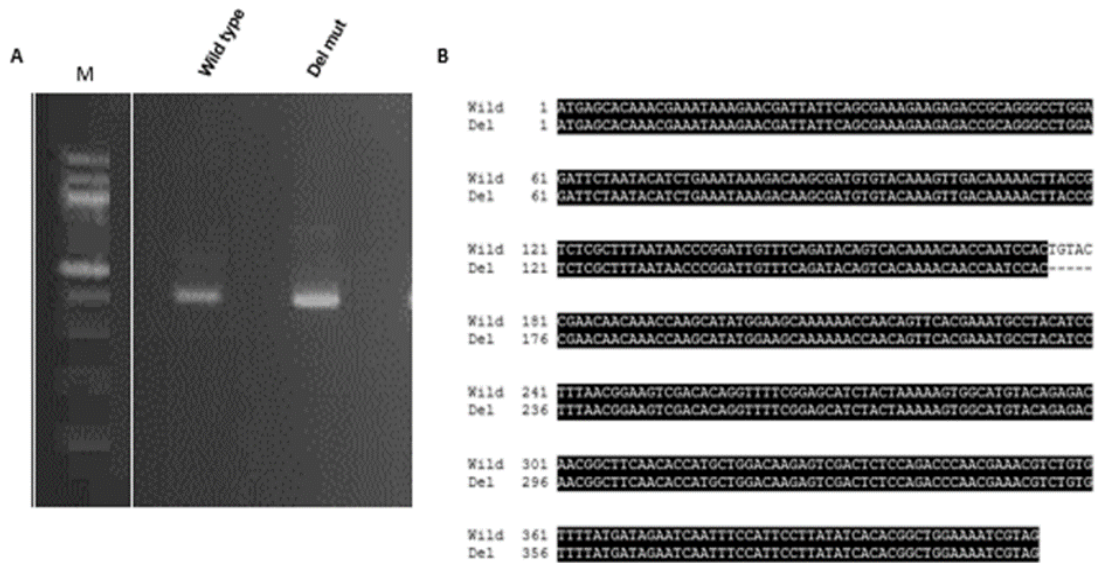


Figure 5-18. Validation of mutation in *pierce1* transcripts of *c.176_180del* maternal zygotic mutants.

A) *pierce1* transcripts amplified by PCR from mutants and WT. B) Sequencing of PCR products showed 5 bp deletion in the *pierce1* transcripts from mutants.

The multi-alignment of *Pierce1* orthologues of human, mouse and zebrafish highlight the conserved regions (Figure 5.19A). Both mutant transcripts were translated in silico using ExPasy (<https://web.expasy.org/translate/>). As shown in Figure 5.19B, the mutations result in frameshifts and premature stop codons in *pierce1* mutant transcripts and would be expected to generate truncated proteins. In the truncated proteins generated from the mutant transcripts, 70% of the conserved residues would be missing.

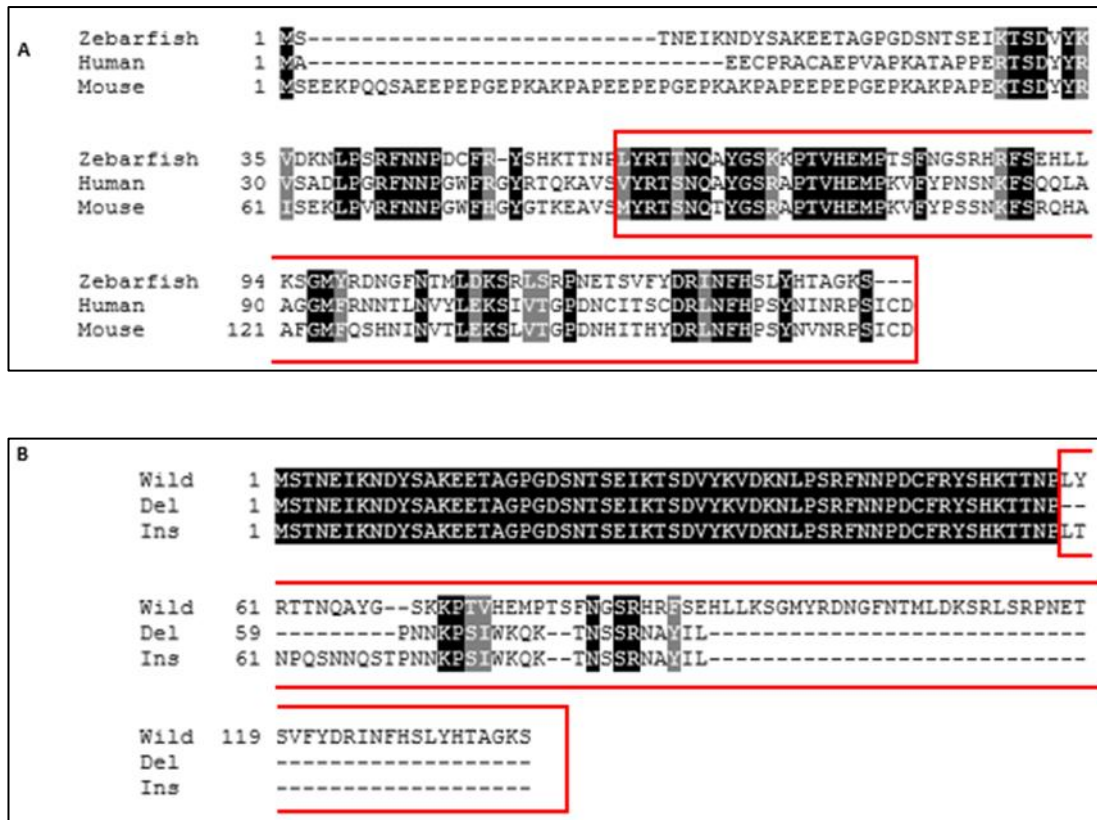


Figure 5-19. Conserved amino acid residues are missing in the mutants.

A) Multi-alignment of Pierce1 from zebrafish, mouse and human using *Clustaw* and *Boxshade*. The conserved residues are shaded in black. B) Multi-alignment of Pierce1 protein sequences generated from WT and mutants' transcripts. 70% of the amino acid residues are lost in the mutants. Species and accession numbers are as follows: Zebrafish (*Danio rerio*, GenBank: NP_001116715.1); Mouse (*Mus musculus*, GenBank: NP_081316.1); Human (*Homo sapiens*, GenBank: NP_001041730.1).

5.2.4.5 Maternal zygotic mutants exhibited mild *situs* abnormalities

After validating the maternal zygotic mutants, we characterised the phenotypes of these maternal zygotic mutants by observing them at 24 hpf, 48 hpf and 72 hpf. In contrast to the morphants, they did not exhibit curved axis, hydrocephalus and heart oedema. Otolith defects and pronephric cyst were not observed. A small proportion exhibited *situs* abnormalities as shown in Figure 5.20. The live imaging of the embryos showed small proportion of

embryos with KV cilia with abnormal motility or immotility (see attached video files).

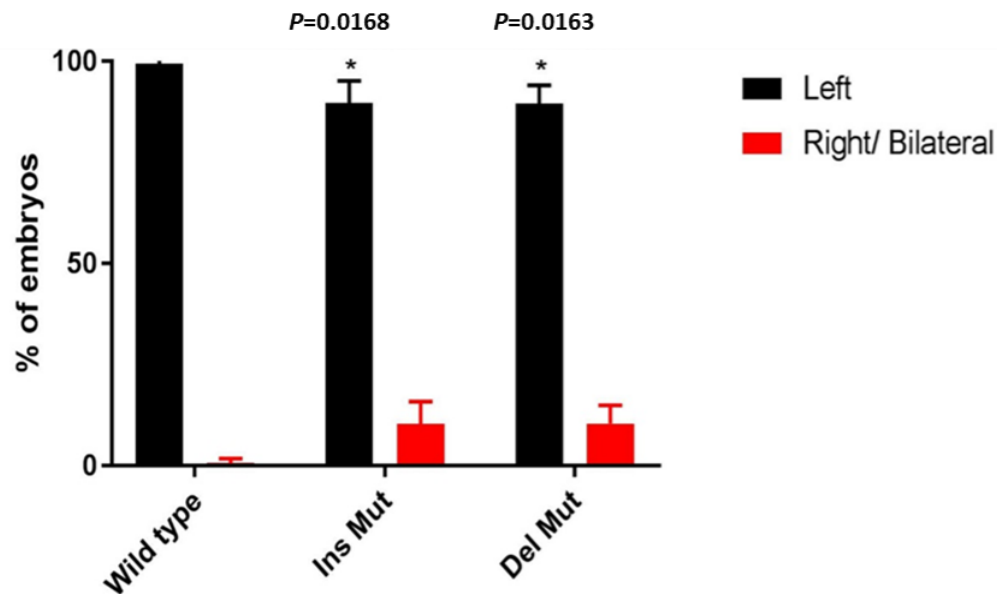


Figure 5-20. Maternal zygotic mutants showed mild situs abnormalities.

In maternal zygotic (mz) mutants from both alleles showed 10-20% embryos with *situs* abnormalities. The difference between WT and mutants is significant. In each trial, 50- 70 embryos for each variable was used. Error bars indicate standard error of mean (SEM) (n=3 independent batches of experiments). *-p<0.05 using 2way ANOVA.

5.3 Discussion

Pierce1 was one of the candidate genes that I chose for further characterisation. It had come up in many ciliary genomic and proteomic screens. Moreover, orthologues of PIERCE1 are only identified in organisms with motile cilia (Mi et al., 2010). It encodes a small protein made up of 167 amino acids in mouse and 137 amino acids in zebrafish. No known functional domains have been identified in this protein and the only identified conserved domain is called DUF4990. In the literature, PIERCE1 was first identified as

a target of TP53 that was also overexpressed in Rb^{-/-} MEFs (Sung et al., 2007, Sung et al., 2010).

To characterise the functional role of PIERCE1, I used zebrafish for *in vivo* investigation. Zebrafish is an increasingly popular vertebrate whole organism model for biomedical research. They have many advantages such as large progeny number, small body size, transparent embryos and abundance of mammalian orthologues (Malicki et al., 2011, Song et al., 2016a).

Initially, I decided to utilise two independent MOs for transient knockdown of *pierce1* in zebrafish embryos. Both morphants showed severe laterality defects and curved axis, phenotypes usually associated with motile cilia defects (Malicki et al., 2011, Song et al., 2016a). Abnormal cilia motility was observed in KV of the morphant embryos that might explain the laterality defects. Immunolabelling of cilia by Acetyl α -tubulin suggested that there was no difference in the cilia morphology in the morphants. In terms of cilia structural analysis, immunostaining has limitations. It can only be used to study cilia number and length. To study cilia architectural defects, electron microscopy would be more beneficial. Such an analysis was not undertaken.

During my study, the same group that identified PIERCE1 as a target of TP53, reported that mouse null mutants of *Pierce1* exhibit severe laterality defects. They reported there was no cilia morphology differences in the motile cilia of mouse embryonic node. In the *pierce1* null embryos, they also found loss of asymmetric expression of *Cerl2*, the earliest flow responding gene, along with randomised expression *Nodal* and *Lefty1/2* (Sung et al., 2016).

These results confirm the findings I had with the MO assays. In addition, using live imaging, I concluded that the laterality defects arise due to abnormal motility of cilia in the KV.

To further understand the functional role of Pierce1 in motile ciliogenesis, I wanted to study the subcellular localisation Pierce1 in KV. Since, no working commercial antibodies were available at the time of my study; I decided to use expression of tagged versions of Pierce1 in zebrafish embryos to detect the localisation. Two tagged versions were utilised to overcome the limitation caused by positioning of the tags; a N-terminus Myc tag and a C-terminus GFP tag. Both tagged versions localised to the cytoplasm. One limitation of this approach is the relative larger size of tags with the small Pierce1 protein can affect the native localisation of the Pierce1 protein. Hence, to get a more reliable data for the localisation, I would ideally wish to use an antibody against Pierce1 that would detect the native protein.

I attempted to rescue the morphants using the 6 x Myc-Pierce1 construct. However, there was no significant difference between rescue and morphants. There are two different ways to interpret this result. Firstly, the tags are interfering the native function of the protein and secondly the morphant phenotypes were caused by off-target effects of the MOs.

Although, initially MOs gained a widespread popularity in the zebrafish community through their ease of usage and rapid results, problems with their application in zebrafish embryos soon emerged. Several research groups reported mutants failing to exhibit expected morphant phenotypes resulting

in perplexing 'pseudophenotypes' (Kok et al., 2015, Place and Smith, 2017, Eve et al., 2017).

Kok *et al* used gene-editing techniques to make zebrafish mutants for 24 genes suspected to be involved in the vascular development. However, mutants for only three of the 24 genes showed phenotypes related to vascular development defects. Previous studies had reported phenotypes in the morphants for more than half of these genes (Kok et al., 2015).

The low concordance between mutant and morphant phenotypes has made many researchers feel sceptical about the MO assay results (Vogan, 2015). Hence, MOs might not be reliable enough to use as a standalone tool to assess gene function. In addition, MOs are only able to generate a transient knock down. Therefore, the phenotypes in adults cannot be characterised.

To validate the phenotypes induced by the transient knockdown by MOs and to assess the phenotypes of the adult fish, I proceeded to generate a zebrafish genetic mutant line for *pierce1*. The small size of the *pierce1* ORF meant only few choices were available for suitable target sites. I decided to use a sgRNA approach to make small indels on exon2 of *pierce1* and dgRNAs approach that target the 5'UTR and exon 2 of *pierce1* that would delete the region spanning in between.

Using the sgRNA, I identified a founder that transmitted 29 bp insertion in the target site of exon2, which would be expected to result in a frame shift and a truncated protein. With the dual-guide CRISPR/Cas9 (dgRNA) genome editing approach, one founder was identified that transmitted a partial deletion of the target region. Several studies have reported that dgRNA can

result in multiple classes of structural variation mediated by non-homologous repair within unique genic segments across a range of sizes (Tai et al., 2016, Certo et al., 2011, Cong et al., 2013). In my allele, there was a partial deletion of intron 1 and a 5 bp deletion in the target region of exon 2. Therefore, this allele was similar to the allele produced by sgRNA approach where the frameshift results in a truncated protein.

The only identified conserved functional domain, known as DUF4990, spans from 11-117 amino acids of the *Pierce1* protein. Both mutant alleles would be expected generate truncated proteins with first 60 amino acids and a disruption of the conserved domain.

The zygotic mutants generated by crossing heterozygous fish did not show any phenotypical difference from WT but I found that there was maternal contribution of *pierce1* mRNA in the embryos. In all animals examined, the earliest stages of development depend on maternal gene products, which are made during oogenesis and deposited in the egg. The phase of maternal control of embryonic development differs among animals and it relies on the onset of zygotic transcription and the stability of the maternal gene products (Abrams and Mullins, 2009, Tadros and Lipshitz, 2009). The initiation of zygotic transcription happens during blastula stage (2.25 hpf -5.25 hpf) in zebrafish embryo development (Kane and Kimmel, 1993, Tadros and Lipshitz, 2009, Langley et al., 2014). My end-point RT-PCR detected presence of *pierce1* transcripts from 1.5 hpf. I considered that the maternal deposition of WT mRNA from the heterozygous mother would be compensating for the mutant phenotype.

Hence, I proceeded to make maternal zygotic mutants for *pierce1* by in-crossing zygotic homozygous mutants. Interestingly, the adult zygotic mutants were viable and fertile indicating that sperm motility is normal, an observation that might be unexpected for a ciliary phenotype.

Unexpectedly, in maternal zygotic mutants from both alleles, only small majority had *situs* abnormalities. Live imaging showed small number of abnormal/ immotile cilia in KV of the mutants and the proportion varied between different embryos. Since, the mutants from both mutant lines (two independent alleles) show few embryos with laterality defects, the laterality defects observed are less likely due to off-target defects. The existence of *pierce1* null mouse mutants that exhibit severe laterality defects like *pierce1* knockdown zebrafish embryos (i.e. morphants) suggest that a compensatory mechanism existing in the zebrafish knockouts (i.e. mutants) that might be masking the mutant phenotype.

Phenotypic differences between knockdowns (e.g., antisense-treated animals) and knockouts (i.e., mutants) have been reported in a number of recent studies in model systems including mouse (White et al., 2013), zebrafish (Kok et al., 2015) and *Arabidopsis* (Bouche and Bouchez, 2001).

Although the off-target effects of the anti-sense reagents can be a reason for these differences, recent studies in zebrafish have given genetic compensation as an alternative explanation. This included a study by Andrea Rossi and colleagues (2015). Knockdown of *egfl7*, an endothelial extracellular-matrix (ECM) gene, in zebrafish lead to severe vascular defects however; the knockouts did not show any significant phenotypes. They found

upregulation of other ECM proteins, specifically Emilins, which might explain this discrepancy partially in *egfl7* mutants but not in the MO embryos. Furthermore, they reported minor or no vascular defects upon *egfl7* MO injections into *egfl7* mutants, suggesting that the phenotypic differences are not due to MO toxicity (Rossi et al., 2015).

In 2017, Anderson *et al* have given a second explanation where they challenged the assumption that complete loss of function (null) phenotypes can always be made by splice site, frameshift, and nonsense mutations. They demonstrated the emergence of transcript variants with restored ORF with alternative mRNA splicing and use of cryptic splice sites in homozygous mutants. Hence, these variants have the potential to translate into at least partially functional proteins (Anderson et al., 2017). However, this phenomenon can be tested by reverse transcription PCR and sequence analysis on homozygous mutant embryos.

I amplified the *pierce1* transcript from both mutant lines and sent the resultant products for sequencing. My data revealed the mutated regions were still intact in the transcript and would result in frameshift and consequently truncated protein. So, I conclude that frame-restoring mRNAs are not found in the *pierce1* mutants. It can also be argued that, through mechanisms such as ribosomal frameshifting and nonsense read through, mRNAs can be translated into full-length proteins. This is difficult to test without a working antibody. Anderson *et al* provided guidelines to tackle this problem including targeting the functional domain of the protein (Anderson et al., 2017). In both *pierce1* mutant alleles, the conserved domain, DUF4990,

should have been disrupted in the truncated protein generated by the mutants.

Dosage compensation was first observed for X-linked genes in *Drosophila* by Muller in 1932 ((MULLER, 1932). Subsequently, in many model organisms, genetic compensation has been reported i.e. mouse (White et al., 2013), zebrafish ((Kok et al., 2015) and *Arabidopsis* (Bouche and Bouchez, 2001). Furthermore, a comprehensive study of 874 genes in over 500,000 human genomes identified 13 individuals harbouring severe disease-causing mutations in 8 different genes, with no reported clinical manifestation of the disease (Chen et al., 2016). Another study on British individuals with Pakistani heritage also reported no significant relationship between genotype and disease manifestations (Narasimhan et al., 2016). Similar findings were reported from a study on individuals from Iceland (Sulem et al., 2015).

Molecular insight into the mechanisms behind genetic compensation is limited. Several mechanisms have been proposed to work behind this phenomenon recently by El-brolosy and Stanier. This include epigenetic changes, mRNA surveillance pathways, ncRNAs, uORFs, RBPs, and miRNAs (El-Brolosy and Stainier, 2017).

In conclusion, *Pierce1* is conserved only in organisms with motile cilia and it has been identified in many ciliary genomic and proteomic screens. Choksi *et al* and my own experiments have shown that *pierce1* functions downstream of *Foxj1*, the master regulator of motile ciliogenesis (Choksi et al., 2014). *pierce1* knockdown in zebrafish showed phenotypes associated

with ciliary defects including severe *situs* abnormalities. Further analysis showed abnormal ciliary motility in KV in the morphants. This was in agreement with the results from mouse null mutants of *perce1* (Sung et al., 2016). However, *perce1* knockout in zebrafish only showed mild *situs* abnormalities. This could be due to genetic compensation mechanisms that mask the mutant phenotype. Many studies have shown difference between knockdowns and knockouts for several genes.

Future work should focus on validating that the mild phenotype in mutants is due to genetic compensatory mechanisms. This could be validated by injecting MOs into the mutants. If there were genetic compensation in the mutants, the mutants would not show severe phenotype as opposed to the WT embryos. It could also seek to characterise the compensatory mechanisms including any upregulation in other genes in the mutants. Ideally the use of an antibody for the protein would help to identify the native protein localisation as this is more reliable than tagged protein expression. This is explored in the next chapter.

Chapter 6 : Localisation of PIERCE1 to multiciliated cells may give clues to its function.

6.1 Preface

PIERCE1 is a novel gene that appears to be important for motile cilia function. The gene was identified in many high throughput genomic screens for ciliary genes as outlined in chapter 4 (Geremek et al., 2011, Hoh et al., 2012, Choksi et al., 2014b, Treutlein et al., 2014b, Nemajerova et al., 2016a). In addition, mouse *Pierce1* null mutant embryos exhibit severe laterality defects consistent with ciliary defects (Sung et al., 2016). Furthermore, knockdown/knockout of *Pierce1* in zebrafish embryos outlined in chapter 5 also showed laterality defects associated with motility defects of cilia in KV.

Since I have only established that PIERCE1 is required for cilia motility, the next step is to understand the biochemical pathway for its function. To understand how PIERCE1 is involved in cilia motility, I have to identify the native localisation of PIERCE1 in ciliated cells. Although, I used tagged expression vectors in zebrafish embryos to understand the subcellular localisation of *Pierce1*, this method has many limitations e.g. expression tags can affect native localisation of the protein.

Fortunately, our collaborator, Dr Dominic Norris (MRC, Harwell, Oxford), gifted us a custom-made polyclonal antibody against full-length mouse PIERCE1 protein raised in rabbit. In this chapter, I outline how we used this antibody in mNEC cultured at the ALI to deduce the expression and localisation of PIERCE1 in primary mouse airway epithelial cells. In addition, I also include

the results from Yeast 2-Hybrid assay carried out with human PIERCE1 on human lung and testis cDNA to find possible interactors.

6.2 Results

6.2.1 Validating PIERCE1 antibody on testis cell lysate by Western blot

To validate the PIERCE1 antibody, we tested it on mouse testis cell lysates (200 mg tissue lysed in 2 ml SDS lysis buffer) by western blot as the gene is highly expressed in testes (Figure 4.2 and 4.3).

As shown in Figure 6.1, different amount of testis tissue lysate (5 μ l to 30 μ l) were loaded on to the gel with SDS lysis buffer as negative control lane. A single band with an apparent molecular mass of just above 20 kDa was detected in all lanes with increasing band densities correlated with increased amount of cell lysate loaded. The predicted molecular mass of the PIERCE1 protein is 18.8 kDa.

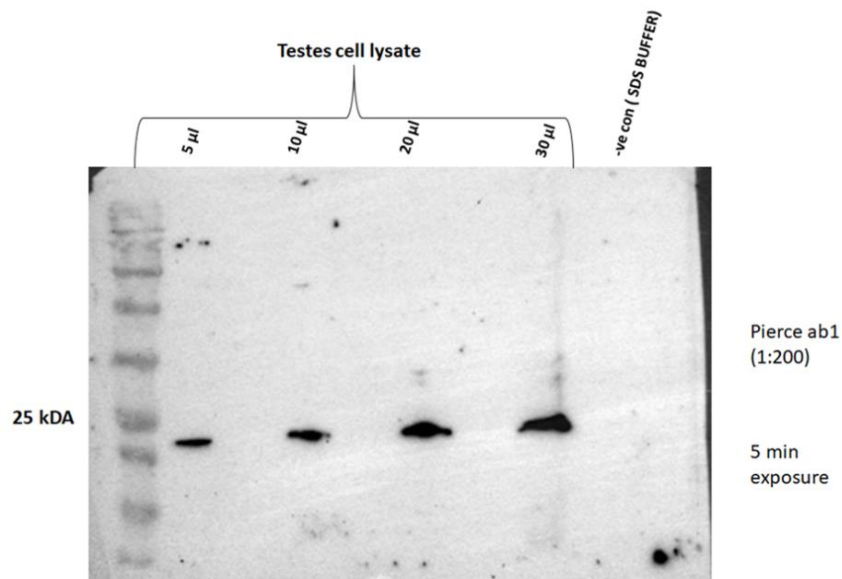


Figure 6-1. Western blot of PIERCE1 in mouse testis tissue lysate.

Increasing amounts of testis tissue lysate (5 µl to 30 µl) was loaded with SDS lysis buffer as negative control. The exposure time was 5 minutes (The blot is representative of n=2).

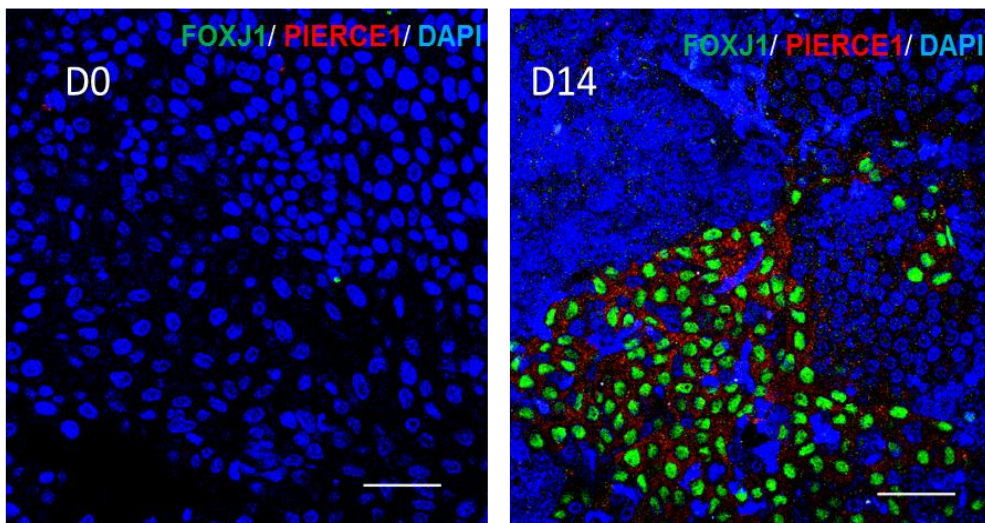
6.2.2 Localisation of PIERCE1 in differentiated mouse airway epithelial cells cultured at the ALI

Next, I wanted to test whether the PIERCE1 antibody could be used to identify the localisation of native PIERCE1 protein in differentiated mNEC cultured at the ALI.

6.2.2.1 PIERCE1 is specifically expressed in ciliated cells

Day 0 and day 14 differentiated mNEC cells were co-stained with an antibody to FOXJ1 that allowed us to visualise the ciliated cells alongside PIERCE1. As shown in Figure 6.2, on day 0 of culture, staining for PIERCE1 and FOXJ1 was absent. At ALI day 14, ciliated cells were found in the cultures, indicated by the staining of FOXJ1 and PIERCE1 was also found to be specifically localised in the ciliated cells. This staining appeared to show a cytoplasmic localisation.

A



B

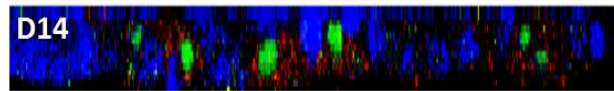


Figure 6-2. PIERCE1 is localised to ciliated cells in ALI mNECs at day 14. Cells were stained with antibodies against FOXJ1 (cilia specific) and PIERCE1. Immunofluorescence confocal images show A) day 0 and day 14 cultures (40x) B) 40x magnification cross section z-stack confocal image of d14 cultures. . Scale bars: 50 μm . (Images are representative of n=3, generated with different cultures)

6.2.4.2 PIERCE1 is localised in the cytoplasm of ciliated cells and does not localise to the cilia axoneme

Cells were also co-stained with ACETYL α -TUBULIN that allows visualisation of the cilia axoneme, and PIERCE1. These cells were then imaged using confocal microscopy to make z-stack images to analyse the localisation of PIERCE1. This technique allows the visualisation of different focal planes in the multi-layered mNEC culture by taking z-stack images through the depth of the cells as shown Figure 6.3.

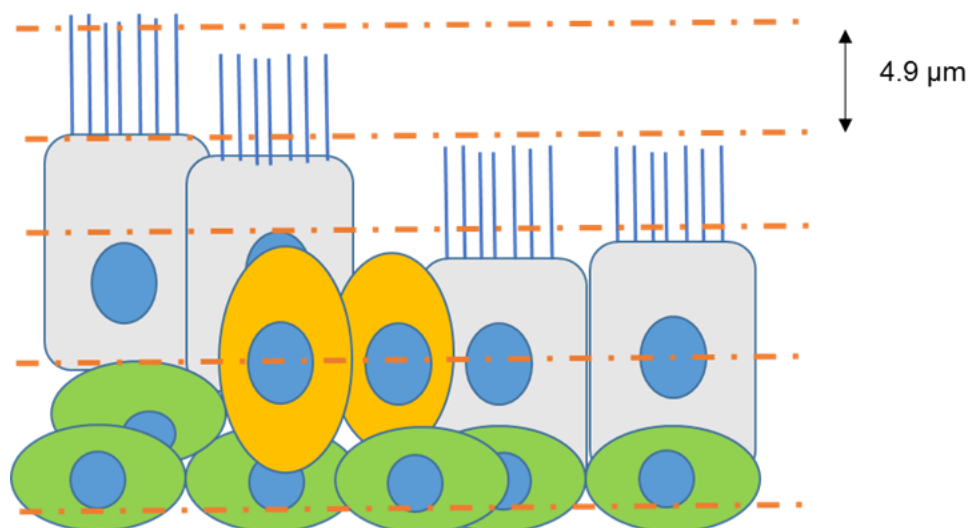


Figure 6-3. Schematic diagram indicating the z-stacks created by the confocal laser scanning microscope from the ALI cultured mNEC samples.

As shown in Figure 6.4, using this technique, I was able to observe that, in the differentiated mNEC, PIERCE1 is localised in the cytoplasm of ciliated cells and does not localise to the cilia axoneme.

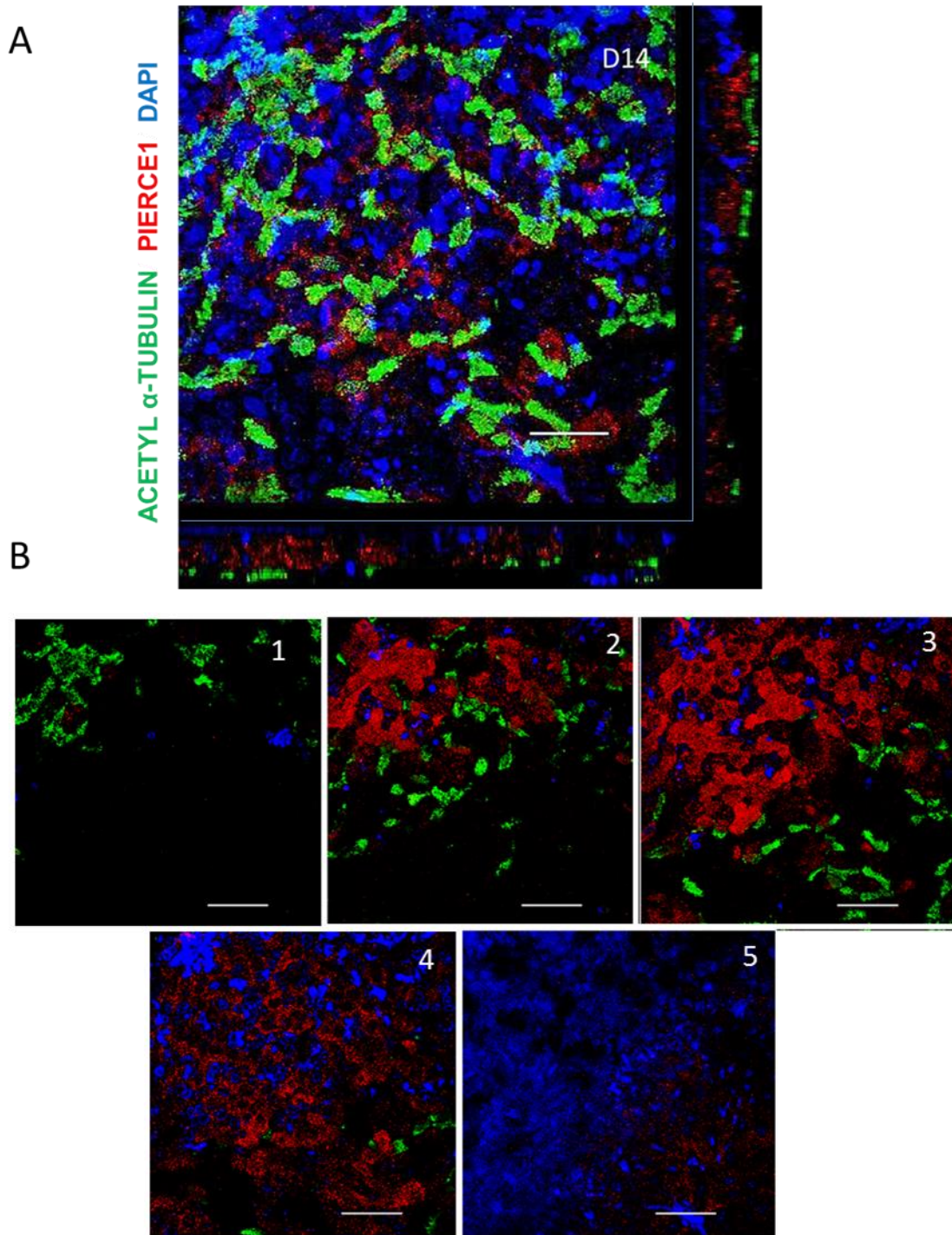


Figure 6-4. PIERCE1 does not localize to cilia axoneme and is localized in the cytoplasm.

Immunofluorescence confocal (40x) image is representative of 3 independent batches of mNEC cultures. At ALI day 14, mNEC were stained with antibodies against ACETYL α -TUBULIN targeting cilia axoneme and PIERCE1. A) Confocal cross-section z-stack image. B) Single z-stack slices from apical surface of the apical (1) to the basal surface (5) of the mNEC culture as indicated in Figure 6.3. Scale bars: 50 μ m.

6.2.3 PIERCE1 is upregulated in mNEC treated with DAPT

In chapter 3, I had shown that MCCs in the mNEC culture at ALI can be increased by DAPT treatment. Therefore, I hypothesized that PIERCE1 expression would also be upregulated in mNECs treated with DAPT. To test this, transcriptional and protein expression of *Pierce1* and *Foxj1* was studied in differentiated mNEC treated with DAPT using real-time PCR and immunofluorescence microscopy.

As shown in Figure 6.5A, transcriptional expression of *Foxj1* and *Pierce1* was significantly increased by around 2-fold in DAPT treated samples. I could show an increased number of ciliated cells (FOXJ1^{+ve}) in DAPT treated mNECs (Figure 3-8). PIERCE1 is also found in FOXJ1^{+ve} cells. Therefore, PIERCE1 may be upregulated in DAPT treated mNEC and PIERCE1 seems to be positively correlated with MCC formation.

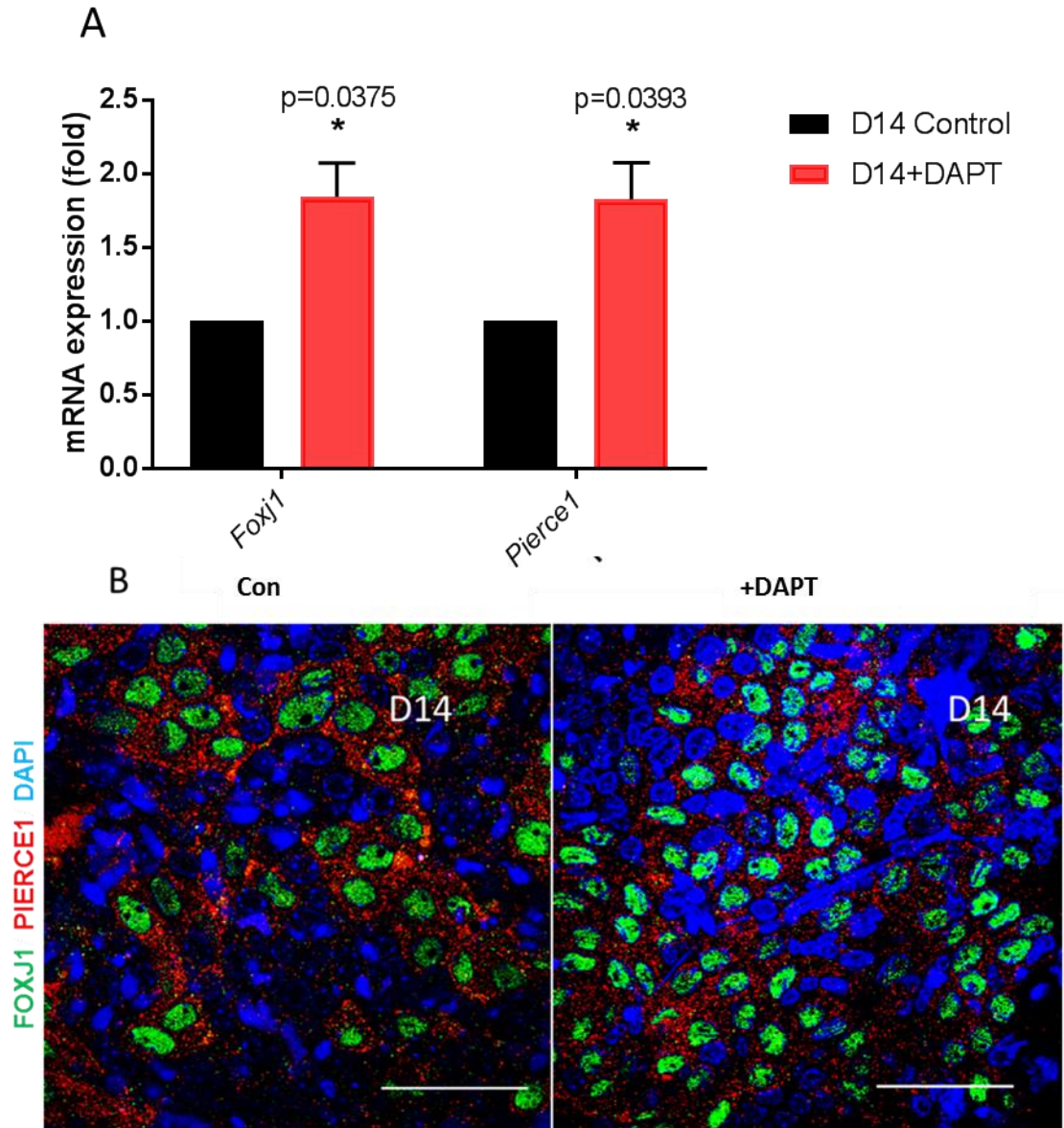


Figure 6-5. *PIERCE1* is upregulated in DAPT treated mNEC.

A. Real-time PCR results of *Foxj1* and *Pierce1* expression DAPT treated mNEC (Scale=50 μ m). The data is representative of 3 batches of cells. Error bars indicate standard error of mean (SEM) (n=3 independent batches of experiments). **-p<0.01 using 2way ANOVA. B. Confocal images show that ciliated cells (FOXJ1^{+ve}) also stain for PIERCE1.

6.2.5 Determining the interactors of PIERCE1

To further understand the molecular functions of PIERCE1, it is essential to uncover the protein partners that it interacts. To do this an unbiased approach was used to identify the interactors of PIERCE1. The yeast two-hybrid system is an *in vivo* method widely used to examine the existence of protein-protein interactions or identify new interacting candidates of a known protein (Chien et al., 1991). A yeast two-hybrid screen was performed using full-length human Pierce1 (1-136 aa), as a bait fusion and screening human lung and testis libraries. A commercial company, Hybrigenics (<https://www.hybrigenics-services.com/>), carried out the screen on our behalf. Although I did not perform this study it is directly relevant to the work in my thesis.

Interestingly, the screens done on both libraries yielded many hits. However, only one candidate came up on both screens (lung and testis) and came up in the category of the highest confidence level. This protein was PIAS2, a E3-type small ubiquitin-like modifier (SUMO) ligase. From the human lung library, two independent clones for PIAS2 was identified with one clone spanning -136...600 nt and the second spanning -115...1167 nt. From the human testis library, two independent clones for PIAS2 were identified with one clone spanning -61...539 nt and the second spanning -59...544 nt. This indicated that PIERCE1 may interact with region spanning from 20 aa- 390 aa of PIAS2. Other hits were placed in the categories of moderate or below confidence. They did not overlap in two screens. The analysis of this protein and its interaction with PIERCE1 is currently on-going.

6.3 Discussion

I previously suggested that *PIERCE1* is a novel gene that is involved in the function of motile cilia. It was identified in many high throughput genomic and proteomic screens for ciliary genes (Geremek et al., 2011, Hoh et al., 2012, Choksi et al., 2014b, Treutlein et al., 2014b, Nemajerova et al., 2016a). Sung *et al* (2016) reported that mouse null embryos of *Pierce1* exhibited severe laterality defects commonly seen in patients with ciliopathies (Sung et al., 2016). To investigate the function of *PIERCE1* *in vivo*, I used zebrafish embryos as my *in vivo* model as described in Chapter 5. The knockdown of *Pierce1* in zebrafish embryos resulted in phenotypes consistent with motile cilia defects and with live imaging, I was able to establish that cilia motility was aberrant in these embryos.

Further investigation regarding the biochemical, molecular, and genetic mechanisms by which *PIERCE1* interacts with other known factors is required to elucidate the precise role of *PIERCE1* during motile ciliogenesis. As a starting point, I decided to study the localisation of *PIERCE1* in ciliated cells.

In Chapter 3, I validated primary mouse airway epithelial cell culture as a good *in vitro* model to investigate the factors associated with ciliogenesis. I decided to use a custom made polyclonal antibody raised against full length mouse *PIERCE1* protein, on differentiated ALI cultured airway epithelial cells to understand its' localisation. Prior to using the antibody for microscopy, I tested it on mouse testis tissue lysate by western blotting. As I described in chapter 4, several online datasets i.e. BioGPS,

Human Protein Atlas, showed that PIERCE1 is highly expressed in testis. Sperm harbours flagella for locomotion. The structure and function of cilia and flagella are very well conserved across evolution (Ibañez-Tallon et al., 2003). I did not quantitate protein levels for this experiment, but I reasoned that since my purpose was only focused on detecting the protein, this method was sufficient. As expected, PIERCE1 was detected by the antibody on the western blot. A very clear band with a size of around 20 kDA was visible across the blot. It is difficult to prove that this is PIERCE1 but as it was close to the predicted size for mouse PIERCE1 protein it seems like a reasonable assumption. I was not able to compete this binding as I did not have access to any recombinant protein.

When I used this antibody on undifferentiated and differentiated mNEC cultured at ALI, PIERCE1 (like FOXJ1) was not detected in undifferentiated mNECs. In contrast, at day 14, PIERCE1 was found to be specifically localised in ciliated cells (FOXJ1⁺ cells). It had a cytoplasmic localisation while FOXJ1 was localised in nucleus. These data were consistent with the data from chapter 5, where I showed that tagged proteins in zebrafish embryos also localised to the cytoplasm. This localisation data confirms that the protein is not found in the cilia axoneme, but my functional data suggest that it is required for normal cilia motility. Further support for the localisation of the protein in ciliated cells comes from the DAPT treatment data which showed that *Pierce1* increased along with ciliated cell numbers.

Having established that PIERCE1 is a cytoplasmic protein found in ciliated cells and is required for cilia motility, I looked in the literature for other known factors that is expressed in the cytoplasm and that are important for

cilia motility. Axonemal dynein arms are large sophisticated devices that fuel cilia motility (Gibbons and Rowe, 1965, Ishikawa, 2017). In 1988, Fawkes *et al* performed studies on *Chlamydomonas* to show that Dynein subunits are pre-assembled in the cytoplasm and then exported into the axoneme, where they are docked onto peripheral microtubules. The underlying mechanisms for this were not clearly understood (Fowkes *et al.*, 1998). In the following years, human genetics and model organisms have contributed major insights into the complex process of axonemal dynein arm assembly and how they are transported into cilia/flagellum by dynein axonemal assembly factors (DNAAFs) which are themselves largely cytoplasmic. Many of these proteins were identified by screening for causative mutations in PCD patients (Loges *et al.*, 2009, Omran *et al.*, 2008, Mitchison *et al.*, 2012, Tarkar *et al.*, 2013). Multiple PCD genes such as *LRRC50/DNAAF1* (Duquesnoy *et al.*, 2009, Loges *et al.*, 2009), *KTU/DNAAF2* (Omran *et al.*, 2008), *PF22/DNAAF3* (Mitchison *et al.*, 2012), *DYX1C1/DNAAF4* (Tarkar *et al.*, 2013), *HEATR2/DNAAF5* (Horani *et al.*, 2012, Diggle *et al.*, 2014), *LRRC6* (Kott *et al.*, 2012, Horani *et al.*, 2013a), *ZMYND10* (Moore *et al.*, 2013, Zariwala *et al.*, 2013, Mali *et al.*, 2018), *SPAG1* (Knowles *et al.*, 2013d), *C21ORF59* (Austin-Tse *et al.*, 2013) and *PIH1D3* (Paff *et al.*, 2017, Olcese *et al.*, 2017), have been shown to be involved in the cytoplasmic assembly of dynein arm subunits and loss of these factors lead to loss of both ODAs and IDAs. Although, the specific functions of these proteins are not clear, by analysis of protein sequence and interactions, some of them seem to interact with ubiquitous chaperone, HSP90 (zur Lage *et al.*, 2018). So, it indicates these cytoplasmic factors may facilitate the proper folding of dynein arms and assembly into the axoneme by working with a chaperone complex.

Since PIERCE1 is localised to the cytoplasm and its loss results in cilia motility defects, it can be hypothesised that PIERCE1 may be a cytoplasmic factor involved in the assembly of dynein arms. Since I did not study the axonemal structure of cilia in zebrafish knockdown experiment in detail e.g. by TEM, we do not know whether there was a loss of ODA and IDA in the cilia axoneme. Until the structure of motile cilia formed in the absence of PIERCE1 is investigated, it will not be possible to draw a conclusion regarding the involvement of PIERCE1 in dynein arms assembly.

To gain further insights into the molecular function of PIERCE1, a Yeast Two-Hybrid assay with LexA bait fusion was very recently carried out to identify the interacting partners of PIERCE1. This was undertaken using human lung and testis cDNA libraries independently. These tissues were chosen as they contain abundant ciliated cells. Protein inhibitor of activated STAT2 (PIAS2) was the only candidate that came up on both screens (lung and testis) and came up in the category with the highest confidence level. PIAS2 is an E3-type small ubiquitin-like modifier (SUMO) ligase (Palvimo, 2007, Rytinki et al., 2009). Many additional candidates came up in each screen with a lower level of confidence. In future, co-immunoprecipitation and mass spectroscopy studies will be carried out to validate the interaction and to look for more interacting partners.

Protein inhibitor of activated signal transducer and activator of transcription 2 (PIAS2) belongs to the PIAS protein family (Moilanen et al., 1999, Kotaja et al., 2002). PIAS proteins are shown to be inhibitors of activated STAT only and modulate and interact with several other proteins, including AR and p53 (Kotaja et al., 2000, Schmidt and Müller, 2002, Kong et al., 2015).

PIAS2 is highly expressed in the testis (Yan et al., 2003). PIAS proteins also acts as E3 ligases involved in the process of sumoylation (Palvimo, 2007). In addition, PIAS2 was shown to be upregulated during mucociliary differentiation of mouse tracheal epithelial cells as it is in the RNA sequencing data set generated by Nemajerovo *et al* (Nemajerova et al., 2016a). Interestingly both PIERCE1 and PIAS2 were identified in whole-genome gene expression profiling of bronchial biopsies from PCD patients and were both placed into the cluster enriched for cilia genes. (Geremek et al., 2011). These findings raise a possibility that PIERCE1 and PIAS2 might be involved in the sumoylation of factors associated with cytoplasmic assembly of dynein arms. Sumoylation is a protein modification process facilitated by E1-activating enzyme, E2-conjugating enzyme and E3 ligating proteins (Wilkinson and Henley, 2010, Flotho and Melchior, 2013). Sumoylation commonly results in change in the molecular interactions of the sumoylated proteins, which ultimately result in changes in protein activity, localization or stability (Flotho and Melchior, 2013, Bi et al., 2014).

Sumoylation has been found to be important in ciliogenesis in different contexts by several groups (McIntyre et al., 2015, Li et al., 2012b). In motile ciliogenesis, the current understanding about the molecular and biochemical pathways involved in the cytoplasmic assembly of dynein arms remains vague. The components of the Ruvbl1-Ruvbl2-Tah1-Pih1 (R2TP) complexes, Pontin (Ruvbl1) and Reptin (Ruvbl2, that normally act as co-chaperones for the assembly of multiple macromolecular protein complexes are also known to be important for the cytoplasmic assembly of dynein arms (Te et al., 2007, Kakihara and Houry, 2012, Li et al., 2017). Zebrafish mutants for both Pontin

and Reptin show cilia motility defects along with reduction in the number of outer and inner dynein arms (Zhao et al., 2013b, Li et al., 2017). Reptin was also shown to interact with Lrrc6, one of the cytoplasmic Dynein assembly factor (Zhao et al., 2013b). Pontin was also shown to be required for the stabilization of axonemal dynein intermediate chain 1 (DNAI1) and DNAI2, one of the initial steps in axonemal dynein arm assembly (Li et al., 2017, zur Lage et al., 2018).

In the canonical pathway, sumoylation was shown to be required for activity of Reptin as part of R2TP complex in cell cycle pathway (Kim et al., 2006). Although it's not clear how Reptin and Pontin functions as part of the cytoplasmic dynein assembly in motile ciliogenesis, it is possible that sumoylation may be required to regulate their activities. This is just one of the many possible examples where sumoylation may play a role in dynein arms assembly in motile ciliogenesis. Since, the current understanding regarding the cytoplasmic assembly of dynein arms is ambiguous, it can only be assumed that the modification process of sumoylation may be important for some factors involved.

In conclusion, I suggest that PIERCE1 is involved in the pre-assembly of dynein arms based on its cytoplasmic localization and consequences upon loss of function. However, the specific functions of this protein and its relationships with cytoplasmic dynein assembly factors remains to be understood. The Y2H assay carried out with the full-length Human Pierce1 (1-136 aa) protein identified PIAS2, as a possible interacting partner of PIERCE1. With this finding, I hypothesise that PIERCE1 and PIAS2 may be involved in the sumoylation of cytoplasmic dynein assembly factors.

Chapter 7 : Discussion

As I described in chapter 1, there are many gaps left in the current understanding of cilia formation and function. Therefore, many components and pathways that make up the cilium and required for its motility are still not known. In order to address this, many groups have conducted large scale proteomic, genomic and transcriptomic screens that have identified a large number of candidates that may have a role in motile ciliogenesis (Ross et al., 2007, Hoh et al., 2012, Choksi et al., 2014b, Choksi et al., 2014c, Stauber et al., 2017) . However, further characterisation of these candidates is required to understand its role and importance in ciliogenesis.

My aim in this thesis was to select putative genes from large scale screens I mentioned in the last paragraph based on the number of studies that have identified the gene as a ciliary gene, *in silico* analysis and expression profile in differentiating *in vitro* cultured mouse primary airway epithelial cells. Once a gene was selected, I aimed to carry out further characterisation of the genes using my *in vitro* model – mouse primary airway epithelial cells cultured at ALI and an *in vivo* model- zebrafish embryos.

In this closing chapter, I will summarise all the significant findings from the thesis and discuss how close I managed to get to my initial aims. I will also explore the limitations and the future potential of my work.

7.1 Establishment of *in vitro* culture of mouse primary airway epithelial cells as a model for studying motile ciliogenesis

First step was to establish the *in vitro* model, mouse primary airway epithelial cell culture at ALI. I successfully managed to isolate cells from mouse trachea and nasal cavity and to grow and differentiate them on ALI following the protocols adapted from other groups (You et al., 2002, Antunes et al., 2007a, Vladar and Brody, 2013) . The differentiation of mTEC and mNEC at the ALI was first validated by studying the expression of markers of basal cells, ciliated cells and secretory by end-point RT-PCR, western blot and immunocytochemistry. Once I validated that the differentiation had occurred, the expression pattern of genes required for ciliogenesis as the cells differentiate at ALI was examined using end-point RT-PCR. An increase in expression was observed, consistent with studies by other groups (Vladar and Brody, 2013, Nemajerova et al., 2016a). Since end-point RT-PCR is only semi-quantitative, it is difficult to deduce further information about the pattern of expression. In the future, I will move on to real time PCR that would allow me to understand the expression pattern of cilia specific genes during the differentiation of airway epithelial cells.

As reviewed by Vladar *et al* and shown by many groups, ciliogenesis in mTEC grown at ALI can be modulated by drug treatment (Pan et al., 2007b, Vladar et al., 2012, Vladar and Brody, 2013, Burke et al., 2014). I decided to test this aspect on mNEC by DAPT (a Notch inhibitor) treatment. Consistent with results from several groups on mTEC cultured at ALI, I saw increase in MCCs in mNEC culture (Stubbs et al., 2012, Tan et al., 2013b, Villa et al., 2016). This was observed by immunofluorescence by looking at the percentage

of FOXJ1^{+ve} cells in the culture. I realised that more reliable way would be to do a real-time PCR to study the mRNA expression levels of *Foxj1*. This was explored in chapter 6. The increase in MCCs in mNEC, like reported in mTECs by other groups, was expected since molecular pathway of MCC formation is conserved even though the cells are from different niches (Brooks and Wallingford, 2014b, Meunier and Azimzadeh, 2016). It showed mNECs can be used like mTECs as a model to understand MCC formation. I also attempted to optimise gene modulation in these cells by siRNA transfection. This was not successful because of limitations such as low transfection efficiency, batch variation, difficulty in growing FACS sorted cell population of interest since primary cells loss their proliferative potential once they are passaged. Recently, different groups have reported various ways of overcoming these issues in this models such as treating the cells with SMAD signalling inhibitors that would consequently increase the proliferative potential of the cells (Mou et al., 2016, Eenjes et al., 2018a, Levardon et al., 2018). However, in the interest of time, I did not pursue the initial plan to carry out gene modulation in this cell culture model.

In addition, recent advances in techniques like single-cell profiling can also be useful to explore using this *in vitro* model to understand the molecular and cellular biology of lung epithelium. This was demonstrated recently by Plasschaert et al (2018) who carried out single-cell profiling of human bronchial epithelial cells grown at ALI and isolated mTECs to acquire a complete map of distinct cell types in airway epithelium. They made a novel discovery of a new cell type known as 'pulmonary ionocyte' that express CFTR, a gene mutated in cystic fibrosis (Plasschaert et al., 2018).

The significant contribution from this work for my research was the validation of differentiation of MCCs in this culture and the capability of modulating multiciliogenesis in the culture.

7.2 *Pierce1* was selected for further characterisation from a list of 10 randomly selected putative ciliary genes

From three recent studies that screened for novel ciliary genes at the time of my research (Ross et al., 2007, Hoh et al., 2012, Choksi et al., 2014c), I selected 10 uncharacterised genes including *Pierce1* that might have had a role in ciliogenesis. Initially, the expression pattern of *Pierce1* during the differentiation of mNECs at ALI was studied. *Pierce1* showed increased expression during differentiation like other established ciliary genes. I used endpoint RT-PCR here. But recently Nemajeravo *et al* carried-out RNA seq at different time points of mTEC differentiation at ALI. Consistent with my findings from mNEC, they also showed *Pierce1* was upregulated during the differentiation of mTEC like many other cilia genes (Nemajerova et al., 2016a).

Secondly, the transcriptional expression of candidate genes was analysed in different whole mouse tissues. Interestingly, *Pierce1* showed enriched expression in motile ciliated tissues denoted by higher band densities. Again, endpoint PCR used here is semi-quantitative, hence a more accurate representation can be made by real time PCR. This distribution of enriched expression in tissue harbouring motile cilia for *Pierce1* was also shown by datasets from bioGPS (Wu et al., 2009) (<http://biogps.org/#goto=genereport&id=69327>). In addition, the Human Protein Atlas (Marx, 2014, Pontén et al., 2011) showed PIERCE1 expression

associated with motile ciliated cells, although the sub-cellular localisation of the protein was not clear (<https://www.proteinatlas.org/ENSG00000160345-C9orf116/tissue>). However, these datasets do not represent all proteins accurately and therefore the data cannot be relied on blindly. Furthermore, the expression in distinct cell types of E18.8 mouse lung using the data from 'LungGens' (Du et al., 2015) showed that *Pierce1* is specifically expressed in ciliated cells. Although none of these data can be used as a standalone tool to establish the functional role of the gene in ciliogenesis, these can be used in combination to make a rational prediction.

Using Cildb, a knowledge database that incorporates ciliary data from various sources and links orthology relationships among 44 species (44 eukaryotes and 3 bacteria) to high throughput ciliary studies (Arnaiz et al., 2014), I was also able to find other screens done in mouse, human and zebrafish that have identified *PIERCE1* as a potential ciliary gene (Ross et al., 2007, Geremek et al., 2011, Geremek et al., 2014, Hoh et al., 2012, Treutlein et al., 2014a, Choksi et al., 2014b, Stauber et al., 2017). Combining all these findings, *PIERCE1* was selected as a strong candidate for further characterisation.

As I mentioned before, recently, Plasschaert *et al* (2018) had carried out single-cell profiling of mTECs and HBECs to obtain a comprehensive map of distinct cell types present in proximal airways (Plasschaert et al., 2018). The single-cell profiling is a very useful technique as it will allow to analyse the difference of individual cells/cell types and can reveal the cell-type specific transcriptional data with good accuracy (Wang and Navin, 2015). If I were to do

my selection of ciliary gene candidates now, I would have incorporated this data as well to select good candidates for further characterisation.

Nevertheless, using the dataset from Plasschaert *et al* (2018) that is available from NCBI GEO under accession number GSE102580, I studied the expression on *PIERCE1* in human and mouse proximal airway epithelial cells. The data can be viewed using a computational tool, SPRING , that allows an interactive visualization of single-cell profiling data and allows to investigate unrestricted gene topology (Weinreb et al., 2018). As Shown in Figure 7.1, in mTEC, *Pierce1* expression is specifically enriched in the ciliated cells as shown by the SPRING plots (Plasschaert et al., 2018).

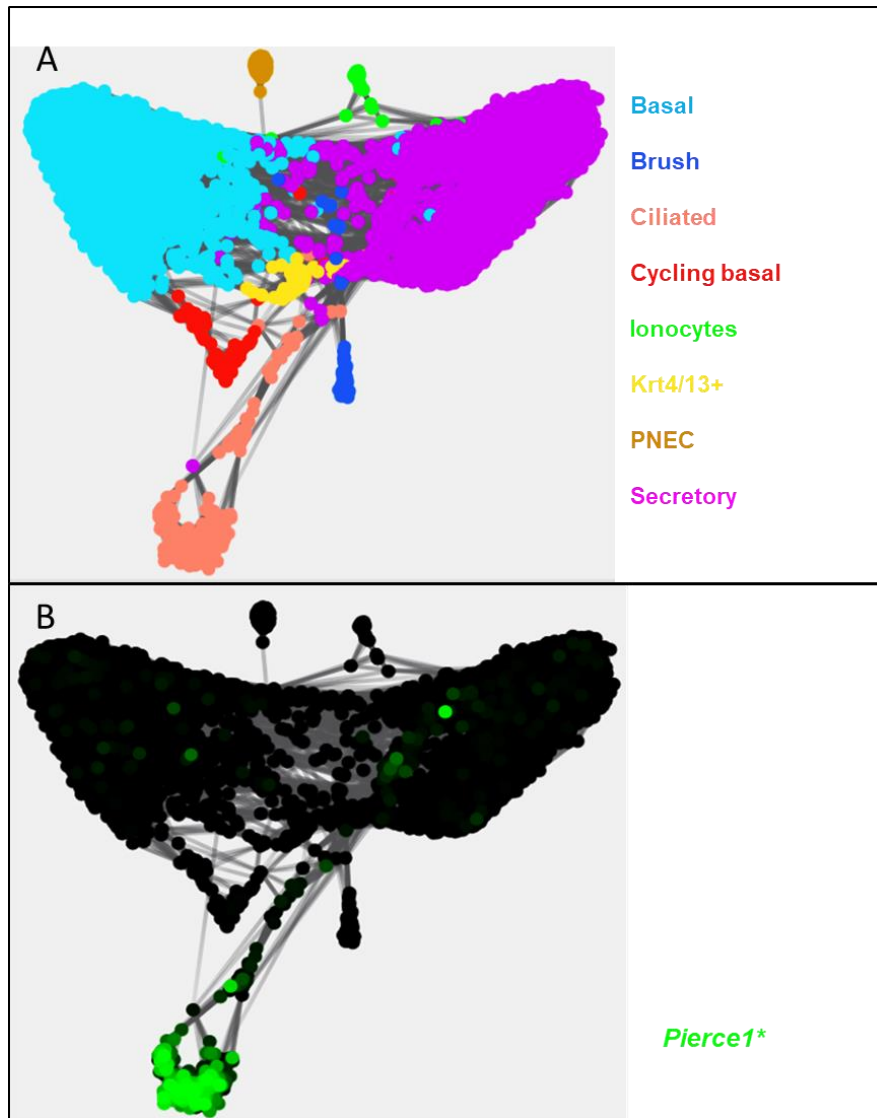


Figure 7-1. Single-cell profiling of mTEC shows enriched expression of *Pierce1* in ciliated cells.

Plasschaert et al (2018) carried out single cell profiling of mTEC to obtain a comprehensive map of all cell types in mouse proximal airway epithelium and revealed novel gene signatures in the distinct cell types. A) SPRING plots of mTEC (n = 3 mice) showing distinct cell type clusters (colour coded) present in the proximal airways. B) SPRING plot showing the distribution of *Pierce1* expression (green colour shaded) in distinct airway epithelial cell clusters. It shows enriched expression in ciliated cells (Plasschaert et al., 2018, Weinreb et al., 2018).

Interestingly (and reassuringly), the ciliated cell enriched expression for *PIERCE1* was also conserved in human bronchial epithelial cell (HBEC) as shown by Figure 7.2 (Plasschaert et al., 2018).

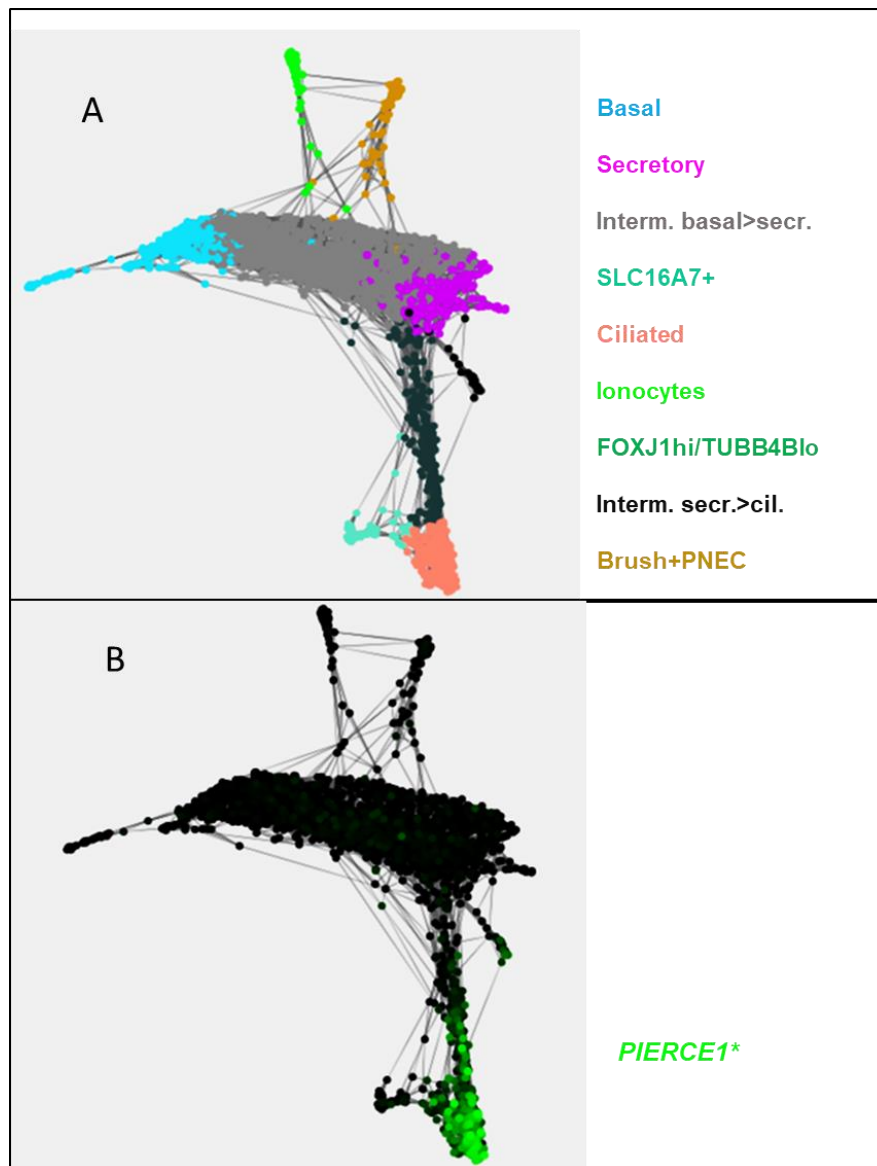


Figure 7-2. Single-cell profiling of HBECs shows enriched expression of *PIERCE1* in ciliated cells.

Plasschaert *et al* (2018) carried out single cell profiling of mTEC to obtain a comprehensive map of all cell types in human proximal airway epithelium and also revealed novel gene signatures in the distinct cell types. A) SPRING plots of HBECs ($n = 3$ donors, 2,970 cells) showing distinct cell type clusters (colour coded) present in the proximal airways. B) SPRING plot showing the distribution of *PIERCE1* expression (green colour shaded) in distinct airway epithelial cell clusters. It shows enriched expression in ciliated cells (Plasschaert et al., 2018, Weinreb et al., 2018).

7.3 *pierce1* zebrafish morphants showed severe situs abnormalities and curved axis associated with cilia defects.

To characterise the functional role of PIERCE1, I used zebrafish for *in vivo* investigation. Zebrafish is a great model for studying motile ciliogenesis as it possess all kind of motile cilia as found in humans (Malicki et al., 2011). Two independent morpholinos were used to transiently knockdown *pierce1* in zebrafish embryos. Both morphants showed severe laterality defects and curved axis usually associated with motile cilia defects. The laterality defects were consistent with the finding on *Pierce1* mouse null embryos (Sung et al., 2016). Abnormal cilia motility was observed in KV of the morphant embryos that explained the occurrence of laterality defects. Immunolabelling the cilia by Acetyl α -tubulin antibodies showed that there was no difference in the cilia morphology in morphants by immunofluorescence. In terms of cilia structural analysis, immunostaining has limitations. It can only be used to study cilia number and length. To study cilia architectural defects, electron microscopy would be more beneficial.

I was able to validate the splice blocking morpholino by RT-PCR and sequencing which showed that the targeted exon/intron boundary was retained in the morphants. However, to my disappointment, the rescue of the morphants by injection of the 6 x Myc-*Pierce1* failed. There are different ways to interpret this result. Firstly: the tags are interfering with the native function of the protein and secondly: morphant phenotypes were caused by the off-target effects of the morpholinos. But this also meant that I could not validate whether the phenotypes of morphants were not due to off-target effects. Since, the reliability of the morpholino assays are controversial these days (Gerety and Wilkinson,

2011, Schulte-Merker and Stainier, 2014), I decided not to use the morpholino assay results as a standalone source to functionally establish *Pierce1* as a ciliary gene. The morpholino assay also does not allow to assess for adult phenotypes e.g. male fertility.

7.4 Maternal zygotic zebrafish mutants of *pierce1* showed mild situs abnormalities

To validate the phenotypes caused by the transient knockdown by morpholinos and to assess the phenotypes of the adult fishes, I proceeded to generate a zebrafish genetic mutant line for *pierce1*.

Using CRIPSR/ Cas9 gene editing technique (Hsu et al., 2014), I generated two mutant alleles in zebrafish, both targeting the exon 2. The only identified conserved functional domain in *PIERCE1*, known as DUF4990, span from 11-117 amino acids of the zebrafish *Pierce1* protein. Both mutant alleles would be expected to generate truncated proteins with first 60 amino acids and disrupted conserved domain. The zygotic mutants generated by crossing heterozygous fishes did not show any phenotypical difference from WT. Since I found maternal contribution of *pierce1* mRNA in the zebrafish embryos, I proposed that the maternal deposition of WT mRNA from heterozygous mother would be compensating for the mutant phenotype.

I next made maternal zygotic mutants for *pierce1* by in-crossing zygotic homozygous mutants. Interestingly, adult zygotic mutants were viable and fertile indicating that sperm motility is normal. In maternal zygotic mutants from both alleles, small majority had *situs* abnormalities. The live imaging showed that few mutant embryos had abnormal/immotile cilia in KV. The existence of

Pierce1 null mouse mutants that exhibit severe laterality defects (Sung et al., 2016) like *pierce1* zebrafish morphants suggest that a compensatory mechanism exists in the zebrafish knockouts (i.e. mutants) that might be masking the mutant phenotype. However, it is interesting to note that the maternal contribution of *pierce1* mRNA did not reflect on the splice morpholino results since maternally contributed mRNA is already spliced. This may be due to the fact that the morpholino is faster in its action in knocking down the *Pierce1* activity whereas creating the genetic mutant take generations. The zebrafish might have developed compensatory mechanisms to recompensate the loss of *Pierce1* functional role. This compensatory mechanisms in combination with maternal contribution was more effective in rescuing the loss of *Pierce1* phenotype. In addition, many groups have reported the same phenomenon where phenotypes exhibited by knockdown experiments does not get recapitulated in the knockouts (White et al., 2013, Kok et al., 2015, Bouche and Bouchez, 2001). Future work would focus on validating that the milder phenotype in mutants is due to genetic compensatory mechanisms. This could be validated by injecting morpholino into the mutants. If there is genetic compensation in the mutants, the mutants would not show severe phenotype as opposed to the WT embryos. We would also seek to characterise the compensatory mechanisms including any upregulation in other genes in the mutants.

In addition, I also attempted to study the subcellular localisation of *Pierce1* in zebrafish embryos. At the time of research, working antibodies against *Pierce1* was not available hence I used expression of tagged versions of *Pierce1* in zebrafish embryos to detect the localisation. Two tagged versions

were utilised to overcome the limitation caused by positioning of the tags; a N-terminus Myc tag and a C-terminus GFP tag. Both tagged versions were localised into the cytoplasm. One limitation of this approach is that the relative larger size of tags with the small Pierce1 protein can affect the native localisation of the Pierce1 protein. Hence, an antibody against Pierce1 that would detect the native protein would be a more reliable approach.

7.5 PIERCE1 has specific expression in multiciliated cells in mouse airway epithelial cells and has a cytoplasmic subcellular localization

So far, I focused on understanding the implications on ciliogenesis when there is absence of PIERCE1. This allowed me to understand what aspect of ciliogenesis require PIERCE1. The findings point towards ciliary motility. So I asked myself how PIERCE1 regulates ciliary motility. To answer this question, we needed to know where PIERCE1 localises in a ciliated cell. Does it localise to the axoneme? We used a custom made polyclonal antibody that was designed against full length mouse Pierce1 protein. This antibody was first validated on western blot on mouse testis cell lysate that detected a protein with predicted size of mouse PIERCE1. Subsequently, the antibody was used to carry out immunohistochemistry on differentiated ALI cultured airway epithelial cells and I observed that PIERCE1 was specifically expressed in ciliated cells as predicted from the datasets like bioGPS, Human Protein Atlas and LungGens. Moreover, the recent single-cell profiling data by Plasschaert *et al* (2018) also showed enriched expression in ciliated cells (Plasschaert et al., 2018).

Furthermore, I have shown that it has a cytoplasmic localisation and the protein did not localise to the axoneme. In the literature, many cytoplasmic proteins, mostly dynein assembly factors, have been found to be required for cilia motility e.g. HEATR2, LRRC50, KTU etc. Absence of these proteins result in abnormal or complete loss of cilia motility due to loss of dynein arms (Duquesnoy et al., 2009, Loges et al., 2009, Omran et al., 2008) (Horani et al., 2012, Diggle et al., 2014). This allows me to propose that PIERCE1 may also

play a similar role. To validate this, we will need to go back to the zebrafish morphants or the mouse null mutants of *ierce1* and analyse the motile cilia architecture using TEM to study the axonemal dynein arms. In the future we will also try to get working antibodies of Pierce1 for human and zebrafish to explore the conservation of the pattern of expression and localisation in ciliated tissues.

7.6 C15ORF65, a paralog of PIERCE1

The milder phenotype observed in *ierce1* zebrafish mutants prompted me to investigate the potential existence of gene redundancy through paralogous genes. Using a web database, KEGG sequence similarity data base (SSDB) (Kanehisa et al., 2016), I was able to identify C15ORF65 as a paralog of PIERCE1. C15ORF65 is also a poorly characterised protein like PIERCE1. Both proteins share the unknown domain of function, DUF4490. Interestingly, *Ccpg1os* (Cell cycle progression 1, opposite strand), mouse orthologue of *C15ORF65* was also shown to have increased expression like *Pierce1* during ALI differentiation of mTEC (Nemajerova et al., 2016b) as shown in Figure 7.3.

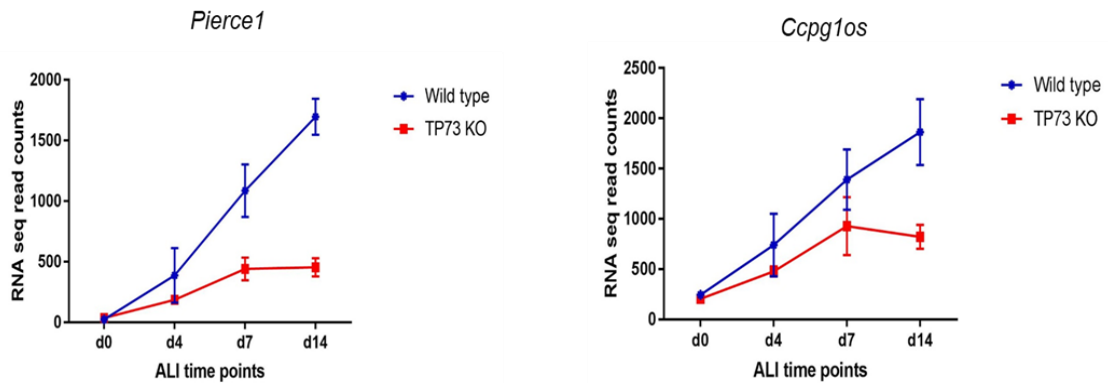


Figure 7-3. Expression of *Pierce1* and *Ccpg1os* in ALI cultured WT mTEC vs *Tp73* KO mTEC.

Nemajerova et al (2016) acquired RNA seq reads from 3 independent cultures for WT and 2 independent cultured of *Tp73*^{-/-} mTEC. Error bars represent standard error of the mean.

Analysis of the Biology Gene Portal System (BioGPS) (Wu et al., 2009) microarray data set (expression in different mouse tissues, *Dataset: GeneAtlas GNF1M, gcrma*), suggests that *Ccpg1os* is abundantly expressed in testis like many ciliary genes (Figure 7.6).



Figure 7-4. *Ccp10s* expression on mouse tissues based on the BioGPS database.

(Dataset: GeneAtlas GNF1M, gcrma; Probeset: gnf1m04869_a_at)

LungGens single cell RNA seq of mouse (E18.5) fetal lung (Du et al., 2015) showed high expression of *Ccp10s* in MCCs as shown in Figure 7.5.

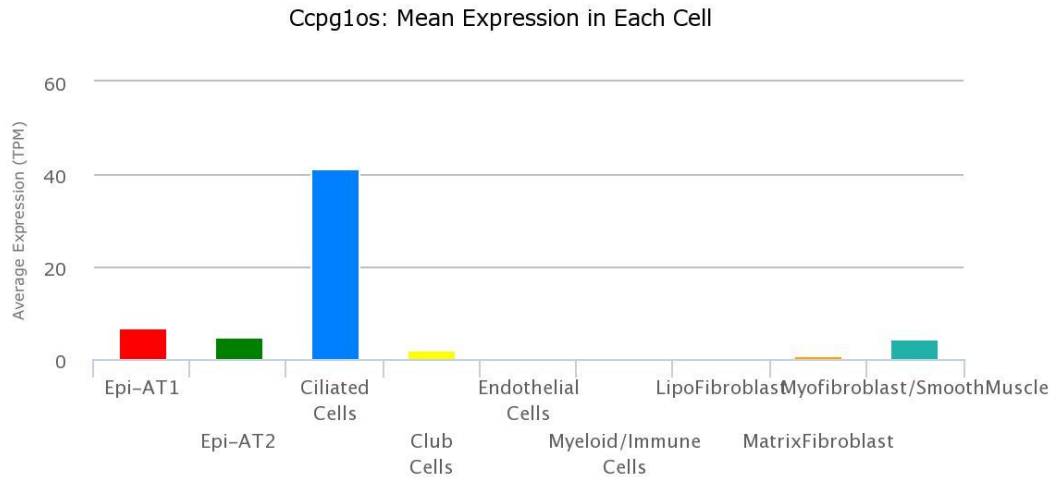


Figure 7-5. Expression of *Ccpq1os* in 9 distinct cell types of E18.5 fetal mouse lung.

The graphs were plotted from the average mean expression data acquired from the LungGENS. The data was collected from contains cells sequenced from E18.5 mouse lung, processed using Fluidigm C1 microfluidics technology. The count of samples for each cell types are as follows: Epi-AT1-7, Epi-AT1-9, Ciliated cells-2, Club cells- 2, Endothelial cells- 18, Myeloid/ Immune cells-8, Lipofibroblast-8, *Matrix* fibroblast- 9 and myofibroblast-9.

These results point towards a possible role for C15ORF65 in motile cilia formation. Based on the conserved sequence similarity and expression pattern with PIERCE1, C15ORF65 could play a similar function. So, it would be useful to explore the functional role of this novel candidate. It would also be useful to study the expression levels of *c15orf65* in *ierce1* zebrafish mutants to understand if it causes gene redundancy.

7.7 PIAS2 is a potential binding partner of PIERCE1

To gain further insights into the molecular function of PIERCE1, a Y2H assay was carried out to identify the interacting partners of PIERCE1 using human lung and testis cDNA libraries independently. Protein inhibitor of activated STAT2 (PIAS2) was the only candidate that came up on both screens (lung and testis) and came up in the category of the highest confidence level. PIAS2 is an E3-type small ubiquitin-like modifier (SUMO) ligase (Palvimo, 2007, Rytinki et al., 2009). In future, co-immunoprecipitation and mass spectroscopy studies can be carried out to validate this interaction and look for more interacting partners. PIAS2 was identified in some ciliary screens and is also upregulated during differentiation of mTEC at ALI (Geremek et al., 2011, Nemaierova et al., 2016a). These findings raise a possibility that PIERCE1 and PIAS2 might be involved in the sumoylation of factors associated with cytoplasmic assembly of Dynein arms. Sumoylation is found to be important in ciliogenesis in different contexts by several groups (McIntyre et al., 2015, Li et al., 2012b). The current understanding regarding the cytoplasmic assembly of dynein arms is ambiguous so in future, I will explore the role of sumoylation in cytoplasmic assembly of dynein arms.

7.7 Proposed role of PIERCE1 in motile ciliogenesis

Overall, it appears that PIERCE1 may be involved in the pre-assembly of dynein arms based on its cytoplasmic localization and loss of ciliary motility upon loss of expression. However, the specific functions of these proteins and their relationships with other cytoplasmic dynein assembly factors are not well understood. Y2H assay carried out with the full-length Human Pierce1 (1-136

aa) protein, on human lung and testis library found PIAS2, as a possible interacting partner of PIERCE1. With this finding, we hypothesise that PIERCE1 and PIAS2 may be involved in the sumoylation of cytoplasmic Dynein assembly factors. A schematic diagram is shown in Figure 7.3 to summarise the proposed functional role of PIERCE1.

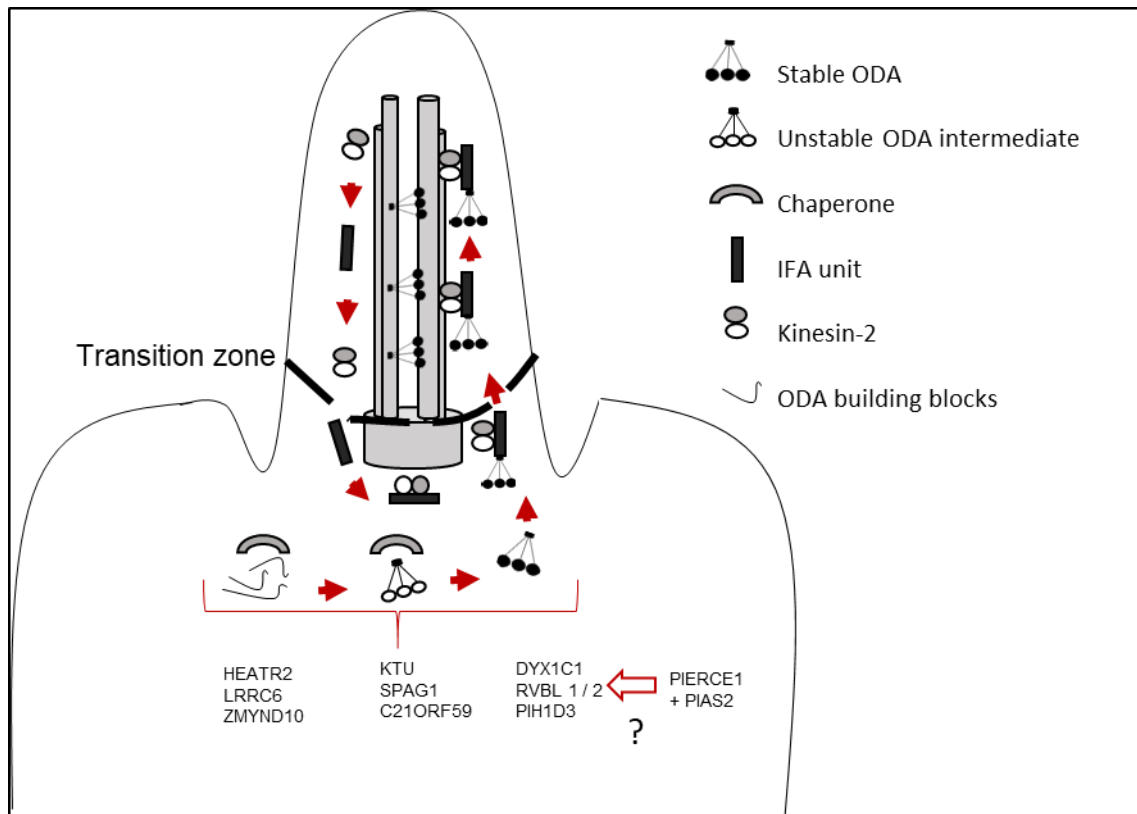


Figure 7-6. Schematic diagram showing the proposed role of PIERCE1.

We hypothesise that PIERCE1 play a role in cytoplasmic assembly of Dynein arms through an E3-type small ubiquitin-like modifier, PIAS2. There are many known cytoplasmic factors that are associated the dynein arms assembly. The absence of these factors results in loss of dynein arms and hence abnormal cilia motility. The molecular pathway these factors act through is still not clear. Likewise, mouse mutants of PIERCE1 and zebrafish *pieerce1* morphants had abnormal cilia motility and is localised in the cytoplasm of ciliated cells. Through Y2H assay, it was shown that PIERCE1 interact with PIAS2.

7.8 PIERCE1 and human diseases?

To my knowledge, mutations in human PIERCE1 have not yet been identified. Since *Pierce1* null mouse embryos and zebrafish morphants show *situs* abnormalities, it is possible that *PIERCE1* mutation would be associated with heterotaxy and congenital heart disease. Su *et al* did not report anything on the status of respiratory functions or male fertility in the adult mice (Sung et al., 2016). Therefore, in future, it would be useful to explore the adult mouse mutant to understand more about the disease phenotypes associated with absence of *Pierce1*. In the meantime, I would also consult ciliopathy disease cohorts to identify and investigate on any association of *PIERCE1* mutation with ciliopathy patients.

7.9 Future directions

The following are some of the areas that can be explored to enhance the contributions from my work.

1. To boost the usefulness of the primary airway epithelial cells cultured at ALI by focusing on formulating how to passage cells without loss of differentiation potential and adapting this culture system for gene modulation techniques like CRISPR and high-throughput screening.
2. *Pierce1* was only one of many uncharacterised genes that may have an important role in motile ciliogenesis. It would be also useful to follow up on other candidates and their role in ciliogenesis.
3. To explore why there is variance in the results from *Pierce1* knockdown and knockout experiments in zebrafish.

4. To test whether loss of PIERCE1 affect localisation of other ciliary components such as dynein arms in zebrafish morphants or mouse *Pierce1* mutants.
5. To validate the interaction of PIERCE1 and PIAS2 by co-immunoprecipitation.
6. To explore further interactors of PIERCE1.

Bibliography

- ABOU ALAIWI, W. A., LO, S. T. & NAULI, S. M. 2009. Primary cilia: highly sophisticated biological sensors. *Sensors (Basel)*, 9, 7003-20.
- ABRAMS, E. W. & MULLINS, M. C. 2009. Early zebrafish development: It's in the maternal genes. *Current opinion in genetics & development*, 19, 396-403.
- AKRAM, K., ANUJAN, P., MCCLOSKEY, B., BINGLE, L. & BINGLE, C. 2014. Validation of an in vitro tracheal model for the study of innate host defence mechanism in respiratory tract infections. *European Respiratory Journal*, 44.
- AKRAM, K., MOYO, N., TOMPKINS, M., TRIPP, R., BINGLE, L., STEWART, J. & BINGLE, C. 2015. An innate defence role for BPIFA1/SPLUNC1 against influenza-A virus infection. *European Respiratory Journal*, 46.
- AKRAM, K. M., MOYO, N. A., LEEMING, G. H., BINGLE, L., JASIM, S., HUSSAIN, S., SCHORLEMMER, A., KIPAR, A., DIGARD, P., TRIPP, R. A., SHOHET, R. V., BINGLE, C. D. & STEWART, J. P. 2017. An innate defense peptide BPIFA1/SPLUNC1 restricts influenza A virus infection. *Mucosal Immunology*, 11, 71.
- AL JORD, A., LEMAITRE, A. I., DELGEHYR, N., FAUCOURT, M., SPASSKY, N. & MEUNIER, A. 2014. Centriole amplification by mother and daughter centrioles differs in multiciliated cells. *Nature*, 516, 104-7.
- ALBERTSON, R. C. & YELICK, P. C. 2005. Roles for fgf8 signaling in left-right patterning of the visceral organs and craniofacial skeleton. *Developmental Biology*, 283, 310-321.
- ALTEN, L., SCHUSTER-GOSSLER, K., BECKERS, A., GROOS, S., ULMER, B., HEGERMANN, J., OCHS, M. & GOSSLER, A. J. D. 2012. Differential regulation of node formation, nodal ciliogenesis and cilia positioning by Noto and Foxj1. *dev.* 072728.
- ANDERSON, J. L., MULLIGAN, T. S., SHEN, M.-C., WANG, H., SCAHILL, C. M., TAN, F. J., DU, S. J., BUSCH-NENTWICH, E. M. & FARBER, S. A. 2017. mRNA processing in mutant zebrafish lines generated by chemical and CRISPR-mediated mutagenesis produces unexpected transcripts that escape nonsense-mediated decay. *PLOS Genetics*, 13, e1007105.
- ANTUNES, M. B., WOODWORTH, B. A., BHARGAVE, G., XIONG, G., AGUILAR, J. L., RATNER, A. J., KREINDLER, J. L., RUBENSTEIN, R. C. & COHEN, N. A. 2007a. Murine nasal septa for respiratory epithelial air-liquid interface cultures. *BioTechniques*, 43, 195-204.
- ANTUNES, M. B., WOODWORTH, B. A., BHARGAVE, G., XIONG, G., AGUILAR, J. L., RATNER, A. J., KREINDLER, J. L., RUBENSTEIN, R. C. & COHEN, N. A. 2007b. Murine nasal septa for respiratory epithelial air-liquid interface cultures. *Biotechniques*, 43, 195-6, 198, 200 passim.
- ARBI, M., PEFANI, D.-E., KYROUSI, C., LALIOTI, M.-E., KALOGEROPOULOU, A., PAPANASTASIOU, A. D., TARAVIRAS, S. & LYGEROU, Z. 2016. GemC1 controls multiciliogenesis in the airway epithelium. *EMBO reports*, 17, 400-413.
- ARNAIZ, O. 2014. Remodeling Cildb, a popular database for cilia and links for ciliopathies. 3, 9.
- ARNAIZ, O., COHEN, J., TASSIN, A.-M. & KOLL, F. 2014. Remodeling Cildb, a popular database for cilia and links for ciliopathies. *Cilia*, 3, 9.
- ARNAIZ, O., MALINOWSKA, A., KLOTZ, C., SPERLING, L., DADLEZ, M., KOLL, F. & COHEN, J. 2009. Cildb: a knowledgebase for centrosomes and cilia. *Database: The Journal of Biological Databases and Curation*, 2009, bap022.
- ASHIQUE, A. M., CHOE, Y., KARLEN, M., MAY, S. R., PHAMLUONG, K., SOLLOWAY, M. J., ERICSON, J. & PETERSON, A. S. 2009. The Rfx4 Transcription Factor Modulates Shh Signaling by Regional Control of Ciliogenesis. *Science Signaling*, 2, ra70.

- AUSTIN-TSE, C., HALBRITTER, J., ZARIWALA, MAIMOONA A., GILBERTI, RENÉE M., GEE, HEON Y., HELLMAN, N., PATHAK, N., LIU, Y., PANIZZI, JENNIFER R., PATEL-KING, RAMILA S., TRITSCHLER, D., BOWER, R., O'TOOLE, E., PORATH, J. D., HURD, TOBY W., CHAKI, M., DIAZ, KATRINA A., KOHL, S., LOVRIC, S., HWANG, D.-Y., BRAUN, DANIELA A., SCHUELER, M., AIRIK, R., OTTO, EDGAR A., LEIGH, MARGARET W., NOONE, PEADAR G., CARSON, JOHNNY L., DAVIS, STEPHANIE D., PITTMAN, JESSICA E., FERKOL, THOMAS W., ATKINSON, JEFFRY J., OLIVIER, KENNETH N., SAGEL, SCOTT D., DELL, SHARON D., ROSENFELD, M., MILLA, CARLOS E., LOGES, NIKI T., OMRAN, H., PORTER, MARY E., KING, STEPHEN M., KNOWLES, MICHAEL R., DRUMMOND, IAIN A. & HILDEBRANDT, F. 2013. Zebrafish Ciliopathy Screen Plus Human Mutational Analysis Identifies C21orf59 and CCDC65 Defects as Causing Primary Ciliary Dyskinesia. *American Journal of Human Genetics*, 93, 672-686.
- BAAS, D., MEINIEL, A., BENADIBA, C., BONNAFE, E., MEINIEL, O., REITH, W. & DURAND, B. 2006. A deficiency in RFX3 causes hydrocephalus associated with abnormal differentiation of ependymal cells. *European Journal of Neuroscience*, 24, 1020-1030.
- BABU, D. & ROY, S. 2013. Left–right asymmetry: cilia stir up new surprises in the node. *Open Biology*, 3.
- BAKER, M. A., HETHERINGTON, L., REEVES, G., MULLER, J. & AITKEN, R. J. 2008a. The rat sperm proteome characterized via IPG strip prefractionation and LC-MS/MS identification. *Proteomics*, 8, 2312-21.
- BAKER, M. A., HETHERINGTON, L., REEVES, G. M. & AITKEN, R. J. 2008b. The mouse sperm proteome characterized via IPG strip prefractionation and LC-MS/MS identification. *Proteomics*, 8, 1720-30.
- BALESTRA, FERNANDO R. & GÖNCZY, P. 2014. Multiciliogenesis: Multicilin Directs Transcriptional Activation of Centriole Formation. *Current Biology*, 24, R746-R749.
- BALESTRINI, A., COSENTINO, C., ERRICO, A., GARNER, E. & COSTANZO, V. 2010. GEMC1 is a TopBP1-interacting protein required for chromosomal DNA replication. *Nature cell biology*, 12, 484.
- BAY, S. N. & CASPARY, T. 2012. What are those cilia doing in the neural tube? *Cilia*, 1, 19.
- BELLOMO, D., LANDER, A., HARRAGAN, I. & BROWN, N. A. 1996. Cell proliferation in mammalian gastrulation: the ventral node and notochord are relatively quiescent. *Dev Dyn*, 205, 471-85.
- BEN ABDELKHALEK, H., BECKERS, A., SCHUSTER-GOSSLER, K., PAVLOVA, M. N., BURKHARDT, H., LICKERT, H., ROSSANT, J., REINHARDT, R., SCHALKWYK, L. C., MÜLLER, I., HERRMANN, B. G., CEOLIN, M., RIVERA-POMAR, R. & GOSSLER, A. 2004. The mouse homeobox gene Not is required for caudal notochord development and affected by the truncate mutation. *Genes and Development*, 18, 1725-1736.
- BI, H., LI, S., WANG, M., JIA, Z., CHANG, A. K., PANG, P. & WU, H. 2014. SUMOylation of GPS2 protein regulates its transcription-suppressing function. *Molecular Biology of the Cell*, 25, 2499-2508.
- BISGROVE, B. W., MAKOVA, S., YOST, H. J. & BRUECKNER, M. 2012. RFX2 is essential in the ciliated organ of asymmetry and an RFX2 transgene identifies a population of ciliated cells sufficient for fluid flow. *Developmental Biology*, 363, 166-178.
- BLATT, E. N., YAN, X. H., WUERFFEL, M. K., HAMILOS, D. L., BRODY, S. L. J. A. J. O. R. C. & BIOLOGY, M. 1999. Forkhead transcription factor HFH-4 expression is temporally related to ciliogenesis. 21, 168-176.
- BLOODGOOD, R. A. 2010. Sensory reception is an attribute of both primary cilia and motile cilia. *Journal of Cell Science*, 123, 505-509.
- BLUM, M., DE ROBERTIS, E. M., WALLINGFORD, J. B. & NIEHRS, C. 2015. Morpholinos: Antisense and Sensibility. *Dev Cell*, 35, 145-9.

- BLUM, M. & OTT, T. 2018. Animal left–right asymmetry. *Current Biology*, 28, R301-R304.
- BOISVIEUX-ULRICH, E., LAINÉ, M.-C. & SANDOZ, D. 1990. Cytochalasin D inhibits basal body migration and ciliary elongation in quail oviduct epithelium. *Cell and Tissue Research*, 259, 443-454.
- BONNAFE, E., TOUKA, M., AITLOUNIS, A., BAAS, D., BARRAS, E., UCLA, C., MOREAU, A., FLAMANT, F., DUBRUILLE, R. & COUBLE, P. 2004. The transcription factor RFX3 directs nodal cilium development and left-right asymmetry specification. *Molecular and cellular biology*, 24, 4417-4427.
- BOON, M., WALLMEIER, J., MA, L., LOGES, N. T., JASPERS, M., OLBRICH, H., DOUGHERTY, G. W., RAIDT, J., WERNER, C., AMIRAV, I., HEVRONI, A., ABITBUL, R., AVITAL, A., SOFERMAN, R., WESSELS, M., O'CALLAGHAN, C., CHUNG, E. M. K., RUTMAN, A., HIRST, R. A., MOYA, E., MITCHISON, H. M., VAN DAELE, S., DE BOECK, K., JORISSEN, M., KINTNER, C., CUPPENS, H. & OMRAN, H. 2014. MCIDAS mutations result in a mucociliary clearance disorder with reduced generation of multiple motile cilia. *Nat Commun*, 5.
- BOUCHE, N. & BOUCHEZ, D. 2001. Arabidopsis gene knockout: phenotypes wanted. *Curr Opin Plant Biol*, 4, 111-7.
- BRAIMAN, A. & PRIEL, Z. 2008. Efficient mucociliary transport relies on efficient regulation of ciliary beating. *Respiratory Physiology & Neurobiology*, 163, 202-207.
- BRANCORSINI, S., DAVIDSON, I. & SASSONE-CORSI, P. 2008. TIPT, a male germ cell-specific partner of TRF2, is chromatin-associated and interacts with HP1. *Cell Cycle*, 7, 1415-22.
- BROADHEAD, R., DAWE, H. R., FARR, H., GRIFFITHS, S., HART, S. R., PORTMAN, N., SHAW, M. K., GINGER, M. L., GASKELL, S. J., MCKEAN, P. G. & GULL, K. 2006. Flagellar motility is required for the viability of the bloodstream trypanosome. *Nature*, 440, 224-7.
- BRODY, S. L., YAN, X. H., WUERFFEL, M. K., SONG, S.-K., SHAPIRO, S. D. J. A. J. O. R. C. & BIOLOGY, M. 2000. Ciliogenesis and left–right axis defects in Forkhead factor HFH-4–null mice. 23, 45-51.
- BROOKS, ERIC R. & WALLINGFORD, JOHN B. 2014a. Multiciliated Cells. *Current Biology*, 24, R973-R982.
- BROOKS, E. R. & WALLINGFORD, J. B. 2014b. Multiciliated cells: a review. *Current biology : CB*, 24, R973-R982.
- BURKE, M. C., LI, F.-Q., CYGE, B., ARASHIRO, T., BRECHBUHL, H. M., CHEN, X., SILLER, S. S., WEISS, M. A., O'CONNELL, C. B., LOVE, D., WESTLAKE, C. J., REYNOLDS, S. D., KURIYAMA, R. & TAKEMARU, K.-I. 2014. Chibby promotes ciliary vesicle formation and basal body docking during airway cell differentiation. *The Journal of Cell Biology*, 207, 123-137.
- CAILLAT, C., FISH, A., PEFANI, D. E., TARAVIRAS, S., LYGEROU, Z. & PERRAKIS, A. 2015. The structure of the GemC1 coiled coil and its interaction with the Geminin family of coiled-coil proteins. *Acta Crystallogr D Biol Crystallogr*, 71, 2278-86.
- CARON, A., XU, X. & LIN, X. 2012. Wnt/beta-catenin signaling directly regulates Foxj1 expression and ciliogenesis in zebrafish Kupffer's vesicle. *Development*, 139, 514-24.
- CARVALHO-SANTOS, Z., AZIMZADEH, J., PEREIRA-LEAL, J. B. & BETTENCOURT-DIAS, M. 2011. Tracing the origins of centrioles, cilia, and flagella. *The Journal of Cell Biology*, 194, 165-175.
- CASPARY, T., LARKINS, C. E. & ANDERSON, K. V. 2007. The graded response to Sonic Hedgehog depends on cilia architecture. *Dev Cell*, 12, 767-78.
- CERTO, M. T., RYU, B. Y., ANNIS, J. E., GARIBOV, M., JARJOUR, J., RAWLINGS, D. J. & SCHARENBERG, A. M. J. N. M. 2011. Tracking genome engineering outcome at individual DNA breakpoints. 8, 671.

- CHEN, J., KNOWLES, H. J., HEBERT, J. L. & HACKETT, B. P. J. T. J. O. C. I. 1998. Mutation of the mouse hepatocyte nuclear factor/forkhead homologue 4 gene results in an absence of cilia and random left-right asymmetry. *102*, 1077-1082.
- CHEN, R., SHI, L., HAKENBERG, J., NAUGHTON, B., SKLAR, P., ZHANG, J., ZHOU, H., TIAN, L., PRAKASH, O., LEMIRE, M., SLEIMAN, P., CHENG, W. Y., CHEN, W., SHAH, H., SHEN, Y., FROMER, M., OMBERG, L., DEARDORFF, M. A., ZACKAI, E., BOBE, J. R., LEVIN, E., HUDSON, T. J., GROOP, L., WANG, J., HAKONARSON, H., WOJCICKI, A., DIAZ, G. A., EDELMANN, L., SCHADT, E. E. & FRIEND, S. H. 2016. Analysis of 589,306 genomes identifies individuals resilient to severe Mendelian childhood diseases. *Nat Biotechnol*, *34*, 531-8.
- CHIEN, C. T., BARTEL, P. L., STERNGLANZ, R. & FIELDS, S. 1991. The two-hybrid system: a method to identify and clone genes for proteins that interact with a protein of interest. *Proceedings of the National Academy of Sciences*, *88*, 9578-9582.
- CHOKSI, S. P., BABU, D., LAU, D., YU, X. & ROY, S. 2014a. Systematic discovery of novel ciliary genes through functional genomics in the zebrafish. *Development*, *141*, 3410.
- CHOKSI, S. P., BABU, D., LAU, D., YU, X. & ROY, S. 2014b. Systematic discovery of novel ciliary genes through functional genomics in the zebrafish. *Development (Cambridge, England)*, *141*, 3410-3419.
- CHOKSI, S. P., BABU, D., LAU, D., YU, X. & ROY, S. 2014c. Systematic discovery of novel ciliary genes through functional genomics in the zebrafish. *Development*, *141*, 3410-9.
- CHOKSI, S. P., LAUTER, G., SWOBODA, P. & ROY, S. 2014d. Switching on cilia: Transcriptional networks regulating ciliogenesis. *Development (Cambridge)*, *141*, 1427-1441.
- CHUNG, M. I., PEYROT, S. M., LEBOEUF, S., PARK, T. J., MCGARY, K. L., MARCOTTE, E. M. & WALLINGFORD, J. B. 2012. RFX2 is broadly required for ciliogenesis during vertebrate development. *Dev Biol*, *363*, 155-65.
- CLEVIDENCE, D. E., OVERDIER, D. G., PETERSON, R. S., PORCELLA, A., YE, H., PAULSON, K. E. & COSTA, R. H. J. D. B. 1994. Members of the HNF-3/forkhead family of transcription factors exhibit distinct cellular expression patterns in lung and regulate the surfactant protein B promoter. *166*, 195-209.
- COLANTONIO, J. R., VERMOT, J., WU, D., LANGENBACHER, A. D., FRASER, S., CHEN, J. N. & HILL, K. L. 2009. The dynein regulatory complex is required for ciliary motility and otolith biogenesis in the inner ear. *Nature*, *457*, 205-9.
- COLE, D. G. 2003. The Intraflagellar Transport Machinery of *Chlamydomonas reinhardtii*. *Traffic*, *4*, 435-442.
- COLE, D. G., DIENER, D. R., HIMELBLAU, A. L., BEECH, P. L., FUSTER, J. C. & ROSENBAUM, J. L. 1998. Chlamydomonas Kinesin-II-dependent Intraflagellar Transport (IFT): IFT Particles Contain Proteins Required for Ciliary Assembly in Caenorhabditis elegans Sensory Neurons. *The Journal of Cell Biology*, *141*, 993.
- CONG, L., RAN, F. A., COX, D., LIN, S., BARRETTO, R., HABIB, N., HSU, P. D., WU, X., JIANG, W., MARRAFFINI, L. A. & ZHANG, F. 2013. Multiplex Genome Engineering Using CRISPR/Cas Systems. *339*, 819-823.
- COWAN, M. J., GLADWIN, M. T. & SHELHAMER, J. H. 2001. Disorders of ciliary motility. *Am J Med Sci*, *321*, 3-10.
- CRUZ, C., RIBES, V., KUTEJOVA, E., CAYUSO, J., LAWSON, V., NORRIS, D., STEVENS, J., DAVEY, M., BLIGHT, K., BANGS, F., MYNETT, A., HIRST, E., CHUNG, R., BALASKAS, N., BRODY, S. L., MARTI, E. & BRISCOE, J. 2010. Foxj1 regulates floor plate cilia architecture and modifies the response of cells to sonic hedgehog signalling. *Development*, *137*, 4271.
- D'AGOSTINO, Y., LOCASCIO, A., RISTORATORE, F., SORDINO, P., SPAGNUOLO, A., BORRA, M. & D'ANIELLO, S. 2016. A Rapid and Cheap Methodology for CRISPR/Cas9 Zebrafish Mutant Screening. *Molecular Biotechnology*, *58*, 73-78.

- DANIELS, M. L. A. & NOONE, P. G. 2015. Genetics, diagnosis, and future treatment strategies for primary ciliary dyskinesia. *Expert opinion on orphan drugs*, 3, 31-44.
- DE JONGE, H. J. M., FEHRMANN, R. S. N., DE BONT, E. S. J. M., HOFSTRA, R. M. W., GERBENS, F., KAMPS, W. A., DE VRIES, E. G. E., VAN DER ZEE, A. G. J., TE MEERMAN, G. J. & TER ELST, A. 2007. Evidence Based Selection of Housekeeping Genes. *PLOS ONE*, 2, e898.
- DEBLANDRE, G. A., WETTSTEIN, D. A., KOYANO-NAKAGAWA, N. & KINTNER, C. 1999. A two-step mechanism generates the spacing pattern of the ciliated cells in the skin of *Xenopus* embryos. *Development*, 126, 4715-28.
- DIDON, L., ZWICK, R. K., CHAO, I. W., WALTERS, M. S., WANG, R., HACKETT, N. R. & CRYSTAL, R. G. 2013. RFX3 Modulation of FOXJ1 regulation of cilia genes in the human airway epithelium. *Respiratory Research*, 14, 70-70.
- DIGGLE, C. P., MOORE, D. J., MALI, G., ZUR LAGE, P., AIT-LOUNIS, A., SCHMIDTS, M., SHOEMARK, A., GARCIA MUNOZ, A., HALACHEV, M. R., GAUTIER, P., YEYATI, P. L., BONTHRON, D. T., CARR, I. M., HAYWARD, B., MARKHAM, A. F., HOPE, J. E., VON KRIEGSHEIM, A., MITCHISON, H. M., JACKSON, I. J., DURAND, B., REITH, W., SHERIDAN, E., JARMAN, A. P. & MILL, P. 2014. HEATR2 Plays a Conserved Role in Assembly of the Ciliary Motile Apparatus. *PLOS Genetics*, 10, e1004577.
- DIRKSEN, E. R. 1971. Centriole morphogenesis in developing ciliated epithelium of the mouse oviduct. *J Cell Biol*, 51, 286-302.
- DU, Y., GUO, M., WHITSETT, J. A. & XU, Y. 2015. 'LungGENS': a web-based tool for mapping single-cell gene expression in the developing lung. *Thorax*, 70, 1092-4.
- DU, Y., KITZMILLER, J. A., SRIDHARAN, A., PERL, A. K., BRIDGES, J. P., MISRA, R. S., PRYHUBER, G. S., MARIANI, T. J., BHATTACHARYA, S., GUO, M., POTTER, S. S., DEXHEIMER, P., ARONOW, B., JOBE, A. H., WHITSETT, J. A. & XU, Y. 2017. Lung Gene Expression Analysis (LGEA): an integrative web portal for comprehensive gene expression data analysis in lung development. *Thorax*, 72, 481-484.
- DUQUESNOY, P., ESCUDIER, E., VINCENSINI, L., FRESHOUR, J., BRIDOUX, A. M., COSTE, A., DESCHILDRE, A., DE BLIC, J., LEGENDRE, M., MONTANTIN, G., TENREIRO, H., VOJTEK, A. M., LOUSSERT, C., CLEMENT, A., ESCALIER, D., BASTIN, P., MITCHELL, D. R. & AMSELEM, S. 2009. Loss-of-function mutations in the human ortholog of *Chlamydomonas reinhardtii* ODA7 disrupt dynein arm assembly and cause primary ciliary dyskinesia. *Am J Hum Genet*, 85, 890-6.
- DYMEK, E. E. & SMITH, E. F. 2007. A conserved CaM- and radial spoke-associated complex mediates regulation of flagellar dynein activity. *The Journal of Cell Biology*, 179, 515-526.
- EENJES, E., MERTENS, T. C. J., BUSCOP-VAN KEMPEN, M. J., VAN WIJCK, Y., TAUBE, C., ROTTIER, R. J. & HIEMSTRA, P. S. 2018a. A novel method for expansion and differentiation of mouse tracheal epithelial cells in culture. *Scientific Reports*, 8, 7349.
- EENJES, E., MERTENS, T. C. J., BUSCOP-VAN KEMPEN, M. J., VAN WIJCK, Y., TAUBE, C., ROTTIER, R. J. & HIEMSTRA, P. S. 2018b. A novel method for expansion and differentiation of mouse tracheal epithelial cells in culture. *Scientific Reports*, 8, 7349.
- EL-BROLOS, M. A. & STAINIER, D. Y. R. 2017. Genetic compensation: A phenomenon in search of mechanisms. *PLoS Genetics*, 13, e1006780.
- ESSNER, J. J., AMACK, J. D., NYHOLM, M. K., HARRIS, E. B. & YOST, H. J. 2005. Kupffer's vesicle is a ciliated organ of asymmetry in the zebrafish embryo that initiates left-right development of the brain, heart and gut. *Development*, 132, 1247-60.
- EVE, A. M. J., PLACE, E. S. & SMITH, J. C. 2017. Comparison of Zebrafish *tmem88a* mutant and morpholino knockdown phenotypes. *PLOS ONE*, 12, e0172227.
- FAHY, J. V. & DICKEY, B. F. 2010. Airway mucus function and dysfunction. *New England Journal of Medicine*, 363, 2233-2247.

- FERRANTE, M. I., ROMIO, L., CASTRO, S., COLLINS, J. E., GOULDING, D. A., STEMPLE, D. L., WOOLF, A. S. & WILSON, S. W. 2008. Convergent extension movements and ciliary function are mediated by *ofd1*, a zebrafish orthologue of the human oral-facial-digital type 1 syndrome gene. *Human molecular genetics*, 18, 289-303.
- FISCH, C. & DUPUIS-WILLIAMS, P. 2012. Ultrastructure of cilia and flagella – back to the future! *Biology of the Cell*, 103, 249-270.
- FLIEGAUF, M., BENZING, T. & OMRAN, H. 2007. When cilia go bad: cilia defects and ciliopathies. *Nat Rev Mol Cell Biol*, 8, 880-93.
- FLOTHO, A. & MELCHIOR, F. 2013. Sumoylation: A Regulatory Protein Modification in Health and Disease. *Annual Review of Biochemistry*, 82, 357-385.
- FOWKES, M. E., MITCHELL, D. R. & MATSUDAIRA, P. 1998. The Role of Preassembled Cytoplasmic Complexes in Assembly of Flagellar Dynein Subunits. *Molecular Biology of the Cell*, 9, 2337-2347.
- FUNK, M. C., BERA, A. N., MENCHEN, T., KUALES, G., THRIENE, K., LIENKAMP, S. S., DENGJEL, J., OMRAN, H., FRANK, M. & ARNOLD, S. J. 2015. Cyclin O (*Ccno*) functions during deuterosome-mediated centriole amplification of multiciliated cells. *Embo j*, 34, 1078-89.
- GAJIWALA, K. S., CHEN, H., CORNILLE, F., ROQUES, B. P., REITH, W., MACH, B. & BURLEY, S. K. 2000. Structure of the winged-helix protein hRFX1 reveals a new mode of DNA binding. *Nature*, 403, 916.
- GARCIA-GONZALO, F. R. & REITER, J. F. 2012. Scoring a backstage pass: Mechanisms of ciliogenesis and ciliary access. *The Journal of Cell Biology*, 197, 697-709.
- GEIMER, S. & MELKONIAN, M. 2004. The ultrastructure of the *Chlamydomonas reinhardtii* basal apparatus: identification of an early marker of radial asymmetry inherent in the basal body. *J Cell Sci*, 117, 2663-74.
- GENETOOLS. 2018. *Morpholino Antisense Oligos* [Online]. 1001 Summerton Way ,Philomath, OR 97370 USA Available: http://www.gene-tools.com/morpholino_antisense_oligos [Accessed].
- GEREMEK, M., BRUINENBERG, M., ZIETKIEWICZ, E., POGORZELSKI, A., WITT, M. & WIJMENGA, C. 2011. Gene expression studies in cells from primary ciliary dyskinesia patients identify 208 potential ciliary genes. *Hum Genet*, 129, 283-93.
- GEREMEK, M., ZIETKIEWICZ, E., BRUINENBERG, M., FRANKE, L., POGORZELSKI, A., WIJMENGA, C. & WITT, M. 2014. Ciliary genes are down-regulated in bronchial tissue of primary ciliary dyskinesia patients. *PLoS One*, 9, e88216.
- GERETY, S. S. & WILKINSON, D. G. 2011. Morpholino artifacts provide pitfalls and reveal a novel role for pro-apoptotic genes in hindbrain boundary development. *Developmental Biology*, 350, 279-289.
- GIBBONS, I. R. & ROWE, A. J. 1965. Dynein: A Protein with Adenosine Triphosphatase Activity from Cilia. *Science*, 149, 424-6.
- GOMPERTS, B. N., GONG-COOPER, X. & HACKETT, B. P. 2004. *Foxj1* regulates basal body anchoring to the cytoskeleton of ciliated pulmonary epithelial cells. *Journal of Cell Science*, 117, 1329-1337.
- GRIESENBACH, U., KITSON, C., ESCUDERO GARCIA, S., FARLEY, R., SINGH, C., SOMERTON, L., PAINTER, H., SMITH, R. L., GILL, D. R., HYDE, S. C., CHOW, Y. H., HU, J., GRAY, M., EDBROOKE, M., OGILVIE, V., MACGREGOR, G., SCHEULE, R. K., CHENG, S. H., CAPLEN, N. J. & ALTON, E. W. 2006. Inefficient cationic lipid-mediated siRNA and antisense oligonucleotide transfer to airway epithelial cells in vivo. *Respir Res*, 7, 26.
- GRIFFIN, K., PATIENT, R. & HOLDER, N. 1995. Analysis of FGF function in normal and no tail zebrafish embryos reveals separate mechanisms for formation of the trunk and the tail. *Development*, 121, 2983-94.

- GUO, X., SHEN, J., XIA, Z., ZHANG, R., ZHANG, P., ZHAO, C., XING, J., CHEN, L., CHEN, W., LIN, M., HUO, R., SU, B., ZHOU, Z. & SHA, J. 2010. Proteomic analysis of proteins involved in spermiogenesis in mouse. *J Proteome Res*, 9, 1246-56.
- HACKETT, B. P., BRODY, S. L., LIANG, M., ZEITZ, I. D., BRUNS, L. A. & GITLIN, J. D. J. P. O. T. N. A. O. S. 1995. Primary structure of hepatocyte nuclear factor/forkhead homologue 4 and characterization of gene expression in the developing respiratory and reproductive epithelium. 92, 4249-4253.
- HAMADA, H. 2016. Roles of Motile and Immotile Cilia in Left-Right Symmetry Breaking. *In: NAKANISHI, T., MARKWALD, R. R., BALDWIN, H. S., KELLER, B. B., SRIVASTAVA, D. & YAMAGISHI, H. (eds.) Etiology and Morphogenesis of Congenital Heart Disease: From Gene Function and Cellular Interaction to Morphology.* Tokyo: Springer Japan.
- HIRST, R. A., JACKSON, C. L., COLES, J. L., WILLIAMS, G., RUTMAN, A., GOGGIN, P. M., ADAM, E. C., PAGE, A., EVANS, H. J., LACKIE, P. M., O'CALLAGHAN, C. & LUCAS, J. S. 2014. Culture of primary ciliary dyskinesia epithelial cells at air-liquid interface can alter ciliary phenotype but remains a robust and informative diagnostic aid. *PLoS One*, 9, e89675.
- HOH, R. A., STOWE, T. R., TURK, E. & STEARNS, T. 2012. Transcriptional program of ciliated epithelial cells reveals new cilium and centrosome components and links to human disease. *PLoS One*, 7, e52166.
- HOH, R. A., STOWE, T. R., TURK, E. & STEARNS, T. 2013. Transcriptional Program of Ciliated Epithelial Cells Reveals New Cilium and Centrosome Components and Links to Human Disease. *PLOS ONE*, 7, e52166.
- HOLTZMAN, M. J., BYERS, D. E., ALEXANDER-BRETT, J. & WANG, X. 2014. The role of airway epithelial cells and innate immune cells in chronic respiratory disease. *Nature Reviews Immunology*, 14, 686.
- HONG, S.-K. & DAWID, I. B. 2009. FGF-dependent left-right asymmetry patterning in zebrafish is mediated by *ler2* and *Fibp1*. *Proceedings of the National Academy of Sciences*, 106, 2230.
- HORANI, A., BRODY, S. L. & FERKOL, T. W. 2014. Picking up speed: advances in the genetics of primary ciliary dyskinesia. *Pediatr Res*, 75, 158-164.
- HORANI, A., DRULEY, TODD E., ZARIWALA, MAIMOONA A., PATEL, ANAND C., LEVINSON, BENJAMIN T., VAN ARENDONK, LAURA G., THORNTON, KATHERINE C., GIACALONE, JOE C., ALBEE, ALISON J., WILSON, KATE S., TURNER, EMILY H., NICKERSON, DEBORAH A., SHENDURE, J., BAYLY, PHILIP V., LEIGH, MARGARET W., KNOWLES, MICHAEL R., BRODY, STEVEN L., DUTCHER, SUSAN K. & FERKOL, THOMAS W. 2012. Whole-Exome Capture and Sequencing Identifies HEATR2 Mutation as a Cause of Primary Ciliary Dyskinesia. *The American Journal of Human Genetics*, 91, 685-693.
- HORANI, A., FERKOL, T. W., SHOSEYOV, D., WASSERMAN, M. G., OREN, Y. S., KEREM, B., AMIRAV, I., COHEN-CYMBERKNOH, M., DUTCHER, S. K., BRODY, S. L., ELPELEG, O. & KEREM, E. 2013a. LRRC6 Mutation Causes Primary Ciliary Dyskinesia with Dynein Arm Defects. *PLOS ONE*, 8, e59436.
- HORANI, A., NATH, A., WASSERMAN, M. G., HUANG, T. & BRODY, S. L. 2013b. Rho-Associated Protein Kinase Inhibition Enhances Airway Epithelial Basal-Cell Proliferation and Lentivirus Transduction. *American Journal of Respiratory Cell and Molecular Biology*, 49, 341-347.
- HOWE, K., CLARK, M. D., TORROJA, C. F., TORRANCE, J., BERTHELOT, C., MUFFATO, M., COLLINS, J. E., HUMPHRAY, S., MCLAREN, K., MATTHEWS, L., MCLAREN, S., SEALY, I., CACCAMO, M., CHURCHER, C., SCOTT, C., BARRETT, J. C., KOCH, R., RAUCH, G.-J., WHITE, S., CHOW, W., KILIAN, B., QUINTAIS, L. T., GUERRA-ASSUNÇÃO, J. A., ZHOU, Y., GU, Y., YEN, J., VOGEL, J.-H., EYRE, T., REDMOND, S., BANERJEE, R., CHI, J., FU, B., LANGLEY, E., MAGUIRE, S. F., LAIRD, G. K., LLOYD, D., KENYON, E., DONALDSON, S.,

- SEHRA, H., ALMEIDA-KING, J., LOVELAND, J., TREVANION, S., JONES, M., QUAIL, M., WILLEY, D., HUNT, A., BURTON, J., SIMS, S., MCLAY, K., PLUMB, B., DAVIS, J., CLEE, C., OLIVER, K., CLARK, R., RIDDLE, C., ELIOTT, D., THREADGOLD, G., HARDEN, G., WARE, D., MORTIMER, B., KERRY, G., HEATH, P., PHILLIMORE, B., TRACEY, A., CORBY, N., DUNN, M., JOHNSON, C., WOOD, J., CLARK, S., PELAN, S., GRIFFITHS, G., SMITH, M., GLITHERO, R., HOWDEN, P., BARKER, N., STEVENS, C., HARLEY, J., HOLT, K., PANAGIOTIDIS, G., LOVELL, J., BEASLEY, H., HENDERSON, C., GORDON, D., AUGER, K., WRIGHT, D., COLLINS, J., RAISEN, C., DYER, L., LEUNG, K., ROBERTSON, L., AMBRIDGE, K., LEONGAMORNLETT, D., MCGUIRE, S., GILDERTHORP, R., GRIFFITHS, C., MANTHRAVADI, D., NICHOL, S., BARKER, G., WHITEHEAD, S., KAY, M., et al. 2013a. The zebrafish reference genome sequence and its relationship to the human genome. *Nature*, 496, 498-503.
- HOWE, K., CLARK, M. D., TORROJA, C. F., TORRANCE, J., BERTHELOT, C., MUFFATO, M., COLLINS, J. E., HUMPHRAY, S., MCLAREN, K., MATTHEWS, L., MCLAREN, S., SEALY, I., CACCAMO, M., CHURCHER, C., SCOTT, C., BARRETT, J. C., KOCH, R., RAUCH, G. J., WHITE, S., CHOW, W., KILIAN, B., QUINTAIS, L. T., GUERRA-ASSUNCAO, J. A., ZHOU, Y., GU, Y., YEN, J., VOGEL, J. H., EYRE, T., REDMOND, S., BANERJEE, R., CHI, J., FU, B., LANGLEY, E., MAGUIRE, S. F., LAIRD, G. K., LLOYD, D., KENYON, E., DONALDSON, S., SEHRA, H., ALMEIDA-KING, J., LOVELAND, J., TREVANION, S., JONES, M., QUAIL, M., WILLEY, D., HUNT, A., BURTON, J., SIMS, S., MCLAY, K., PLUMB, B., DAVIS, J., CLEE, C., OLIVER, K., CLARK, R., RIDDLE, C., ELLIOT, D., THREADGOLD, G., HARDEN, G., WARE, D., BEGUM, S., MORTIMORE, B., KERRY, G., HEATH, P., PHILLIMORE, B., TRACEY, A., CORBY, N., DUNN, M., JOHNSON, C., WOOD, J., CLARK, S., PELAN, S., GRIFFITHS, G., SMITH, M., GLITHERO, R., HOWDEN, P., BARKER, N., LLOYD, C., STEVENS, C., HARLEY, J., HOLT, K., PANAGIOTIDIS, G., LOVELL, J., BEASLEY, H., HENDERSON, C., GORDON, D., AUGER, K., WRIGHT, D., COLLINS, J., RAISEN, C., DYER, L., LEUNG, K., ROBERTSON, L., AMBRIDGE, K., LEONGAMORNLETT, D., MCGUIRE, S., GILDERTHORP, R., GRIFFITHS, C., MANTHRAVADI, D., NICHOL, S., BARKER, G., et al. 2013b. The zebrafish reference genome sequence and its relationship to the human genome. *Nature*, 496, 498-503.
- HOYER-FENDER, S. 2010. Centriole maturation and transformation to basal body. *Seminars in Cell & Developmental Biology*, 21, 142-147.
- HSU, PATRICK D., LANDER, ERIC S. & ZHANG, F. 2014. Development and Applications of CRISPR-Cas9 for Genome Engineering. *Cell*, 157, 1262-1278.
- HWANG, W. Y., FU, Y., REYON, D., MAEDER, M. L., TSAI, S. Q., SANDER, J. D., PETERSON, R. T., YE, J. R. & JOUNG, J. K. 2013a. Efficient genome editing in zebrafish using a CRISPR-Cas system. *Nat Biotechnol*, 31, 227-9.
- HWANG, W. Y., FU, Y., REYON, D., MAEDER, M. L., TSAI, S. Q., SANDER, J. D., PETERSON, R. T., YE, J. R. J. & JOUNG, J. K. 2013b. Efficient In Vivo Genome Editing Using RNA-Guided Nucleases. *Nature biotechnology*, 31, 227-229.
- IBAÑEZ-TALLON, I., HEINTZ, N. & OMRAN, H. 2003. To beat or not to beat: roles of cilia in development and disease. *Human Molecular Genetics*, 12, R27-R35.
- IOANNOU, A., SANTAMA, N. & SKOURIDES, P. A. 2013. *Xenopus laevis* nucleotide binding protein 1 (xNubp1) is important for convergent extension movements and controls ciliogenesis via regulation of the actin cytoskeleton. *Developmental Biology*, 380, 243-258.
- ISHIKAWA, T. 2017. Axoneme Structure from Motile Cilia. *Cold Spring Harb Perspect Biol*, 9.
- IVLIEV, A. E., T HOEN, P. A., VAN ROON-MOM, W. M., PETERS, D. J. & SERGEEVA, M. G. 2012. Exploring the transcriptome of ciliated cells using in silico dissection of human tissues. *PLoS One*, 7, e35618.
- JACKSON, P. K. & ATTARDI, L. D. 2016. p73 and FoxJ1: Programming Multiciliated Epithelia. *Trends in cell biology*, 26, 239-240.

- JAIN, R., JAVIDAN-NEJAD, C., ALEXANDER-BRETT, J., HORANI, A., CABELLON, M. C., WALTER, M. J. & BRODY, S. L. 2012. Sensory functions of motile cilia and implication for bronchiectasis. *Frontiers in bioscience (Scholar edition)*, 4, 1088-1098.
- JING, J. C., CHEN, J. J., CHOU, L., WONG, B. J. F. & CHEN, Z. 2017. Visualization and Detection of Ciliary Beating Pattern and Frequency in the Upper Airway using Phase Resolved Doppler Optical Coherence Tomography. *Scientific Reports*, 7, 8522.
- KAKIHARA, Y. & HOURY, W. A. 2012. The R2TP complex: discovery and functions. *Biochim Biophys Acta*, 1823, 101-7.
- KALNINS, V. I. & PORTER, K. R. 1969. Centriole replication during ciliogenesis in the chick tracheal epithelium. *Z Zellforsch Mikrosk Anat*, 100, 1-30.
- KAMURA, K., KOBAYASHI, D., UEHARA, Y., KOSHIDA, S., IJIMA, N., KUDO, A., YOKOYAMA, T. & TAKEDA, H. 2011. Pkd11 complexes with Pkd2 on motile cilia and functions to establish the left-right axis. *Development*, 138, 1121.
- KANE, D. A. & KIMMEL, C. B. 1993. The zebrafish midblastula transition. *Development*, 119, 447-456.
- KANEHISA, M., SATO, Y., KAWASHIMA, M., FURUMICHI, M. & TANABE, M. 2016. KEGG as a reference resource for gene and protein annotation. *Nucleic Acids Res*, 44, D457-62.
- KATHIRIYA, I. S. & SRIVASTAVA, D. 2000. Left-right asymmetry and cardiac looping: implications for cardiac development and congenital heart disease. *Am J Med Genet*, 97, 271-9.
- KAWASUMI, A., NAKAMURA, T., IWAI, N., YASHIRO, K., SAIJOH, Y., BELO, J. A., SHIRATORI, H. & HAMADA, H. 2011. Left-right asymmetry in the level of active Nodal protein produced in the node is translated into left-right asymmetry in the lateral plate of mouse embryos. *Developmental Biology*, 353, 321-330.
- KENNEDY, M. P., OMRAN, H., LEIGH, M. W., DELL, S., MORGAN, L., MOLINA, P. L., ROBINSON, B. V., MINNIX, S. L., OLBRICH, H., SEVERIN, T., AHRENS, P., LANGE, L., MORILLAS, H. N., NOONE, P. G., ZARIWALA, M. A. & KNOWLES, M. R. 2007. Congenital heart disease and other heterotaxic defects in a large cohort of patients with primary ciliary dyskinesia. *Circulation*, 115, 2814-21.
- KIM, J. H., CHOI, H. J., KIM, B., KIM, M. H., LEE, J. M., KIM, I. S., LEE, M. H., CHOI, S. J., KIM, K. I., KIM, S. I., CHUNG, C. H. & BAEK, S. H. 2006. Roles of sumoylation of a reptin chromatin-remodelling complex in cancer metastasis. *Nat Cell Biol*, 8, 631-9.
- KISTLER, W. S., HORVATH, G. C., DASGUPTA, A. & KISTLER, M. K. 2009. Differential expression of Rfx1-4 during mouse spermatogenesis. *Gene Expression Patterns*, 9, 515-519.
- KLEIN, T. J. & MLODZIK, M. 2005. PLANAR CELL POLARIZATION: An Emerging Model Points in the Right Direction. *Annual Review of Cell and Developmental Biology*, 21, 155-176.
- KLOS DEHRING, DEBORAH A., VLADAR, ESZTER K., WERNER, MICHAEL E., MITCHELL, JENNIFER W., HWANG, P. & MITCHELL, BRIAN J. 2013. Deuterosome-Mediated Centriole Biogenesis. *Developmental Cell*, 27, 103-112.
- KNEZEVIC, V., RANSON, M. & MACKEM, S. 1995. The organizer-associated chick homeobox gene, *Gnot1*, is expressed before gastrulation and regulated synergistically by activin and retinoic acid. *Developmental biology*, 171, 458-470.
- KNIGHT-JONES, E. W. 1954. Relations between Metachronism and the Direction of Ciliary Beat in Metazoa. *Quarterly Journal of Microscopical Science*, s3-95, 503-521.
- KNOWLES, M. R. & BOUCHER, R. C. 2002. Mucus clearance as a primary innate defense mechanism for mammalian airways. *J Clin Invest*, 109, 571-7.
- KNOWLES, M. R., DANIELS, L. A., DAVIS, S. D., ZARIWALA, M. A. & LEIGH, M. W. 2013a. Primary ciliary dyskinesia. Recent advances in diagnostics, genetics, and characterization of clinical disease. *Am J Respir Crit Care Med*, 188, 913-22.
- KNOWLES, M. R., DANIELS, L. A., DAVIS, S. D., ZARIWALA, M. A. & LEIGH, M. W. 2013b. Primary Ciliary Dyskinesia. Recent Advances in Diagnostics, Genetics, and Characterization of

- Clinical Disease. *American Journal of Respiratory and Critical Care Medicine*, 188, 913-922.
- KNOWLES, MICHAEL R., OSTROWSKI, LAWRENCE E., LOGES, NIKI T., HURD, T., LEIGH, MARGARET W., HUANG, L., WOLF, WHITNEY E., CARSON, JOHNNY L., HAZUCHA, MILAN J., YIN, W., DAVIS, STEPHANIE D., DELL, SHARON D., FERKOL, THOMAS W., SAGEL, SCOTT D., OLIVIER, KENNETH N., JAHNKE, C., OLBRICH, H., WERNER, C., RAIDT, J., WALLMEIER, J., PENNEKAMP, P., DOUGHERTY, GERARD W., HJEIJ, R., GEE, HEON Y., OTTO, EDGAR A., HALBRITTER, J., CHAKI, M., DIAZ, K. A., BRAUN, DANIELA A., PORATH, JONATHAN D., SCHUELER, M., BAKTAI, G., GRIESE, M., TURNER, EMILY H., LEWIS, ALEXANDRA P., BAMSHAD, MICHAEL J., NICKERSON, DEBORAH A., HILDEBRANDT, F., SHENDURE, J., OMRAN, H. & ZARIWALA, MAIMOONA A. 2013c. Mutations in SPAG1 Cause Primary Ciliary Dyskinesia Associated with Defective Outer and Inner Dynein Arms. *The American Journal of Human Genetics*, 93, 711-720.
- KNOWLES, M. R., OSTROWSKI, L. E., LOGES, N. T., HURD, T., LEIGH, M. W., HUANG, L., WOLF, W. E., CARSON, J. L., HAZUCHA, M. J., YIN, W., DAVIS, S. D., DELL, S. D., FERKOL, T. W., SAGEL, S. D., OLIVIER, K. N., JAHNKE, C., OLBRICH, H., WERNER, C., RAIDT, J., WALLMEIER, J., PENNEKAMP, P., DOUGHERTY, G. W., HJEIJ, R., GEE, H. Y., OTTO, E. A., HALBRITTER, J., CHAKI, M., DIAZ, K. A., BRAUN, D. A., PORATH, J. D., SCHUELER, M., BAKTAI, G., GRIESE, M., TURNER, E. H., LEWIS, A. P., BAMSHAD, M. J., NICKERSON, D. A., HILDEBRANDT, F., SHENDURE, J., OMRAN, H. & ZARIWALA, M. A. 2013d. Mutations in SPAG1 cause primary ciliary dyskinesia associated with defective outer and inner dynein arms. *Am J Hum Genet*, 93, 711-20.
- KOK, F. O., SHIN, M., NI, C. W., GUPTA, A., GROSSE, A. S., VAN IMPEL, A., KIRCHMAIER, B. C., PETERSON-MADURO, J., KOURKOULIS, G., MALE, I., DESANTIS, D. F., SHEPPARD-TINDELL, S., EBARASI, L., BETSHOLTZ, C., SCHULTE-MERKER, S., WOLFE, S. A. & LAWSON, N. D. 2015. Reverse genetic screening reveals poor correlation between morpholino-induced and mutant phenotypes in zebrafish. *Dev Cell*, 32, 97-108.
- KONG, X., MA, S., GUO, J., MA, Y. A. N., HU, Y., WANG, J. & ZHENG, Y. 2015. Ubiquitously expressed transcript is a novel interacting protein of protein inhibitor of activated signal transducer and activator of transcription 2. *Molecular Medicine Reports*, 11, 2443-2448.
- KONNO, A., SHIBA, K., CAI, C. & INABA, K. 2015. Branchial Cilia and Sperm Flagella Recruit Distinct Axonemal Components. *PLOS ONE*, 10, e0126005.
- KOTAJA, N., AITTO-MÄKI, S., SILVENNOINEN, O., PALVIMO, J. J. & JÄNNE, O. A. 2000. ARIP3 (androgen receptor-interacting protein 3) and other PIAS (protein inhibitor of activated STAT) proteins differ in their ability to modulate steroid receptor-dependent transcriptional activation. *Molecular Endocrinology*, 14, 1986-2000.
- KOTAJA, N., VIHINEN, M., PALVIMO, J. J. & JANNE, O. A. 2002. Androgen receptor-interacting protein 3 and other PIAS proteins cooperate with glucocorticoid receptor-interacting protein 1 in steroid receptor-dependent signaling. *Journal of Biological Chemistry*.
- KOTT, E., DUQUESNOY, P., COPIN, B., LEGENDRE, M., DASTOT-LE MOAL, F., MONTANTIN, G., JEANSON, L., TAMALET, A., PAPON, J.-F., SIFFROI, J.-P., RIVES, N., MITCHELL, V., DE BLIC, J., COSTE, A., CLEMENT, A., ESCALIER, D., TOURÉ, A., ESCUDIER, E. & AMSELEM, S. 2012. Loss-of-Function Mutations in LRRC6, a Gene Essential for Proper Axonemal Assembly of Inner and Outer Dynein Arms, Cause Primary Ciliary Dyskinesia. *American Journal of Human Genetics*, 91, 958-964.
- KOZMINSKI, K. G., BEECH, P. L. & ROSENBAUM, J. L. 1995. The Chlamydomonas kinesin-like protein FLA10 is involved in motility associated with the flagellar membrane. *J Cell Biol*, 131, 1517-27.

- KRAMER-ZUCKER, A. G., OLALE, F., HAYCRAFT, C. J., YODER, B. K., SCHIER, A. F. & DRUMMOND, I. A. 2005. Cilia-driven fluid flow in the zebrafish pronephros, brain and Kupffer's vesicle is required for normal organogenesis. *Development*, 132, 1907-1921.
- KREILING, J. A., WILLIAMS, G. & CRETON, R. 2007. Analysis of Kupffer's vesicle in zebrafish embryos using a cave automated virtual environment. *Developmental dynamics: an official publication of the American Association of Anatomists*, 236, 1963-1969.
- KROLL, K. L. 2007. Geminin in embryonic development: coordinating transcription and the cell cycle during differentiation. *Front Biosci*, 12, 409.
- KYROUSI, C., ARBI, M., PILZ, G.-A., PEFANI, D.-E., LALIOTI, M.-E., NINKOVIC, J., GÖTZ, M., LYGEROU, Z. & TARAVIRAS, S. 2015. Mcidas and GemC1 are key regulators for the generation of multiciliated ependymal cells in the adult neurogenic niche. *Development*, 142, 3661.
- LABUN, K., MONTAGUE, T. G., GAGNON, J. A., THYME, S. B. & VALEN, E. 2016. CHOPCHOP v2: a web tool for the next generation of CRISPR genome engineering. *Nucleic Acids Res*, 44, W272-6.
- LANGLEY, A. R., SMITH, J. C., STEMPLE, D. L. & HARVEY, S. A. 2014. New insights into the maternal to zygotic transition. *Development*, 141, 3834-3841.
- LECHTRECK, K. F., DELMOTTE, P., ROBINSON, M. L., SANDERSON, M. J. & WITMAN, G. B. 2008. Mutations in Hydin impair ciliary motility in mice. *J Cell Biol*, 180, 633-43.
- LEIGH, M. W. 2012. 71 - Primary Ciliary Dyskinesia. In: WILMOTT, R. W., BOAT, T. F., BUSH, A., CHERNICK, V., DETERDING, R. R. & RATJEN, F. (eds.) *Kendig & Chernick's Disorders of the Respiratory Tract in Children (Eighth Edition)*. Philadelphia: W.B. Saunders.
- LEVARDON, H., YONKER, L. M., HURLEY, B. P. & MOU, H. 2018. Expansion of Airway Basal Cells and Generation of Polarized Epithelium. *Bio-protocol*, 8, e2877.
- LI, J. B., GERDES, J. M., HAYCRAFT, C. J., FAN, Y., TESLOVICH, T. M., MAY-SIMERA, H., LI, H., BLACQUE, O. E., LI, L., LEITCH, C. C., LEWIS, R. A., GREEN, J. S., PARFREY, P. S., LEROUX, M. R., DAVIDSON, W. S., BEALES, P. L., GUAY-WOODFORD, L. M., YODER, B. K., STORMO, G. D., KATSANIS, N. & DUTCHER, S. K. 2004. Comparative genomics identifies a flagellar and basal body proteome that includes the BBS5 human disease gene. *Cell*, 117, 541-52.
- LI, S., FERNANDEZ, J.-J., MARSHALL, W. F. & AGARD, D. A. 2012a. Three-dimensional structure of basal body triplet revealed by electron cryo-tomography. *The EMBO Journal*, 31, 552-562.
- LI, Y., ZHANG, Q., WEI, Q., ZHANG, Y., LING, K. & HU, J. 2012b. SUMOylation of the small GTPase ARL-13 promotes ciliary targeting of sensory receptors. *The Journal of Cell Biology*, 199, 589-598.
- LI, Y., ZHAO, L., YUAN, S., ZHANG, J. & SUN, Z. 2017. Axonemal dynein assembly requires the R2TP complex component Pontin. *Development*, 144, 4684-4693.
- LINDEMANN, C. B. 2003. Structural-Functional Relationships of the Dynein, Spokes, and Central-Pair Projections Predicted from an Analysis of the Forces Acting within a Flagellum. *Biophysical Journal*, 84, 4115-4126.
- LIU, Y., PATHAK, N., KRAMER-ZUCKER, A. & DRUMMOND, I. A. 2007. Notch signaling controls the differentiation of transporting epithelia and multiciliated cells in the zebrafish pronephros. *Development*, 134, 1111-22.
- LOGES, N. T., OLBRICH, H., BECKER-HECK, A., HÄFFNER, K., HEER, A., REINHARD, C., SCHMIDTS, M., KISPERT, A., ZARIWALA, M. A., LEIGH, M. W., KNOWLES, M. R., ZENTGRAF, H., SEITHE, H., NÜRNBERG, G., NÜRNBERG, P., REINHARDT, R. & OMRAN, H. 2009. Deletions and Point Mutations of LRRC50 Cause Primary Ciliary Dyskinesia Due to Dynein Arm Defects. *The American Journal of Human Genetics*, 85, 883-889.

- LOPES, S. S., LOURENCO, R., PACHECO, L., MORENO, N., KREILING, J. & SAUDE, L. 2010. Notch signalling regulates left-right asymmetry through ciliary length control. *Development*, 137, 3625-32.
- LUCAS, J. S., ADAM, E. C., GOGGIN, P. M., JACKSON, C. L., POWLES-GLOVER, N., PATEL, S. H., HUMPHREYS, J., FRAY, M. D., FALCONNET, E., BLOUIN, J. L., CHEESEMAN, M. T., BARTOLONI, L., NORRIS, D. P. & LACKIE, P. M. 2012. Static respiratory cilia associated with mutations in Dnahc11/DNAH11: a mouse model of PCD. *Hum Mutat*, 33, 495-503.
- MA, L., QUIGLEY, I., OMRAN, H. & KINTNER, C. 2014. Multicilin drives centriole biogenesis via E2f proteins. *Genes Dev*, 28, 1461-71.
- MALI, G. R., YEYATI, P. L., MIZUNO, S., DODD, D. O., TENNANT, P. A., KEIGHREN, M. A., ZUR LAGE, P., SHOEMARK, A., GARCIA-MUNOZ, A., SHIMADA, A., TAKEDA, H., EDLICH, F., TAKAHASHI, S., VON KREISHEIM, A., JARMAN, A. P. & MILL, P. 2018. ZMYND10 functions in a chaperone relay during axonemal dynein assembly. *Elife*, 7.
- MALICKI, J., AVANESOV, A., LI, J., YUAN, S. & SUN, Z. 2011. Analysis of cilia structure and function in zebrafish. *Methods Cell Biol*, 101, 39-74.
- MARCET, B., CHEVALIER, B., LUXARDI, G., CORAUX, C., ZARAGOSI, L.-E., CIBOIS, M., ROBBERMESANT, K., JOLLY, T., CARDINAUD, B., MOREILHON, C., GIOVANNINI-CHAMI, L., NAWROCKI-RABY, B., BIREMBAUT, P., WALDMANN, R., KODJABACHIAN, L. & BARBRY, P. 2011. Control of vertebrate multiciliogenesis by miR-449 through direct repression of the Delta/Notch pathway. *Nat Cell Biol*, 13, 693-699.
- MARQUES, S., BORGES, A. C., SILVA, A. C., FREITAS, S., CORDENONSI, M. & BELO, J. A. 2004. The activity of the Nodal antagonist Cerl-2 in the mouse node is required for correct L/R body axis. *Genes & Development*, 18, 2342-2347.
- MARSHALL, C. B., MAYS, D. J., BEELER, J. S., ROSENBLUTH, J. M., BOYD, K. L., SANTOS GUASCH, G. L., SHAVER, T. M., TANG, L. J., LIU, Q., SHYR, Y., VENTERS, B. J., MAGNUSON, M. A. & PIETENPOL, J. A. 2016. p73 Is Required for Multiciliogenesis and Regulates the Foxj1-Associated Gene Network. *Cell Rep*, 14, 2289-300.
- MARX, V. 2014. An atlas of expression. *Nature*, 509, 645.
- MCCLINTOCK, T. S., GLASSER, C. E., BOSE, S. C. & BERGMAN, D. A. 2008. Tissue expression patterns identify mouse cilia genes. *Physiol Genomics*, 32, 198-206.
- MCGRATH, J. & BRUECKNER, M. 2003. Cilia are at the heart of vertebrate left-right asymmetry. *Curr Opin Genet Dev*, 13, 385-92.
- MCGRATH, J., SOMLO, S., MAKOVA, S., TIAN, X. & BRUECKNER, M. 2003. Two Populations of Node Monocilia Initiate Left-Right Asymmetry in the Mouse. *Cell*, 114, 61-73.
- MCINTYRE, J. C., JOINER, A. M., ZHANG, L., IÑIGUEZ-LLUHÍ, J. & MARTENS, J. R. 2015. SUMOylation regulates ciliary localization of olfactory signaling proteins. *Journal of Cell Science*, 128, 1934-1945.
- MEUNIER, A. & AZIMZADEH, J. 2016. Multiciliated Cells in Animals. *Cold Spring Harb Perspect Biol*, 8.
- MI, H., DONG, Q., MURUGANUJAN, A., GAUDET, P., LEWIS, S. & THOMAS, P. D. 2010. PANTHER version 7: improved phylogenetic trees, orthologs and collaboration with the Gene Ontology Consortium. *Nucleic Acids Research*, 38, D204-D210.
- MITCHELL, D. R. 2017. Evolution of Cilia. *Cold Spring Harb Perspect Biol*, 9.
- MITCHISON, H. M., SCHMIDTS, M., LOGES, N. T., FRESHOUR, J., DRITSOULA, A., HIRST, R. A., O'CALLAGHAN, C., BLAU, H., AL DABBAGH, M., OLBRICH, H., BEALES, P. L., YAGI, T., MUSSAFFI, H., CHUNG, E. M. K., OMRAN, H. & MITCHELL, D. R. 2012. Mutations in axonemal dynein assembly factor DNAAF3 cause primary ciliary dyskinesia. *Nature Genetics*, 44, 381.

- MOILANEN, A.-M., KARVONEN, U., POUKKA, H., YAN, W., TOPPARI, J., JÄNNE, O. A. & PALVIMO, J. J. 1999. A testis-specific androgen receptor coregulator that belongs to a novel family of nuclear proteins. *Journal of Biological Chemistry*, 274, 3700-3704.
- MOORE, D. J., ONOUFRIADIS, A., SHOEMARK, A., SIMPSON, M. A., ZUR LAGE, P. I., DE CASTRO, S. C., BARTOLONI, L., GALLONE, G., PETRIDIS, S., WOOLLARD, W. J., ANTONY, D., SCHMIDTS, M., DIDONNA, T., MAKRYTHANASIS, P., BEVILLARD, J., MONGAN, N. P., DJAKOW, J., PALS, G., LUCAS, J. S., MARTIN, J. K., NIELSEN, K. G., SANTONI, F., GUIPPONI, M., HOGG, C., ANTONARAKIS, S. E., EMES, R. D., CHUNG, E. M., GREENE, N. D., BLOUIN, J. L., JARMAN, A. P. & MITCHISON, H. M. 2013. Mutations in ZMYND10, a gene essential for proper axonemal assembly of inner and outer dynein arms in humans and flies, cause primary ciliary dyskinesia. *Am J Hum Genet*, 93, 346-56.
- MORIMOTO, M., LIU, Z., CHENG, H.-T., WINTERS, N., BADER, D. & KOPAN, R. 2010. Canonical Notch signaling in the developing lung is required for determination of arterial smooth muscle cells and selection of Clara versus ciliated cell fate. *Journal of Cell Science*, 123, 213-224.
- MOU, H., VINARSKY, V., TATA, P. R., BRAZAUSKAS, K., CHOI, S. H., CROOKE, A. K., ZHANG, B., SOLOMON, G. M., TURNER, B., BIHLER, H., HARRINGTON, J., LAPEY, A., CHANNICK, C., KEYES, C., FREUND, A., ARTANDI, S., MENSE, M., ROWE, S., ENGELHARDT, J. F., HSU, Y. C. & RAJAGOPAL, J. 2016. Dual SMAD Signaling Inhibition Enables Long-Term Expansion of Diverse Epithelial Basal Cells. *Cell Stem Cell*, 19, 217-231.
- MULAY, A. 2017. *The Role of BPIFA1 in Otitis Media*. PhD, University of Sheffield.
- MULLER, H. 1932. Further studies on the Nature and causes of gene mutations. *Proc 6th Int Congr Genet 1*:, 213–255.
- MULLER, O. 1786. *Animalcula infusoria; fluvia tilia et marina, que detexit, systematice descripsit et ad vivum delineari curavit. Typis N. Molleri, Havniae.*
- MURPHY, D. B., SEEMANN, S., WIESE, S., KIRSCHNER, R., GRZESCHIK, K. H. & THIES, U. J. G. 1997. The human hepatocyte nuclear factor 3/fork head gene FKHL13: genomic structure and pattern of expression. 40, 462-469.
- MUSA, M., WILSON, K., SUN, L., MULAY, A., BINGLE, L., MARRIOTT, H. M., LECLAIR, E. E. & BINGLE, C. D. 2012. Differential localisation of BPIFA1 (SPLUNC1) and BPIFB1 (LPLUNC1) in the nasal and oral cavities of mice. *Cell and Tissue Research*, 350, 455-464.
- NAKACHI, M., NAKAJIMA, A., NOMURA, M., YONEZAWA, K., UENO, K., ENDO, T. & INABA, K. 2011. Proteomic profiling reveals compartment-specific, novel functions of ascidian sperm proteins. *Mol Reprod Dev*, 78, 529-49.
- NARASIMHAN, V., HJEIJ, R., VIJ, S., LOGES, N. T., WALLMEIER, J., KOERNER-RETTBERG, C., WERNER, C., THAMILSELVAM, S. K., BOEY, A., CHOKSI, S. P., PENNEKAMP, P., ROY, S. & OMRAN, H. 2015. Mutations in CCDC11, which Encodes a Coiled-Coil Containing Ciliary Protein, Causes Situs Inversus Due to Dysmotility of Monocilia in the Left–Right Organizer. *Human Mutation*, 36, 307-318.
- NARASIMHAN, V. M., HUNT, K. A., MASON, D., BAKER, C. L., KARCZEWSKI, K. J., BARNES, M. R., BARNETT, A. H., BATES, C., BELLARY, S., BOCKETT, N. A., GIORDA, K., GRIFFITHS, C. J., HEMINGWAY, H., JIA, Z., KELLY, M. A., KHAWAJA, H. A., LEK, M., MCCARTHY, S., MCEACHAN, R., O'DONNELL-LURIA, A., PAIGEN, K., PARISINOS, C. A., SHERIDAN, E., SOUTHGATE, L., TEE, L., THOMAS, M., XUE, Y., SCHNALL-LEVIN, M., PETKOV, P. M., TYLER-SMITH, C., MAHER, E. R., TREMBATH, R. C., MACARTHUR, D. G., WRIGHT, J., DURBIN, R. & VAN HEEL, D. A. 2016. Health and population effects of rare gene knockouts in adult humans with related parents. *Science*, 352, 474-7.
- NASEVICIUS, A. & EKKER, S. C. 2000. Effective targeted gene 'knockdown' in zebrafish. *Nat Genet*, 26, 216-20.

- NEMAJEROVA, A., KRAMER, D., SILLER, S. S., HERR, C., SHOMRONI, O., PENA, T., GALLINAS SUAZO, C., GLASER, K., WILDUNG, M., STEFFEN, H., SRIRAMAN, A., OBERLE, F., WIENKEN, M., HENNION, M., VIDAL, R., ROYEN, B., ALEVRA, M., SCHILD, D., BALS, R., DÖNITZ, J., RIEDEL, D., BONN, S., TAKEMARU, K.-I., MOLL, U. M. & LIZÉ, M. 2016a. TAp73 is a central transcriptional regulator of airway multiciliogenesis. *Genes & Development*, 30, 1300-1312.
- NEMAJEROVA, A., KRAMER, D., SILLER, S. S., HERR, C., SHOMRONI, O., PENA, T., GALLINAS SUAZO, C., GLASER, K., WILDUNG, M., STEFFEN, H., SRIRAMAN, A., OBERLE, F., WIENKEN, M., HENNION, M., VIDAL, R., ROYEN, B., ALEVRA, M., SCHILD, D., BALS, R., DONITZ, J., RIEDEL, D., BONN, S., TAKEMARU, K., MOLL, U. M. & LIZE, M. 2016b. TAp73 is a central transcriptional regulator of airway multiciliogenesis. *Genes Dev*, 30, 1300-12.
- NEMAJEROVA, A., KRAMER, D., SILLER, S. S., HERR, C., SHOMRONI, O., PENA, T., SUAZO, C. G., GLASER, K., WILDUNG, M. & STEFFEN, H. 2016c. TAp73 is a central transcriptional regulator of airway multiciliogenesis. *Genes & development*, 30, 1300-1312.
- NEWBY, C. M., SABIN, L. & PEKOSZ, A. 2007. The RNA binding domain of influenza A virus NS1 protein affects secretion of tumor necrosis factor alpha, interleukin-6, and interferon in primary murine tracheal epithelial cells. *Journal of virology*, 81, 9469-9480.
- NICHOLS, J. E., NILES, J. A., VEGA, S. P., ARGUETA, L. B., EASTAWAY, A. & CORTIELLA, J. 2014. Modeling the lung: Design and development of tissue engineered macro- and micro-physiologic lung models for research use. *Exp Biol Med (Maywood)*, 239, 1135-69.
- NIGG, E. A. & RAFF, J. W. 2009. Centrioles, centrosomes, and cilia in health and disease. *Cell*, 139, 663-78.
- NIGG, E. A. & STEARNS, T. 2011. The centrosome cycle: Centriole biogenesis, duplication and inherent asymmetries. *Nat Cell Biol*, 13, 1154-60.
- NONAKA, S., TANAKA, Y., OKADA, Y., TAKEDA, S., HARADA, A., KANAI, Y., KIDO, M. & HIROKAWA, N. 1998a. Randomization of Left–Right Asymmetry due to Loss of Nodal Cilia Generating Leftward Flow of Extraembryonic Fluid in Mice Lacking KIF3B Motor Protein. *Cell*, 95, 829-837.
- NONAKA, S., TANAKA, Y., OKADA, Y., TAKEDA, S., HARADA, A., KANAI, Y., KIDO, M. & HIROKAWA, N. 1998b. Randomization of Left–Right Asymmetry due to Loss of Nodal Cilia Generating Leftward Flow of Extraembryonic Fluid in Mice Lacking KIF3B Motor Protein. *Cell*, 95, 829-837.
- NONAKA, S., YOSHIBA, S., WATANABE, D., IKEUCHI, S., GOTO, T., MARSHALL, W. F. & HAMADA, H. 2005. De Novo Formation of Left–Right Asymmetry by Posterior Tilt of Nodal Cilia. *PLoS Biology*, 3, e268.
- NORRIS, D. P. 2012. Cilia, calcium and the basis of left-right asymmetry. *BMC Biology*, 10, 102-102.
- NORRIS, D. P. & GRIMES, D. T. 2012. Cilia Discern Left from Right. *Science*, 338, 206.
- OLBRICH, H., SCHMIDTS, M., WERNER, C., ONOUFRIADIS, A., LOGES, NIKI T., RAIDT, J., BANKI, NORA F., SHOEMARK, A., BURGOYNE, T., AL TURKI, S., HURLES, MATTHEW E., KÖHLER, G., SCHROEDER, J., NÜRNBERG, G., NÜRNBERG, P., CHUNG, EDDIE M. K., REINHARDT, R., MARTIN, JUNE K., NIELSEN, KIM G., MITCHISON, HANNAH M. & OMRAN, H. 2012. Recessive HYDIN Mutations Cause Primary Ciliary Dyskinesia without Randomization of Left-Right Body Asymmetry. *The American Journal of Human Genetics*, 91, 672-684.
- OLCESE, C., PATEL, M. P., SHOEMARK, A., KIVILUOTO, S., LEGENDRE, M., WILLIAMS, H. J., VAUGHAN, C. K., HAYWARD, J., GOLDENBERG, A., EMES, R. D., MUNYE, M. M., DYER, L., CAHILL, T., BEVILLARD, J., GEHRIG, C., GUIPPONI, M., CHANTOT, S., DUQUESNOY, P., THOMAS, L., JEANSON, L., COPIN, B., TAMALET, A., THAUVIN-ROBINET, C., PAPON, J.-F., GARIN, A., PIN, I., VERA, G., AURORA, P., FASSAD, M. R., JENKINS, L., BOUSTRED,

- C., CULLUP, T., DIXON, M., ONOUFRIADIS, A., BUSH, A., CHUNG, E. M. K., ANTONARAKIS, S. E., LOEBINGER, M. R., WILSON, R., ARMENGOT, M., ESCUDIER, E., HOGG, C., GROUP, U. K. R., AMSELEM, S., SUN, Z., BARTOLONI, L., BLOUIN, J.-L. & MITCHISON, H. M. 2017. X-linked primary ciliary dyskinesia due to mutations in the cytoplasmic axonemal dynein assembly factor PIH1D3. *Nature Communications*, 8, 14279.
- OMRAN, H. 2010. NPHP proteins: gatekeepers of the ciliary compartment. *The Journal of Cell Biology*, 190, 715-717.
- OMRAN, H., KOBAYASHI, D., OLBRICH, H., TSUKAHARA, T., LOGES, N. T., HAGIWARA, H., ZHANG, Q., LEBLOND, G., O'TOOLE, E., HARA, C., MIZUNO, H., KAWANO, H., FLIEGAUF, M., YAGI, T., KOSHIDA, S., MIYAWAKI, A., ZENTGRAF, H., SEITHE, H., REINHARDT, R., WATANABE, Y., KAMIYA, R., MITCHELL, D. R. & TAKEDA, H. 2008. Ktu/PF13 is required for cytoplasmic pre-assembly of axonemal dyneins. *Nature*, 456, 611.
- OSTROWSKI, L. E., BLACKBURN, K., RADDE, K. M., MOYER, M. B., SCHLATZER, D. M., MOSELEY, A. & BOUCHER, R. C. 2002a. A proteomic analysis of human cilia: identification of novel components. *Mol Cell Proteomics*, 1, 451-65.
- OSTROWSKI, L. E., BLACKBURN, K., RADDE, K. M., MOYER, M. B., SCHLATZER, D. M., MOSELEY, A. & BOUCHER, R. C. 2002b. A Proteomic Analysis of Human Cilia: Identification of Novel Components. *Molecular & Cellular Proteomics*, 1, 451-465.
- OSTROWSKI, L. E., DUTCHER, S. K. & LO, C. W. 2011. Cilia and Models for Studying Structure and Function. *Proceedings of the American Thoracic Society*, 8, 423-429.
- PAFF, T., LOGES, N. T., APREA, I., WU, K., BAKEY, Z., HAARMAN, E. G., DANIELS, J. M. A., SISTERMANS, E. A., BOGUNOVIC, N., DOUGHERTY, G. W., HÖBEN, I. M., GROßE-ONNEBRINK, J., MATTER, A., OLBRICH, H., WERNER, C., PALS, G., SCHMIDTS, M., OMRAN, H. & MICHA, D. 2017. Mutations in PIH1D3 Cause X-Linked Primary Ciliary Dyskinesia with Outer and Inner Dynein Arm Defects. *American Journal of Human Genetics*, 100, 160-168.
- PAINTRAND, M., MOUDJOU, M., DELACROIX, H. & BORNENS, M. 1992. Centrosome organization and centriole architecture: their sensitivity to divalent cations. *J Struct Biol*, 108, 107-28.
- PALVIMO, J. J. 2007. PIAS proteins as regulators of small ubiquitin-related modifier (SUMO) modifications and transcription. *Biochemical Society Transactions*, 35, 1405-1408.
- PAN, J., YOU, Y., HUANG, T. & BRODY, S. L. 2007a. RhoA-mediated apical actin enrichment is required for ciliogenesis and promoted by Foxj1. *Journal of Cell Science*, 120, 1868-1876.
- PAN, J., YOU, Y., HUANG, T. & BRODY, S. L. 2007b. RhoA-mediated apical actin enrichment is required for ciliogenesis and promoted by Foxj1. *J Cell Sci*, 120, 1868-76.
- PARK, T. J., HAIGO, S. L. & WALLINGFORD, J. B. 2006. Ciliogenesis defects in embryos lacking inturned or fuzzy function are associated with failure of planar cell polarity and Hedgehog signaling. *Nat Genet*, 38, 303-311.
- PARK, T. J., MITCHELL, B. J., ABITUA, P. B., KINTNER, C. & WALLINGFORD, J. B. 2008. Dishevelled controls apical docking and planar polarization of basal bodies in ciliated epithelial cells. *Nat Genet*, 40, 871-879.
- PATEL, A. & HONORÉ, E. 2010. Polycystins and renovascular mechanosensory transduction. *Nature Reviews Nephrology*, 6, 530.
- PAZOUR, G. J., AGRIN, N., LESZYK, J. & WITMAN, G. B. 2005. Proteomic analysis of a eukaryotic cilium. *J Cell Biol*, 170, 103-13.
- PAZOUR, G. J. & WITMAN, G. B. 2003. The vertebrate primary cilium is a sensory organelle. *Curr Opin Cell Biol*, 15, 105-10.

- PEEL, N., STEVENS, N. R., BASTO, R. & RAFF, J. W. 2007. Overexpressing Centriole-Replication Proteins In Vivo Induces Centriole Overduplication and De Novo Formation. *Current Biology*, 17, 834-843.
- PEFANI, D.-E., DIMAKI, M., SPELLA, M., KARANTZELIS, N., MITSIKI, E., KYROUSI, C., SYMEONIDOU, I.-E., PERRAKIS, A., TARAVIRAS, S. & LYGEROU, Z. 2011. Idas, a Novel Phylogenetically Conserved Geminin-related Protein, Binds to Geminin and Is Required for Cell Cycle Progression. *Journal of Biological Chemistry*, 286, 23234-23246.
- PENNEKAMP, P., KARCHER, C., FISCHER, A., SCHWEICKERT, A., SKRYABIN, B., HORST, J., BLUM, M. & DWORNICZAK, B. 2002. The Ion Channel Polycystin-2 Is Required for Left-Right Axis Determination in Mice. *Current Biology*, 12, 938-943.
- PIPERNO, G. & MEAD, K. 1997. Transport of a novel complex in the cytoplasmic matrix of Chlamydomonas flagella. *Proceedings of the National Academy of Sciences of the United States of America*, 94, 4457-4462.
- PIPERNO, G., SIUDA, E., HENDERSON, S., SEGIL, M., VAANANEN, H. & SASSAROLI, M. 1998. Distinct mutants of retrograde intraflagellar transport (IFT) share similar morphological and molecular defects. *Journal of Cell Biology*, 143, 1591-1601.
- PITULESCU, M. E., TEICHMANN, M., LUO, L. & KESSEL, M. 2009. TIPT2 and geminin interact with basal transcription factors to synergize in transcriptional regulation. *BMC Biochem*, 10, 16.
- PLACE, E. S. & SMITH, J. C. 2017. Zebrafish atoh8 mutants do not recapitulate morpholino phenotypes. *PLOS ONE*, 12, e0171143.
- PLASSCHAERT, L. W., ŽILIONIS, R., CHOO-WING, R., SAVOVA, V., KNEHR, J., ROMA, G., KLEIN, A. M. & JAFFE, A. B. 2018. A single-cell atlas of the airway epithelium reveals the CFTR-rich pulmonary ionocyte. *Nature*, 560, 377-381.
- PONTÉN, F., SCHWENK, J. M., ASPLUND, A. & EDQVIST, P. H. D. 2011. The Human Protein Atlas as a proteomic resource for biomarker discovery. *Journal of Internal Medicine*, 270, 428-446.
- POWNALL, M. E. & ISAACS, H. V. 2010. Developmental Biology. *FGF Signalling in Vertebrate Development*. San Rafael (CA): Morgan & Claypool Life Sciences

Copyright (c) 2010 by Morgan & Claypool Life Sciences.

- PRAETORIUS, H. A. & SPRING, K. R. 2001. Bending the MDCK cell primary cilium increases intracellular calcium. *J Membr Biol*, 184, 71-9.
- QUIGLEY, I. K. & KINTNER, C. 2017. Rfx2 Stabilizes Foxj1 Binding at Chromatin Loops to Enable Multiciliated Cell Gene Expression. *PLOS Genetics*, 13, e1006538.
- RAMACHANDRAN, S., KRISHNAMURTHY, S., JACOBI, A. M., WOHLFORD-LENANE, C., BEHLKE, M. A., DAVIDSON, B. L. & MCCRAY, P. B. 2013. Efficient delivery of RNA interference oligonucleotides to polarized airway epithelia in vitro. *American Journal of Physiology - Lung Cellular and Molecular Physiology*, 305, L23-L32.
- RAMSDELL, A. F. 2005. Left-right asymmetry and congenital cardiac defects: getting to the heart of the matter in vertebrate left-right axis determination. *Dev Biol*, 288, 1-20.
- RAN, F. A., HSU, P. D., LIN, C. Y., GOOTENBERG, J. S., KONERMANN, S., TREVINO, A. E., SCOTT, D. A., INOUE, A., MATOBA, S., ZHANG, Y. & ZHANG, F. 2013. Double nicking by RNA-guided CRISPR Cas9 for enhanced genome editing specificity. *Cell*, 154, 1380-9.
- RAWLINS, E. L., OKUBO, T., XUE, Y., BRASS, D. M., AUTEN, R. L., HASEGAWA, H., WANG, F. & HOGAN, B. L. M. 2009. The role of Scgb1a1(+) Clara cells in the long-term maintenance and repair of lung airway, but not alveolar, epithelium. *Cell Stem Cell*, 4, 525-34.
- RAWLINS, E. L., OSTROWSKI, L. E., RANDELL, S. H. & HOGAN, B. L. M. 2007. Lung development and repair: Contribution of the ciliated lineage. *Proceedings of the National Academy of Sciences*, 104, 410-417.

- REYNOLDS, S. D. & MALKINSON, A. M. 2010. Clara cell: progenitor for the bronchiolar epithelium. *Int J Biochem Cell Biol*, 42, 1-4.
- ROCK, J. R., GAO, X., XUE, Y., RANDELL, S. H., KONG, Y.-Y. & HOGAN, B. L. M. 2011. Notch-dependent differentiation of adult airway basal stem cells. *Cell stem cell*, 8, 639-648.
- ROCK, J. R., ONAITIS, M. W., RAWLINS, E. L., LU, Y., CLARK, C. P., XUE, Y., RANDELL, S. H. & HOGAN, B. L. 2009. Basal cells as stem cells of the mouse trachea and human airway epithelium. *Proceedings of the National Academy of Sciences*, 106, 12771-12775.
- ROKICKI, W., ROKICKI, M., WOJTACHA, J. & DŽELIJIĆ, A. 2016. The role and importance of club cells (Clara cells) in the pathogenesis of some respiratory diseases. *Kardiochirurgia i Torakochirurgia Polska = Polish Journal of Cardio-Thoracic Surgery*, 13, 26-30.
- ROSENBAUM, J. L., MOULDER, J. E. & RINGO, D. L. 1969. Flagellar elongation and shortening in *Chlamydomonas*. The use of cycloheximide and colchicine to study the synthesis and assembly of flagellar proteins. *J Cell Biol*, 41, 600-19.
- ROSS, A. J., DAILEY, L. A., BRIGHTON, L. E. & DEVLIN, R. B. 2007. Transcriptional profiling of mucociliary differentiation in human airway epithelial cells. *Am J Respir Cell Mol Biol*, 37, 169-85.
- ROSSI, A., KONTARAKIS, Z., GERRI, C., NOLTE, H., HOLPER, S., KRUGER, M. & STAINIER, D. Y. 2015. Genetic compensation induced by deleterious mutations but not gene knockdowns. *Nature*, 524, 230-3.
- ROSSMAN, C. M., FORREST, J. B., LEE, R. M. & NEWHOUSE, M. T. 1980. The dyskinetic cilia syndrome. Ciliary motility in immotile cilia syndrome. *Chest*, 78, 580-2.
- ROY, S. 2009. The motile cilium in development and disease: emerging new insights. *Bioessays*, 31, 694-9.
- RYAN, R., FAILLER, M., REILLY, M. L., GARFA-TRAORE, M., DELOUS, M., FILHOL, E., REBOUL, T., BOLE-FEYSOT, C., NITSCHKÉ, P., BAUDOUIN, V., AMSELEM, S., ESCUDIER, E., LEGENDRE, M., BENMERAH, A. & SAUNIER, S. 2018. Functional characterization of tektin-1 in motile cilia and evidence for TEKT1 as a new candidate gene for motile ciliopathies. *Human Molecular Genetics*, 27, 266-282.
- RYTINKI, M. M., KAIKKONEN, S., PEHKONEN, P., JÄÄSKELÄINEN, T. & PALVIMO, J. J. 2009. PIAS proteins: pleiotropic interactors associated with SUMO. *Cellular and Molecular Life Sciences*, 66, 3029.
- SALATHE, M. 2007. Regulation of mammalian ciliary beating. *Annu Rev Physiol*, 69, 401-22.
- SARMAH, B., WINFREY, V. P., OLSON, G. E., APPEL, B. & WENTE, S. R. 2007. A role for the inositol kinase Ipk1 in ciliary beating and length maintenance. *Proc Natl Acad Sci U S A*, 104, 19843-8.
- SATIR, P. 1995. Landmarks in cilia research from leeuwenhoek to US. *Cell Motility*, 32, 90-94.
- SATIR, P. 2017. CILIA: before and after. *Cilia*, 6, 1.
- SATIR, P. & CHRISTENSEN, S. T. 2007. Overview of structure and function of mammalian cilia. *Annual Review of Physiology*. Palo Alto: Annual Reviews.
- SATIR, P. & CHRISTENSEN, S. T. 2008. Structure and function of mammalian cilia. *Histochemistry and Cell Biology*, 129, 687-693.
- SATIR, P., GUERRA, C. & BELL, A. J. 2007. Evolution and persistence of the cilium. *Cell Motil Cytoskeleton*, 64, 906-13.
- SATIR, P., PEDERSEN, L. B. & CHRISTENSEN, S. T. 2010. The primary cilium at a glance. *J Cell Sci*, 123, 499-503.
- SCHMIDT, D. & MÜLLER, S. 2002. Members of the PIAS family act as SUMO ligases for c-Jun and p53 and repress p53 activity. *Proceedings of the National Academy of Sciences*, 99, 2872-2877.
- SCHULTE-MERKER, S. & STAINIER, D. Y. R. 2014. Out with the old, in with the new: reassessing morpholino knockdowns in light of genome editing technology. *Development*, 141, 3103.

- SCHWEICKERT, A., VICK, P., GETWAN, M., WEBER, T., SCHNEIDER, I., EBERHARDT, M., BEYER, T., PACHUR, A. & BLUM, M. 2010. The Nodal Inhibitor Coco Is a Critical Target of Leftward Flow in *Xenopus*. *Current Biology*, 20, 738-743.
- SCHWEICKERT, A., WEBER, T., BEYER, T., VICK, P., BOGUSCH, S., FEISTEL, K. & BLUM, M. 2007. Cilia-driven leftward flow determines laterality in *Xenopus*. *Curr Biol*, 17, 60-6.
- SEDAGHAT, M. H., SHAHMARDAN, M. M., NOROUZI, M. & HEYDARI, M. 2016. Effect of Cilia Beat Frequency on Muco-ciliary Clearance. *Journal of Biomedical Physics & Engineering*, 6, 265-278.
- SERUGGIA, D. & MONTOLIU, L. 2014. The new CRISPR-Cas system: RNA-guided genome engineering to efficiently produce any desired genetic alteration in animals. *Transgenic Res*, 23, 707-16.
- SHAH, A. S., BEN-SHAHAR, Y., MONINGER, T. O., KLINE, J. N. & WELSH, M. J. 2009. Motile Cilia of Human Airway Epithelia Are Chemosensory. *Science*, 325, 1131-1134.
- SHAPIRO, A. J., DAVIS, S. D., POLINENI, D., MANION, M., ROSENFELD, M., DELL, S. D., CHILVERS, M. A., FERKOL, T. W., ZARIWALA, M. A., SAGEL, S. D., JOSEPHSON, M., MORGAN, L., YILMAZ, O., OLIVIER, K. N., MILLA, C., PITTMAN, J. E., DANIELS, M. L. A., JONES, M. H., JANAHI, I. A., WARE, S. M., DANIEL, S. J., COOPER, M. L., NOGEE, L. M., ANTON, B., EASTVOLD, T., EHRNE, L., GUADAGNO, E., KNOWLES, M. R., LEIGH, M. W. & LAVERGNE, V. 2018. Diagnosis of Primary Ciliary Dyskinesia. An Official American Thoracic Society Clinical Practice Guideline. *Am J Respir Crit Care Med*, 197, e24-e39.
- SHINOHARA, K., CHEN, D., NISHIDA, T., MISAKI, K., YONEMURA, S. & HAMADA, H. 2015. Absence of Radial Spokes in Mouse Node Cilia Is Required for Rotational Movement but Confers Ultrastructural Instability as a Trade-Off. *Developmental Cell*, 35, 236-246.
- SHINOHARA, K. & HAMADA, H. 2017. Cilia in Left-Right Symmetry Breaking. *Cold Spring Harb Perspect Biol*, 9.
- SHINOHARA, K., KAWASUMI, A., TAKAMATSU, A., YOSHIBA, S., BOTILDE, Y., MOTOYAMA, N., REITH, W., DURAND, B., SHIRATORI, H. & HAMADA, H. 2012. Two rotating cilia in the node cavity are sufficient to break left-right symmetry in the mouse embryo. *Nature Communications*, 3, 622.
- SILVERMAN, M. A. & LEROUX, M. R. 2009. Intraflagellar transport and the generation of dynamic, structurally and functionally diverse cilia. *Trends in Cell Biology*, 19, 306-316.
- SMITH, E. F. & YANG, P. 2004. The radial spokes and central apparatus: mechano-chemical transducers that regulate flagellar motility. *Cell Motil Cytoskeleton*, 57, 8-17.
- SMITH, J. C., NORTHEY, J. G., GARG, J., PEARLMAN, R. E. & SIU, K. W. 2005. Robust method for proteome analysis by MS/MS using an entire translated genome: demonstration on the ciliome of *Tetrahymena thermophila*. *J Proteome Res*, 4, 909-19.
- SONG, R., WALENTEK, P., SPONER, N., KLIMKE, A., LEE, J. S., DIXON, G., HARLAND, R., WAN, Y., LISHKO, P., LIZE, M., KESSEL, M. & HE, L. 2014. miR-34/449 miRNAs are required for motile ciliogenesis by repressing cp110. *Nature*, 510, 115-120.
- SONG, Z., ZHANG, X., JIA, S., YELICK, P. C. & ZHAO, C. 2016a. Zebrafish as a Model for Human Ciliopathies. *J Genet Genomics*, 43, 107-20.
- SONG, Z., ZHANG, X., JIA, S., YELICK, P. C. & ZHAO, C. 2016b. Zebrafish as a Model for Human Ciliopathies. *Journal of Genetics and Genomics*, 43, 107-120.
- SOROKIN, S. P. 1968. Reconstructions of centriole formation and ciliogenesis in mammalian lungs. *Journal of Cell Science*, 3, 207-230.
- STAINIER, D. Y., KONTARAKIS, Z. & ROSSI, A. 2015. Making sense of anti-sense data. *Dev Cell*, 32, 7-8.
- STAUBER, M., WEIDEMANN, M., DITTRICH-BREIHZOLZ, O., LOBSCHAT, K., ALTEN, L., MAI, M., BECKERS, A., KRACHT, M. & GOSSLER, A. 2017. Identification of FOXJ1 effectors during ciliogenesis in the foetal respiratory epithelium and embryonic left-right organiser of the mouse. *Dev Biol*, 423, 170-188.

- STEIN, S. & KESSEL, M. 1995. A homeobox gene involved in node, notochord and neural plate formation of chick embryos. *Mech Dev*, 49, 37-48.
- STEINMAN, R. M. 1968. An electron microscopic study of ciliogenesis in developing epidermis and trachea in the embryo of *Xenopus laevis*. *Am J Anat*, 122, 19-55.
- STOLC, V., SAMANTA, M. P., TONGPRASIT, W. & MARSHALL, W. F. 2005. Genome-wide transcriptional analysis of flagellar regeneration in *Chlamydomonas reinhardtii* identifies orthologs of ciliary disease genes. *Proc Natl Acad Sci U S A*, 102, 3703-7.
- STOOKE-VAUGHAN, G. A., HUANG, P., HAMMOND, K. L., SCHIER, A. F. & WHITFIELD, T. T. 2012. The role of hair cells, cilia and ciliary motility in otolith formation in the zebrafish otic vesicle. *Development*, 139, 1777.
- STUBBS, J., VLADAR, E., AXELROD, J. & KINTNER, C. 2012. Multicilin promotes centriole assembly and ciliogenesis during multiciliate cell differentiation. *Nature cell biology*, 14, 140.
- STUBBS, J. L., OISHI, I., IZPISUA BELMONTE, J. C. & KINTNER, C. 2008. The forkhead protein *Foxj1* specifies node-like cilia in *Xenopus* and zebrafish embryos. *Nat Genet*, 40, 1454-60.
- SULEM, P., HELGASON, H., ODDSON, A., STEFANSSON, H., GUDJONSSON, S. A., ZINK, F., HJARTARSON, E., SIGURDSSON, G. T., JONASDOTTIR, A., JONASDOTTIR, A., SIGURDSSON, A., MAGNUSSON, O. T., KONG, A., HELGASON, A., HOLM, H., THORSTEINSDOTTIR, U., MASSON, G., GUDBJARTSSON, D. F. & STEFANSSON, K. 2015. Identification of a large set of rare complete human knockouts. *Nat Genet*, 47, 448-52.
- SULIK, K., DEHART, D. B., IANGAKI, T., CARSON, J. L., VRABLIC, T., GESTELAND, K. & SCHOENWOLF, G. C. 1994. Morphogenesis of the murine node and notochordal plate. *Dev Dyn*, 201, 260-78.
- SUNG, Y. H., BAEK, I. J., KIM, Y. H., GHO, Y. S., OH, S. P., LEE, Y. J. & LEE, H. W. 2016. *PIERCE1* is critical for specification of left-right asymmetry in mice. *Sci Rep*, 6, 27932.
- SUNG, Y. H., KIM, H. J., DEVKOTA, S., ROH, J., LEE, J., RHEE, K., BAHK, Y. Y. & LEE, H. W. 2010. *Pierce1*, a novel p53 target gene contributing to the ultraviolet-induced DNA damage response. *Cancer Res*, 70, 10454-63.
- SUNG, Y. H., KIM, H. J. & LEE, H. W. 2007. Identification of a novel Rb-regulated gene associated with the cell cycle. *Mol Cells*, 24, 409-15.
- TABIN, C. J. & VOGAN, K. J. 2003. A two-cilia model for vertebrate left-right axis specification. *Genes & Development*, 17, 1-6.
- TADROS, W. & LIPSHITZ, H. D. 2009. The maternal-to-zygotic transition: a play in two acts. *Development*, 136, 3033-3042.
- TAI, D. J. C., RAGAVENDRAN, A., MANAVALAN, P., STORTCHEVOI, A., SEABRA, C. M., ERDIN, S., COLLINS, R. L., BLUMENTHAL, I., CHEN, X., SHEN, Y., SAHIN, M., ZHANG, C., LEE, C., GUSELLA, J. F. & TALKOWSKI, M. E. 2016. Engineering microdeletions and microduplications by targeting segmental duplications with CRISPR. *Nature neuroscience*, 19, 517-522.
- TAKEDA, S. & NARITA, K. 2012. Structure and function of vertebrate cilia, towards a new taxonomy. *Differentiation*, 83, S4-S11.
- TAN, F. E., VLADAR, E. K., MA, L., FUENTEALBA, L. C., HOH, R., ESPINOZA, F. H., AXELROD, J. D., ALVAREZ-BUYLLA, A., STEARNS, T., KINTNER, C. & KRASNOW, M. A. 2013a. *Myb* promotes centriole amplification and later steps of the multiciliogenesis program. *Development (Cambridge, England)*, 140, 4277-4286.
- TAN, F. E., VLADAR, E. K., MA, L., FUENTEALBA, L. C., HOH, R., ESPINOZA, F. H., AXELROD, J. D., ALVAREZ-BUYLLA, A., STEARNS, T., KINTNER, C. & KRASNOW, M. A. 2013b. *Myb* promotes centriole amplification and later steps of the multiciliogenesis program. *Development*, 140, 4277-86.

- TAN, S. Y., ROSENTHAL, J., ZHAO, X. Q., FRANCIS, R. J., CHATTERJEE, B., SABOL, S. L., LINASK, K. L., BRACERO, L., CONNELLY, P. S., DANIELS, M. P., YU, Q., OMRAN, H., LEATHERBURY, L. & LO, C. W. 2007. Heterotaxy and complex structural heart defects in a mutant mouse model of primary ciliary dyskinesia. *J Clin Invest*, 117, 3742-52.
- TARKAR, A., LOGES, N. T., SLAGLE, C. E., FRANCIS, R., DOUGHERTY, G. W., TAMAYO, J. V., SHOOK, B., CANTINO, M., SCHWARTZ, D., JAHNKE, C., OLBRICH, H., WERNER, C., RAIDT, J., PENNEKAMP, P., ABOUHAMED, M., HJEIJ, R., KÖHLER, G., GRIESE, M., LI, Y., LEMKE, K., KLENA, N., LIU, X., GABRIEL, G., TOBITA, K., JASPERS, M., MORGAN, L. C., SHAPIRO, A. J., LETTEBOER, S. J. F., MANS, D. A., CARSON, J. L., LEIGH, M. W., WOLF, W. E., CHEN, S., LUCAS, J. S., ONOUFRIADIS, A., PLAGNOL, V., SCHMIDTS, M., BOLDT, K., UK10K, ROEPMAN, R., ZARIWALA, M. A., LO, C. W., MITCHISON, H. M., KNOWLES, M. R., BURDINE, R. D., LOTURCO, J. J. & OMRAN, H. 2013. DYX1C1 is required for axonemal dynein assembly and ciliary motility. *Nature Genetics*, 45, 995.
- TE, J., JIA, L., ROGERS, J., MILLER, A. & HARTSON, S. D. 2007. Novel subunits of the mammalian Hsp90 signal transduction chaperone. *Journal of proteome research*, 6, 1963-1973.
- TERRÉ, B., PIERGIOVANNI, G., SEGURA-BAYONA, S., GIL-GÓMEZ, G., YOUSSEF, S. A., ATTOLINI, C. S.-O., WILSCH-BRÄUNINGER, M., JUNG, C., ROJAS, A. M., MARJANOVIĆ, M., KNOBEL, P. A., PALENZUELA, L., LÓPEZ-ROVIRA, T., FORROW, S., HUTTNER, W. B., VALVERDE, M. A., BRUIN, A., COSTANZO, V. & STRACKER, T. H. 2016. GEMC1 is a critical regulator of multiciliated cell differentiation. *The EMBO Journal*, 35, 942-960.
- THOMAS, J., MORLÉ, L., SOULAVIE, F., LAURENÇON, A., SAGNOL, S. & DURAND, B. 2010. Transcriptional control of genes involved in ciliogenesis: a first step in making cilia. *Biology of the Cell*, 102, 499-513.
- TICHELAAR, J. W., WERT, S. E., COSTA, R. H., KIMURA, S., WHITSETT, J. A. J. J. O. H. & CYTOCHEMISTRY 1999. HNF-3/forkhead homologue-4 (HFH-4) is expressed in ciliated epithelial cells in the developing mouse lung. 47, 823-831.
- TILLEY, A. E., WALTERS, M. S., SHAYKHIEV, R. & CRYSTAL, R. G. 2014. Cilia Dysfunction in Lung Disease. *Annu Rev Physiol*.
- TILLEY, A. E., WALTERS, M. S., SHAYKHIEV, R. & CRYSTAL, R. G. 2015. Cilia dysfunction in lung disease. *Annu Rev Physiol*, 77, 379-406.
- TIMME-LARAGY, A. R., KARCHNER, S. I. & HAHN, M. E. 2012. Gene knockdown by morpholino-modified oligonucleotides in the zebrafish model: applications for developmental toxicology. *Methods in molecular biology (Clifton, N.J.)*, 889, 51-71.
- TREUTLEIN, B., BROWNFIELD, D. G., WU, A. R., NEFF, N. F., MANTALAS, G. L., ESPINOZA, F. H., DESAI, T. J., KRASNOW, M. A. & QUAKE, S. R. 2014a. Reconstructing lineage hierarchies of the distal lung epithelium using single-cell RNA-seq. *Nature*, 509, 371-5.
- TREUTLEIN, B., BROWNFIELD, D. G., WU, A. R., NEFF, N. F., MANTALAS, G. L., ESPINOZA, F. H., DESAI, T. J., KRASNOW, M. A. & QUAKE, S. R. 2014b. Reconstructing lineage hierarchies of the distal lung epithelium using single-cell RNA-seq. *Nature*, 509, 371.
- TSAO, P.-N., VASCONCELOS, M., IZVOLSKY, K. I., QIAN, J., LU, J. & CARDOSO, W. V. 2009. Notch signaling controls the balance of ciliated and secretory cell fates in developing airways. *Development (Cambridge, England)*, 136, 2297-2307.
- UHLEN, M., OKSVOLD, P., FAGERBERG, L., LUNDBERG, E., JONASSON, K., FORSBERG, M., ZWAHLEN, M., KAMPF, C., WESTER, K., HOBBER, S., WERNERUS, H., BJÖRLING, L. & PONTEN, F. 2010. Towards a knowledge-based Human Protein Atlas. *Nature Biotechnology*, 28, 1248.
- VAN LEEWENHOEK, A. 1932. *Anthony Van Leewenhoek and His "little Animals"*, Dover.
- VAREILLE, M., KIENINGER, E., EDWARDS, M. R. & REGAMEY, N. 2011. The Airway Epithelium: Soldier in the Fight against Respiratory Viruses. *Clinical Microbiology Reviews*, 24, 210-229.

- VELAND, I. R., AWAN, A., PEDERSEN, L. B., YODER, B. K. & CHRISTENSEN, S. T. 2009. Primary cilia and signaling pathways in mammalian development, health and disease. *Nephron. Physiology*, 111, p39-p53.
- VIJ, S., RINK, J. C., HO, H. K., BABU, D., EITEL, M., NARASIMHAN, V., TIKU, V., WESTBROOK, J., SCHIERWATER, B. & ROY, S. 2012. Evolutionarily Ancient Association of the FoxJ1 Transcription Factor with the Motile Ciliogenic Program. *PLOS Genetics*, 8, e1003019.
- VILLA, M., CROTTA, S., DINGWELL, K. S., HIRST, E. M. A., GIALITAKIS, M., AHLFORS, H., SMITH, J. C., STOCKINGER, B. & WACK, A. 2016. The aryl hydrocarbon receptor controls cyclin O to promote epithelial multiciliogenesis. *Nature Communications*, 7, 12652.
- VLADAR, E. K. & AXELROD, J. D. 2008. Dishevelled links basal body docking and orientation in ciliated epithelial cells. *Trends in Cell Biology*, 18, 517-520.
- VLADAR, ESZTER K., BAYLY, ROY D., SANGORAM, ASHVIN M., SCOTT, MATTHEW P. & AXELROD, JEFFREY D. 2012. Microtubules Enable the Planar Cell Polarity of Airway Cilia. *Current Biology*, 22, 2203-2212.
- VLADAR, E. K. & BRODY, S. L. 2013. Analysis of ciliogenesis in primary culture mouse tracheal epithelial cells. *Methods Enzymol*, 525, 285-309.
- VLADAR, E. K. & MITCHELL, B. J. 2016. It's a family act: the geminin triplets take center stage in motile ciliogenesis. *The EMBO Journal*, 35, 904-906.
- VLADAR, E. K. & STEARNS, T. 2007. Molecular characterization of centriole assembly in ciliated epithelial cells. *The Journal of Cell Biology*, 178, 31-42.
- VOGAN, K. 2015. Zebrafish mutants versus morphants. *Nature Genetics*, 47, 105.
- VON DASSOW, G., SCHMIDT, J. E. & KIMELMAN, D. 1993. Induction of the Xenopus organizer: expression and regulation of Xnot, a novel FGF and activin-regulated homeo box gene. *Genes & Development*, 7, 355-366.
- WAGNER, M. K. & YOST, H. J. 2000. Left-right development: The roles of nodal cilia. *Current Biology*, 10, R149-R151.
- WALLMEIER, J., AL-MUTAIRI, D. A., CHEN, C. T., LOGES, N. T., PENNEKAMP, P., MENCHEN, T., MA, L., SHAMSELDIN, H. E., OLBRICH, H., DOUGHERTY, G. W., WERNER, C., ALSABAH, B. H., KOHLER, G., JASPERS, M., BOON, M., GRIESE, M., SCHMITT-GROHE, S., ZIMMERMANN, T., KOERNER-RETTBERG, C., HORAK, E., KINTNER, C., ALKURAYA, F. S. & OMRAN, H. 2014. Mutations in CCNO result in congenital mucociliary clearance disorder with reduced generation of multiple motile cilia. *Nat Genet*, 46, 646-51.
- WANG, W., WU, S., SHI, Y., MIAO, Y., LUO, X., JI, M., YAO, K. & HE, J. 2015. c-MYB regulates cell growth and DNA damage repair through modulating MiR-143. *FEBS Letters*, 589, 555-564.
- WANG, Y. & NAVIN, N. E. 2015. Advances and Applications of Single Cell Sequencing Technologies. *Molecular cell*, 58, 598-609.
- WEINREB, C., WOLOCK, S. & KLEIN, A. M. 2018. SPRING: a kinetic interface for visualizing high dimensional single-cell expression data. *Bioinformatics*, 34, 1246-1248.
- WHEATLEY, D. N., WANG, A. M. & STRUGNELL, G. E. 1996. Expression of primary cilia in mammalian cells. *Cell biology international*, 20, 73-81.
- WHITE, J. K., GERDIN, A. K., KARP, N. A., RYDER, E., BULJAN, M., BUSSELL, J. N., SALISBURY, J., CLARE, S., INGHAM, N. J., PODRINI, C., HOUGHTON, R., ESTABEL, J., BOTTOMLEY, J. R., MELVIN, D. G., SUNTER, D., ADAMS, N. C., TANNAHILL, D., LOGAN, D. W., MACARTHUR, D. G., FLINT, J., MAHAJAN, V. B., TSANG, S. H., SMYTH, I., WATT, F. M., SKARNES, W. C., DOUGAN, G., ADAMS, D. J., RAMIREZ-SOLIS, R., BRADLEY, A. & STEEL, K. P. 2013. Genome-wide generation and systematic phenotyping of knockout mice reveals new roles for many genes. *Cell*, 154, 452-64.
- WICKSTEAD, B. & GULL, K. 2011. The evolution of the cytoskeleton. *Journal of Cell Biology*, 194, 513-525.

- WILKINSON, K. A. & HENLEY, J. M. 2010. Mechanisms, regulation and consequences of protein SUMOylation. *The Biochemical journal*, 428, 133-145.
- WILLIAMS, C. L., LI, C., KIDA, K., INGLIS, P. N., MOHAN, S., SEMENEC, L., BIALAS, N. J., STUPAY, R. M., CHEN, N., BLACQUE, O. E., YODER, B. K. & LEROUX, M. R. 2011. MKS and NPHP modules cooperate to establish basal body/transition zone membrane associations and ciliary gate function during ciliogenesis. *J Cell Biol*, 192, 1023-41.
- WILSON, C. W., NGUYEN, C. T., CHEN, M.-H., YANG, J.-H., GACAYAN, R., HUANG, J., CHEN, J.-N. & CHUANG, P.-T. 2009. Fused has evolved divergent roles in vertebrate Hedgehog signalling and motile ciliogenesis. *Nature*, 459, 98.
- WLOGA, D. & GAERTIG, J. 2010. Post-translational modifications of microtubules. *Journal of Cell Science*, 123, 3447-3455.
- WU, C., OROZCO, C., BOYER, J., LEGLISE, M., GOODALE, J., BATALOV, S., HODGE, C. L., HAASE, J., JANES, J., HUSS, J. W. & SU, A. I. 2009. BioGPS: an extensible and customizable portal for querying and organizing gene annotation resources. *Genome Biology*, 10, R130-R130.
- WU, M., LU, W., SANTOS, R. E., FRATTINI, M. G. & KELLY, T. J. 2014. Geminin inhibits a late step in the formation of human pre-replicative complexes. *J Biol Chem*, 289, 30810-21.
- WU, Y., HU, X., LI, Z., WANG, M., LI, S., WANG, X., LIN, X., LIAO, S., ZHANG, Z., FENG, X., WANG, S., CUI, X., WANG, Y., GAO, F., HESS, R. A. & HAN, C. 2016. Transcription Factor RFX2 Is a Key Regulator of Mouse Spermiogenesis. *Scientific Reports*, 6, 20435.
- YAN, W., SANTTI, H., JANNE, O. A., PALVIMO, J. J. & TOPPARI, J. 2003. Expression of the E3 SUMO-1 ligases PIASx and PIAS1 during spermatogenesis in the rat. *Gene Expr Patterns*, 3, 301-8.
- YAN, X., ZHAO, H. & ZHU, X. 2016. Production of Basal Bodies in bulk for dense multicilia formation. *F1000Res*, 5.
- YOSHIBA, S., SHIRATORI, H., KUO, I. Y., KAWASUMI, A., SHINOHARA, K., NONAKA, S., ASAI, Y., SASAKI, G., BELO, J. A., SASAKI, H., NAKAI, J., DWORNICZAK, B., EHRLICH, B. E., PENNEKAMP, P. & HAMADA, H. 2012. Cilia at the Node of Mouse Embryos Sense Fluid Flow for Left-Right Determination via Pkd2. *Science*, 338, 226.
- YOSHISUE, H., PUDDICOMBE, S. M., WILSON, S. J., HAITCHI, H. M., POWELL, R. M., WILSON, D. I., PANDIT, A., BERGER, A. E., DAVIES, D. E., HOLGATE, S. T. & HOLLOWAY, J. W. 2004. Characterization of ciliated bronchial epithelium 1, a ciliated cell-associated gene induced during mucociliary differentiation. *Am J Respir Cell Mol Biol*, 31, 491-500.
- YOU, Y. & BRODY, S. L. 2013. Culture and differentiation of mouse tracheal epithelial cells. *Methods Mol Biol*, 945, 123-43.
- YOU, Y., HUANG, T., RICHER, E. J., SCHMIDT, J.-E. H., ZABNER, J., BOROK, Z., BRODY, S. L. J. A. J. O. P.-L. C. & PHYSIOLOGY, M. 2004a. Role of f-box factor foxj1 in differentiation of ciliated airway epithelial cells. 286, L650-L657.
- YOU, Y., HUANG, T., RICHER, E. J., SCHMIDT, J. E., ZABNER, J., BOROK, Z. & BRODY, S. L. 2004b. Role of f-box factor foxj1 in differentiation of ciliated airway epithelial cells. *Am J Physiol Lung Cell Mol Physiol*, 286, L650-7.
- YOU, Y., RICHER, E. J., HUANG, T. & BRODY, S. L. 2002. Growth and differentiation of mouse tracheal epithelial cells: selection of a proliferative population. *Am J Physiol Lung Cell Mol Physiol*, 283, L1315-21.
- YU, X., LAU, D., NG, C. P. & ROY, S. 2011. Cilia-driven fluid flow as an epigenetic cue for otolith biomineralization on sensory hair cells of the inner ear. *Development*, 138, 487.
- YU, X., NG, C. P., HABACHER, H. & ROY, S. 2008. Foxj1 transcription factors are master regulators of the motile ciliogenic program. *Nat Genet*, 40, 1445-53.
- YUKITAKE, H., FURUSAWA, M., TAIRA, T., IGUCHI-ARIGA, S. M. M. & ARIGA, H. 2002. AAT-1, a Novel Testis-specific AMY-1-binding Protein, Forms a Quaternary Complex with AMY-

- 1, A-kinase Anchor Protein 84, and a Regulatory Subunit of cAMP-dependent Protein Kinase and Is Phosphorylated by Its Kinase. *Journal of Biological Chemistry*, 277, 45480-45492.
- ZARIWALA, M. A., GEE, H. Y., KURKOWIAK, M., AL-MUTAIRI, D. A., LEIGH, M. W., HURD, T. W., HJEIJ, R., DELL, S. D., CHAKI, M., DOUGHERTY, G. W., ADAN, M., SPEAR, P. C., ESTEVE-RUDD, J., LOGES, N. T., ROSENFELD, M., DIAZ, K. A., OLBRICH, H., WOLF, W. E., SHERIDAN, E., BATTEN, T. F., HALBRITTER, J., PORATH, J. D., KOHL, S., LOVRIC, S., HWANG, D. Y., PITTMAN, J. E., BURNS, K. A., FERKOL, T. W., SAGEL, S. D., OLIVIER, K. N., MORGAN, L. C., WERNER, C., RAIDT, J., PENNEKAMP, P., SUN, Z., ZHOU, W., AIRIK, R., NATARAJAN, S., ALLEN, S. J., AMIRAV, I., WIECZOREK, D., LANDWEHR, K., NIELSEN, K., SCHWERK, N., SERTIC, J., KOHLER, G., WASHBURN, J., LEVY, S., FAN, S., KOERNER-RETTBERG, C., AMSELEM, S., WILLIAMS, D. S., MITCHELL, B. J., DRUMMOND, I. A., OTTO, E. A., OMRAN, H., KNOWLES, M. R. & HILDEBRANDT, F. 2013. ZMYND10 is mutated in primary ciliary dyskinesia and interacts with LRRC6. *Am J Hum Genet*, 93, 336-45.
- ZHAO, H., ZHU, L., ZHU, Y., CAO, J., LI, S., HUANG, Q., XU, T., HUANG, X., YAN, X. & ZHU, X. 2013a. The Cep63 paralogue Deup1 enables massive de novo centriole biogenesis for vertebrate multiciliogenesis. *Nat Cell Biol*, 15, 1434-1444.
- ZHAO, L., YUAN, S., CAO, Y., KALLAKURI, S., LI, Y., KISHIMOTO, N., DIBELLA, L. & SUN, Z. 2013b. Reptin/Ruvbl2 is a Lrrc6/Seahorse interactor essential for cilia motility. *Proceedings of the National Academy of Sciences*, 110, 12697-12702.
- ZHOU, F., NARASIMHAN, V., SHBOUL, M., CHONG, Y. L., REVERSADE, B. & ROY, S. 2015. Gmnc Is a Master Regulator of the Multiciliated Cell Differentiation Program. *Current Biology*, 25, 3267-3273.
- ZUO, W., ZHANG, T., WU, D. Z. A., GUAN, S. P., LIEW, A.-A., YAMAMOTO, Y., WANG, X., LIM, S. J., VINCENT, M. & LESSARD, M. 2015. p63+ Krt5+ distal airway stem cells are essential for lung regeneration. *Nature*, 517, 616.
- ZUR LAGE, P., STEFANOPOULOU, P., STYCZYNSKA-SOCZKA, K., QUINN, N., MALI, G., VON KRIEGSHEIM, A., MILL, P. & JARMAN, A. P. 2018. Ciliary dynein motor preassembly is regulated by Wdr92 in association with HSP90 co-chaperone, R2TP. *The Journal of Cell Biology*.

Appendix 1

Table 1: Preparation of mTEC-plus media

Components	For 250 ml Media	For 50 ml Media
Insulin (10 µg /ml)	1250 µl	250 µl
Transferrin (5 µg /ml)	250 µl	50 µl
CT (0.1 µg/ml.)	250 µl	50 µl
EGF (25 ng/ml.)	1250 µl	250 µl
BPE (30µg/ml)	7.5 mg	1.5 mg
FBS	12.5 ml	2.5 ml
DMEM/F12 media +10% Pen/Strep)	233.5 ml	46.7 ml
RA-B ((10,000x), (5 × 10 ⁻⁴ M) * (Use 1µl/10ml)	25 µl (Add just before use)	5 µl (Add just before use)

Table 2: Preparation of mTEC-SF media

Components	For 250 ml Media	For 50 ml Media
Insulin (5µg/ml)	625 µl	125 µl
Transferrin (5µg/ml)	250 µl	50 µl
CT (0.025µg/ml)	62.5 µl	12.5 µl
EGF (5ng/ml)	250 µl	50 µl
BPE (30µg/ml)	7.5 mg	1.5 mg (100 µl)
BSA (1mg/ml)	2.5 ml	500 µl
DMEM/F12 media +10% Pen/Strep)	248.7 ml	49.1 ml
RA-B (10,000x) (Use 1µl/10ml)	25 µl (Add just before use)	5 µl (Add just before use)

Appendix 2

2.1 Buffers used in Western blotting

Western Blotting Running buffer (10X)

Tris	30.3g
Glycine	2.9g
20% SDS solution	50mls
Water	Up to 1000ml

Western Blotting transfer buffer

Tris	2.9g
Glycine	1.45g
20% SDS solution	925 μ l
Methanol	100mls
Water	Up to 500mls

TBS (10X)

Tris-HCl 1M pH8.0	100ml
Sodium chloride	97.3g
Water	Up to 1000ml

TBS/0.05% Tween (10X)

Tris-HCl 1M pH8.0	100ml
Sodium chloride	97.3g
Tween-20	5ml
Water	Up to 1000ml

0.2M Sodium hydroxide (Caution! Corrosive)

Sodium hydroxide	4g
Water	Up to 500ml

2x SDS Lysis Buffer

1M DTT	1ml
20% SDS solution	1ml
Glycerol	2ml
Tris-HCl 0.5M pH6.8	1.25ml
0.2% bromophenol blue	200µl
Protease Inhibitor tablet	1 tablet
Water	4.55ml

2.2 Buffers in Agarose Gel Electrophoresis

50X TAE buffer

Tris free base	242 g
Disodium EDTA	18.61 g
Glacial Acetic Acid	57.1 ml
DDI H ₂ O	Fill up to 1 litre

Appendix 3

Table 1: RT-PCR primers ordered for mouse genes

Genes	Primers (Fwd-Forward, Rev-Reverse)
<i>Oaz1</i>	Fwd- ACAGAGGAGCCGACGTCTAA Rev- CCAAGAAAGCTGAAGGTTC
<i>Mtekt1</i>	Fwd- CAGTGCGAAGTGGTAGACG Rev- TTCACCTGGATTTCTCCTG
<i>Bpifa1</i>	Fwd- GGTGCACAACATTGCTGAAT Rev- CAAGAGGCAGGAGACTGAG
<i>Krt5</i>	Fwd- ACCTTCGAAACACCAAGCAC Rev- TGA CTGGTCCA ACTCCTTCC
<i>Foxj1</i>	Fwd- GGCCACCAAGATCACTCTGTA Rev- TGTTCAA AAGGACAGGTTGTGG
<i>Mcidas</i>	Fwd- CCCCTGACCAACAGTGACTT Rev- TTAGGGTCACGATTGTGCAG
<i>Myb</i>	Fwd- CAGGAATCGGATGAATCTGG Rev- CGTGCTCAGGCTGTTCTCTG
<i>Dnah11c</i>	Fwd- TTGTGTGGCTTTCTGGGTTT Rev- GGTGGAGGCCATGAAGGTAT
<i>Cbe1</i>	Fwd- GGATGGAGTCAGTTTCGAGGA Rev- TGGCCTGGTCAAAGCTTTAC
<i>Pierce1</i>	Fwd- GGGTGGTTTCATGGCTACG Rev- ACATTCCAAAAGCTGCGTGT
<i>Riken Cdna 1700013f07</i>	Fwd- GTGGGCTTCTAAGAAATCGCTG Rev- GCCACCATCATTTTTCCGGG
<i>Riken Cdna 1700001119 (C5orf49 Homolog)</i>	Fwd- GCA GAAGCC ACC TAA CCT GA Rev- ACA GTC CTT TCT TGT TCC TCC T

<i>Riken Cdna 4833427g06 (C11orf88 Homolog)</i>	Fwd- GAA AGC TCC TGA GTC ACC A Rev- CAT CTC GCG TTT TGG CCT TT
<i>Lrrc4b</i>	Fwd- GGA ACA GGC TGG AGG AAC AA Rev- TGG ATA TCA GAC ACA TCC AGC AGT
<i>Riken Cdna 1700028p14 (C9orf35 Homolog)</i>	Fwd- CGG AGC CAG TGT TGG TGT AT Rev- TTC TCG GAT CTG GTG GGG AT
<i>Maats1</i>	Fwd- TGA AAT GGA GAA CCG CCG AA Rev- TCC ATG ATG CTT TAT TTG TGA TGG A
<i>Erich2</i>	Fwd- AGT GTG GTG ACT GTT GGT CC Rev- TTC AAC GTG TTC TCC AGG GG
<i>Spata24</i>	Fwd- CAG TGT GTC TCG CCT TCG AT Rev- CAG CTT TCT CCT CCA CCA GTT

Table 2: RT-qPCR primers ordered for mouse genes

Gene	Fwd Primer	Rev Primer
<i>Pierce1</i>	GTGGTTTCATGGCTACGGGA	AAAAGCTGCGTGTTGTCTGG
<i>Foxj1</i>	TGGATCACGGACAACCTTCTG	TCTTGAAGGCCCCACTGA
<i>Hprt</i>	GATCAGTCAACGGGGGACAT	GGTCCTTTTCACCAGCAAGC

Appendix 4

Table 1: RT-PCR primers ordered for zebrafish work

Purpose	Fwd	Rev
<i>ierce1</i> splice MO test	TCAGCGAAAGAAGAGA CCGC	AGATTGTTGCGTGCATTGTT
<i>ierce1</i> sgRNA mutation check	TACTCACAGGCATTTT GTGAAC	TGAGTTTGAAATCAAACAAG CA
5'UTR - <i>ierce1</i> - 3'UTR (checking dgRNA mutation in <i>ierce1</i>)	GGTCACATTACGTCAC CTGGTT	AATAGCGTTCCTCATTTTCA
<i>ierce1</i> dgRNA homozygous detection	AAAAACAATGCACGCA ACAA	ACGGTCATGGAAAACCTTGGGA
<i>actin</i> (loading control for endpoint PCR)	CTCTTCCAGCCTTCCT TCCT	CCACCGATCTGCTTGCTGAT
EcoR1- <i>ierce1</i> full coding region-XbaI (For amplifying full <i>ierce1</i> protein coding region, and cloning <i>ierce1</i> in to 6 x Myc tag zebrafish expression vector)	GCGAATTCGATGAGCA CAAACGAAATAAAG	GCTCTAGATTACGATTTTCCA GCCGTG
BamH1 - <i>ierce1</i> full coding region-EcoR1 (Cloning <i>ierce1</i> into C-terminus GFP tagged zebrafish expression vector)	GGATCCATGAGCACAA ACGAAATAAAG	GAATTCCTACGATTTTCCAGC CGTGTG

Table 2: RT-qPCR primers ordered for zebrafish

Gene	Fwd Primer	Rev Primer
<i>pierce1</i>	CCAAGCATATGGAAGCAAAA	TTCGTTGGGTCTGGAGAGTC
<i>rplpo</i>	ATGATAACGGCAGTGTCTA CAGC	GATGATAGTGTGAGGGAT GGAAG

Table 3: Oligo sequences used in the synthesis of the gRNA sequences used to target the *pierce1* locus for Cas9-mediated genomic editing

Primer name	Sequence
<i>pierce1</i> sgRNA1 Fwd	GAAATTAATACGACTCACTATATGGTTTGTGTTCCGGTA CAGGTTTTAGAGCTAGAAATA
<i>pierce1</i> sgRNA 5'UTR Fwd	GAAATTAATACGACTCACTATAGTGTGAGGCATTATC C GTGGTTTTAGAGCTAGAAATAGC
gRNA Rev	AAAAGCACCGACTCGGTGCCACTTTTTCAAGTTGATAA CGGACTAGCCTTATTTAACTTGCTA TTTCTAGCTCTAAAAC


```

Mouse      1  -----MLQPQETFSNPALRDEDKHLGNLWASKKS
Human     1  -----MERSESRRRRLEEAPKL
Chimpanzee 1  -----MERSESRRRRLEEAPKL
Zebrafish 1  -----MPQERDPFFPPRYENDETLTGR-KEIQKL
Frog      1  MSTKGQIYEPRVLSIGICFHRLSPYTRSGHQMPHSRDPYFPFQYENDDTFQGR-Q-MQRT
consensus 1  . . . . .

Mouse     30  LYKNPAHLAQQQEPWSRLSSTETATSRSDT-FFDSKIPKDDLDFRLATLYNHHTGAEKN
Human    18  PYKNPHTLAQQQEPWSRLNSTFTITSMRRDAYYFDPEIPKDDLDFRLAALYNHHTGTAKN
Chimpanzee 18  PYKNPHTLAQQQEPWSRLNSTFTITSMRRDAYYFDPEIPKDDLDFRLAALYNHHTGTAKN
Zebrafish 29  SDDKETHLAQNDEPWRRLHNTITEASSRRTVFEHYDITTPKDSLDIHLKAAYDHHGLGKQN
Frog     59  NGKQSNLSLPQKEEPWHRLNSTATLSSDRRAVYYDPEAESDLSLDFTLKSLYDHTGLLND
consensus 61  . . . . * . * . * . * . * . * . * . * . * . * . * . * . * . * . .

Mouse     89  KTEILLHQETIEDIQGTKIQFPGECFHAPSAPITSRITIRHWINPKKESIHHSIOGSIVSP
Human    78  KSEILLNQKTIQDTYRTKIQFPGEFLTPPTPPITFLANIRHWINPKKESIHHSIOGSIVSP
Chimpanzee 78  KSEILLNQKTIQDTYRTKIQFPGEFLTPPTPPITFLANIRHWINPKKESIHHSIOGSIVSP
Zebrafish 89  KSQIVMOMETVIGADNGTKKN-KELE---DSVCD AENKGIKVVVDITKRSIYSIKGSIESH
Frog    119  RNETLYORETLEENHGRIKRNVRKE---IKVSQEEVPSVKQWVSEQRSNAYSINGAIVSH
consensus 121 . . . . . * . . . . . . . . . . * . . . . * . * . * . * . * . * .

Mouse    149  HTAATNGGYSRKN DGGFFST
Human   138  HTAATNGGYSRKN DGGFFST
Chimpanzee 138  HTAATNGGYSRKN DGGFFST
Zebrafish 145  HTASTNRGYSRKN DGGFFST
Frog    176  HTAATNRGYSRKN DGGYYSI
consensus 181  ***.*** ***** ***.**

```

Figure.2.; Sequence alignment of C1ORF194 orthologs. Sequences were aligned using Clustal X and shaded by BOXSHADE. Shaded residues indicate $\geq 80\%$. Species and accession numbers are as follows: Mouse (*Mus musculus*, GenBank: NP_083590.1); Human (*Homo sapiens*, GenBank: NP_001116433.1); Chimpanzee (*Pan troglodytes* GenBank: PNI54343.1) Zebrafish (*Danio rerio*, GenBank: NP_001107082.1); Frog (*Xenopus laevis*, GenBank: XP_018101963.1).

```

Zebrafish      1  -----MEV LSEAKSKPLSTL
Chicken       1  -----MASPATAGAGEQGGTVED--GGSGLGRRRPPPPVSSL
Mouse        1  MEELAKKERRAMPDGGGLKKEGKVEEAEAGKEEGREEEGGEEVETSETIRGKPRPLPSAL
Human        1  -----MEDDEEETTASTIRGKPRPPPPVSAQ
Chimpanzee   1  -----MEDDEEETTASTIRGKPRPPPPVSAQ
consensus    1  . . . . . * . *

Zebrafish     16  SVFSFIPPRRTEPKEMRYFNCSIKAPERSLYDCLHQSIEGEDNKLHRDDRKHAKARGLDI
Chicken      35  SAFSYIPPRREGPAELSYHRVAQTGGVSTYDSIFKRPEGYNEKLHRC DREHARSRLNV
Mouse       61  FAFSYIPPRHQGPKERSYFSREGQTGIVSLYDCVFKRRLDYNOKLHRDDREHAKNLGLHI
Human       26  SAFSYIPPRRLDPKEHSYNYRPARTGIIISLYDCIFKRRLDYDOKLHRDDREHAKSLGLHV
Chimpanzee  26  SAFSYIPPRRLDPKEHSYNYRPARTGIIISLYDCVFKRRLDYDOKLHRDDREHAKSLGLHV
consensus   61  ..**.*. . . . . * . . . . . * . . . . . * . . . . . * . .

Zebrafish     76  FSEESSRPAPVLCSSVYGRFSPLHYDSSRSFARVAHRSDFYKNKGLTWSVEEGYGSVT
Chicken     95  NDEEMARPVAVLSSSEYGRRTDKHTEQQIRSHARINCVAQAFYRKNGITCILEKPSRLD
Mouse     121  NEEEQERTVPEVLMSSVYGRINQPIEPLNRDYGHVSHVKTDFYRKNEIPSIKGPFGHIN
Human     86  NEEEQERPVGVLTSVYGRINQPIEPLNRDFGRANHVQADFYRKNDIPSLKEPFGGHIA
Chimpanzee 86  NEEEQERPVGVLTSVYGRINQPIEPLNRDFGHANHVQADFYRKNDIPSLKEPFGGHIA
consensus  121  ..** *.. ** **.*. . . . . * . . . . . * . . . . . * . . . . .

Zebrafish    135  EV
Chicken     155  EC
Mouse      181  FA
Human      146  ES
Chimpanzee 146  ES
consensus   181  *

```

Figure.3. Sequence alignment of C5ORF49 orthologs. Sequences were aligned using Clustal X and shaded by BOXSHADE. Shaded residues indicate $\geq 80\%$. Species and accession numbers are as follows: Mouse (*Mus musculus*, GenBank: XP_001144715.1); Human (*Homo sapiens*, GenBank: NP_001083053.1); Chimpanzee (*Pan troglodytes* GenBank: XP_001144715.1) Zebrafish (*Danio rerio*, GenBank: XP_002665577.1); Chicken (*Gallus gallus*, GenBank: XP_003640829.1).

```

Human      1 METGPSEEPSGRKESQEMCPPGLLVFAGSSEQDANLAKQFWISASMYPPSESQVLVLRDS
Chimpanzee 1 METGPSEELSGRKESQEMCPPGLLVFAGSSEQDANLAKQFWISASMYPPSESQVLVLRDS
Mouse      1 METGPRGCPGRKESQEICSPGLLVFTGCSEQDANLAKQFWLGASMYPTTESQVLVLRGS
Frog       1 -----MEDSWAGDCAYTVFSGSCERDWSLCKIFWNSVTIQPPLESRLVS-GDI
Zebrafish  1 MSEELD---EEVLDGLTEVEKLYTVEHGASQEDVAYAKLFWNSLSLCPPIESRLVS-SDI
consensus  1 . . . . . ** * .. * ..* ** . . . * . ** ** .

Human      61 SQRLEPVARPRRSRGSSENSHSSQSFLHASNKNRDIFAEALKIQESEEKVKYLOKAKTRDEI
Chimpanzee 61 SQRLEPVARPRRSRGSSENSHSSQSFLHASNKNRDIFAEALKIQESEEKVKYLOKAKTRDEI
Mouse      61 SQRLEPVARNSKVVLRRE-KSSVQPFPPDQDKDAIIFAKAQRIQESSEERAKYLOKAKTRDEI
Frog       48 EQRLEPAGSTKQN----KNITHQQSVENPKMEYFLFEAQKQYLYLKEKANYLNKANKREEI
Zebrafish  57 RQRLEPVAKTPNTT----NAAANQAPWSK-RNEEIQQDAYLRQKQEEKQRYMEMAKNRDQI
consensus  61 *** .*. . . . . . . . . * * . . . . . * . . . . .

Human      121 LQLLRKQREERISKELISLPYKPKAKEHKAKKVVS----ESDKEDQEEVKTLID
Chimpanzee 121 LQLLRKQREERISKELISLPYKPKAKEHKAKKVVS----ESDKEDQEEVKALD
Mouse      120 LQLLRKQREERISKELISLPYKPKDKVPKSKVLS----ESGLRDQEEVKALE
Frog       104 IELLKQREERIKKEEISQAYKPKITEKRSRS-DSGCDAEVLEIRAVORLQ
Zebrafish  112 IALLKQORDERIKKEMTAYKHKPKKGLKLEKRLAPKTLSSDVDEDCQEVQKLO
consensus  121 . ** .***.*** **.*. .** . . . . . . . . . . . . . . . * *

```

Figure 4.; Sequence alignment of C11ORF88 orthologs. Sequences were aligned using Clustal X and shaded by BOXSHADE. Shaded residues indicate $\geq 80\%$. Species and accession numbers are as follows: Mouse (*Mus musculus*, GenBank: NP_808370.1); Human (*Homo sapiens*, GenBank: NP_997313.2); Chimpanzee (*Pan troglodytes* GenBank: PNI40766.1) Zebrafish (*Danio rerio*, GenBank: NP_001093491.2); Frog (*Xenopus laevis* GenBank: XP_018081396.1).


```

Mouse      1  -----MLQPQETFSNPALRDEDKHLGNLWASKKS
Human      1  -----MERSPSRRRRLEEAPKL
Chimpanzee 1  -----MERSPSRRRRLEEAPKL
Zebrafish  1  -----MPQERDFPPFPRYENDFTLTGR-KEIQKL
Frog       1  MSTKGGIYEPVRLSIGICFHRLSPYTRSGHQMPHSRDPYFPQYENDDTFOGK-Q-MQRT
consensus  1  . . . . .

Mouse      30  LYKNPAHLAQQODPWSRLSSTPTATSRSRDT-FEDSKIPEKDDLDFRLATLYNHHTGAFKN
Human      18  PYKNPHTLAQQQEPWSRLNSTPTITSMRRDAYYFDPEIPKDDLDFRLAALYNHHTGTFKN
Chimpanzee 18  PYKNPHTLAQQQEPWSRLNSTPTITSMRRDAYYFDPEIPKDDLDFRLAALYNHHTGTFKN
Zebrafish  29  SDDKPTHLAQNDEPWRLHNTTTEASSRRTVVFHYDTTTPKDSLDTLKAAYDHHGLFQN
Frog       59  NGKQSNSLPQKEEPWHRLNSTATLSSDRRAVYYDPEAPSDSLDFTLKSLYDHHHTGLLND
consensus  61  . . . . * . * . * * . * . * . . . * * . * * . * . * . .

Mouse      89  KTEILLHQETIEDIQGTKIQFPGECFHAPSAPITSRTTIRHWINPKKESIHHSIOGSIVSP
Human      78  KSEILLNQKITQDTYRTKIQFPGEFLTPPTPPITFLANIRHWINPKKESIHHSIOGSIVSP
Chimpanzee 78  KSEILLNQKITQDTYRTKIQFPGEFLTPPTPPITFLANIRHWINPKKESIHHSIOGSIVSP
Zebrafish  89  KSQTVMOMETVGDNGTKRN-KELE---DSVCD AENKGIKVVVDTKKASLYSIKGSIESH
Frog       119  RNETLYORETLTENHGRIDKNRVKE---IKVSQEEVPSVKQWVSPQRSNAYSINGAIVSH
consensus  121  . . . . * . . . . . . . . . * . . . . * * . * * .

Mouse      149  HTAATNGGYSRKNDDGGFFST
Human      138  HTAATNGGYSRKKDDGGFFST
Chimpanzee 138  HTAATNGGYSRKKDDGGFFST
Zebrafish  145  HTASTNRGYSRKKDDGGFFST
Frog       176  HTAATNRGYSRKKDDGGYST
consensus  181  ***.* * * * * * * * * .

```

Figure.2.; Sequence alignment of C1ORF194 orthologs. Sequences were aligned using Clustal X and shaded by BOXSHADE. Shaded residues indicate $\geq 80\%$. Species and accession numbers are as follows: Mouse (*Mus musculus*, GenBank: NP_083590.1); Human (*Homo sapiens*, GenBank: NP_001116433.1); Chimpanzee (*Pan troglodytes* GenBank: PNI54343.1) Zebrafish (*Danio rerio*, GenBank: NP_001107082.1); Frog (*Xenopus laevis*, GenBank: XP_018101963.1).

```

Zebrafish      1  -----MEVLSEAKSKPLSTL
Chicken       1  -----MASPATAGAGEQGGDVED--GSSGLGRRRPPVSSL
Mouse        1  MEELAKKERRAMPDGGGLKKEGKVEEEAGKEEGREEEGGEEEPVTSETLRGKRRPLPISAL
Human        1  -----MEDDEEETTASTLRGKRRPPVSAQ
Chimpanzee   1  -----MEDDEEETTASTLRGKRRPPVSAQ
consensus    1  . . . . . * . *

Zebrafish     16  SVFSIIPPRTEPKEMRYFNCSIKAPERSLYDCI HQSIEGIDNKLHRDDRKHAKARGLDI
Chicken      35  SAFSYIPPRREGPAELSYFHRVACTGGVSTYDSIFKRPEGYNEKLHRCREHARSRLNV
Mouse       61  PAFSYIPPRHQGPKEISYFSREGQTGIVSLYDCVFKRRLDYNOKLHRDDREHAKNLGLHI
Human       26  SAFSYIPPRRLDPKEHSYYYRPARTGIIISLYDCIFKRRLDYDOKLHRDDREHAKSLGLHV
Chimpanzee  26  SAFSYIPPRRLDPKEHSYYYRPARTGIIISLYDCIFKRRLDYDOKLHRDDREHAKSLGLHV
consensus   61  ..**.***.* * . * . . . . * . * . . . . . * . * . . . . * . * . . . . * . * .

Zebrafish     76  FSEESSRPAPVLCSSVYGRFSPLHYD--SSRSFARVAHIRSDFYKNGITWSVEEGYGSVIT
Chicken     95  NDEEMARPVAVLSSSYGRRIDKHTEQQIRSHARINCVQAEFYRKNGITCTLEKPSRLD
Mouse     121  NEEEQERTVFPVLMSSVYGRINQPIEPLNRDYGHVSHVKTDFYRKNEIPSLKGPFGGHIN
Human     86  NEEEQERPVGVLTSVYGRINQPIEPLNRDFGRANHVQADFYRKNDIPSLKGPFGGHIA
Chimpanzee 86  NEEEQERPVGVLTSVYGRINQPIEPLNRDFGRANHVQADFYRKNDIPSLKGPFGGHIA
consensus  121  ..** * . * . * . * . . . . * . . . . . * . * . * . . . . .

Zebrafish    135  PV
Chicken     155  PC
Mouse      181  PA
Human      146  PS
Chimpanzee 146  PS
consensus  181  *

```

Figure.3. Sequence alignment of C5ORF49 orthologs. Sequences were aligned using Clustal X and shaded by BOXSHADE. Shaded residues indicate $\geq 80\%$. Species and accession numbers are as follows: Mouse (*Mus musculus*, GenBank: XP_001144715.1); Human (*Homo sapiens*, GenBank: NP_001083053.1); Chimpanzee (*Pan troglodytes* GenBank: XP_001144715.1) Zebrafish (*Danio rerio*, GenBank: XP_002665577.1); Chicken (*Gallus gallus*, GenBank: XP_003640829.1).

```

Human      1 METGPSEEPSGRKESQEMCPPGLLVFAGSSEQDANLAKQFWISASMYPPSESQVLVLRDSD
Chimpanzee 1 METGPSEELSGRKEEQEMCPPGLLVFAGSSEQDANLAKQFWISASMYPPSESQVLVLRDSD
Mouse      1 METGPRGCPGRKESQEICSPGLLVFTGCEQDANLAKQFWLGASMYPTTESQVLVLRGSD
Frog       1 -----MEDSWAGDCRYTVFSGSCERDVSLCKTFWNSVTLQPPLESRLVS-GDI
Zebrafish  1 MSEELD---EEVLDGLTEVEKLYTVFHGASQEDVAYAKLFWNSLSLQPPLESRLVS-SDI
consensus  1 . . . . . ** * .. * .. * ** . . . * . ** ** .

Human      61 SQRLEPVARPRRSRGSSENSHSSCSFHFLASNKNRDIFAEALKIQESEEEKVKYLOKAKTRDEI
Chimpanzee 61 SQRLEPVARPRRSRGSSENSHSSCSFHFLASNKNRDIFAEALKIQESEEEKVKYLOKAKTRDEI
Mouse      61 SQRLEPVARNSKVVLRRE-KSSVQFPFFDQDKDAIIFAKAQRIQESSEKAKYLOKAKTRDEI
Frog       48 EQRLRAAGSTKQN----KNITHQQSVENPKMEYFLFEAQKQOYLKFKANYLNKANKREEI
Zebrafish  57 RQRLKVAKTPNIT----NAAANQAPWSK-RNEEIQQDQAYLRQKQEEKQRYMEMAKNRDQI
consensus  61 *** .*. . . . . . . . . * * .*. .*. .*. .*. .*.

Human      121 LQLLRKQREERISKELISLQPKPKAKEHAKKVVVSDSDKEDQEEVKTLD
Chimpanzee 121 LQLLRKQREERISKELISLQPKPKAKEHAKKVVVSDSDKEDQEEVKAID
Mouse      120 LQLLRKQREERISKELISLQPKPKDKVPKSKVLS----ESGLRDQEEVKALE
Frog       104 IELLKQREERIKKEEISQAYKPKQITEKRSRS-DSGCDQAEVLEIRAVQRLQ
Zebrafish  112 IALLKQORDERIKKEMIAFKKPKKGGKLEEKRLAPKTLSSDVDEQKEVOKLQ
consensus  121 . **.*.***.*** **.*. .** . . . . . . . . . . . . . *

```

Figure 4.; Sequence alignment of C11ORF88 orthologs. Sequences were aligned using Clustal X and shaded by BOXSHADE. Shaded residues indicate $\geq 80\%$. Species and accession numbers are as follows: Mouse (*Mus musculus*, GenBank: NP_808370.1); Human (*Homo sapiens*, GenBank: NP_997313.2); Chimpanzee (*Pan troglodytes* GenBank: PNI40766.1) Zebrafish (*Danio rerio*, GenBank: NP_001093491.2); Frog (*Xenopus laevis* GenBank: XP_018081396.1).

```

Zebrafish      1 MR TTVTSLP S LLL L-----VQ L R LL --- -----QE VGA
Frog           1 -M T ----LCT RILG KLI I KQ-V L  TAL----- L G SP
Human          1 -- A AR--G  --P PPG S PHGA F  FS PLGA GGGVAVTSAA G S P
Chimpanzee    1 -- A AR--G  --P PPG S PHGA F  FS PLGA GGGVAVTSAA G S P
Mouse         1 MAQA IR--G  --L PPG S PHGA L  FS PLRA GGGVAVTSAA G S P
consensus     1 . . . . . * . . . . * . . . . .

```

```

Zebrafish      38 AV A QH E DN SN T
Frog           40 AP A V E S N
Human          55 VA A A P G
Chimpanzee    55 VA A A P G
Mouse         57 AA A A P S
consensus     61 ..** *.*****.*.*.* ***. * .*****. ****.*.*****

```

```

Zebrafish      98 Q Q N L
Frog           100 N N S
Human          115 K S
Chimpanzee    115 K S
Mouse         117 K S
consensus     121 *****.* ***** * .*****.*.*****.*****.*****

```

```

Zebrafish      158 G H V G P
Frog           160
Human          175
Chimpanzee    175
Mouse         177
consensus     181 .***.*****.*.***.***.**.*****.*****.*****

```

```

Zebrafish      218 E S SV N S H
Frog           220 H I
Human          235 T
Chimpanzee    235 T
Mouse         237 T
consensus     241 *****.*.*****.*****.... *****.*****.*.*****

```

```

Zebrafish      278 Q V PY
Frog           280 N S PN M
Human          295 AG
Chimpanzee    295 AG
Mouse         297 AG
consensus     301 *****.*.*****.*****.*****.*****.* **.*.*****

```

```

Zebrafish      338
Frog           340
Human          355
Chimpanzee    355
Mouse         357
consensus     361 *****.*.*****.*****.*****.*****

```

```

Zebrafish      398 R V A -----
Frog           400 TD-----
Human          415 PVAAGGTGSGGGP PGG
Chimpanzee    415 PVAAGGTGSGGGP PGG
Mouse         417 PVAAGGPG--GGGPGG
consensus     421 *****.*.*****.*****.*.***.*..

```

```

Zebrafish 441 -----V VN          TGE SALRTFNE FIHI    PS HL HEVV TT S
Frog      444 -----PS TD          VEETK-----PTDKE    PTV-R  ITY-----
Human     475 GGVGGG GG          QPG ALQP--RG EKEP    TD -V  GGR GD A
Chimpanzee 475 GGVGGG GG          QPG ALQP--RG EKEP    TD -V  GGR GD A
Mouse     475 GG-AGGAGG        QPG AQQP--RG EKEP    TD -A  GGR D- A
consensus 481          . *****... ..          . **** . * . . .

Zebrafish 496 SL---- IFGSSS P A KPT          P --YPSG
Frog      485 ----- SLT      S T          G I
Human     532 GPASS APA      P A          E A
Chimpanzee 532 GPASS APA      P A          E A
Mouse     530 APASA APA      P A          E A
consensus 541          ... ..* *.. **.*... .. *****

Zebrafish 550      V          A A          G      RGS ISGGST PQI S G Q
Frog      540          TA-----P
Human     592          SVA AA---A A-S G V
Chimpanzee 592          SVA AA---A A-S G V
Mouse     590          SVA AA---A A-G A V
consensus 601 **..*****.*...*****.*.... . . . . *

Zebrafish 610 SLRLHHPEI N N A A      Y- KPHH NNNMMGLGL    LNNNNNPPSPCSQVQTPI
Frog      580 -N-----      H-      Y----T      NN TGTLN-----
Human     648 -S-----      -      HH VAA      SS PS -----
Chimpanzee 648 -S-----      -      HH VAA      SS PS -----
Mouse     646 -S-----      -      HH VAA      GG P- -----
consensus 661          ...**.... ***** . *.... . . .

Zebrafish 669 SCTQVPVSAGSTS SIPSPMPLPTLGIHGSLK LMGK Q PQI
Frog      611 -----      ----- --KN M          S
Human     683 -----      ----- KGP
Chimpanzee 683 -----      ----- KGP
Mouse     680 -----      ----- KG-
consensus 721          *          .. ...*...*****.*****

Zebrafish 729
Frog      639
Human     713
Chimpanzee 713
Mouse     709
consensus 781 *

```

Figure 5. Sequence alignment of LRRC4B orthologues. Sequences were aligned using Clustal X and shaded by BOXSHADE. Shaded residues indicate $\geq 80\%$. Species and accession numbers are as follows: Zebrafish (*Danio rerio*, GenBank: XP_684717.3); Frog (*Xenopus laevis* GenBank: OCT56939.1) Human (*Homo sapiens*, GenBank: NP_001073926.1); Chimpanzee (*Pan troglodytes*, Uniprot: H2QGY2) Mouse (*Mus musculus*, GenBank: NP_937893.1).

```

Mouse      1  MGTFFDQCHECFESKERWYEIGPTDLLERKGSILTRSHHKKYSEPVLVYSWHRNREAFPK
Human      1  MDSLDRSCQDWCDCRKHQWLEIGPPDLVERKGSILTRSHHKKYSKPVLVYSWHRDREAFPK
Chimpanzee 1  MDSLDRSCQDWCDCRKHQWLEIGPPDLVERKGSILTRSHHKKYSKPVLVYSWHRDREAFPK
Frog       1  -----MSLYAMPDLVERKGSILYLRSHHWVTYGRITTLVSGWHQONREAFPK
Spotted gar 1  -----MYYSRPTLVSNWHQONREAFPK
consensus 1  . . . . . * . . . . . * . . . . . * . . . . . * . . . . . *

Mouse      61  DYDIES-PETVKNLCMSTYRFRGSD-SPRNMSEAREQMAQVLVKNKDLVEK-KRTGLLDEE
Human      61  GYDIEG-PEKVKKLCNSTYRRLGTDESPIWTSETHEKLSQMCINTEWVEM-KSKALLNEE
Chimpanzee 61  DYDIEG-PEKVKKLCNSTYRRLGTDESPIWTSETHEKLSQMCINTEWAEM-KSKALLNEE
Frog       44  DYDLDTLELGRKNLCHSTYRSLGKVTETDVKITTEEQLSQVCLKDDYEARDVPKSMVNEE
Spotted gar 22  DYDLTVCSGKKNLLRSTYRNLGRCGNTDWSITTEGQLSQCHLKKDYEIRETPKPLVKAE
consensus 61  .**.. .. * * .**..* . . * . . . . . * . . . . . * . . . . . *

Mouse      118  TLCPGILERDPELPPPTGFRDVPMSPPDPRKPCFSTTYSEDETPQYEPYPFAC-PRREY
Human      119  TVSSGIIERTGLPATGFGAVFRRHPPDWSKMCALTTYSEDYVPPYDYQPHAY-PCQDDY
Chimpanzee 119  TVSSGIIERTGLPATGFGAVFRRHPPDWSKMCALTTYSEDYVPPYDYQPHAY-PCQDDY
Frog       104  TIDAVDVYRQIGS--YERGSVLRHDKDHGKIHLETTYHNDYSFPPQP---TMIPHAPQC
Spotted gar 82  NFNSAYFERETRRREKTFSEVLRHQAGHNKIDMDTTYALDYLPYSYSTQSCVGDQAE
consensus 121  .. . . * . . . . * . . . . * . . . . * . . . . * . . . . . *

Mouse      177  SIVHRKCRSQFTDLNGSKRLGINTWHDESGIYANSEAKOKLYALARNPIVFL--
Human      178  SIVHRKCRSQFTDLNGSKREGINTWHDESGIYANSQVKKLYPLTSGPIVFEI--
Chimpanzee 178  SIVHRKCRSQFTDLNGSKREGINTWHDESGIYANSQVKKLYPLTSGPIVFEI--
Frog       159  PAAYKKCHSQFTDTADYRRDGRNTWODESGIYGNHQLKHSLEKKS-CPITPHL-
Spotted gar 142  SAAYRRCSQFTDTADYRRDGRNTWODESGVYGNSHIRRRVPELS-HPITPHIL
consensus 181  . . . . * . . . . * . . . . * . . . . * . . . . * . . . . *

```

Figure 6.; Sequence alignment of C9ORF135 orthologues. Sequences were aligned using Clustal X and shaded by BOXSHADE. Shaded residues indicate $\geq 80\%$. Species and accession numbers are as follows: Mouse (*Mus musculus*, GenBank: EDL41604.1), Human (*Homo sapiens*, GenBank: NP_001010940.1); Chimpanzee (*Pan troglodytes*, XP_520445.3); Frog (*Xenopus laevis* GenBank: XP_018099332.1); Spotted gar (*Lepisosteus oculatus*, GenBank XP_015221901.1).

Zebrafish 1 -----VSVTRTFDK NE NKGFRQ T T A V GRE R
 Frog 1 -----MRIMSETVTH PGPGARYRP A T AH SFR
 Mouse 1 QTVTIQEPRPNDQRIPIYQCREVRR -KGGFA T I AQ Q
 Human 1 HAVTIEEPQAQPQVSQTRYRE SR GSHISS A I TQ Q
 Chimpanzee 1 HAVTIEEPQAQPQVSQTRYRE SR GSHISS A I TQ Q
 consensus 1 .. . * ** .***** . * . . . * . . . *

Zebrafish 49 QASLD E N I D P H Q RLEA G D R YA Q Q Q TG
 Frog 48 Q S D Q V P E V K RLQLK Q D R RA Q LN K AQ
 Mouse 60 T I S N R N F H YWSK LH T E QEAK EV RLQAA
 Human 61 T I S R K N I Y YWSK P S E HK K E R TT
 Chimpanzee 61 T I S R K N I Y YWSK P S E HK K E Q TT
 consensus 61 . . * . . . * . . . * * * * . * . . . * . . . * . . . *

Zebrafish 109 IVSGAV--THAPNPAN VD K L A PD F P S LLSSD-GDD
 Frog 108 SQVPTLP Q LGATGG D L V P L S A LSPAP----D
 Mouse 120 MDTSFQM K KDEDPD N F L L LSPV TQPLLLTPSS Y
 Human 121 TDASFQM K VYEDPE N F F F Y S A PYTFPPTST
 Chimpanzee 121 TDASFQM K VYEDPE N F F F Y S A PYTFPPTST
 consensus 121 . . * . * . * . * . * . * . * . * . * . * . * *

Zebrafish 166 SPT FQR V S T S R PGT S T H L
 Frog 164 PAT LVR I S A A SG- N L
 Mouse 180 AII TKS T A V QD- N Q
 Human 181 LSI SKS T A V A QD- T Q
 Chimpanzee 181 LSI SKS T A V QD- T Q
 consensus 181 * . * . * . * . * . * . * . * . * . * . * . * . * . * . * . *

Zebrafish 226 K I P N L L E Q T T LQ
 Frog 223 P S V L D Q K A K
 Mouse 239 P N SV A NA G L Q
 Human 240 A S T F N Q I E
 Chimpanzee 240 A S T F N Q I E
 consensus 241 . * . * . * . * . * . * . * . * . * . * . * . * . * . * . *

Zebrafish 286 Q E E K E DAS QR NE KK RSDY IA L RK N E D
 Frog 283 Q K K DT DSH R AE E KQ RKKH TA T MN K E N
 Mouse 299 D N N NDQ Y L EA AQ RKKH SD M GK K Q D
 Human 300 N N N NAR L EG -----
 Chimpanzee 300 N N N NAR L EG AK Q RTH ST V RK K E N
 consensus 301 * . . * . * . * . . . * . * *

Zebrafish 346 K SD M A T QT RNSNRST SH S Q AS SPS L Q
 Frog 343 K ND T S I YF RLAEQYL SP N Q AN PDF Q R
 Mouse 359 S SN V S L RF NNSEDFV NH N E SS PDF Q R
 Human 330 -----
 Chimpanzee 360 K SD V S L CF NNSEDFV NY N E SC PDF Q R
 consensus 361 . *

Zebrafish 406 V PKV---TK S RR L MKT Q KEE VC-RVEK PL F KEKPVP PP
 Frog 403 V VRT-TTRS K VL R EQV S LAN TKTQASK PL E IEKPAP PE
 Mouse 419 P PQIITTKA K RM Y AEV K VDK NKGLEGT SL Q NPISQA LP
 Human 330 -----
 Chimpanzee 420 A PKVITTKA K RL Y AEV K LDK NKVLEAK PP Q NPIPQP LP
 consensus 421 . *

Zebrafish 462 T EKPPEG E R ST Q E W T K QDK
 Frog 462 R QDPPEG E K L A T GQ
 Mouse 479 S EMTSYE G I V L S K
 Human 330 -----
 Chimpanzee 480 T EMTSNE E I V C K
 consensus 481 * . * . * . * . * . * . * . * . * . * . * . * . *

```

Zebrafish 522 EV          DFQID EAQ  SFT A S  GV V  L
Frog      522      A          E G H A   L  SE   EV S
Mouse     539          N H D L   N  D   RV A
Human     376          N H H V   N  G   RA A
Chimpanzee 540        N H H V   N  G   RA A
consensus 541 *..***.***** . . . . . *.* . **.******

Zebrafish 582 T      D          ER R      Q    QD DM      T INQ
Frog      582 A          ER R      Q  Q  Q  D      SATEH
Mouse     599 A          QK LQQ  M   E    Q  T      N EER
Human     436 V          KQ L      E    H  S      N EAN
Chimpanzee 600 V        KQ L      E    H  S      N EAN
consensus 601 .****.*.*****.* * ..**.*. . . . . *.*.****.* **

Zebrafish 642 A      E H K E N T A  ETMNSQ          R      MDF      HS
Frog      642      E Q K E D  Q  SS R          TS      RS
Mouse     659      K E I E N  E NR Y          DF      NA
Human     496      A E M K D  E SR Y          YF      NA
Chimpanzee 660      A E M K D  E SR Y          YF      NA
consensus 661 ..*** ** . ** . * *.* ** ..*****.***** ..**.*

Zebrafish 702      Q  RL  SPG TVPTEPQSPSYRASS  ILNHILS-----QVEEVVP
Frog      702      Q  Q   CGD QAF ESRNTFSG GS PRDATLQDTHDIETQ LLQ TCCIESPYS
Mouse     719      L  E   HSN ETM EEQVYKEL SEDF-----ELEEE ESL -----
Human     556      L  Q   HSY ESM QKKLTEGE DE S-----NA--- MLL -----
Chimpanzee 720      L  Q   HSY ESM QKRLTEGE DE S-----NA--- MLL -----
consensus 721 *.*. **.* * . . . . . . . . . .

Zebrafish 747 GNLTSRDPEPTQNTLTSHT -----TE-DTHNTDGKK-ADSAQQQL-----
Frog      762 GNVSTLEREATLQDICGTE  VPAQDICGTKREVPA DICGTERETPAQDICGTEREVPA
Mouse     761 -----S VPTVSVSKTSTIKPT DEGEG-----
Human     595 -----T-----NENNS-----
Chimpanzee 759 -----T-----NENNS-----
consensus 781 .. . . . . . . . . . .

Zebrafish -----
Frog      822 QDICGTERETPAQDICGTERETPAQDICGTEGEVPAQDKCGERETPAQDICGTEGERET
Mouse     -----
Human     -----
Chimpanzee -----
consensus 841

Zebrafish -----
Frog      882 PTQDICGTERERETPAQDICSTEGEVPAQDICGTEREEEEQCDTHGTD
Mouse     -----
Human     -----
Chimpanzee -----
consensus 901

```

Figure 7.; Sequence alignment of MAATS1 orthologues. Sequences were aligned using Clustal X and shaded by BOXSHADE. Shaded residues indicate $\geq 80\%$. Species and accession numbers are as follows: Zebrafish (*Danio rerio*, GenBank: XP_001333344.3); Frog (*Xenopus laevis* GenBank: OCT93569.1); Mouse (*Mus musculus*, GenBank: EDK97973.1), Human (*Homo sapiens*, GenBank: NP_001307245.1); Chimpanzee (*Pan troglodytes*, XP_016797207.1).

```

Zebrafish      1 MNRLQCVGRPSEVSSKLSSEKEVPPLKLLSASLGDPAAKEAVERKAKQTKLKINEKTEGQA
Frog           1 -----MVS RVEIRSATP-----RTNGPGKLEVLGPE-----DFSTETCSLA
Human          1 -----
Chimpanzee    1 -----
Mouse         1 -----
consensus     1

Zebrafish     61 PAQTSETASNMKLLSSSTRQOKPKPEGKTDGMDSSLLTTKQNAFQK--SETLNP SLKAHSS-
Frog          37 PQF-----SNFETDLTNAI--KTVANEK GKQLQVLGPQENVFVFPSTTSRPV-SAGGRQ
Human          1 -----
Chimpanzee    1 -----
Mouse         1 -----
consensus     61

Zebrafish    118 --NSSRGYNASKAPSRNVT-----THGH-KPP-KQVPSIMTALERKQEECEVQ
Frog          89 WSVGRKMYSPTKQISLCAVKVLSQSFDS ENCKPLQKMSPNATVKKSVPEGLDENSECVPQ
Human          1 -----METVNEPETGEVSKDAVIVKQEKRNNEYCLO
Chimpanzee    1 -----METVNEPETGEVSKDAVIVKQEKRNNEYCLO
Mouse         1 -----METVDETKAGETSKDLVLAKQEGNSDYCLK
consensus    121          ..          . . . . .

Zebrafish    162 SESVHELHTQAPGEVLSANDKESPEAQHDEEENE SDEGLVPLELFAEFLQAVMIKNYOLA
Frog         149 HVEK-EVV-----TDKDKSSDEDKSSDEKEAVPLELLAEFLKAVMADYKVA
Human         31 DIDD-KLSESAED----DGEDDTNDEDDDEDSNP KKNTQAPLELMAEFLRAEMAREYOLA
Chimpanzee   31 DIDD-KLSESAED----DGEDDTNDEDDDEDSNP KKNTQAPLELMAEFLRAEMACEYOLA
Mouse        31 DIEE-NLSDSTDG----DGEEDSSND--DDEGPTKKATQAPLELMAEFLRAEMGRDYOLA
consensus   181 .. .          . . . . *..          ****.***** * . . . .

Zebrafish    222 KKLCQMIL IYEPQNSEAKWFLPLIEEKLLMEADEESDDDDLESDTSDNDDEDDDDDE
Frog         196 HKLCQMI L IYEPENREAKEFFPLIEKRVQMEDGNTDSEDTENSEDTEGSESDSESESE
Human         86 KKLCQMI L IYEPENBEAKEFFPLIEEMLLMEKTONHEQDGENSDEDS-SGESKGESDEEL
Chimpanzee   86 KKLCQMI L IYEPENBEAKEFFPLIEEMLLMEKTONHEQDGEDSDEDS-SGESKGESDEEL
Mouse        84 KKLCQMI L IYEPENPVAKEFFSLIEEMLLKEKAQDEED-BEDSDEDS-SSESEVDSSEDEG
consensus   241 .*****.***.* .***.***. ....* . . . . *.. . . . .

Zebrafish    282 SSSSDTDEESIDSTDDTLSSSC
Frog         256 SSSSDTSSDDTSE-DESVP---
Human        145 SSSSDEGEDGS-----
Chimpanzee   145 SSSSDEGEDGS-----
Mouse        142 SSSSDECEDGS-----
consensus   301 * .*** . . .

```

Figure 8.; Sequence alignment of ERICH2 orthologues. Sequences were aligned using Clustal X and shaded by BOXSHADE. Shaded residues indicate $\geq 80\%$. Species and accession numbers are as follows: Zebrafish (*Danio rerio*, GenBank: XP_009300384.1); Frog (*Xenopus laevis* GenBank: XP_018091376.1); Human (*Homo sapiens*, GenBank: NP_001276876.1); Chimpanzee (*Pan troglodytes*, XP_001135926.1); Mouse (*Mus musculus*, GenBank: XP_011238042.1).

```

Chimpanzee 1 MATPLGWSKAGSGSVCLAFDQLRDVIESQEELIHQLRNVMLQDENFVSKEEFQAVEKKL
Mouse      1 MATPLGWSKAGSGSVCLAFDQLRDVIESQEELIHQLRNVMLQDENFVSKEEFHEIEKKL
Human     1 MATPLGWSKAGSGSVCLAFDQLRDVIESQEELIHQLRNVMLQDENFVSKEEFQAVEKKL
Pig      1 MATPLGWSKAGSGSVCLAFDQLRDVIESQEELIHQLRNVMLQDENFVSKEEFQAVEKKL
consensus 1 ***** .***** *****.....*****

Chimpanzee 61 VEEKAAHAKTKVLLAKEEEKLQFALGEVEVLSKQLEKEKLAFEKALSSVKSRLQESSKK
Mouse     61 VEEKAAHAKTKALLAKEEEKLQFALGEVEVLSKQLEKEKMAFEKALSSVKSRLVQESSKK
Human    61 VEEKAAHAKTKVLLAKEEEKLQFALGEVEVLSKQLEKEKLAFEKALSSVKSRLVQESSKK
Pig     61 VEEKAAHAKTKVLLAKEEEKLQFALGEVEVLSKQLEKEKLAFEKALSSVKSRLQESSKK
consensus 61 ***** .***** .***** .*****

Chimpanzee 121 DQLITKCNEIESHIIKQEDILNGKENEIKELQQVISQOKQIE SPPPAGSVAGIT-----
Mouse    121 DQLITKCNEIESHIIKQEDILNGKENEIKELQQVISQOKQIFRNHISDFRIQKQOET YMA
Human   121 DQLITKCNEIESHIIKQEDILNGKENEIKELQQVISQOKQIFRNHMSDFRIQKQOES YMA
Pig    121 DQLITKCNEIESHIIKQEDILNGKENEIKELQQVISQOKQIFRNHMSDFRIQKQOEN YMA
consensus 121 ***** .***** .***** .*****

Chimpanzee 175 -CLT---SGSRSSRRATWPKCWTRSIRKPKQGHVVRPAATSIPGKNKMAAAFLFSGCNPQPL
Mouse    181 QVLDQKRKKATGMRRARSRCQCSREK-----
Human   181 QVLDQKHKKASGTROARSHORPREK-----
Pig    181 QVLDQKHKKASGTROARSHORPREK-----
consensus 181 ..*.....* *.....

Chimpanzee 231 PSLWESPASSPCYFPPSWVVVEVHKVGACSLGEEGLCLLVGTTASFGYLIPSYINSPG
Mouse
Human
Pig
consensus 241

Chimpanzee 291 YPVIFHPTPSVLVNLTLPT
Mouse
Human
Pig
consensus 301

```

Figure 9.; Sequence alignment of SPATA24 orthologues. Sequences were aligned using Clustal X and shaded by BOXSHADE. Shaded residues indicate $\geq 80\%$. Species and accession numbers are as follows: Chimpanzee (*Pan troglodytes*, GeneBank: PNI22565.1); Mouse (*Mus musculus*, GenBank: NP_083761.1); Human (*Homo sapiens*, GenBank: NP_919272.1); Pig (*Sus scrofa*, GeneBank: NP_001171393).

```

Pig      1  MFLFSRKTKTPISTYSDSYRAPSISKEVYKDPPLWAWEANKEVTPGLTHTAQRHVDPEAL
Mouse    1  MFLFSRKTKTPISTYSDSYRAPSISKEVYKDPPLWAWEANKEVTPGLTQTMHRHVDPEAL
Human    1  MFLFSRKTRTPISTYSDSYRAPSISKEVYKDPPLCAWEANKFLTTPGLTHTMERHVDPEAL
Chimpanzee 1  MFLFSRKTRTPISTYSDSYRAPSISKEVYKDPPLCAWEANKFLTTPGLTHTMERHVDPEAL
consensus 1  *****.*****.*****.*****.*****.*****.*****.*****

Pig      61  QKMVKCAVQDYSYKGSISGHPYLPKEYWLSQEEADKCNPNYLCGNRYNTWRMGPYSCIGW
Mouse    61  QKMKCAVQDYTYKSSISGHPYLPKEYWLSPEEDKCCPSYLDNDRYNTWRTSPCS-NYW
Human    61  QKMAKCAVQDYTYRGSISGHPYLPKEYWLSQEEADKCSPNYLGSDWYNTWRMEPYNSCC
Chimpanzee 61  QKMAKCAVQDYTYRGSISGHPYLPKEYWLSQEEADKCSPNYLGSDRYNTWRMEPYNSCC
consensus 61  *** ***.***.*..**.*.....*...*** **..*****.***

Pig      121  NRCNVYLPQLPKEAGMETVVRGMPLVYPPKPERLNAYEREVVNMLNSLSRNQPLPQITP
Mouse    120  NKYTGCLPRLSKDTGME-SVRGMPLYEPPKQERLNAYEREVVNMLNSLSRNRTLPQITP
Human    121  NKYTYLPLPKEARMETAVRGMPLCPPERLNAYEREVVNMLNSLSRNQQLPRITP
Chimpanzee 121  NKYTYLPLPKEARMETEVRGMPLCPPERLNAYEREVVNMLNSLSRNQQLPRITP
consensus 121  *... ***.***.*..**.*.....*...*****.*****.*****.*** **

Pig      181  RCGCDPLPGRLPEHGYESACSGRHYCLRGMDYYVAGPCTERRLRPLCAEQPTVRSVSP
Mouse    179  RCGCVDPLPGRLPEHGYESPCSGRHYCLRGMDYCTTREPSTERRLRPLCSCQPTECVALR
Human    181  RCGCVDPLPGRLPEHGYESACSGRHYCLRGMDYYASGAPCTDRRLRPLCREQPTMCTSLR
Chimpanzee 181  RCGCVDPLPGRLPEHGYESACSGRHYCLRGMDYYASGSPCTDRRLRPLCREQPTMCTSLR
consensus 181  ****.*****.*****.*****.*****.*****.*****.*****

Pig      241  CEHRPQGMHCAVLTPPQSYYPCPNLRWDTSHFKKTGGPQRNNYVHVHPEFVSETYPDYHCW
Mouse    239  SPARNAMCCYNS--PAIILPVSEF-----
Human    241  APARNAVCCYNS--PAVILPISEF-----
Chimpanzee 241  APARNAVCCYNS--PAVILPISEF-----
consensus 241  ..*....*... *.....*...

```

Figure 10.; Sequence alignment of CBE1 orthologues. Sequences were aligned using Clustal X and shaded by BOXSHADE. Shaded residues indicate $\geq 80\%$. Species and accession numbers are as follows: Pig (*Sus scrofa*, GeneBank: XP_020920344.1); Mouse (*Mus musculus*, GenBank: NP_001041470.1); Human (*Homo sapiens*, GenBank: NP_115985.2); Chimpanzee (*Pan troglodytes*, GeneBank: XP_520543.3).

